

Sheffield Hallam University

Investigation of disintegration and arcing in electric fuses

BROWN, Robert Ernest

Available from the Sheffield Hallam University Research Archive (SHURA) at:

<http://shura.shu.ac.uk/7111/>

A Sheffield Hallam University thesis

This thesis is protected by copyright which belongs to the author.

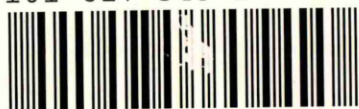
The content must not be changed in any way or sold commercially in any format or medium without the formal permission of the author.

When referring to this work, full bibliographic details including the author, title, awarding institution and date of the thesis must be given.

Please visit <http://shura.shu.ac.uk/7111/> and <http://shura.shu.ac.uk/information.html> for further details about copyright and re-use permissions.

CITY CAMPUS, POND STREET,
SHEFFIELD, S1 1WB.

101 617 343 1



REFERENCE

ProQuest Number: 10694282

All rights reserved

INFORMATION TO ALL USERS

The quality of this reproduction is dependent upon the quality of the copy submitted.

In the unlikely event that the author did not send a complete manuscript and there are missing pages, these will be noted. Also, if material had to be removed, a note will indicate the deletion.



ProQuest 10694282

Published by ProQuest LLC (2017). Copyright of the Dissertation is held by the Author.

All rights reserved.

This work is protected against unauthorized copying under Title 17, United States Code
Microform Edition © ProQuest LLC.

ProQuest LLC.
789 East Eisenhower Parkway
P.O. Box 1346
Ann Arbor, MI 48106 – 1346

Investigation of Disintegration and Arcing in Electric Fuses

Robert Ernest Brown

A thesis submitted in partial fulfilment of the requirements of
Sheffield Hallam University
for the degree of Doctor of Philosophy.

Electronics Research Group
School of Engineering
Sheffield Hallam University
Sheffield, UK

March 2000



This thesis is dedicated to my wife Jackie, my two sons Nicholas and Cameron,
and to my parents.

Acknowledgements

I would like to declare my deepest love, respect and gratitude to my wife Jackie, for her constant support, encouragement and dedication during our time together but particularly during the time period of this project.

I would like to express my love for my two sons Nicholas and Cameron who have been a constant motivation and source of delight. I am grateful that, whilst conducting this project my extra time at home has allowed me to be a big part in their young lives.

I would sincerely like to thank and express my love to my Mother and Father who, I consider acknowledge the worth of education and learning and have helped in every way possible to allow me to fulfil my aspirations in this respect.

My sincere thanks are expressed to my wives parents, for their help in many ways but particularly in relieving me of my paternal duties, which has provided me with the time to complete this project.

On behalf of my family, I wish to express our sincere thanks to all our friends who have been sources of help in many ways, and who have provided sanctuary from the world of fuses.

I wish to express my deepest gratitude to Professor Peter M. McEwan, my Director of Studies for his help and encouragement and without whose guidance and interest, the completion of this project would not have been possible.

Furthermore, I wish to express my thanks to my friends and colleagues at Sheffield Hallam University. To Dr. Jon Travis my second supervisor. To John Burgan for all his help and for allowing me free access to his 'Aladdin's cave of electronic bits'. My thanks to Len Evans, for his help and for free access to his 'DIY store and tool cupboard' and my thanks to Roger Roddis for allowing me to use the 'best scopes from his lab' for the period of this project.

My thanks are also expressed to GE POWER CONTROLS Ltd., Liverpool, UK, and particularly to Dave Crellin for his support and assistance in the acquisition of fuse samples, arranging fuse testing at Trafford Park and in the loan of video equipment.

In conclusion, I am sure all of these individuals are pleased with my achievement, but I am proud of them and will be indebted to them always, because they have been so big a part of it.

The Author.

Following secondary education at South Grove Comprehensive School, Rotherham, in August 1975 the author commenced apprenticeship training in Instrumentation and Electronics with British Steel Corporation

On completion of the apprenticeship in August 1979 the author took up a Junior Technician position within the Instrument Department at British Steel, Rotherham where during the next thirteen years the author progressed to the position of Senior Process Control Technician

The author moved to Vancouver, Canada in March 1993, where he took up the position of Instrument Maintenance Engineer with Sealand Sales/Crescent Controls Ltd.

In October 1993 the author returned to the UK and to higher education, initially at Rotherham College of Arts and Technology but then at Sheffield Hallam University where in June 1996 he obtained a Bachelor of Engineering First Class Honours Degree in Electronic Systems and Control Engineering.

In October 1996 the author embarked on the three year Ph.D. research project present in this thesis.

Declaration.

I hereby declare that this thesis is entirely my own work, and has not been submitted in support of an application of another degree or qualification of this, or any other university, institute of learning or industrial organisation.

Robert Ernest Brown

March 2000

Abstract

This thesis essentially presents the experimental investigation of the fundamental phenomena of electric fuse element disintegration and its causation and influence on the subsequent fragmentation of the fuse elements when subjected to excessive fault currents. The basis of the study involved experimental observation of disintegration of fuse elements and the analysis of the dynamic responses of current-carrying conductors, which precipitate disintegration. The experimental techniques employed utilised commercially available video cameras to capture images of element disruptions during disintegration of fuse elements subjected to low short-circuit and high overload currents. Specialist experimental image capturing techniques and hardware implementations were developed to enable investigation of element disintegration caused by high short-circuit fault currents. Disintegration phenomena of fuse elements for all fault cases were compared within different time domains, which included specialist techniques to investigate disintegration of elements in sand and against glass substrates. Disintegration phenomena of elements in unconfined media such as air and water also constituted the studies. The studies diverged, finally, into experimental observations of the temporal development of arc initiation and extinction phenomena of fault current limiting of HBC fuses using spectroscopic analysis of the arc light radiation. The range of studies covered have led to new understandings of fundamental current limiting behaviour of HBC and open type fuses which contribute, in a small way, to the knowledge base of the subject and hopefully will be an aid to improved designs and development of new types of electric fuse.

List of Figures.

Chapter 1

Figure		Page
1.1(i)	TIS63 HBC fuse – rated 63 amp, 415 volt, GE Power Control Ltd.,	2
1.1(ii)	Typical components of HBC fuse construction	2
1.2	The range and application of cartridge fuses [2]	3
1.3	Common types of fuse element and notch geometries	5
1.4	Oscillograms indicating the variance of the shape of fuse voltage waveforms relative to temporal disintegration phenomena	11/12
1.5	Referred time periods of fuse element disintegration relative to a typical fuse voltage waveform	12
1.6	Simplified diagram of a fuse arc	13
1.7	Fuse arcing period equivalent circuit model.	15
1.8(i)	UR31 20Amp 300 Volt Semiconductor film substrate fuse, Yoden Fuse Company, Japan	17
1.8(ii)	Yoden UR31 fuse, film substrate element	17
1.9	Film substrate fuse element with 'Z' plane restrictions	18
1.10	Pre-arcing time current characteristic of Yoden UR61-30A semiconductor film substrate fuse.	19

Chapter 2.

2.1	Clear patterns of disintegration observed in post operation fuse remnants	22
2.2	Unduloid formations observed in post operation conductor remnants[32]	24
2.3	Striated disintegration pattern observed in post operation fuse fulgurites[32].	30
2.4	Striated disintegration pattern observed in images of fast exploding wires[71].	30
2.5	Segmented disintegration observed in conductor remnants[32].	31
2.6	Hibner's [57] resistance gradient fuse model.	36
2.7	Gomez McEwan [58] Striated mechanism of fuse voltage Increase based on the average arclet voltage during the pre-peak arc voltage period.	40

2.8	Gomez [10] Striated mechanism of fuse voltage decrease based on the average arclet voltage during the post-peak arc voltage period.	41
2.9	Arcing period predicted fuse voltage waveforms by Gomez [10] arclet voltage model and experimental HBC wire element fuse voltage waveforms.	42
2.10	Arcing period predicated fuse voltage and current waveforms by Dolgowski's [59] 'empirically determined' fuse arc model and experimental HBC fuse voltage and current waveforms	45
2.11	Arcing period predicted fuse voltage and current waveforms by Wright and Beaumont's [21] 'arc physic' HBC fuse arc model and experimental HBC fuse voltage and current waveforms	46
2.12	Arcing period predicted fuse voltage and current waveforms by Daalder and Schreurs [26] 'hybrid' HBC fuse arc model and experimental HBC fuse voltage and current waveforms.	48

Chapter 3.

3.1	HBC conductive film substrate fuse element notch geometries	52
3.2	Experimental fuse cartridge 'A' (shown without filler) and fuse terminal post arrangement	53
3.3	Experimental fuse test facility.	54
3.4	Experimental low voltage fuse test facility circuit schematic (excluding generator sets).	54
3.5	Example of an experimental HBC conductive film substrate fuse element.	70
3.6	Fuse cartridge 'B' used to hold conductive film substrate fuse elements.	71
3.7	Medium speed video camera experimental arrangement.	77
3.8	Medium speed video camera and filter arrangement.	78
3.9	Fast speed video camera	78
3.10	Fast speed video camera, light sensor, TSL 1401.	79
3.11	Fast speed video camera, optical system.	80
3.12	Fast speed video camera control electronics and sensor output capture oscilloscopes	81
3.13	Interconnection schematic diagram for fast speed video camera control, optical system, sensor output capture oscilloscopes and fuse test facility.	82
3.14	Structured timing sequence of TSL 1401 serial input (SI) pulses	83

3.15	Structured oscilloscope capture of TSL 1401 sensor output	83
3.16	Alignment arrangement of optical system and homogenous light source	84
3.17	Simplified block diagram of camera test arrangement with patterned encoded wheel	85
3.18	Patterned encoded wheel designed to simulate sequential arc ignition.	85
3.19	Normalised TSL 1401 sensor output. (Integration time = 1.5ms)	85
3.20	HBC conductive film substrate fuse holder showing horizontal and vertical datum's for accurate positioning of fuse elements.	86
3.21	HBC conductive film substrate holder with additional substrate clamping plate with vertical alignment datum's	86
3.22	Fuse test circuit with additional crowbar thyristor and variable resistor arrangement which allowed commutated disintegration of fuse elements relative to fuse voltage	88
3.23	Fuse test circuit with additional crowbar thyristor which, when triggered from the fast video camera control allowed commutated disintegration of fuse elements relative to latching of the fast video comparator.	89

Chapter 4

4.1	Images of random 'catenary' shaped element disposition. (Medium speed video camera images)	92
4.2	Sequenced images displaying temporal development of unduloid formation in a 0.2032 \varnothing mm/60mm silver wire element, (Medium speed video camera images)	93
4.3	Close up image of the connection between end cap and a 0.2032 \varnothing mm/60mm silver wire element about 40ms after the instant of disintegration (Slow speed video image)	93
4.4	Image of a 0.2032 \varnothing mm/60mm silver wire element with disintegration initiating in the vicinity of an element end cap connection point. (Medium speed video image)	94
4.5	Sequenced images displaying the onset of disintegration of a 0.2032 \varnothing mm/60mm wire element before the formation of unduloids (Slow speed video camera images)	94
4.6	Sequenced images displaying the formation of unduloids before the onset of disintegration of a 0.2032 \varnothing mm/60mm wire element (Medium speed video camera images)	94
4.7	Image of 0.2032 \varnothing mm/60mm silver wire element remnants expelled away from the point of arc ignition (Slow speed video camera image)	95

4.8	Images of the 'whipping' action of attached remnants of an 0.2032Ømm/60mm silver wire element around a 'pivot' point in the vicinity of the end cap element connection point	95
4.9	Images indicating the variance of the number of arc ignitions observed during the disintegration of a 0.2032Ømm/60mm silver wire element (Medium speed video camera images)	96
4.10	Fuse voltage and current waveforms during the time period of disintegration of a standard fuse with a 0.2032Ømm/60mm silver wire element	96
4.11	Sequenced images displaying the sequential ignition of arcs evidential of sequential disintegration of a 0.2032Ømm/60mm silver wire element (Medium speed video camera images)	97
4.12	Fuse voltage and current waveforms during the long time period of fault current conduction of a standard fuse with a 0.2032Ømm/60mm silver wire element	97
4.13	Images of the thermal contraction of a 0.2032Ømm/60mm silver element after current commutation (Slow speed video camera images)	98
4.14	Unduloid formations observed in the remnants of a 0.2032Ømm/60mm silver wire element. Disintegration commutated 160ms after current initiation.	99
4.15	Image of fuse remnants indicating the location of a large temperature gradient (Slow speed video camera image).	99
4.16	Images of random element end cap connection location of disintegration in a vertically orientated 0.2032Ømm/60mm silver element (Camera rotated through 90o) (Medium speed video camera images)	100
4.17	Images of axial movement of a 0.2032Ømm silver wire element indicating shear forces acting in the vicinity of the end cap element connection. (Slow speed video camera images)	101
4.18	Sequenced images of the disintegration of a 0.2Ømm/60mm Copper wire suspended in air (Medium speed video camera images)	101
4.19	Sequenced images of the disintegration of a 0.2032Ømm/30mm Silver wire suspended in water (Medium speed video camera images)	102
4.20	Sequenced images of parallel 0.2032Ømm/60mm silver wire elements (Axial element separation = 3mm) indicating the weak influence of electromagnetic forces and the dominance of thermal dilation forces (Slow speed video camera images)	102
4.21	Sequenced images of parallel 0.2032Ømm/60mm silver wire elements (Axial element separation = 1mm) indicating the fusion of elements and familiar disintegration pattern (Slow speed video camera images)	103

4.22	Images, captured during long time period disintegration of HBC conductive film substrate fuses, indicating the random shape of element longitudinal deformation (Medium speed video camera images)	105
4.23	Images, captured during long time period disintegration of HBC conductive film substrate fuses indicating the location of initial fragmentation of the fuse element.	105
4.24	Typical oscillograms of fuse voltage captured at the fragmentation instant of HBC conductive film substrate fuse elements (Long time period disintegration investigation)	106
4.25	Typical oscillograms of fuse voltage and fuse current captured during long time period fault current conduction Element = 0.2032Ømm/25mm silver wire, Filler = fine quartz.	106
4.26	Images of element remnants indicating uniformly embedded quartz granules, minimal axial deformation of the element in the vicinity of the end cap and the location of arc ignition.	107
4.27	Images, captured during very short time period disintegration of standard fuses, indicating the random disposition of catenary shaped elements. (Medium speed video camera images)	110
4.28	Images captured during very short time period disintegration of standard fuses showing the location of initial fragmentation of the fuse element. (Medium speed video camera images)	111
4.29	Sequenced images indicating continued element fragmentation after forced current commutation and correlated fuse voltage and current oscillograms captured during very short time period disintegration of standard fuses. (Medium speed video camera images)	111
4.30	Sequenced images captured during very short time period disintegration of standard fuses indicating the evolution of spheroids in non-current carrying copper element remnants after forced current commutation (Medium speed video camera images).	112
4.31	Sequenced images of arcing and correlated fuse voltage and current oscillograms captured during very short time period disintegration of standard fuses indicating sequential element fragmentation and arc ignition	113
4.32	Oscillograms of fuse voltage and current for standard fuse during very short time period fault conditions.	113
4.33	Image of fuse remnants indicating the minimal axial deformation of the element in the vicinity of the end cap, the location of arc ignition, and element fragmentation.	114
4.34	Images captured during very short time period disintegration of HBC conductive film substrate fuses, indicating the random shape of element longitudinal deformation (Medium speed video camera images).	116
4.35	Images captured during very short time period disintegration of HBC conductive film substrate fuses indicating the location of initial fragmentation of the fuse element.	116

4.36	Correlated video images, voltage oscillograms and images of fuse fulgurites which evidence element fragmentation by sequential arc ignition during very short time period disintegration of HBC conductive film substrate fuses	117
4.37	Sequenced images and correlated voltage oscillographs indicating temporal development of element fragmentation evidenced by the ignitions of a series of short arcs along the length of the element.	118
4.38	Image of fuse fulgurite and voltage oscillogram indicating the total dispersion of the fuse element by arcing phenomena during the period of arc ignition, Element = 0.2Ømm/25mm copper wire, Filler = fine quartz.	118
4.39	Typical oscillogram of HBC conductive film substrate fuse voltage and current during very short time period fault conditions, Element = 0.2Ømm/25mm copper wire, Filler = fine quartz.	119
4.40	Images of element spheroid and segmented remnants and element 'stubs' after current diversion	120

Chapter 5

5.1	Sequenced video images and correlated voltage and current oscillograms which evidence temporal segmented fragmentation of a wire fuse element embedded in epoxy resin	124
5.2	X-rays of fuse remnants and correlated fuse current and voltage oscillograms for fuses constructed with fillers of different compaction density.	127
5.3	Fuse voltage oscillograms inditing the characteristic 'S' shaped pattern of disintegration	129
5.4	Fuse voltage oscillograms presented by Wolny[19][78] indicating the variance of the rate of rise of fuse voltage relative to current density and element confinement during the disintegration of wire fuse elements.	129
5.5	Sequenced images indicating the development of arcing during the pre-peak arc voltage period and correlated fuse voltage and current oscillograms captured during disintegration in short notch element conductive film substrate fuses.	131/132
5.6	Sequenced images indicating arcing phenomena in the post-peak arc voltage period and correlated fuse voltage oscillographs captured during disintegration in wire element conductive film substrate fuses	133
5.7	Sequenced images indicating arcing phenomena in the post-peak arc voltage period of disintegration in short notched conductive film substrate fuses	134
5.8	Sequenced images indicating arcing phenomena and correlated voltage oscillograms of disintegration in short notch conductive film substrate fuse elements suspended in water.	136/137

5.9	Sequenced images indicating the light radiating from a short notch conductive film substrate fuse and correlated fuse voltage and current oscillogram captured about the instant of fault current diversion.	138
5.10	Sequenced images of patterned light /darkness captured during the investigation to establish the degree of image lag for the fast video camera.	139
5.11	Fuse voltage and current oscillograms captured during the investigation of the substrate influence on arcing phenomena in the post-peak arc voltage time period.	140
5.12	Sequenced images indicating arcing phenomena and correlated fuse voltage and current oscillograms captured during the post-peak arc voltage period of disintegration in conductive film substrate fuses.	141
5.13	Diagram of optical spectrum analyser interfaced to the fuse test facility	143
5.14	Experimental arrangement used in the spectroscopic analysis of HBC conductive film substrate fuse arcing phenomena.	143
5.15	Experimental arrangement of OSA and fuse enclosure (Shown without top cover and opaque shroud)	144
5.16	Typical arc light spectrum and correlated fuse voltage oscillogram captured during the post-peak arc voltage time period of disintegration in a short notch silver HBC conductive film fuse	145
5.17	Mean arc light spectrum captured during the post peak arc voltage time period in the disintegration of a conductive film substrate fuse with a 0.2Ømm/25mm copper wire element embedded in fine quartz.	146
5.18	Mean arc light spectrum captured during the post peak arc voltage time period in the disintegration of a conductive film substrate fuse with a short notch silver element embedded in fine quartz.	146
5.19	Mean arc light spectrum captured during the post peak arc voltage period in the disintegration of a conductive film substrate fuse with a 0.2Ømm/25mm copper wire element suspended in water.	147
5.20	Mean arc light spectrum captured during the post peak arc voltage period in the disintegration of a conductive film substrate fuse with a short notch silver element suspended in water.	147
5.21	Typical arc light spectrum and correlated fuse voltage oscillogram captured during the pre-peak arc voltage time period of disintegration in a short notch silver HBC conductive film substrate fuse	149
5.22	Mean arc light spectrum captured during the pre-peak arc voltage time period of the disintegration of a conductive film substrate fuse with a short notch silver element embedded n fine quartz.	149
5.23	Arc light spectrums captured during the disintegration of short notch silver element conductive film substrate fuses immersed in sand.	150
5.24	Independent data sources indicating the electrical resistivity of silica quartz as a function of temperature	152

List of Tables

Chapter 2

Table		Page
2.1	Classifications of the disintegration of electrical conductors	22
2.2	Measured and calculated values of Joule integrals for the disintegration time periods of a wire element HBC fuse [57].	38

Chapter 3

3.1	Primary chemical components and ratios of quartz fillers	52
3.2	Relevant technical specifications for epoxy resin (RS© 199-1468)	53
3.3	Maximum wire diameters - disintegration initiated at voltage zero and occurs at the instant of peak supply voltage	57
3.4	Primary chemical components and ratios of substrate materials.	71

Nomenclature

List of Principal Symbols

Symbol	Description
$v(t)$	Instantaneous value of voltage
$v_f(t)$	Instantaneous value of fuse voltage
$i(t)$	Instantaneous value of current
$I_f(t)$	Instantaneous value of fuse current
R_c	Equivalent circuit resistance
L_c	Equivalent circuit inductance

Glossary of Terms

Term	Definition
Conductive Film Substrate Fuse	A fuse, constructed with a random geometry element pressed against a substrate by rear acting pressure of a constricting medium.
Fulgurite	The fused remnants of silica quartz granular filler.
Hydrographic Bonding	A technique using water glass (<i>Sodium Silicate</i>) to bond granular fuse fillers.

Glossary of Abbreviations

Acronym	Definition
I1	Maximum fuse breaking capacity duty BS EN 602909
I2	Maximum arc energy fuse test duty BS EN 602909

Contents

Chapter 1

A Synopsis of the Role of the Fuse and the Project Objectives.

1.1	Introduction.	1
1.2	General Consideration of Fuse Requirements.	1
1.3	Typical HBC Fuse Construction	2
1.3.1	<i>Material, Physical, Objective and Transient Properties of HBC Fuses</i>	4
1.3.2	<i>Fuse Elements</i>	4
1.3.3	<i>Fuse Fillers</i>	7
1.3.4	<i>Fuse End Caps</i>	8
1.3.5	<i>Fuse Cartridge</i>	9
1.4	Investigation Objectives	9
1.4.1	<i>Fuse Element Disintegration</i>	10
1.4.2	<i>Electric Arcs</i>	13
1.4.3	<i>The Theory of Fuse Operation</i>	15
1.5	Scope of the Investigation of Disintegration in HBC Conductive Film Substrate Fuses	16
1.5.1	<i>Conductive Film Substrate Fuse Elements</i>	17
1.6	Chapter Propositions and Key Findings.	19

Chapter 2

Phenomena of Electrical Conductor Disintegration and Modelling Techniques of HBC Fuse Disintegration and Arcing Phenomena

2.1	Introduction	21
2.2	Classifications of Fuse Element Disintegration	21
2.3	Phenomenological Aspects of Single Break Disintegration	22
2.3.1	<i>Summary of Propositions and Accepted Phenomena of Single Break Disintegration</i>	23
2.3.2	<i>Key Findings relating to the Phenomena of Single Break Disintegration</i>	24

2.4	Phenomenological Aspects of Unduloid Disintegration	24
2.4.1	<i>Summary of Propositions and Accepted Phenomena of Unduloid Disintegration</i>	28
2.4.2	<i>Key Findings relating to the Phenomena of Unduloid Disintegration</i>	29
2.5	Phenomenological Aspects of Striated Disintegration	29
2.5.1	<i>Summary of Propositions and Accepted Phenomena of Striated Disintegration</i>	33
2.5.2	<i>Key Findings relating to the Phenomena of Striated Disintegration.</i>	34
2.6	Implications of Electrical Conductor Disintegration in Modelling the Arcing Period of HBC Fuse Operation.	35
2.7	Disintegration Models of the Arcing Period of Fuse Operation.	35
2.7.1	<i>Resistance Gradient Model of the Disintegration of a HBC Fuse</i>	36
2.7.2	<i>Key Aspects of Resistance Gradient Modelling of the Disintegration of a HBC Fuse</i>	38
2.7.3	<i>Arclet Voltage Model of the Disintegration of a HBC Fuse</i>	39
2.7.4	<i>Key Aspects of the Arclet Voltage Model of the Disintegration of a HBC Fuse.</i>	43
2.8	HBC Fuse Arcing Phenomena.	44
2.8.1	<i>HBC Fuse Arc Models</i>	44
2.8.2	<i>Notable Attributes of HBC Fuse Arc Models</i>	48
2.9	Summarising Comparisons of Fuse Arc Models and Disintegration Models of the Arcing Period of HBC Fuse Operation	49
2.10	Chapter Summary and Propositions	49

Chapter 3

Experimental Techniques

3.1	Introduction	51
3.2	Experimental HBC Fuse Construction	51
3.2.1	<i>Fuse Elements</i>	52
3.2.2	<i>Arc Quenching Mediums</i>	52

3.2.3	<i>Cartridges and End Caps</i>	53
3.3	Experimental Low Voltage Fuse Test Facility.	54
3.3.1	<i>Energy Sources.</i>	55
3.3.2	<i>Current Switching and Fault Application Control.</i>	55
3.3.3	<i>Accuracy of Current Switching</i>	56
3.3.4	<i>Disintegration Capabilities of Fuse Test Facility .</i>	56
3.3.5	<i>Summary of Fuse Test Facility Capacity.</i>	57
3.4	Element Disintegration and Arc Parameter Data Capture.	58
3.4.1	<i>Historical Methods of Fuse Data Capture.</i>	58
3.4.1.1	<i>Examination of Fully Disintegrated Fuses</i>	58
3.4.1.2	<i>Key Findings and Propositions - Examination of Fully Disintegrated Fuses.</i>	60
3.4.1.3	<i>Examination of Commutated Disintegration Fuses.</i>	60
3.4.1.4	<i>Key Findings and Propositions - Examination of Commutated Disintegration Fuses.</i>	61
3.4.2	<i>Transient Methods of Data Capture.</i>	62
3.4.2.1	<i>Fuse Voltage and Arc Voltage.</i>	62
3.4.2.2	<i>Arc Light</i>	63
3.4.2.3	<i>Fuse Material Density</i>	66
3.4.2.4	<i>Key Findings and Propositions - Transient Data Capture.</i>	66
3.4.3	<i>Techniques to Observe HBC Fuse Element Disintegration.</i>	68
3.4.3.1	<i>Key Findings and Propositions - Techniques to Observe HBC Fuse Element Disintegration.</i>	69
3.5	Investigation Applied Experimental Techniques	69
3.5.1	<i>Method to View Disintegration of HBC Substrate Fuse Elements.</i>	70
3.5.1.1	<i>Experimental HBC Substrate Fuse Element Construction.</i>	70
3.5.1.2	<i>Experimental Fuse Cartridge 'B'</i>	71
3.5.2	<i>Methods of Data Capture</i>	72
3.5.3	<i>Fuse Terminal Data Capture.</i>	72
3.5.3.1	<i>Fuse Current.</i>	72
3.5.3.2	<i>Fuse Voltage.</i>	73

3.5.3.3	<i>Digital Storage Oscilloscopes - DSO</i>	73
3.5.3.4	<i>DSO - Personal Computer (PC) - Data Transfer and Data Conversion</i>	73
3.5.3.5	<i>Accuracy of Fuse Current and Voltage Measurements.</i>	74
3.5.4	<i>Video Image Data.</i>	74
3.5.4.1	<i>Slow Speed Video Camera</i>	75
3.5.4.2	<i>Experimental Use and Event Time Correlation : Slow Speed Video Camera.</i>	76
3.5.4.3	<i>Medium Speed Video Camera.</i>	76
3.5.4.4	<i>Experimental Use and Event Time Correlation: Medium Speed Video Camera</i>	77
3.5.4.5	<i>Fast Speed Video Camera</i>	78
3.5.5	<i>Techniques to Terminate Disintegration of HBC Substrate Fuse Elements</i>	87
3.5.5.1	<i>Commutation Relative to Fuse Voltage.</i>	88
3.5.5.2	<i>Commutation Relative to Fast Video Camera Comparator Latch.</i>	88
3.6	Chapter Summary and Propositions	89

Chapter 4

Experimental Observations of the Causation Phenomena of Fuse Element Disintegration

4.1	Introduction	91
4.2	Experimental Approach and Chapter Format	91
4.3	Investigation of Disintegration in the Long Time Domain	91
4.3.1	<i>Description of Temporal Observations of Wire Disintegration in Air.</i>	92
4.3.2	<i>Issues and Propositions Originating from Temporal Observations</i>	98
4.3.3	<i>Additional Observations of the Influences of Component Forces acting about the Locations of Element Disintegration</i>	100
4.3.4	<i>Additional Observations of Proposed Influencing Phenomena on the Formation of Unduloids.</i>	101
4.3.5	<i>Key Findings in the Investigation of Unduloid Formation in Wires Suspended in Unconfined Media.</i>	103

4.3.6	<i>Description of Temporal Observations of Disintegration of Conductive Film Substrate fuses Immersed in Sand.</i>	104
4.3.7	<i>Issues and Propositions Originating from Temporal Observations of Element Disintegration</i>	106
4.3.8	<i>Key Findings in the Investigation of Disintegration of Wires in Confined Media.</i>	108
4.4	Conclusions of Disintegration in the Long Time Domain.	109
4.5	Investigation of Disintegration in the Very Short Time Domain.	109
4.5.1	<i>Temporal Observations of the Disintegration of Wires in Air</i>	110
4.5.2	<i>Issues and Propositions Originating from Temporal Observations of Element Disintegration.</i>	114
4.5.3	<i>Investigation Key Findings for Wires in Unconfined Media.</i>	115
4.5.4	<i>Temporal Observations of the Disintegration of Conductive Film Substrate Fuses Immersed in Sand</i>	115
4.5.5	<i>Issues and Propositions Originating from Temporal Observations of Wire Disintegration</i>	119
4.5.6	<i>Investigation Key Findings for Wires in Confined Media</i>	120
4.6	Conclusions of Very Short Time Domain Investigations of Disintegration.	121
4.7	Chapter Conclusions.	122

Chapter 5

Review and Evaluation of Further Experimental Observations of Fuse Element Disintegration and Arcing Phenomena, Project Summary and Conclusions.

5.1	Introduction.	123
5.2	Review of Observations to Determine the Causation Phenomena of Fuse	123
5.2.1	<i>Issues and Propositions Originating from Observations.</i>	124
5.2.2	<i>Key Findings of the Investigation of Very Short Time Domain Disintegration of Encapsulated Wires</i>	125
5.2.3	<i>Evaluation of the Phenomena of Wire Fragmentation in Confined Media in the Very Short Time Domain.</i>	125

5.3	Review of Observations of the Extent of Fuse Element Fragmentation and Arcing due to the Forces of Wire Confinement.	126
5.3.1	<i>Evaluation of the Observations of the Extent of Wire Fragmentation and Arcing due to the Forces of Wire Confinement.</i>	128
5.4	Review of Observations of the Rate of Rise of Fuse Arc Ignition Voltage due to the Forces of Wire Confinement.	128
5.4.1	<i>Evaluation of the observations of the Rate of Rise of Fuse Arc Ignition Voltage due to the Forces of Wire Confinement.</i>	129
5.5	Review of Experimental Observations of the Temporal Development of Disintegration and Arcing in Conductive Film Substrate Fuses.	130
5.5.1	<i>Observations of Arcing Phenomena about the Peak Arc Voltage Instant.</i>	130
5.5.2	<i>Observations of Post-Peak Arc Voltage Period Arcing Phenomena</i>	132
5.5.3	<i>Issues Originating from Post-Peak Arc Voltage Period Observations</i>	135
5.5.4	<i>Image Phenomena.</i>	135
5.5.5	<i>Arc Light Hysteresis.</i>	137
5.5.6	<i>Electronic Hardware Phenomena.</i>	139
5.5.7	<i>Fuse Construction Phenomena.</i>	140
5.5.8	<i>Proposition of Fault Current Commutation by Fuse Fugurites.</i>	142
5.5.9	<i>Spectroscopic Analysis of Arcing in Conductive Film Substrate Fuses.</i>	142
5.5.10	<i>Spectroscopic Analysis Experimental Arrangements.</i>	143
5.5.11	<i>Analysis of Post-peak Arc Voltage Time Period Arc Light Spectra</i>	145
5.5.12	<i>Analysis of Pre-peak Arc Voltage Time Period Arc light Spectra.</i>	148
5.5.13	<i>Comparison of Arc Light Spectrum Captured during Separate Periods of Fuse Element Disintegration.</i>	150
5.5.14	<i>Evaluation of Spectroscopic Studies of Fuse Arcing.</i>	150
5.6	Evaluation of the Electrical Conductivity of Silica	152
5.7	Key Findings of the Experimental Observations of the Temporal Development of Disintegration and Arcing in Conductive Film Substrate Fuses.	153
5.8	Project Summary, Evaluation, Recommendations and Conclusions.	154
5.8.1	<i>Summary.</i>	154

5.8.2	<i>Evaluation of Study.</i>	155
5.8.3	<i>Recommendations for Future Work.</i>	155
5.8.4	<i>Recommendations of the Project to the Operation of Fuses.</i>	156
5.8.5	<i>Recommendations for the Construction of Practical HBC Conductive Film Substrate Fuses.</i>	156
5.8.6	<i>Contributions to Knowledge.</i>	157
5.8.7	<i>Publications.</i>	157

References	158
-------------------	-----

Appendices

A1	Fuse Test Facility, Energy Sources and Induction Motor Specifications.	166
A2	Fuse Test Facility, Thyristor Specifications	167
A3	Fuse Test Facility, Differential Probe Specifications	168
A4	Fuse Test Facility: Point on Wave Switch Control Unit - Schematic Diagrams	169
A5	Fuse Test Facility, Digital Storage Oscilloscope Specifications	179
A6	Slow Speed Video Camera Specifications	182
A7	Medium Speed Video Camera Specifications	183
A8	Fast Speed Video Camera Testing Results.	184
A9	Fast Speed Video Camera Commissioning Results	188
A10	Fast Speed Video Camera Specifications	190
A11	Analysis of the Dynamic Behaviour of Current Carrying Wires up to Melting Temperature.	200
A12	Finite Element CAD Analysis of Wire Displacement and Stress Distribution	225
A13	Evaluation of the Extent of Fragmentation of a Cylindrical Column Suspended in Un-Confined and Constricted Media.	228
A14	Fuse Test Facility, Optical Spectrum Analyser Interfacing.	229

Preface

Structure of the Thesis

This Thesis is divided into five Chapters, the first of which initially presents an overview of the role and construction of high breaking capacity fuses as a basis for the introduction of the project study areas of disintegration and arcing in electric fuses. Moreover, in this section of the chapter the objectives of the project are clearly stated. The latter half of the chapter discusses the theory of fuse operation to help link observations of fuse element disintegration and arcing phenomena, to the simulation of fuse operation by mathematical model which is proposed as the wider scope of this project.

Chapter two discusses the past work of other researchers in the study fields of fuse element disintegration and modelling of the arcing period of fuse operation. Consequently, this chapter provides the comprehensive knowledge framework against which this study is based.

Experimental techniques are discussed in Chapter three and since the results presented in this thesis generally comprise observations from experimentation, this chapter addresses all aspects of past and current experimental practices. Therefore, the chapter is subdivided and initially the experimental techniques used in past investigations are discussed from which some degree of integrity of the techniques is importantly estimated. The chapter concludes by presenting the experimental techniques used in this project.

Chapters four and five present the results and evaluations of the numerous investigations of disintegration and arcing phenomena obtained from this project. Finally, the project conclusions, recommendations and contributions to knowledge emanating from the work are discussed and conclude Chapter five and this Thesis.

Chapter 1

A Synopsis of the Role of the Fuse and the Project Objectives.

1.1 Introduction.

This Chapter introduces and summarises the objectives and scope of the fuse research work reported in this thesis.

The fundamental requirements of electric fuses are initially discussed and the variances of the main types are briefly presented. The remainder of the Chapter and subsequently the report are focused on high breaking capacity fuses (HBC).

Chapter one is presented in three sections and the first presents an overview of high breaking capacity fuses in which the constructional details and the properties of the individual components of the fuse assembly are discussed.

Chosen areas for investigation are introduced in section two. These are conductor disintegration phenomena, arc formation, fuse operation and fault current interruption.

The development of new HBC fuse designs, fuse prototype testing and simulation of fuse operation are briefly discussed in section three. Attributes of HBC conductive film substrate fuses, their suggested role in optimising disintegration, arc formation and subsequently controlling arcing to benefit fault current interruption are also introduced and conclude the Chapter.

1.2 General Consideration of Fuse Requirements.

A fuse is generally accepted to be the simplest form of protection device used to avoid damage to an electrical system by excess currents. This view stems from the simple construction of the wire type fuse and often leads to the assumption that the operation of a fuse is also simple. In general terms, the fuse is an electrical conductor, which melts when subjected to excessive current and due to disintegration subsequently interrupts current flow. The fuse is then irreparably damaged and can be viewed as being forfeited in the process of protecting the electrical system. Edison [1] acknowledged this and described the role of the fuse as a 'weak link' in an electrical circuit.

Besides interrupting fault currents a fuse should conduct current for all conditions except those classed as faults. Furthermore after operation a fuse should present a high resistance to current flow. These attributes are fundamental to the role of the fuse but are commonly overlooked by all but the specialist.

More complex attributes of fuse operation, of interest to fuse designers and specialist users, are the requirements to avert potentially circuit-damaging disturbances generated during disintegration and furthermore to quickly force current interruption. These and other attributes are important in the role of semi-conductor and high breaking capacity current limiting fuses. Due to the diversity of fuse operating requirements, the range of fuse types is now vast as summarised in Figure 1.2 [2].

The work reported in this thesis concentrated on HBC conductive film substrate fuses. The fault current operation of HBC conductive film substrate fuses is fundamentally the same as standard HBC fuses, however the rationale for investigating this type of fuse will be addressed in Subsection 1.5. Consequently, the attributes of HBC fuses and conductive film substrate fuses will be addressed solely hereon.

1.3 Typical HBC Fuse Construction

An example of a commercially available HBC fuse and a diagram displaying typical construction are shown in Figures 1.1i and 1.1ii.

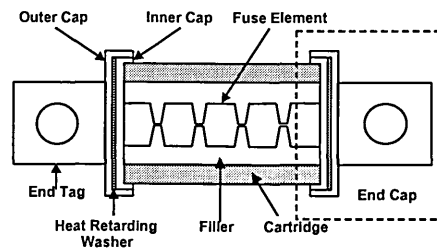
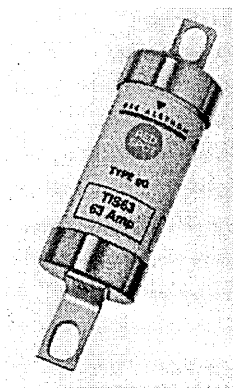


Figure 1.1(i) TIS63 HBC fuse – rated 63 amp, 415 volt, GE Power Control Ltd.

Figure 1.1(ii) Typical components of HBC fuse construction

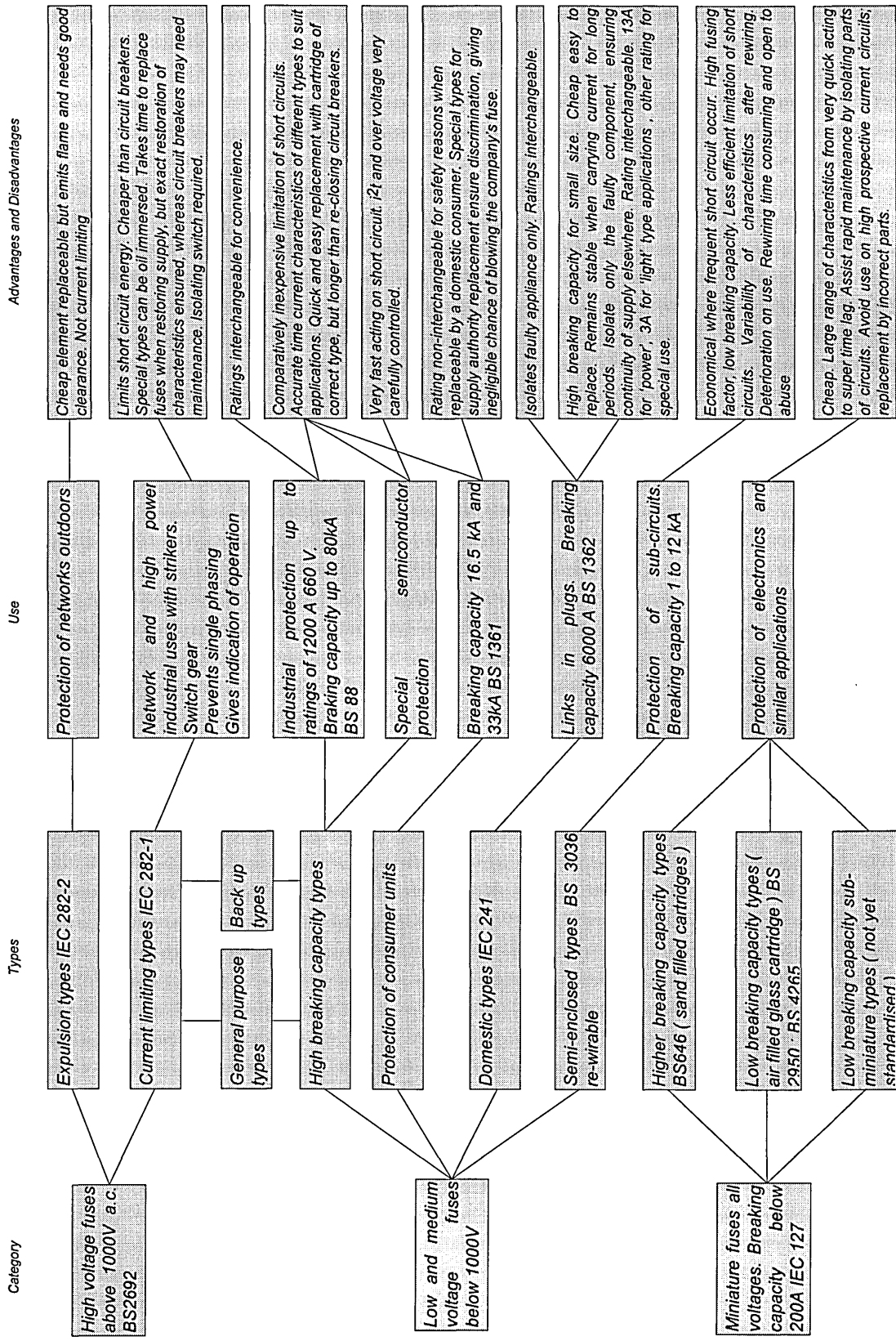


Figure 1.2 The range and application of cartridge fuses [2]

An HBC fuse comprises an element, normally positioned centrally within a cartridge and surrounded by a granular filler, which occupies the space between the element and the inner walls of the cartridge. The element is attached at both ends to inner caps, which seal the ends of the cartridge. An insulating washer is often sandwiched between the inner cap and outer cap, to which an end tag is attached. The inner cap, washer, outer cap and end tag are collectively referred to as the fuse end cap.

Each component of the fuse assembly influences the overall performance of the fuse. The properties of each component are carefully chosen to collectively control fuse operation for a particular application and can be subdivided and analysed under the classifications of material, physical, objective and transient properties.

1.3.1 Material, Physical, Objective and Transient Properties of HBC Fuses

Materials used in the construction of individual components of the fuse assembly have been developed in practice over many years, consequently optimum materials have now been determined for each component and are referred to as material properties. Moreover, due to the numerous applications of fuses, their physical attributes such as size, shape and methods of construction vary widely and are referred to as physical properties. The overall fuse-operating characteristic is derived from the individual component characteristics. Consequently, the operating response with respect to time of a component may be referred to as its objective or transient properties.

Considerations of fuse component properties are important when designing a fuse to operate and efficiently clear fault currents for particular applications. Subsections 1.3.2~1.3.5 will address the properties of HBC fuse components.

1.3.2 Fuse Elements

HBC fuse elements are generally manufactured from silver or copper. Other materials such as aluminium, lead and tin have been used [3][4][5] but are accepted to be inferior alternatives.

Fuse elements have many physical properties. Element geometry is variable and may be in the form of wire or flat ribbon. Wire elements are normally cut from lengths, which have been hard drawn to precise diameters or alternatively from lengths of hard drawn wire further conditioned by soft annealing processes. Ribbon is most often cut to

specified widths from wide sheets rolled to a precise thickness. The size of the fuse element is dependent on its intended application and this is determined initially from simulations of fuse performance and confirmed by practical fuse tests in accordance with the test duty requirements of the fuse.

HBC fuses may contain a single element or multiple elements connected in parallel. The elements most often have several areas of varying width referred to as ‘constrictions or notches’. A single element may have parallel notches or ‘bridges’. The objectives of the notches are to create areas of maximum current density and thus induce melting and subsequently arcing initially within the centre location of the notch. The attributes of notches and their geometry will be addressed in Subsections 1.4 and 1.5. Notches in HBC wire element fuses are manufactured by connecting several wires together to create nodes and further connecting the nodes with single wires. Alternatively, separate wires of different diameters are joined to form a constricted wire element. In both cases soldering techniques are used to connect the wires. Notch creation in ribbon elements is achieved by roll indentation methods, mechanically stamping the notch using accurately machined press tools or photo chemical etching techniques. Several fuse elements are shown in Figure 1.3, indicating the wide range of element and notch geometries that are used in the construction of commercial fuses.

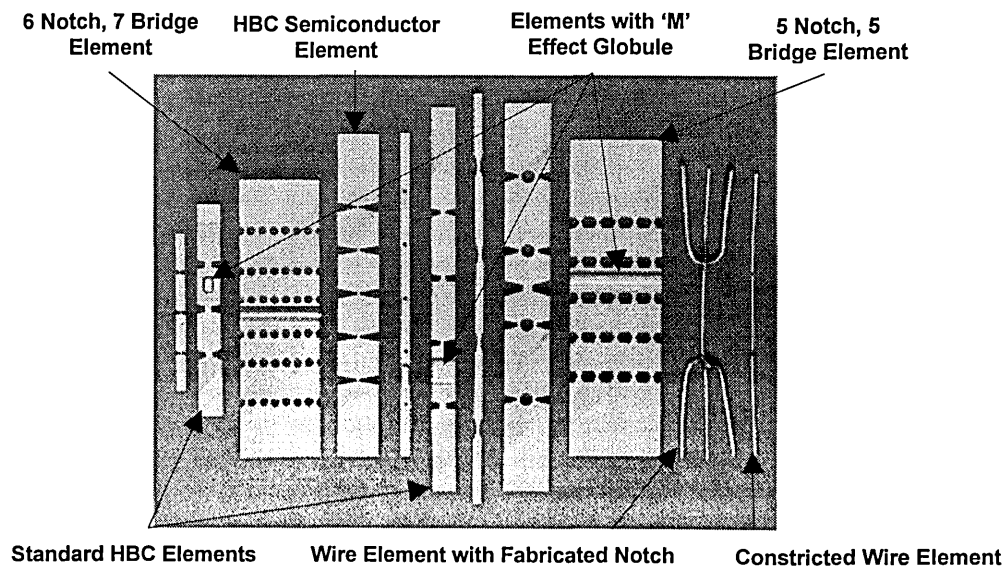


Figure 1.3 Common types of fuse element and notch geometries

Some comprehension of fuse objectives can be obtained by examining the desirable transient properties of fuse element materials [6]. These are,

- High thermal and electrical conductivity
- Low specific heat capacity
- Low melting and vaporisation temperatures
- Low latent heat
- Low density

At rated current levels and currents up to the minimum fusing level, the fuse must be able to establish and maintain steady state thermal equilibrium conditions. In these circumstances the electrical power input to the fuse element is conducted away from the element and dissipated as heat. Consequently, it is justifiable to use materials with high thermal and electrical conductivity's to accomplish this.

Rapid fuse operation and current interruption is an expected requirement during high fault current conditions. The time period from the instant of fault current application to the instant of element vaporisation is minimised by using materials with low specific heat capacities, low melting and low vaporisation temperatures. A key feature is that the energy let through to the protected circuit during this time period is minimised.

Frequently elements manufactured from materials having desirable properties for high over current protection, present inadequate protection for low overload currents over long time periods. However, the transient properties of such element materials may be altered for long time periods by using a technique such as the 'M' effect. This technique, named after the founder, A.W. Metcalf [7] produces a eutectic alloy of the element material with a second metal (usually deposited as a solder globule on the fuse element). The eutectic temperature is lower than the melting temperature of the element material, which hence activates interruption at low over current levels.

After gold, silver is considered the best element material since it permits high current handling due to its high thermal ($4.18\text{W/mK}\times 10^2$) and electrical conductivity ($1.31\Omega\text{m}\times 10^{-8}$) and low specific heat capacity (232J/kgK). Additionally, minimal surface oxidation occurs when silver is near its melting temperature (961°C). This is an advantage over copper, for the preheating and melting behavior of copper is greatly influenced by oxidation when surrounded by air [5]. However, when copper is encased

in sand or quartz filler oxidation is greatly reduced and consequently the choice between silver and copper is usually resolved by economics.

1.3.3 Fuse Fillers

A granular filler material is mostly used in the cavity between the fuse element and the cartridge walls of an HBC fuse. Silica quartz is the most frequently used filler material and its role has been comprehensively investigated [5][8]. Materials such as river sand, marble chalk, lime [5], and other combinations such as mica and water glass and special ceramics [9] have been used and assessed as filler mediums. Generally, their attributes are inferior to silica, which is also beneficially cheap, abundant and chemically stable.

Commonly, granules of approximately equal size are used to fill the fuse cartridge. Size grading is achieved by sifting the quartz through standard mesh sieves. Filler grain size is proposed to influence the minimum fusing current of wire fuse elements [5]. Moreover, it has been observed that granular size and packing density influences the electrode fall voltage of electric arcs ignited during disintegration of fuse elements [10]. The physical attributes of filler have been acknowledged and incorporated in empirically determined models of fuse arcs [11] and element disintegration [12]. The nominal granular size of filler used in HBC fuses is 300 microns [6], and it is proposed that grains in the size range 250~500 microns are best suited for arc quenching [5]. Filler is poured into the cartridge and then mechanically vibrated to a specific compaction density. A nominal value of 1.6g/mm^3 has been proposed [10].

The many transient properties of filler have a significant influence on the overall behaviour of the fuse. In particular it influences the heating process of the fuse element by providing a thermal sink. Additionally the filler restricts movement of the fuse element, due to thermal expansion, and consequently imparts mechanical forces on the fuse element.

Five independent transient properties of filler material which aid the extinction of electric arcs ignited during the disintegration of HBC fuses have been identified [8].

1. During the arcing period of fuse operation the filler withdraws energy from an electric arc/arcs by fusion.

2. During fusion the filler forms a molten shield which contains the arcs within the solid filler in the cartridge and thus prevents merging of the arcs and flashover between individual elements.
3. The filler allows pressure to build up within the molten shield, which assists arc extinction.
4. The filler provides conductance when very hot which has a damping effect on circuit transients.
5. The filler provides insulation against the thermal and mechanical shock of operation.

Moreover on cooling, the electrical conductance of the filler is extremely low which assists the insulation post operation fuse requirement [13].

1.3.4 Fuse End Caps

The HBC fuse end cap arrangement comprises the inner cap, washer and outer cap to which an end tag is attached. The inner and outer caps are generally fabricated from copper or brass, and are usually plated with tin or silver. The washer is nominally fabricated from fireproof fibre materials.

Many end cap designs exist but commonly in the UK, the inner and outer caps are cylindrical and designed to press fit together. Minimal electrical contact resistance is required between the inner and outer caps, which is aided by tin or silver plating. End tags of various shapes and dimensions also exist to suit the variety of contact and fitting arrangements found in practice. The inner cap is first pressed onto the fuse cartridge. The fuse element is subsequently attached through a central hole to the inner cap by soldering or spot welding. The outer cap is pressed onto the inner cap sandwiching the fireproof washer and collectively adequately seal the fuse cartridge.

The end cap assembly must seal the fuse cartridge efficiently to stop ingress of moisture and aid satisfactory operation of the fuse during short circuit and low over current fault conditions. The seal is severely tested under short circuit conditions when very high pressures have to be contained. The fireproof washer additionally provides end cap protection from the effects of prolonged arcing where seal failure and fuse terminal flashover could occur. Furthermore, the end caps contribute a cooling effect at the ends of the fuse element, which is improved by the increased emissivity provided

by tin or silver plating of the end caps and fuses with significant ratings have been designed relative to these attributes [14]. Also, during fuse operation the end caps present physical barriers to movement of the fuse element induced by thermal expansion.

1.3.5 Fuse Cartridge

The cartridge is usually constructed of a ceramic material although others, such as glass reinforced plastic are also used.

Traditionally the shape of the cartridge is tubular in the UK, and rectangular versions are used in continental European designs. The choice of cartridge shape has an effect on the minimum fusing current and the mechanical strength of the fuse. The cartridge wall thickness can range from 2mm~15mm and up to 100mm for the outer cartridge diameter [6].

The cartridge should have good electrical insulating properties in addition to good thermal conducting properties. It should also be non-porous and capable of withstanding significant thermal and mechanical shocks.

1.4 Investigation Objectives

Fuse operation is generally subdivided into two principal time periods. That occurring between the instant of fault application to the instant of element disintegration and arc ignition is referred to as the pre-arcing period and that from the instant of arc ignition to the instant of current interruption is referred to as the arcing period.

During the pre-arcing period, the temperature of the fuse element, its resistance and voltage potential will increase due to joule heating. Continued joule heating induces a change in the physical state of the fuse and at some time instant a break will occur in the element. Disintegration of the fuse element then begins and dependent on circuit and conductor conditions, a gaseous glow discharge followed by an electric arc may form. This marks the start of the arcing period of fuse operation.

A notch in a fuse element presents a restriction to current flow during the pre-arcing period and therefore is a location of maximum current density. Notches can be considered as 'manufactured' locations of maximum current density. Consequently,

melting and vaporisation of the element and subsequently disintegration and arc ignition will initially occur within the notch.

Alternatively, locations of maximum current density can occur due to non-homogenous construction of the fuse element and/or inherent phenomena of fault current conduction. Consequently, melting and vaporisation of the element and subsequently disintegration and arc ignition will take place naturally.

It is the objective of this investigation to observe temporal disintegration and arc formation in electrical conductors and attempt to quantify and establish by experimentation an understanding of the inherent mechanisms of disintegration.

Disintegration can be defined as the fragmentation or break up of the fuse element when carrying fault current. Furthermore arc formation in fuse elements is a consequence of disintegration and circuit conditions at the time instant of disintegration and this is fundamental to the theory of fuse operation. The following discussions introduce temporal aspects of disintegration, arc formation, and the theory of HBC fuse operation, which are the principal study fields of this investigation.

1.4.1 Fuse Element Disintegration

Temporal disintegration phenomena are dependent on the specific energy delivered to the fuse element [16][17][18]. Understanding of the phenomena is still far from complete.

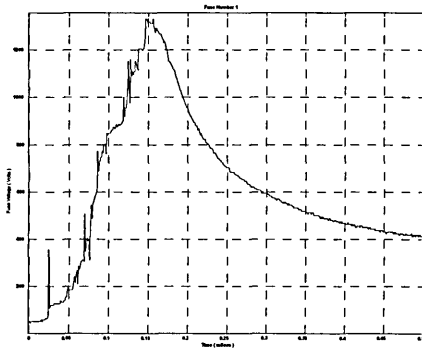
Bennett [17] attempted to classify electrical conductor disintegration relative to the specific energy delivered to the conductor and skin effect phenomena. Three temporal modes of disintegration were defined.

- Slow Disintegration – Slow conductor vaporisation, due to the fractional difference between conductor specific energy and dissipated energy.
- Fast Disintegration – Rapid conductor vaporisation, due to the sufficiently high conductor specific energy.
- Super Fast Disintegration – Induced by rapid discharge of energy from fast circuits provoking skin effect dominance. A rare mode.

This study is associated with the disintegration of HBC fuses where current densities come within the order of magnitude range, $10^1 \sim 10^4 \text{A/mm}^2$, and therefore only the slow and fast modes of disintegration are encountered [19].

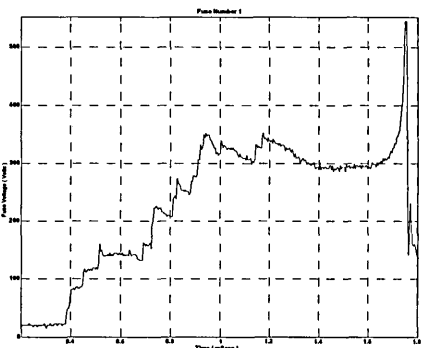
Other phenomena, such as specific power, current density, surface stability of a liquefied conductor, electromagnetic forces, kinetic forces and radiation effects, are also accountable in the classification and study of conductor disintegration. Consequently, previous research of these phenomena will be addressed (Subsections 2.2~2.5) and observations of some of these phenomena from this investigation will subsequently be presented and quantified in Chapter 4.

Due to temporal disintegration phenomena multiple breaks in the fuse element and multiple arcing can occur. As a result the study of the temporal disintegration of the fuse element can be associated with the shape of the fuse terminal voltage waveform which is evidence of arcing captured during disintegration (Figures 1.4i~1.4iii). For example, the positive slope of the voltage developed across the fuse can give an indication of transient fragmentation of the fuse element and hence some temporal classification of disintegration can be assumed. Moreover, the maximum fuse voltage can be related to the number of breaks in the fuse element [10].



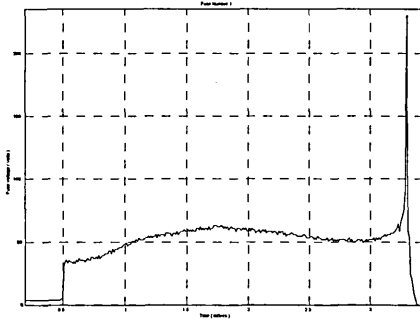
Fuse Element = 0.2134mm \varnothing / 30mm
 Element Material = Copper
 Fuse Filler Material = Fine Quartz
 Prospective Current = 320 amps
 Supply Voltage = 240 volts RMS 50 Hz.
 Fault Initiated at Voltage Zero
 Pre-Arcing Time \approx 7ms
 Peak Arc Voltage \approx 1292 volts
 Time Base 50 μ s/div

(1.4i) Fuse voltage waveform, captured during very short time period disintegration of a wire fuse element



Fuse Element = 0.2mm \varnothing / 25mm
 Element Material = Copper
 Fuse Filler Material = Fine Quartz
 Supply Voltage = 110 volts RMS 50 Hz.
 Fault Initiated at Voltage Zero
 Pre-Arcing Time \approx 31ms
 Peak Arc Voltage \approx 360 volts
 Time Base 200 μ s/div

(1.4ii) Fuse voltage waveform, captured during short time period disintegration of a wire fuse element



Fuse Element = 0.2mm \varnothing / 25mm
 Element Material = Copper
 Fuse Filler Material = Fine Quartz
 Supply Voltage = 100 volts RMS 50 Hz.
 Fault Initiated at Voltage Zero
 Pre-Arcing Time \approx 89ms
 Peak Arc Voltage \approx 65 volts
 Time Base 500 μ s/div

(1.4iii) Fuse voltage waveform, captured during long time period disintegration of a wire fuse element

Figure 1.4 Oscillograms indicating the variance of the shape of fuse voltage waveforms relative to temporal disintegration phenomena

Temporal disintegration of the conductor can also be described and referred to by subdivision of the fuse voltage waveform into distinct time periods [10] as indicated in Figure 1.5.

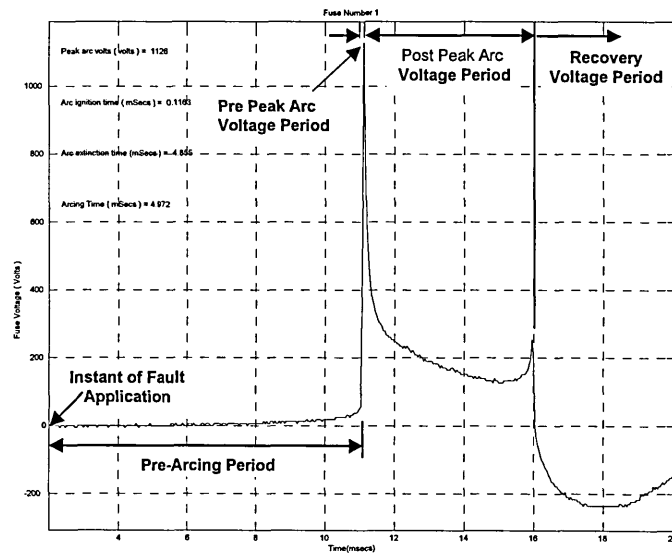


Figure 1.5 Referred time periods of fuse element disintegration relative to a typical fuse voltage waveform

At the start of the arcing period of fuse operation and significantly during the pre-peak arc voltage time period the fuse voltage rapidly increases due to the formation of electric arcs. This phenomenon is critical to good fuse operation. During the post-peak arc voltage period the development of established arcs optimises fuse operation. It

is useful to consider the basic attributes of electric arcs and their formation since the temporal development of disintegration, is usually evidenced by arcing.

1.4.2 Electric Arcs

The fuse voltage waveforms captured during fuse disintegration (Figures 1.4i~1.4iii), show that at the start of the arcing period the fuse voltage increases at a considerable rate. This is due to the formation of an electric arc, which is a self-sustained gaseous discharge, having a relatively low voltage potential and capable of supporting high current flow between anode and cathode electrodes [20]. At atmospheric pressures and above, a high-pressure arc, subsequently referred to as a fuse arc, has the familiar characteristic of an intensely brilliant core.

A fuse arc (Figure 1.6) is accepted to be composed of three regions [21]. The cathode fall region, anode fall region and positive column.

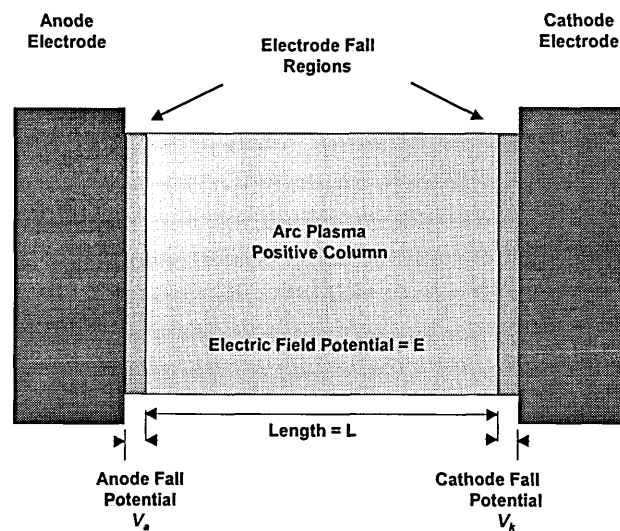


Figure 1.6 Simplified diagram of a fuse arc

The cathode and anode regions are longitudinally small ($\approx 10^{-3}$ mm) and a voltage potential is associated with each region. For element materials with low boiling points (silver and copper), the cathode fall potential drop (V_k) is substantially constant. However, the voltage potential associated with the anode fall region (V_a) could be any value between zero and the atomic ionisation potential of the element material [21]. It is suggested that the anode fall voltage depends on the mechanism

prevailing in the electrode region [22]. For a silver element Wright and Beaumont [21] proposed a cathode fall voltage of 10 volts and an anode fall voltage of 7.56 volts for use with their model of a fuse arc burning in metallic vapour.

Collectively the voltage associated with both electrode fall regions is referred to as the arc root voltage (V_{ak}). A value of 20~25 volts was indicated by voltage oscillograms captured during disintegration of silver wires in air by Baxter [5]. Values in the range 100~150 volts were suggested from investigations of strip element disintegration in filler by Lestrup [23]. Consequently, element geometry is suggested to account for the variance of the arc root voltage magnitude (20~200 volts) by Hibner [24]. Furthermore, the arc root voltage magnitude has been observed to be a function of filler material and packing density [10] and element current density [11] .

The positive column occupies the space between the electrode fall regions and its length (l) is accepted to be the gap size between the electrodes due to the small size of the electrode fall regions [21]. The length of the positive column is dependent on the power input and the transient interaction between the arc and its environment, which cause electrode and filler erosion. The voltage associated with the positive column is the product of the column length and electric field strength or column gradient (E), which additionally is a function of arc conductivity (ρ) and current density (J). Consequently, the determination of fuse arc column gradient is complex and has attracted limited investigations [25][26].

The voltage components of the three regions of the electrical arc can be combined to form the simple mathematical model of fuse arc voltage (Eq. 1.1).

$$v_{arc}(t) = V_{ak} + El(t) \quad \text{Eq.1.1}$$

The components of arc models and their attributes will be addressed in Subsection 2.8.

A consequence of element disintegration into a number of multiple fragments (n) is the formation of numerous series arcs. Thus the temporal fuse arc voltage is given by Equation 1.2.

$$V_{fuse}(t) = (n(V_{ak} + El))(t) \quad \text{Eq.1.2}$$

This temporal development of fuse voltage is fundamental to the operation of fuses.

1.4.3 The Theory of Fuse Operation

The accepted equivalent circuit model applicable during the arcing period of fuse operation is presented in Figure 1.7

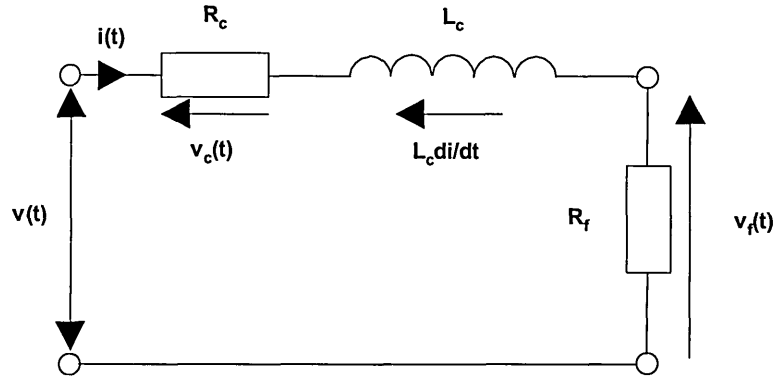


Figure 1.7 Fuse arcing period equivalent circuit model.

From analysis, the circuit voltage components can be described by Equation 1.3.

$$v_s(t) = L_c \frac{di}{dt} + i(t)R_c + v_{fuse}(t) \quad \text{Eq.1.3}$$

and thus the change in circuit fault current is given by Equation 1.4

$$\frac{di}{dt} = \frac{v_s(t) - v_{fuse}(t) - i(t)R_c}{L_c} \quad \text{Eq.1.4}$$

Increasing fuse voltage (v_{fuse}) is beneficial to limiting the rate of increase of fault current and the sudden voltage increase, consequential of arc ignition, has a significant effect on reducing this rate. Moreover, dependent on the magnitude of arc voltage the rate of current flow can be reversed, which forces the fuse current and more significantly, the circuit current toward zero, i.e. when the inequality $v(t) \geq v_s(t)$ is satisfied. Consequently, it is proposed that this phenomena and the pre-peak arc voltage period are of most significance to fuse operation.

This process occurs in all fuses but differs in character and degree dependent upon fuse type and significantly on the phenomena of disintegration. At the instant of peak arc voltage it is assumed that the circumstances described by Equation 1.5 exist.

$$V_{fuse} = n_{max}(V_{arc}) \quad \text{Eq.1.5}$$

Consequently, in the post-peak arc voltage period the temporal development of fuse voltage, given by Equation 1.4, is significant in prolonging and optimising current reduction. Merging of series arcs is generally accepted to occur [19][5][10][26] and the associated loss of arc root voltage is considered to reduce the overall fuse voltage, which is observed in fuse voltage oscillograms. It is proposed in Chapter 5 that this phenomena and the post-peak arc voltage period are of secondary importance to fuse operation.

1.5 Scope of the Investigation of Disintegration in HBC Conductive Film Substrate Fuses

Fuse designs are closely related to application conditions. For new designs some parameters can be derived from mathematical models but, generally prototype fuses have to be manufactured to enable precise characteristics to be determined by practical testing (type testing).

In the pre-arcing period of HBC fuse operation the physical boundaries of fuse components are well defined and consequently their transient interaction has been accurately simulated using computer programmed mathematical models [13][27].

However, in the arcing period the component boundaries are less well defined due to the disintegrating fuse element, which is composed of matter, that passes through three states over a period of time. Consequently, the transient interaction between the element and its surroundings is more difficult to predict. Mathematical models have been presented which claim to simulate fuse arcing [21][11][26], but are only considered moderately accurate and applicable to specific HBC fuse types. These will be discussed in Subsection 2.8.

It is clear that the simulation of the full operation of a fuse is still limited. In this work a different approach is considered to generate the fuse model. This consists of modelling the disintegration of the fuse and the subsequent temporal changes in fuse voltage during disintegration and the arcing period rather than direct fuse arc modelling. Also understanding the fundamental phenomena of electrical conductor disintegration could lead directly to the control of fuse arcing by variation of element geometry. Film substrate fuse elements permit infinite variation of element geometries, and hence

provide a practical solution for geometry investigation. The various attributes of the foregoing are briefly discussed and conclude this Chapter.

1.5.1 Conductive Film Substrate Fuse Elements

A commercially available film substrate fuse and film substrate element marketed for semiconductor protection by the Yoden Fuse Company, Japan are shown in Figures 1.8i~1.8ii.

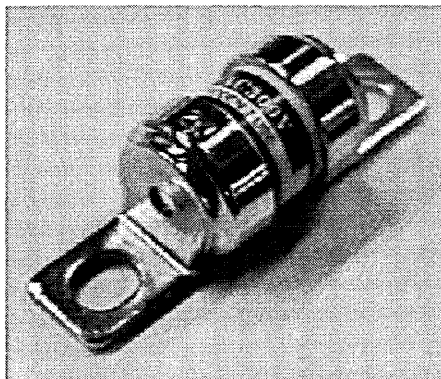


Figure 1.8(i) UR31 20Amp 300 Volt Semiconductor film substrate fuse, marketed by Yoden Fuse Company, Japan

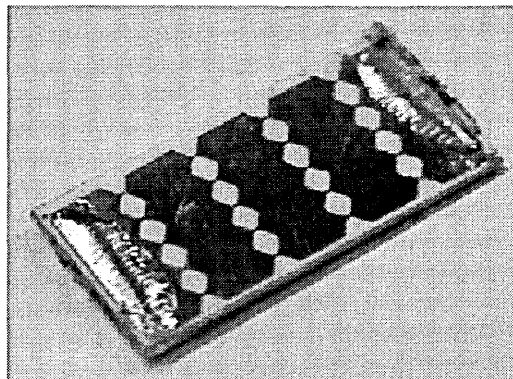


Figure 1.8(ii) Yoden UR31 fuse, film substrate element

The UR31-20A fuse element shown in Figure 1.8(ii) is constructed from a copper film laid on an alumina substrate. Silver is also used for element films and magnesia, silica and berylia have been proposed as possible substrate materials [15]. The UR31 element has a conventional geometry design comprising 4 notches and 5 bridges and has a film thickness 15 microns and a substrate thickness 1mm.

The way film substrate elements may permit infinite variation of element geometries is indicated in Figure 1.9 which displays a film fuse element where element restrictions are formed in the fuse 'Z' plane by multiple layers of films. The film deposition technique is generally by vapour deposition, however electroplating and screen-printing methods have been used in development studies [83]. Film techniques provide excellent dimensional accuracy in the fabrication of element and notch geometries.

Collectively, the film substrate element is a robust assembly, which is advantageous in manufacture. The assembly is soft soldered between inner caps, packed

in sand and sealed in the fuse cartridge. Other construction details correspond to standard methods previously described, yet for the UR31 fuse the filler was bonded with a hydrographic material [28].

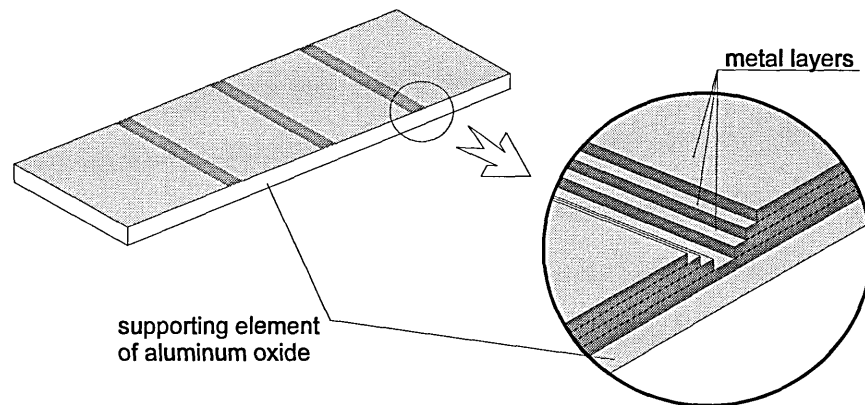


Figure 1.9 Film substrate fuse element with 'Z' plane restrictions

Conductive film substrate fuses are used for high voltage fuse applications and were also developed to comply with the stringent fuse protection requirements of energy sensitive semiconductor devices. In these latter circumstances fast acting fuses with controlled transient arc voltage levels are required. These are generally referred to as 'semiconductor' fuses and contain thin wide strip elements with short narrow restrictions. However, semiconductor element designs can have the adverse effect of increasing fuse body temperatures and consequently standard semiconductor fuses are designed with significant heat dissipation attributes and recommended to have mounting positions with substantial natural or forced convection cooling .

Conductive film substrate fuses have improved element heat dissipation capabilities due to the intimate contact between the conductive film element and the supporting substrate. This allows much higher current densities to be achieved than conventional 'semiconductor' elements with similar geometries at the same rated current.

The pre-arcing time current characteristic for a Yoden UR61, 30amp 660volt film substrate fuse is shown in Figure 1.10. These results claim to indicate reduced circuit let through energy for large over currents compared to other fuse types.

Moreover, the dimensional accuracy of element and notch geometries due to the film deposition techniques is thought to equalize the arc power across the notches and thus prevent concentration of arc energy. This attribute is claimed to further reduce the total energy let through to the circuit during operation of the fuse [29] compared to similar rated fuses.

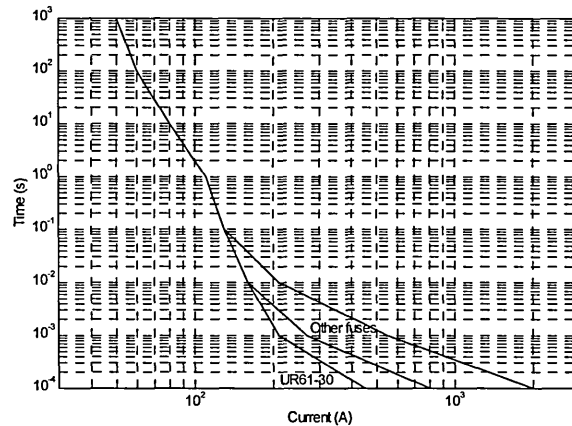


Figure 1.10 Pre-arcing time current characteristic of the Yoden UR61-30A semiconductor film substrate fuse

1.6 Chapter Propositions and Key Findings.

This Chapter has considered fuse requirements and introduced a wide array of fuse types. Properties of fuses and particularly those of conventional HBC fuses and HBC conductive film fuses have also been discussed.

To observe temporal disintegration and arc formation in electrical conductors and quantify and establish the principal mechanisms by experimentation is the objective of this investigation.

The theory of fuse operation is dependent upon the temporal character of the fuse voltage developed during the arcing period which, is a function of element disintegration and arc formation phenomena, particularly during the pre-peak arc voltage period.

Film substrate fuse elements permit infinite variation of element geometries. Consequently, the use of conductive film elements designed to account for inherent disintegration phenomena to improve fuse arcing performance, and provide efficient protection for energy sensitive devices is proposed. Moreover, modelling of fuse

disintegration rather than direct fuse arc modelling is considered to reduce complexity and improve the application of models to a wider range of fuse element geometries.

Therefore, it is proposed to discuss the phenomena of electrical conductor disintegration and the attempts of previous researchers to model fuse disintegration or direct arc modelling of the arcing period of fuse operation in the following Chapter.

Chapter 2

The Phenomena of Electrical Conductor Disintegration and Modelling Techniques of HBC Fuse Disintegration and Arcing Phenomena

2.1 Introduction

This Chapter presents propositions from previous investigations of electrical conductor disintegration phenomena and modelling of arcing in HBC fuse operation. The two principal aspects which are examined are (i) to rationalise previous attempts to classify disintegration phenomena and (ii) conclude the deliberations of each disintegration classification and propose alternative explanations where applicable.

The development of the proposed explanation of electrical conductor disintegration in modelling the arcing period of HBC fuse operation are discussed in the final section of this Chapter. The attributes of two ‘disintegration’ models are presented and the attributes of fuse arc models are briefly discussed and conclude this Chapter.

2.2 Classifications of Fuse Element Disintegration

There are many phenomena associated with the disintegration of electrical conductors. Consequently, the disintegration of electrical conductors and significantly the disintegration of fuse elements need to be categorised relative to criteria of specific phenomena to clarify the arcing behaviour. Several classifications of electrical conductor disintegration have been proposed, as elaborated.

Bennett [17] (Subsection 1.4.1) categorises the phenomena of specific energy and skin effect associated with wire explosions as slow, fast and super fast. Significantly, the phenomena of fuse element disintegration only comply with the criteria of the slow and fast explosion categories based on the magnitude of current density, in the range $10^1 \sim 10^4 \text{ A/mm}^2$, in the fuse element during disintegration. Super fast explosions of electrical conductors in practice are not feasible due to the inherent inductance of practical circuits [30].

Lipski [31], classified low voltage HBC fuse element disintegration from observations of post operation fuse remnants using disintegration pattern criteria associated to the prospective fault current (I_p). The main patterns identified were single break, unduloid, and striated. Two further patterns, chaotic and mixed were also defined

as a blend of two of the main pattern features. The main patterns of unduloid and striated disintegration are shown in Figure 2.1.

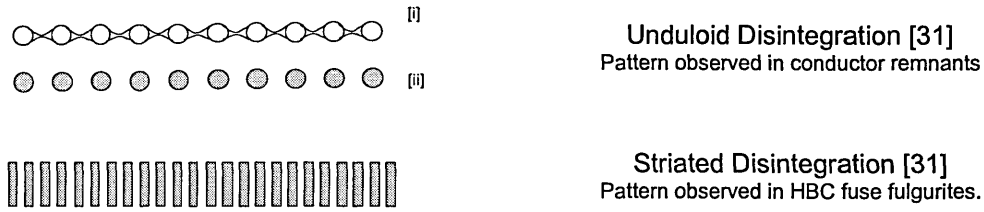


Figure 2.1 Clear patterns of disintegration observed in post operation fuse remnants

Wolny [30], presented rationalisation of both classifications relative to the criteria of fault current level and the mode of arcing (Table 2.1).

Phenomena	Disintegration Classification				
	Slow Disintegration $e_{i/p}(t) > e_{o/p}(t)$	Slow Disintegration $e_{i/p}(t) > e_{o/p}(t)$	Slow Disintegration $e_{i/p}(t) > e_{o/p}(t)$	Fast Disintegration $e_{i/p}(t) \gg e_{o/p}(t)$	Fast Disintegration $e_{i/p}(t) \gg e_{o/p}(t)$
Specific Energy [17]					
Disintegration Pattern $I_n = f(I_p)$ [31]	Single $I_p \leq 6I_n$	Chaotic $4I_n \leq I_p \leq 12I_n$	Unduloid $8I_n \leq I_p \leq 15I_n$	Mixed $12I_n \leq I_p \leq 17I_n$	Striated $I_p > 17I_n$
Fault Current Level Arcing Mode [30]	Low Overload Single Arc Ignition	Low Overload Single Arc Ignition	High Overload / Short Circuit Single Arc / Multiple Arc Ignition	Short Circuit Multiple Arc Ignition	Short Circuit Multiple Arc Ignition

Table 2.1 Classifications of the disintegration of electrical conductors

2.3 Phenomenological Aspects of Single Break Disintegration

A limited number of reports present investigations into single break disintegration of electrical conductors.

Wolny [30], proposed that element disintegration with a single break will occur at low overload fault currents with current densities in the order of 10^1 A/mm^2 and in short fuse elements only. This is a result of element temperature distribution which, is influenced by axial heat flow. The temperature distribution of long elements is influenced less by axial heat flow and consequently several breaks may occur. A mechanism for the clearance of low overload fault currents is proposed which is based

on the gap between the two stubs in the element break increasing to a distance sufficient to withstand the source voltage. During the disintegration of HBC fuse elements it is suggested that the only way this can occur is by element burn back due to arcing. No other transient disintegration phenomena are considered in the report to account for current interruption.

Other investigations discuss low overload fault current conditions and single arc phenomena as a consequence of single break disintegration.

Baxter [33] investigated arcing characteristics of HBC fuses during clearance of low overload fault currents. It is proposed that a single arc may be established which can account for modest current reduction phenomena during which he suggests that increased circuit resistance (R_c) induces stable conditions, which prolong arcing. He further proposes that elongation of the arc occurs to a point where the current is interrupted and in some circumstances this process can consume the whole of the fuse element. Analysis of free air arcs and quartz arcs are presented and arc volt-ampere characteristics are developed. The effects of varying circuit conditions, element geometry and fuse cartridge seal on arcing phenomena are also addressed.

Ofte and Rondeel [34] investigated high voltage HBC fuse arcing phenomena near the minimum breaking current. It is proposed that arcing phenomena for these current levels are fundamentally different from arcing phenomena at short circuit current level, observing the arcing time to be longer, less distinct and suggesting the fuse is not current limiting. A transient mechanism for arc commutation between parallel restrictions and subsequent current interruption is presented. Moreover, a case for fuse failure is presented and suggested to be a function of fuse insulation and source voltage. Consequently the high voltage withstand attributes of silica sand are discussed.

2.3.1 Summary of Propositions and Accepted Phenomena of Single Break Disintegration

The sparsity of research investigations of this classification of disintegration is clearly due to the poor current limiting performance of HBC fuses at the indicated levels of fault current. Arcing conditions are considered to be the most onerous and occur with highly inductive circuits at low overload fault currents [13]. Moreover, arcing conditions are suggested to be stable due to increased circuit resistance, when arcing is persistent [33]. Most research interest has therefore been focused on arcing phenomena and attempts to increase fuse efficiency during these extreme conditions.

The pattern of single break disintegration is accepted to occur in short fuse elements for current densities in the order 10^1 A/mm^2 and gap creation is relatively slow [30]. Influences of element environment and element deformation have been addressed as an aside during unduloid phenomena investigations [5]. The classification, which produces the clear pattern of unduloid disintegration, will subsequently be presented.

2.3.2 Key Findings relating to the Phenomena of Single Break Disintegration

The axial conductor temperature distribution of current carrying conductors is known to be uneven. Consequently, single break disintegration is assumed to occur at the hottest point which is usually at the center of the conductor [5].

In-depth investigation and quantification of the causation phenomena of single breaks in electrical conductors and significantly in HBC fuse elements are incomplete. Phenomena such as thermo-mechanical, gravitational and electromagnetic forces for example have not been addressed to account for single breaks in elements.

2.4 Phenomenological Aspects of Unduloid Disintegration

A significant number of reports have presented investigations of the phenomena of the second main classification - unduloid formation and disintegration.

Unduloid disintegration is characterised by the clear pattern of disintegration shown in Figure 2.2, which can be observed from inspection of post operation conductor remnants.

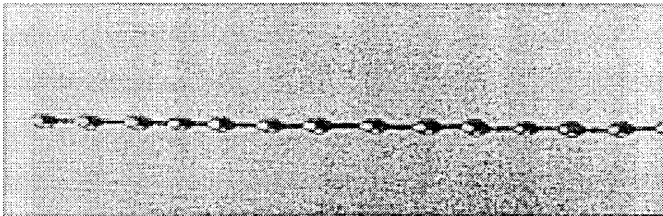


Figure 2.2 Unduloid formations observed in post operation conductor remnants [32]

It is important in this study of disintegration in HBC fuses to indicate that a limited amount of ‘transient’ data has been found which supports the proposal that the phenomena of

unduloid formation is the significant phenomenon in the disintegration of HBC fuses. This is possibly due to the enclosed environment of the HBC fuse element, which makes transient data capture difficult to achieve. Consequently, the majority of unduloid investigations have been carried out on electrical conductors suspended in air and observations captured ‘historically’. Observations and proposals arising from these investigations will be presented, however it is accepted that the temporal disintegration of HBC fuses could be different.

The phenomena of unduloid formations require moderate current densities within the range $10^2 \sim 10^3 \text{ A/mm}^2$. This is classified as high overload/low short circuit fault current conditions [30]. Logically, in these circumstances it is proposed conductor disintegration is followed by multiple arc ignition. The number of unduloids, and breaks produce multiple arcs, hence the current limiting effect is improved in fuse operation for this classification of disintegration.

Observations of ‘red hot balls’ emanating from an electrical conductor on passing ‘electrical fire’ were made by Nairne [35]. It is accepted that Nairne most likely carried out the first investigations of the disintegration of electrical conductors and inadvertently observed the phenomena of unduloid disintegration. Subsequently Nairne has been proposed as the true inventor of the electric fuse [36].

Kleen [37] carried out the first systematic investigations of unduloid formation to account for the ‘striated pattern’ observed on glass plates when condensing vapour clouds emanating from exploding wires suspended in air. From his observations, Kleen proposed a modulus of unduloid formation (Eq. 2.1) based on the theory of wavelength of instability of a liquid cylinder [38]

$$\lambda_{unduloid} = 5.34d \quad \text{Eq. 2.1}$$

Kleen proposed a mechanism for disintegration assuming that the liquid cylinder and unduloid (Figure 2.1i) were unstable and would transpose to a stable sphere (Figure 2.1ii) near the wavelength of instability. Surface tension forces and capillary pressure were proposed for this phenomena in Kleen’s postulations of unduloid formation, however, relatively static conditions were assumed and other forces to be elaborated later were ignored.

Carne [39] proposed that unduloid formation was dependent on the relationship between conductor radial temperature gradient and the radial melting temperature gradient, as a consequence of conductor surface cooling and electromagnetic pinch pressure, respectively. Accordingly, Carne proposed that unduloids are formed when melting develops from the surface of the conductor towards its centre. The formation mechanism is dependent on the rate of heating and current density. Carne applied Rayleigh’s [40] general theory for the breakup of a liquid cylinder under surface tension forces during which, he suggests, the cylinder will break up into globules of regular

modulus (Eq. 2.2) relative to specific element parameters, alternatively, irregular break up would occur.

$$\lambda_{unduloid} = 4.51d \quad \text{Eq. 2.2}$$

Carne also presented unduloid formation criteria (Eq 2.3, 2.4) for sand filled fuses with copper or silver elements dependent on element diameter (d [mm]) and current density (J [A/mm²])

$$dJ_{copper} \geq 400 \quad \text{Eq. 2.3}$$

$$dJ_{silver} \geq 380 \quad \text{Eq. 2.4}$$

In principle, Carne proposed that unduloid formation was a result of surface tension and magnetic pinch forces.

Carne's criteria for the formation of unduloids were found to be inconsistent. Numerous investigations reported the formation of unduloids in electrical conductors at lower current densities [41][42][43]. Moreover, it was found that unduloids could form on wires held in a heat source [44], which questioned formation postulations accountable to electromagnetic forces.

Photographic evidence is referred to which displays the significance of surface tension force and eliminates electromagnetic effects from the formation of unduloids [30]. Vermij [45][46] presented some results which proposes that the theory of unduloid formation and disintegration of wires suspended in air corresponds with most of Kleen's postulations in that the instability wavelength neither depends on current or the element surroundings.

Meyer and Rinderer presented work on unduloid formation based on Rayleigh's theorem [43] and concluded that electromagnetic and element material did influence formation phenomena and, significantly, the unduloid modulus.

Baxter [5] proposed that unduloid formation was a combination of surface tension and electromagnetic pinch effects suggesting three conductor-melting mechanisms to account for formation.

1. The wire melts as a chain of solid and liquid portions along its axis.
2. The wire melts as a system of concentric solid and liquid cylinders.
 - (a) with a solid core and liquid annulus.
 - (b) with a liquid core and solid annulus.

3. The liquid particles are uniformly dispersed throughout the mass of wire.

Baxter eliminated the first case by calculation and measurement but was unable to differentiate cases two and three from observation of oscillographic records. The influence of skin effect phenomena and conductor surface oxidation on surface melting was also reported.

Lipski and Furdal [44] reported the influence of conductor surface conditions on unduloid formation. Consequently, it was proposed that unduloids would form on hard drawn wires but not on soft annealed wires. These observations were later questioned by the same workers due to omission of surface oxidation, which was not thought initially to be significant [41].

Zimny [47] presented a magneto thermo viscous elastic theory to describe longitudinal wave motion caused by the fault current surge. It was proposed that these vibrations are dependent on the conductor's internal structure, which is influenced by its 'thermal career'. Zimny proposed that if the structure rather than the surface of the conductor was conditioned during fabrication, the theory could prove that conditions for unduloid formation were different for hard and soft wires. The axial displacement (U) caused by longitudinal vibrations is given by Equation 2.5. Zimny proposed the value of real component obeys the inequality $Re(\omega) > 0$, such that the vibrations become unstable and wire disintegration occurs.

$$U = A_0 e^{(\omega t + jkz)} \quad \text{Eq. 2.5}$$

Where

A_0 = Amplitude

j = Complex number defining the attenuation and temporal variation

ω = f (conductor material, temperature, k)

k = Wave number = $2\pi/\lambda$

λ = Wave length

r = Radius of the conductor

z = Normalised axial coordinate

Nasilowski [32] presented comprehensive experimental observations of unduloid formations in copper and silver wires suspended in air and embedded in quartz sand for sand granule sizes in the range 0.2~0.4mm. Unduloids were observed to form only on wires with a diameter smaller than 1mm and for moderate current densities ($< 3 \times 10^3 \text{ A/mm}^2$). The internal structures of unduloids were also analysed microscopically. Nasilowski observed post-melting crystallization of the conductor surface with an original grain structured core and concluded that unduloid formation

was a function of the type of surface melting which agreed with Carne's theory. Additionally, the modulus of unduloid formation was observed to be the same regardless of wire materials and filler medium. Consequently, an empirically determined relationship (Eq. 2.6), dependant only on element diameter (d [mm]), was presented for the modulus of unduloid formation.

$$\lambda_{unduloid} = 16/3d \quad \text{Eq. 2.6}$$

2.4.1 Summary of Propositions and Accepted Phenomena of Unduloid Disintegration

In summary, the phenomena of unduloid formation have been observed in many investigations, which propose that the mechanism of disintegration is dependent on the instability of a liquefied cylinder [37][39][45][43] and the evolution of the cylinder into stable spheres. As a result of this mechanism, it is assumed that multiple arc ignitions occur [30][5]

It is proposed that the stability of the liquid cylinder is subject solely to surface tension force [37][45] and a combination of surface tension force and electromagnetic forces in some cases [39][43]. Cylinder instability due to electromagnetic forces is questionable since in separate cases unduloids have been observed to form due to stored thermal energy [46] and externally applied thermal energy [44]. Thermo-elastic wave forces have also been presented to account for unduloid formation in a single case [47].

Unduloid formation is assumed to be slow [30] due to the moderate current densities ($10^2 \sim 10^3 \text{ A/mm}^2$) and the long pre-formation time periods ($>30\text{ms}$ [48]).

Conductor environment is suggested to be insignificant to the modulus of unduloid formation [32] due to adiabatic heating conditions during fault current conduction [30].

Unduloids are formed when the conductor is not fully molten [32][44], the conductor having a liquid surface and solid core. Moreover, the axial temperature distribution is proposed to be relatively flat to account for the consistency of unduloid modulus [30]. Alternatively, it is assumed uneven temperature distribution would induce single break disintegration, which would occur at the hottest point, usually at the centre of the conductor [5].

In general the modulus of unduloid formation λ determined empirically from observations of post operation conductor remnants of initial diameter d is $\approx 5.3d$ [32] and analytically is $\approx 2.25d$ [45][37][38] or $4.51d$ [39][40].

The modulus of unduloid formation has been observed to increase with current density [43]. Moreover, for higher current densities in the order 10^4A/mm^2 the clear pattern of striated disintegration is observed in post operation fuse remnants [32][49].

2.4.2 Key Findings relating to the Phenomena of Unduloid Disintegration

The observations of unduloid formations due to stored thermal energy [46] and formations when an external heat source is applied to the conductor [44] are significant to this investigation. The observations indicate that unduloids can form after current interruption, which could be misinterpreted in transient disintegration analysis.

The reports presenting unduloid formation as a function of conductor metallurgical surface conditions are important. The question is posed, for conductor conditions, which conflict with positive unduloid formation conditions, “what is the principal phenomena of disintegration”?. Consequently, it is suggested that some other fundamental phenomena could be accountable for the element disintegration and the formation of unduloids could be second rank in this process.

No previous data for the temporal development of unduloids has been formed consequently, this is assumed to be slow. No reports have been submitted either that propose thermo-elastic wave motion to be the principal phenomena of conductor disintegration in this classification.

2.5 Phenomenological Aspects of Striated Disintegration

A significant number of reports present investigations of the phenomena of striated disintegration which is characterised by the clear line pattern observed from inspection of post operation sand filled fuse remnants (Figure 2.3), or from images of fast exploding wires suspended in air (Figure 2.4).

As in the case of the study of unduloid formation, only a limited amount of ‘transient’ observations of striated disintegration of HBC fuse elements have been reported. Again, this is possibly due to the enclosed environment of the HBC fuse element. Consequently, the majority of observations of HBC fuse striated disintegration have been obtained ‘historically’ from examination of post arcing fuse remnants referred to as fulgurites.

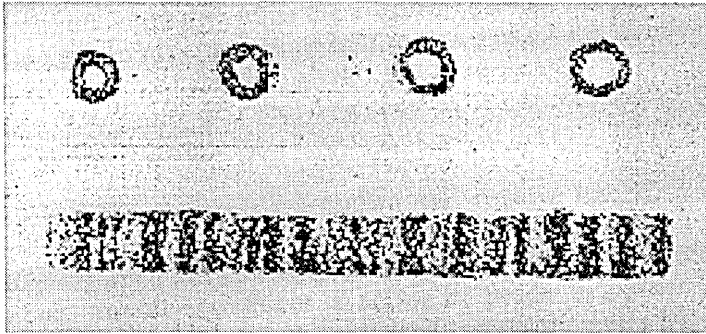


Figure 2.3 Striated disintegration pattern observed in post operation fuse fulgurites [32]

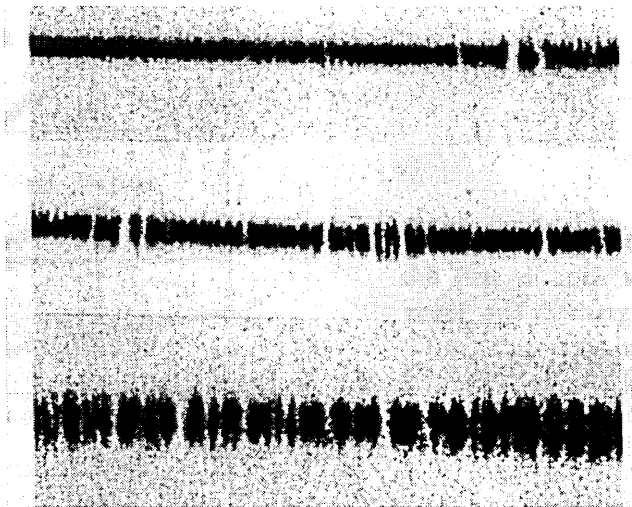


Figure 2.4 Striated disintegration pattern observed in images of fast exploding wires [71]

Numerous transient images of striated disintegration of exploding wires have been presented, yet these circumstances are suggested to be different from those in HBC fuse operation [30]. This is a result of the fast ‘capacitor dominant’ circuits most commonly used to induce this type of disintegration.

Observations and proposals arising from investigations concerned with striated disintegration of HBC fuse elements will be presented.

Striated disintegration of electrical

conductors requires current densities satisfying the inequality constraint $> 10^4 \text{ A/mm}^2$. In these cases fault currents are classified at short circuit level [30]. Significantly, in these circumstances it is proposed conductor disintegration is followed by multiple arc ignition and fulgurite formation which is evidence of striated disintegration. The number of striations and consequently arcs can vary. However, due to their increased number in fuse operation, the current limiting effect is significantly improved for this classification of disintegration.

It is interesting to note that Kleen [37] first observed striated patterns formed on a glass plate from a disintegrating wire and subsequently presented the first postulations of unduloid formations in wires to account for this. Nasilowski [32] is accepted to be the first to observe and suggest different phenomena pertaining to the classifications of unduloid and striated disintegration of wires. Nasilowski found inadvertently that a heated wire on colliding with a solid structure broke up into segments (Figure 2.5) rather than spheroids and reasoned that some vibration phenomena must accompany the

phenomena of wire disintegration. The internal structure of conductor segments was analysed microscopically. Nasilowski observed a post melting dendrite structure in transverse cracks between segments which was different from the internal structure of unduloids. Conclusions were drawn that the cracks were formed during current conduction. Consequently, the hypothesis of mechanical vibration aiding disintegration

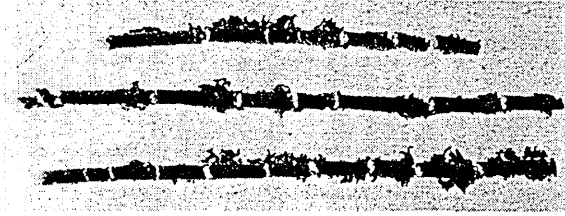


Figure 2.5 Segmented disintegration observed in conductor remnants [32]

was investigated by capturing vibration related data during fault current conduction and disintegration of wire elements, yet for these experiments the elements were embedded in sand. Analysis of the data indicated small amplitude vibrations during the pre-

arcing period and much higher amplitude vibrations during the arcing period. No theoretical analysis of the vibrations was presented. Nasilowski continued to differentiate unduloid and segmented or ‘striated’ disintegration by presenting analysis of historical fulgurite data. Subsequently, the spacing of fulgurite striations were observed to be smaller than the spacing of spheroids observed in conductor remnants consequential of unduloid disintegration. An empirically determined striation modulus was presented (Eq. 2.7) complementary to the unduloid modulus (Eq. 2.6).

$$\lambda_{striated} = 0.555 + 2.08d \quad \text{Eq. 2.7}$$

Furthermore, striated disintegration was observed for higher current densities than unduloid disintegration. Thus to differentiate the two disintegration classifications a current density relationship for silver wires was also presented (Eq. 2.8)

$$J = (1.02/d) - 0.705 \quad \text{Eq. 2.8}$$

Arai [50] presented flash X-Ray images of disintegrating wires suspended in air or alternatively embedded in sand when subjected to large currents. Inspection of sequenced images was proposed to indicate the transient development of striated disintegration, which is suggested to be phenomenologically distinct from unduloid disintegration. Arai considered that wires of large diameters with large current densities disintegrated relative to the striated phenomena and small diameter wires with moderate

current densities deformed into unduloids. This was attributed to electromagnetic pinch forces in the striation case and the combination of electromagnetic pinch and surface tension forces in the case of unduloids. Additionally, it was observed through conductor temperature measurement that striated deformation occurred after complete liquefaction of the wire element, which became corrugated due to the combined action of thermal expansion, surface tension and electromagnetic pinch. The compressive contact between the liquefied conductor and the sand grains was also considered influential on deformation. Subsequently, Arai derived a relationship for the time required to break a striated constriction using the pinch force theory of Maecker [51].

Based on the observations of Arai, Lipski [52] investigated the relationship between the sand particle size and the number of element breaks indicated in striated fulgurites. However, little evidence was presented to support the notion of particle size influencing element deformation and subsequent fragmentation.

Lipski [52][53] developed the arc pinch force interaction theory to justify the striated pattern observed in fulgurites. Lipski assumed full liquefaction of the fuse element and considered the forces of arcing in striated constrictions balanced lateral electromagnetic pinch forces. Following the first break that could occur in any random constriction, a mechanism for the break up of the element was suggested dependent on the interaction of both forces.

Hrynczuk [54] investigated magnetic thermal elastic vibrations in exploding wires suspended in air. Due to language constraints, reports of these investigations have not been fully interpreted. However, the current density range of the theories presented by Hrynczuk, suggest this work is applicable to the striated disintegration of fuses [30]. Hrynczuk proposed that the magnetic forces acting on a cylindrical conductor are initially in a balanced condition. Subsequently the forces are offset by wire buckle due to thermal dilation and additionally by the forces of wire inertia and elasticity. Hrynczuk presented mathematical relationships relative to wave motion of the wire. Consequently, an indication of the instant of element rupture relative to vibration stability of the wire could be determined by comparing electrodynamic forces with mechanical forces.

Jakubiuk [55] presented a theory of electro-thermal disintegration of exploding wires which associates wire disruption with the thermal instability of a conductor due to non homogenous locations of resistance at a high rate of current density increase. The theory is applicable for current densities in the order of 10^4 A/mm^2 and so to striated disintegration of fuse elements. Jakubiuk suggested that for specific wavelengths of

temperature disturbance, hydrodynamic expansion occurs at inhomogeneous resistance locations which is followed by wire rupture.

Hibner [49][24][12][56][18] presented extensive investigations of HBC strip element fuse disintegration in the striated classification. Hibner's interest was modelling of fuse disintegration rather than investigating the causation phenomena of striated disintegration. A technique referred to as the resistance gradient method was used to model fuse disintegration and this work will be addressed later (Subsection 2.7.1). Numerous empirical relationships were presented mostly derived from investigations of strip elements of width $\leq 10\text{mm}$ yet some relationships were presented for HBC fuses with wire elements. Significantly, Hibner presented a relationship for the modulus of striation of silver elements (Eq. 2.9) together with conformity relationships to ensure striated disintegration (Eq. 2.10~2.11).

$$\lambda_{striated} = kS^{\alpha} \quad \text{Eq. 2.9}$$

Where

$$\alpha = 0.21-0.3015(\text{Strip Elements})$$

$$\alpha = 0.3(\text{Wire Elements})$$

$$S = \text{Element CSA}$$

$$Li^2/2Sl \geq 25 \text{ Wsmm}^{-3} \quad \text{Eq. 2.10}$$

Where

$$i = \text{Fusing current}$$

$$l = \text{Element length}$$

$$J \geq 4660S^{-0.29} \quad \text{Eq. 2.11}$$

2.5.1 Summary of Propositions and Accepted Phenomena of Striated Disintegration

The phenomena of striated disintegration have been addressed in numerous investigations of HBC fuse element rupture and wire explosions. Evidence of this class of disintegration is obtained historically from post arcing fulgurites in the case of HBC fuses and from photographic and other imaging techniques in the case of exploding wires suspended in air. The amount of data displaying temporal development of striated disintegration in HBC fuses is limited.

Striated disintegration can occur in HBC fuses with wire or strip elements and is associated with high current densities $> 10^4 \text{A/mm}^2$.

The modulus of striated disintegration is smaller than that of unduloids. Most relationships describing the modulus have been empirically determined and are a function of static element parameters. Images of exploding wires indicate a much

smaller modulus. Consequently it is suggested that the modulus of striation must also be a function of other criteria.

Two principal mechanisms for fuse element striation are suggested. Electromagnetic phenomena or vibration theories are proposed.

Electro-thermal phenomenon is proposed to be only part of the complete mechanism of striated disintegration.

2.5.2 Key Findings relating to the Phenomena of Striated Disintegration.

Proposed theories for the phenomena of striated disintegration are conflicting and are conceived from different temporal observations of disintegration.

The classification of striated disintegration was originally identified and defined from the appearance of post operation conductor segments. Microscopic analysis of these segments indicated a solid conductor core and evidence of conductor melting in transverse cracks [32]. Consequently disintegration due to vibration phenomena have been proposed [32][54][47].

Alternatively, fulgurite evidence of striated disintegration assumes complete liquefaction of the conductor [50][52]. Consequently disintegration due to electromagnetic phenomena are alternatively proposed.

In summary there is no evidential proof to confirm the state of the conductor at the initiation of striated disintegration, consequently the assumption that element deformation precedes element rupture in the mechanism of striated disintegration cannot be strictly substantiated. Therefore, the principal phenomena of this classification are still unaccounted for.

Empirical relationships have been presented for the modulus of striation based on historical fulgurite evidence. However limited accounts of the influence of the fuse element environment on the modulus of striation have been presented even though this has been observed to be significantly smaller in the case of exploding wires suspended in air.

There is a limited amount of transient data to suggest that the number of fulgurite striations increase with time.

2.6 Implications of Electrical Conductor Disintegration in Modelling the Arcing Period of HBC Fuse Operation.

The mathematical relationships presented previously are considered significant to the general discussion of disintegration but in most cases the relationships form parts of models which fully simulate disintegration of a fuse.

The operation of a fuse is collectively the interaction of the transient properties of all its components and therefore to fully simulate fuse operation requires the collective modelling of numerous transient phenomena. Consequently, the task of simulating fuse operation has been approached differently since the chosen phenomena and the methods to simulate and evaluate their transient interaction are arbitrary.

It has been proposed (Subsection 1.4) that the instant of disintegration begins on the fragmentation or break up of the fuse element. Dependent on circuit conditions, arc ignitions will subsequently occur. This phenomenon initiates the arcing period of fuse operation. It is proposed to present the attributes of two types of fuse ‘arcing period’ models. These will subsequently be referred to as ‘disintegration models and arc models’.

Disintegration models simulate the ‘arcing period’ of fuse operation relative to the time zones of disintegration (Figure 1.5, Subsection 1.4.1) and the temporal voltage developed across the fuse.

Arc models simulate fuse operation relative to the temporal voltage developed across an arc (Eq. 1.1 Subsection 1.4.2).

It is anticipated that following the forgoing discussions, the simplicity of the ‘disintegration’ approach to modelling, in comparison to the complexity of ‘arc’ modelling, may become apparent and will add significance to the scope of this investigation.

2.7 Disintegration Models of the Arcing Period of Fuse Operation.

Disintegration models of the arcing period of HBC fuse operation relate to the short circuit fault current conditions. Consequently, the models are applicable for the striated classification of element disintegration. It is proposed to discuss two models.

Hibner [57], presented a model of fuse disintegration relative to fuse resistance in each time zone of HBC fuse operation. Hibner refers to this method as the resistance gradient method.

Gomez and McEwan [58], presented a mechanistic disintegration model relative to the voltage developed across a single arc or ‘arclet’ during multiple arc-striated disintegration of HBC fuses. This model will subsequently be referred to as an arclet voltage disintegration model.

2.7.1 Resistance Gradient Model of the Disintegration of a HBC Fuse

Hibner proposed that a disintegrating HBC fuse can be considered as a variable resistor, its value being a function of the length of a disintegrated fuse element and the gradient of resistance in the time period of operation determined by the switches shown in Figure 2.6. Relationships for the fuse resistance in each time period were determined empirically from measurements of voltage and current.

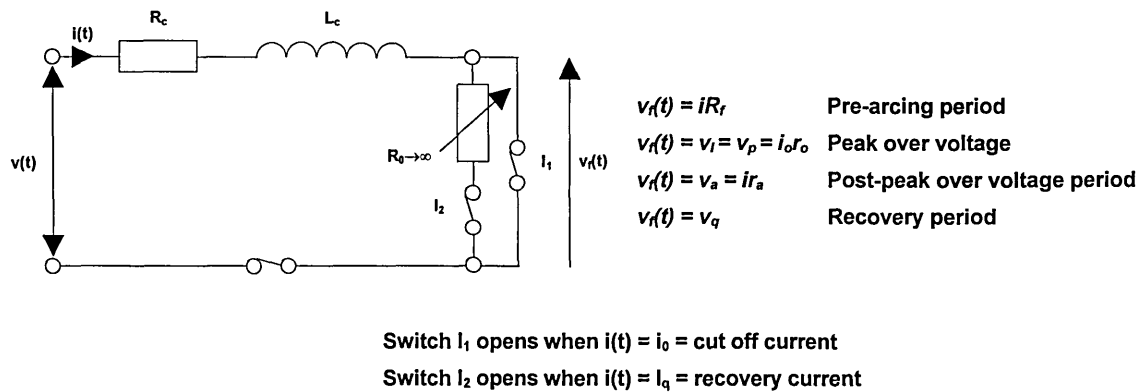


Figure 2.6 Hibner's [57] resistance gradient fuse model

The temporal component of fuse voltage $v_f(t)$ is considered in the four periods of fuse operation.

Pre-arcing Period

It is suggested that for LV fuses rated > 6 A the component $v_f(t)$ is,

$$v_f(t) = i(t)R_f \approx 0 \tag{Eq. 2.12.}$$

Where

$R_f = \text{Element resistance before disintegration}$

Peak Over Voltage Period

The peak over-voltage (V_p) is proposed to occur about the moment of the cut off current [56].

$$V_p = i_o r_o = \rho_o l_d (i_o / S_d)^{0.5} \quad \text{Eq. 2.13}$$

Where,

$$r_o = r_d = \rho_o l_d (S_d i_o)^{-0.5} \quad \text{Eq. 2.14}$$

And,

r_o = Disintegrated element resistance at the instant of peak arc voltage
 r_d = Fuse element resistance during the arcing period

i_o = Cut off current
 l_d = Length of disintegrated element
 S_d = Area of smallest element CSA
 $\rho_o = 0.5 \Omega A^{0.5}$ (Wire Elements)
 $\rho_o = 0.4 \Omega A^{0.5}$ (Strip Elements)

Post-peak Over Voltage Period

Indications of disintegrated fuse resistivity in the post peak over voltage period indicated that the relationship (Eq. 2.14) could be used yet with a lower value. Consequently, the fuse voltage component (v_a) for this period is,

$$v_a = \rho_a l_d (i / S_d)^{-0.5} \quad \text{Eq. 2.15}$$

Where

$$\rho_a = 0.4 \pm 0.1 \Omega A^{0.5}$$

Recovery Voltage Period

The recovery voltage component (v_q) was not considered in the reported analysis.

Application of the Voltage Components during the Time Periods of Disintegration

Equation 2.16, allows determination of the temporal value of current ($i(t)$) for the pre-arcing period assuming $v_f(t) = 0$ (Eq. 2.12). Moreover, given the Joule pre-arcing integral $S_d^2 K$ ($A^2 s$) Equation 2.17 gives the cut off current (i_o)

$$e(t) = R_c i(t) + L_c \frac{di}{dt} \quad \text{Eq. 2.16}$$

$$\int_0^t i^2 dt = S_d^2 K \quad \text{Eq. 2.17}$$

Given the value of cut off current the arcing period temporal current ($i(t)$) can be determined (Eq. 2.18-20) and consequently the arcing period Joule integral

$$e(t) = R_c i(t) + L_c \frac{di}{dt} + v_f(t) \quad \text{Eq. 2.18}$$

Where

$$v_f(t) = V_p \text{ (Eq. 2.13 – Pre peak arc voltage period)} \quad \text{Eq. 2.19}$$

$$v_f(t) = v_a \text{ (Eq.2.15 – Post peak arc voltage period)} \quad \text{Eq. 2.20}$$

Predictions of the Resistance Gradient Model of the Disintegration of a HBC Fuse

Hibner qualifies the resistance gradient model by displaying the accuracy between measured and predicted values of let through energy for the time periods of disintegration for HBC fuses of varying element geometries. The results for a wire element HBC fuse are shown (Table 2.2).

Wire Element - $S_d^2 K = 6800 \text{ (A}^2\text{s)}$			
Joule Integral	Measured	Calculated	Error
Cut Off Current	$i_o = 3150\text{A}$	$i_o=3177$	Good
Pre-arcing Period	6840	6800	Good
Arcing period	3323	2682	-19.2%
Total	10163	9486	-6.7%

Table 2.2 Measured and calculated values of Joule integrals for the disintegration time periods of a wire element HBC fuse [57].

2.7.2 Key Aspects of Resistance Gradient Modelling of the Disintegration of a HBC Fuse

Hibner imposes stringent conditions for the use of the resistance gradient model of disintegration, which aids discussion in relation to the previous deliberations of the phenomena of electrical conductor disintegration.

A short circuit level of fault current is proposed which implies striated rather than unduloid disintegration phenomena. Moreover it is suggested that the model is only applicable where fulgurite evidence indicates the occurrence of striated disintegration and consequently further restricts its use to HBC fuses. Empirically determined conformity relationships (Eq. 2.9~2.10) are suggested for circuit energy and current density which conditions striated disintegration. Restrictions are imposed on pre disintegration element and post disintegration fulgurite geometries

A considerable amount of experimental work was carried out from which the resistance relationships for the time periods of disintegration were derived for selected element geometries. Consequently, the accuracy of the model predictions is good and promotes the fuse resistance modelling technique.

The model is empirically based and withdraws from accounting directly for transient phenomena of disintegration. However, numerous transient phenomena are assumed,

- $v_f(t) = i(t)R_f \approx 0$ (Eq. 2.12) occurs from the assumption of adiabatic heating during the pre-arcing period
- No temporal development of striated disintegration was taken into account. The peak over-voltage (V_p) is proposed to occur at a discontinuity about the moment of the cut-off current. Consequently the time period between initiation of disintegration and the peak over voltage is assumed non existent.
- No temporal development of arcing is accounted for. Consequently, it is assumed that no change in length of disintegrated fuse parts occurs in the assumed multi arc burning time period, referred to as the post peak over voltage time period.

In conclusion it is proposed that the resistance gradient model of HBC fuse striated disintegration can be readily applied to determine the short circuit performance of prototype fuses given the empirical resistance relationships match the transient properties of proposed fuse components. The model appears simplistic of disintegration phenomena, however this must be viewed as an endorsement to the immense amount of work which underlies the models derivation.

A model, which is equally simple to apply, yet accounts directly for temporal development of striated disintegration is the arclet voltage disintegration model [58]. This model will subsequently be discussed.

2.7.3 Arclet Voltage Model of the Disintegration of a HBC Fuse

Gomez and McEwan [58], based the arclet voltage disintegration model on the temporal development of striated disintegration relative to an arc voltage conformity relationship (Eq. 2.21). This proposes that the voltage developed across an arc (V_{arc}) does not exceed twice the arc electrode fall voltage (V_{ak}).

$$V_{arc} \leq 2V_{ak} \qquad \text{Eq. 2.21}$$

Consequently, during multiple arc striated disintegration the temporal development of the fuse voltage (v_f) is a function of the number of arcs (n), subsequently referred to as arclets, and the arc voltage

$$v_f(t) = n(t)v_{arc}(t) \quad \text{Eq. 2.22}$$

The voltage inequality (Eq. 2.21) was determined empirically from examination of commutated disintegration fuses and fuse terminal voltage. Attributes of the data capturing technique, referred to as ‘examination of commutated disintegration fuses’, will be presented in Chapter 3 Subsection 3.4.1.3.

Pre-peak Arc Voltage Period

Gomez and McEwan determined empirically a value for the electrode fall voltage (V_{ak}) of an arclet burning in quartz and the time period (t_k) between sequential arclet ignitions. This allowed a mechanism for the temporal development of the increase in fuse voltage, during the arclet ignition period, to be proposed (Figure 2.7) based on the postulation that successive arclets would ignite to comply with the arclet voltage inequality. The period of arclet ignitions was referred to as the pre-peak arc voltage period (Figure 1.5).

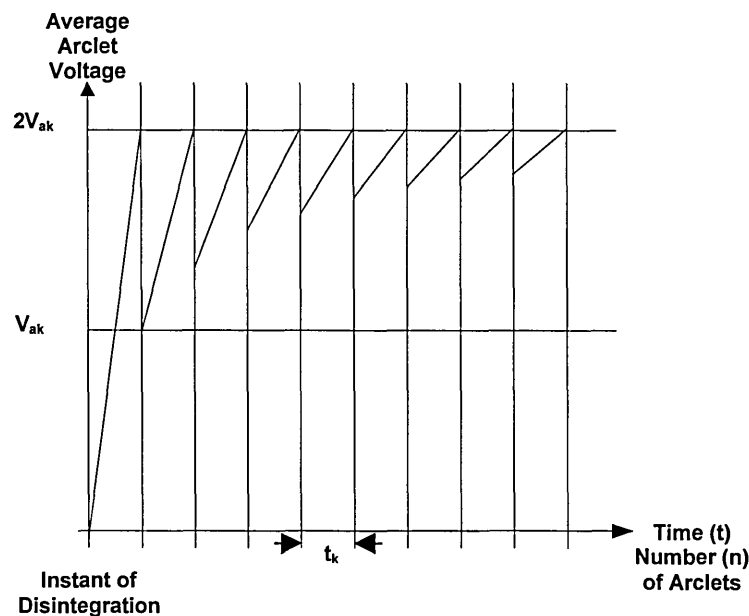


Figure 2.7 Gomez McEwan [58] striated mechanism of fuse voltage increase based on the average arclet voltage during the pre-peak arc voltage period.

It was further suggested that the temporal development of arclet ignitions would continue to a maximum number (n_{max}) (Eq. 2.23), complying with the modulus of striated disintegration observations [32][49] and the length of fuse element (l).

$$n_{max} = l/\lambda_{striated} \quad \text{Eq. 2.23}$$

Subsequently the relationship (Eq. 2.24) for the value of peak fuse over-voltage was proposed for the maximum number of arclets.

$$V_{fuse\ max} = n_{max} 2V_{ak} \quad \text{Eq. 2.24}$$

Post-peak Arc Voltage Period

The use of the arclet inequality relationship was extended by Gomez [10] to the time period after the instant of peak fuse over-voltage. This was referred to as the post peak arc voltage period (Figure 1.5). It was postulated that the merging of adjacent arclets occurred in this period. Consequently, a mechanism for the temporal decrease in fuse voltage during the period was proposed (Figure 2.8).

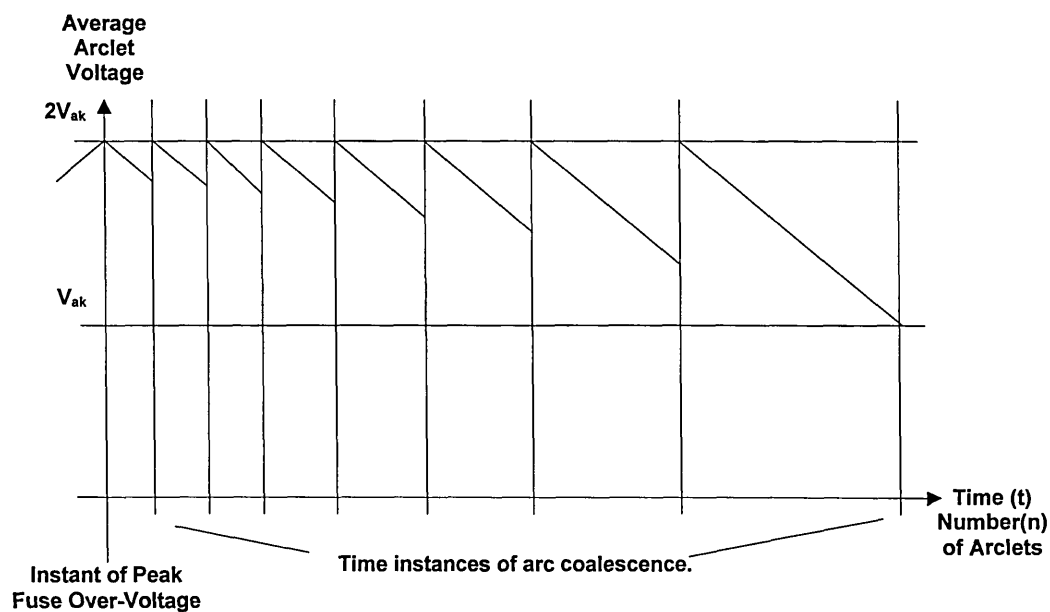


Figure 2.8 Gomez [10] striated mechanism of fuse voltage decrease based on the average arclet voltage during the post-peak arc voltage period.

This was based on the postulation that the loss of an arc electrode fall voltage and the subsequent decrease in average arclet voltage, due to elongation, would occur to comply with the arclet voltage inequality.

Applications of the Arclet Voltage Model

Gomez carried out comprehensive investigations into the relevance of the mechanism to the disintegration of HBC fuses with various notch geometries and fillers of different granulation size and compaction densities. It was found that the mechanism could be applied to predict, with good accuracy, the temporal disintegration of the fuses. It is proposed that the only detriments of the model are its reliance on the pre-knowledge of the electrode fall voltage (V_{ak}) and time period of arclet ignition (t_k). The values of electrode fall voltage are suggested to be fairly standard for specific element material, fillers and compaction densities.

Predictions of the Arclet Voltage Model of the Disintegration of a HBC Fuse

Gomez, qualifies the arclet voltage by displaying the accuracy between measured and predicted values of fuse voltage for the time periods of disintegration of HBC fuses with varying element geometries embedded in different fillers with different compaction densities. The results for an HBC fuse comprising a silver wire element ($0.6\text{mm}\varnothing / 35\text{mm}$) embedded in standard quartz (size $300\mu\text{m}$ density $=1.6\text{ g/ mm}^3$) are shown in Figure 2.9.

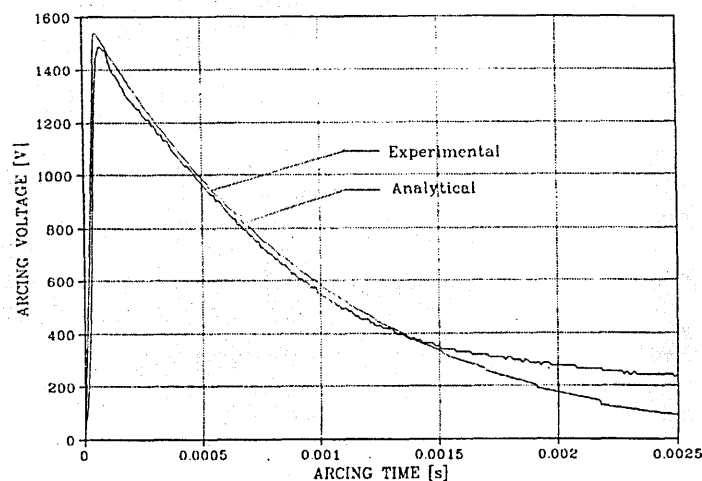


Fig. 2-14 Experimental and Predicted Arc Voltage Traces

Figure 2.9

Arcing period predicted fuse voltage waveforms by Gomez [10] arclet voltage model and experimental HBC wire element fuse voltage waveforms

2.7.4 Key Aspects of the Arclet Voltage Model of the Disintegration of a HBC Fuse.

The investigations of Gomez and McEwan and the arclet voltage model are suggested to be significant advances in the studies of the disintegration of electrical conductors and arcing phenomena in HBC fuses. This is proposed since the work links two previously independent study fields by presenting a justifiable and simple mechanism for the temporal development of HBC fuse voltage.

The mechanism of arclet voltage ignition is based on the sequential fragmentation of the fuse element. This phenomenon had been observed previously for unduloid disintegration of wires suspended in air [45][5]. The evidence presented by Gomez and McEwan to prove the occurrence of this phenomenon in the disintegration of HBC fuses is weak, yet it is suggested here that the accuracy of the predicted course of fuse voltage uphold its integrity.

There is no scientific evidence to uphold the arclet voltage inequality relationship (Eq. 2.21) consequently, it is proposed that this is statistically based on empirical observations.

No accounts are presented for the causation phenomena of disintegration, however, it is suggested that important observations of striated disintegration phenomena have been obtained yet under interpreted. It was postulated that an arclet electrode fall voltage is a function of filler material and compaction density. Hibner [56][57] and Dolegowski [59] also acknowledged this but applied the knowledge indirectly in their empirical relationships. The results of Gomez and McEwan indicate the influence of element surroundings on the modulus of striation and subsequently the number of arclets. Fuse voltage is a function of both phenomena. This creates a paradoxical situation to empirically determine a value for the electrode fall voltage (V_{ak}) and subsequently a relationship for the peak over-voltage. Does the maximum number of arclets increase or does the electrode fall voltage increase or both due to the influence of element surroundings?. The influence of filler granulation size on the modulus of striation has been investigated and dispelled [52]. Consequently the modulus of striation could be a function of filler compaction density only.

The phenomenon of arc merger or arc coalescence was assumed to occur during the post-peak over voltage period. This phenomena is accepted [5][30][26][25] to account for the reduction of fuse voltage observed in the post-peak over voltage period. No observations have been reported to confirm this phenomenon occurs in the

disintegration of HBC fuses. However the accuracy of the predicted course of fuse voltage by the arclet voltage model could lead to justification for the phenomena's occurrence.

In conclusion it is proposed that the arclet voltage model based on HBC fuse striated disintegration can be readily applied as a simple algorithm and will accurately determine the pre-peak arc voltage short circuit performance of prototype fuses given a minimum of predetermined operational data. The method also gives reasonably acceptable predictions of the post-peak arc voltage period arcing performance.

2.8 HBC Fuse Arcing Phenomena.

The arclet voltage model was based on inherent striated disintegration phenomena of HBC fuse elements. Alternatively, and to introduce the final section of this Chapter, HBC fuse arc models are based on arcing phenomena induced in fuse elements at manufactured locations of maximum current density. The concern of this investigation was to study HBC fuse element disintegration that is evidenced only in some cases by fuse arcing. Consequently, in-depth examination of arcing phenomena and determination of arcing parameters was not an investigation objective, however it is proposed to discuss, generally, the attributes of HBC fuse arc models to aid comparisons of arcing period modeling techniques.

2.8.1 HBC Fuse Arc Models

A fuse arc is a self-sustained gaseous discharge having a low voltage potential and capable of supporting high current flow between anode and cathode electrodes [20]. A fuse arc model predicts the course of the voltage (v_{arc}) developed across the electrodes supporting a single arc. Consequently, for HBC fuse elements with numerous restrictions (n) the fuse voltage (v_f) is determined thus,

$$v_f(t) = nv_{arc}(t) \quad \text{Eq. 2.25}$$

Numerous models have been presented which predict the course of arc voltage. These have been classified relative to the analytical or empirical approach to modelling investigations [10]. It is proposed to briefly present the attributes of one model from each of the historical model categories : empirically determined, arc physic and hybrid.

Empirically Determined HBC Fuse Arc Model

A simple arc voltage relationship was developed previously (Subsection 1.4.2) and is reintroduced (Eq. 2.26).

$$v_{arc}(t) = V_{ak} + El(t) \quad \text{Eq. 2.26}$$

Dolegowski [59] presented relationships for the coefficients of Equation 2.26 as function of physical parameters of HBC fuse construction. Extensive investigations were carried out during short circuit fault current fuse operation and various data types were captured. Coefficient relationships including many empirical constants were formed from graphical interpretation of the data.

Collectively the relationships form an 'empirical determined' model of an HBC fuse arc (Eq. 2.27) which is very complex and can only be solved numerically.

$$v_f(t) = n \left\{ \left[V_{ak} = f\left(\frac{i}{j}\right) \right] + \int_0^t \frac{i(t) \left[V_{ak} = f\left(\frac{i}{j}\right) \right]}{A_e (c_v \Delta T + L_f + L_v)} \frac{K_f (J^\beta) e^{\frac{t}{\tau_2}}}{\left(\frac{dl}{dt} + \frac{l}{\tau_1} \right) e^{\frac{t}{\tau_1}} + \frac{\int_0^t i^2 e^{\frac{t}{\tau_2}} dt}{E_{max} i_{max} \tau_2}} \right\} \quad \text{Eq. 2.27}$$

The model gives good predictions of fuse voltage during short circuit fault current conditions for the HBC fuse designs investigated (Figure 2.10).

Phenomena of disintegration are not acknowledged and a single arc is assumed to form in each element restriction. During disintegration of elements with multiple restrictions the fuse voltage is given by Equation 2.25.

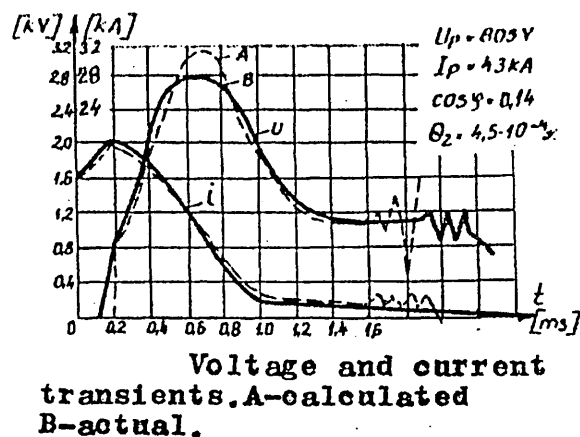


Figure 2.10

Arcing period predicted fuse voltage and current waveforms by Dolgowski's [59] 'empirically determined' fuse arc model and experimental HBC fuse voltage and current waveforms

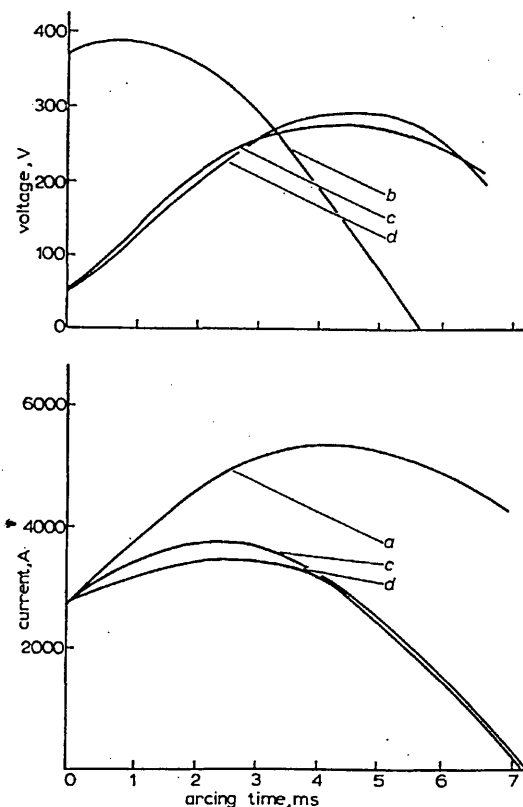
Arc Physic HBC Fuse Arc Model

Wright and Beaumont [21] presented an 'Arc physic' model of a HBC fuse arc relevant for short circuit fault current conditions. This was based on elementary particle analysis of transient electrode processes and positive column conductance (Eq. 2.28).

$$v_{arc}(t) = V_{ak} + i(t)l / (\sigma A) \quad \text{Eq. 2.28}$$

Particle energy exchanges in the location of the electrode ends were considered and a relationship for the rate of electrode burn back or the arc elongation (l) was proposed. Moreover, column conductivity (σ) was determined relative to the atomic and electron densities of the positive column. The cross section of the arc (A) was derived by considering the energy to melt the quartz filler and the volumetric changes of the fulgurite due to fusion.

The relationship presented for the arc voltage (Eq. 2.28) is composed of ten independent equations based on simplifying assumptions and consequently the model is considered complex. However, the accuracy of fuse voltage predictions are satisfactory (Figure 2.11) for the design of HBC fuse investigated, although very difficult to repeat for other fuse designs. Furthermore, the model allows determination of average values of other arc parameters, i.e. arc pressure, arc temperature etc. Disintegration phenomena are



Current and voltage waveforms

- (a) Waveform of prospective current
- (b) Waveform of open circuit voltage
- (c) Computed waveforms
(Values calculated at intervals of 0.8 ms)
- (d) Waveforms obtained by experiment

Figure 2.11

Arcing period predicted fuse voltage and current waveforms by Wright and Beaumont's [21] 'arc physic' HBC fuse arc model and experimental HBC fuse voltage and current waveforms.

unaccounted for and a single arc is assumed to form in each element restriction. Consequently, the fuse voltage is given by Equation 2.25, during disintegration of elements with multiple restrictions.

Hybrid HBC Fuse Arc Model

Daalder and Schreurs [26] presented a model of a HBC fuse arc (Eq. 2.29), relevant to short circuit fault current conditions based on elementary particle analysis of the positive column voltage gradient (E) and the empirical determination of arc size parameters (l, A).

$$v_{arc}(t) = \int_0^l E dx = \int_0^l \frac{\rho I}{A} dx \quad \text{Eq. 2.29}$$

Where

ρ = Specific resistance of the positive column

The relationships derived for the coefficients of Equation 2.29 are mathematically complex and require empirical determination of the constants. Consequently, the model is specific to HBC fuse type. The model predicts arc voltage after arc ignition, hence the absence of electrode phenomena relationships (V_{ak}) in Equation 2.30.

$$\frac{dD^2}{dt} = \frac{q(Z \ln A)^{0.4} I^{1.4} \gamma \left(1 - \frac{\rho_s}{\rho_l}\right)}{b^{1.4} H} \quad \text{Eq. 2.30}$$

$$D = \sqrt{(D_o^i)^2 + Bt} \quad \text{Eq. 2.31}$$

$$B = \frac{q(Z \ln A)^{0.4} I^{1.4} \gamma \left(1 - \frac{\rho_s}{\rho_l}\right)}{b^{1.4} H} \quad \text{Eq. 2.32}$$

Where

D_o^i = Initial thickness of the arc channel

Z = Ion charge

A = Coulomb cut-off

q = Empirical constant

b = Arc column width

H = Energy per unit volume required to raise the temperature of quartz from ambient to fusion

ρ_l = Specific mass of quartz in a liquid state

ρ_s = Specific mass of quartz in a solid state

γ = Flow rate ratio of quartz

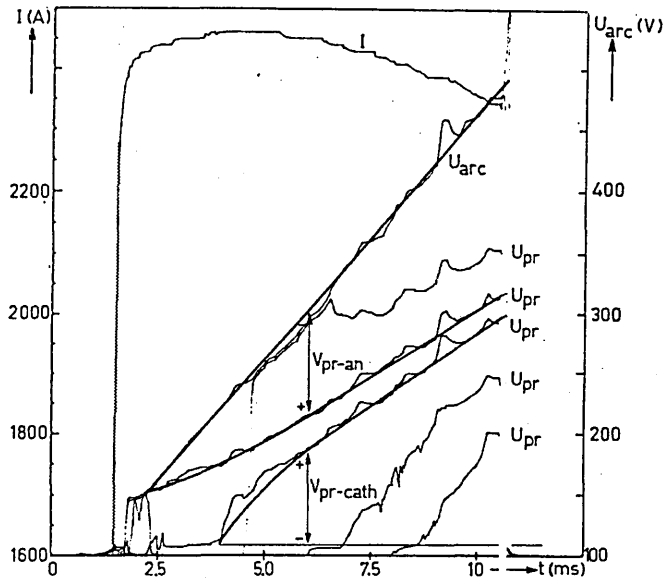


Figure 2.12 Arcing period predicted fuse voltage and current waveforms by Daalder and Schreurs [26] 'hybrid' HBC fuse arc model and experimental HBC fuse voltage and current waveforms.

The 'hybrid' model gave satisfactory results (Figure 2.12) for the HBC fuse types investigated.

Causation phenomena of disintegration are not acknowledged and a single arc is assumed to form in each element restriction. Consequently, the fuse voltage during disintegration of elements with multiple restrictions is given by Equation 2.25.

2.8.2 Notable Attributes of HBC Fuse Arc Models

A significant amount of research has been carried out into electric arc phenomena and specific phenomena of HBC fuse arcs. The models discussed represent a small part of this work but were selected since they simulate completely the temporal development of arc voltage.

The three arc models are mathematically complex but propose to simulate the voltage developed across a single arc during short circuit fault current conditions and the accuracies of predictions were good. The models require determination of empirical constants, which restricts their use to specific fuse types and were derived from investigations that used fuse elements with a single narrow restriction. For circumstances where elements have multiple restrictions Equation 2.25 is used to predict the fuse voltage. In doing this with all the models, two assumptions are made,

- A single arc is formed in each of the element restrictions.
- All arcs ignite together.

At present the single arc circumstances cannot be challenged and the model results uphold this assumption.

However, assuming all arcs ignite together is analogous to homogenous arcing conditions in each of the restrictions. Consequently the situation where numerous 'series' arc models simulate fuse voltage is a practicality. Only Dolegowski's model attempts to simulate these circumstances and the prediction accuracy is good.

Alternatively, given sequential arc ignition, inhomogeneous arcing is suggested. In these circumstances the complexity of modelling fuse voltage is still more vastly increased because different conditions apply for each 'series' arc models.

2.9 Summarising Comparisons of Fuse Arc Models and Disintegration Models of the Arcing Period of HBC Fuse Operation

It has been demonstrated that HBC fuse arc models are extremely complex. To apply the models to simulate multiple arcing in elements with multiple restrictions, the assumption of simultaneous arc formation must be made. This neglects inherent disintegration phenomenon and will incur errors in simulating all but the highest magnitude fault current conditions.

Model accountability of sequential arc formation would incorporate and accept disintegration phenomena but detrimentally increase model complexity. However, the accuracy of simulation would improve if a 'practical' model were possible.

Alternatively, disintegration models, which simulate fuse voltage in specific time periods of disintegration naturally account for disintegration phenomena. The models are simple to apply, given predetermined time period relationships, and prediction accuracy is very good.

2.10 Chapter Summary and Propositions

In summary, disintegration phenomena of electrical conductors and particularly those relevant to the disintegration of HBC fuses have been discussed for three classifications of disintegration. Observed and proposed disintegration phenomena have been identified for each of the classifications and unresolved issues of disintegration have been presented. Implications of disintegration phenomena on fuse voltage modelling techniques have been discussed and the attributes of 'disintegration models' and 'fuse arc models' have been presented for subjective comparisons of the modelling

techniques. In conclusion, this Chapter has presented the knowledge framework for this investigation

In the following Chapter it is proposed to discuss experimental arrangements of previous investigations of electrical conductor disintegration phenomena and then present the experimental techniques used in this investigation to advance understanding of the disintegration in HBC conductive film substrate fuses.

Chapter 3

Experimental Techniques

3.1 Introduction

This Chapter describes experimental techniques used in the investigation of the disintegration of HBC conductive film substrate fuses in three sections.

The first section presents the construction of the experimental HBC fuses and, a basic description of the fuse test facility comprising energy sources, current switching methods and fault application control. The accuracy, with respect to time and repeatability, of the test circuit measurements, together with the disintegration capabilities of the fuse test facility, determined during commissioning trials, concludes the section.

The second section presents the significant experimental techniques devised specifically to capture data relating to the disintegration of HBC fuse elements by previous researchers. The attributes of the techniques are addressed, and the significant ones are identified. Consequently, the approach taken to capture data of the disintegration of HBC conductive film substrate fuses in this investigation, is presented.

Section three presents the experimental techniques used in this investigation.

3.2 Experimental HBC Fuse Construction

The experimental investigation, conducted into the disintegration phenomena of HBC conductive film substrate fuse elements was carried out at a fundamental level using fuses of very basic design and construction to allow for changes in construction of the fuse and subtle alteration of fuse classification. A principal aim was that the fuse construction parameters, used during experimentation, should be very similar to those of commercially available HBC fuses. The disintegrations of the various experimental fuses were to be identical to commercially available fuses for the same fault conditions as elaborated herewith.

3.2.1 Fuse Elements

Experimental HBC substrate fuse elements were fabricated from copper or silver. Copper (purity > 99%), and silver (purity >99%) wire and strip elements of various diameter, thickness and length were used. Strip elements had rectangular notches chemically etched at specific longitudinal intervals. Three types of notch geometries were also used. These are shown in Figures 3.1(i~iii).

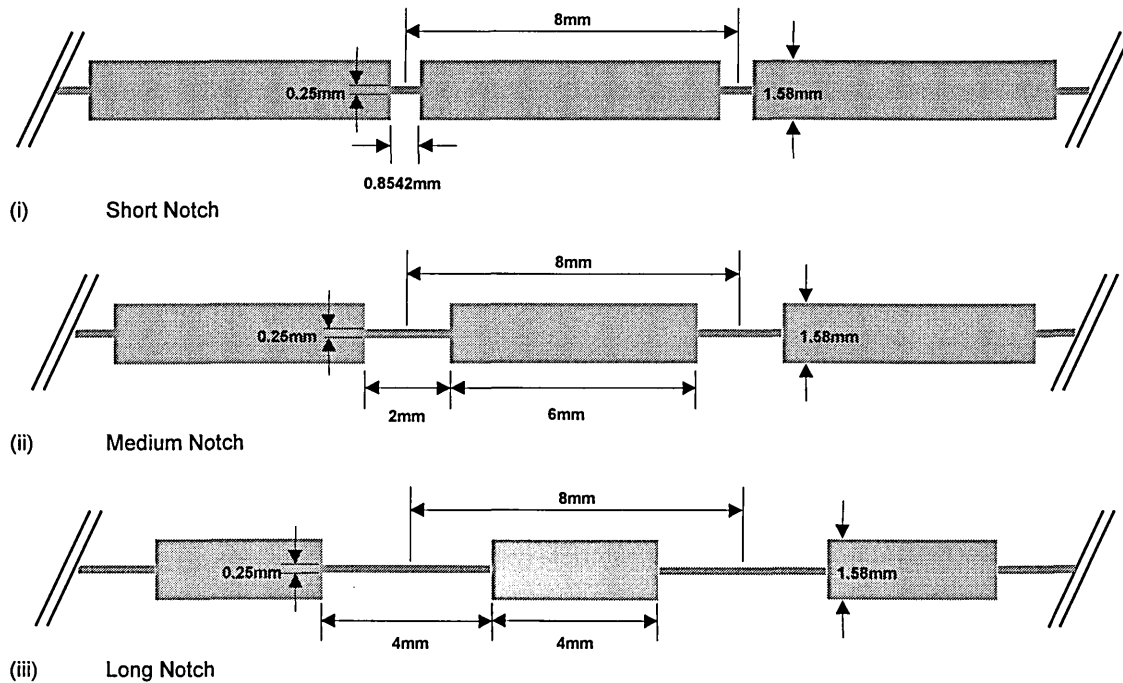


Figure 3.1 HBC conductive film substrate fuse element notch geometries

3.2.2 Arc Quenching Mediums

Several different fuse fillers were used as arc quenching mediums. These were quartz sand, water, air, and epoxy resin.

Two types of quartz fillers were used of different granulation size. These were referred to as fine quartz, (granulation size ≈ 300 microns) and standard quartz, (granulation size ≈ 500 microns). The quartz chemical components and ratios were,

Chemical Component	SiO ₂ %	Na ₂ O %	Al ₂ O ₃ %	K ₂ O %	Fe ₂ O ₃ %	ZrO ₂ %
Fine Quartz	99.75	0.02	0.08	0.04	0.08	0.02
Standard	99.85	0.02	0.06	0.05	0.04	0.02

Table 3.1 Primary chemical components and ratios of quartz fillers

The quartz was compacted by mechanical vibration methods for all fuse samples tested, to a commercial standard. In all cases the vibration time period was at least 5 minutes.

Water used for arc quenching was obtained from the domestic supply. The water temperature was allowed to normalise to ambient, $\approx 23^{\circ}\text{C}$ before use and re-freshed water was used in the construction of each fuse.

The epoxy resin used was distributed by RS© (199-1468). The adhesive and hardening constituents of the resin were mixed in unity ratio. After mixing, the resin was poured around the active fuse element and allowed to cure for a minimum time period of 24 hours before use.

Dielectric Strength	14kVmm ⁻¹
Volume Resistivity	1×10 ¹⁴ Ωcm
Thermal Conductivity	0.377 Wm-K ⁻¹

Table 3.2 Relevant technical specifications for epoxy resin (RS© 199-1468)

3.2.3 Cartridges and End Caps

The fuse cartridges were fabricated from 6mm thick Lexion™ sheet. Two cartridges were constructed but only the cartridge ‘A’ specification is presented here. The cartridge B’ specification is presented later (Subsection 3.5.1.2), to aid clarity.

Figure 3.2 shows a photograph of cartridge ‘A’, of internal dimensions 153 mm (*l*) × 53 mm (*w*) × 69 mm (*d*). The cartridge has a removable lid to allow packing with filler, which is secured with screws to seal the cartridge. The fuse elements are soldered using 60:40 solder, between two copper terminal posts located centrally inside the cartridge. The terminal posts were 4mm in diameter and each post was bolted to one end of a 10mm diameter brass rod, which terminated to the external circuit cables.

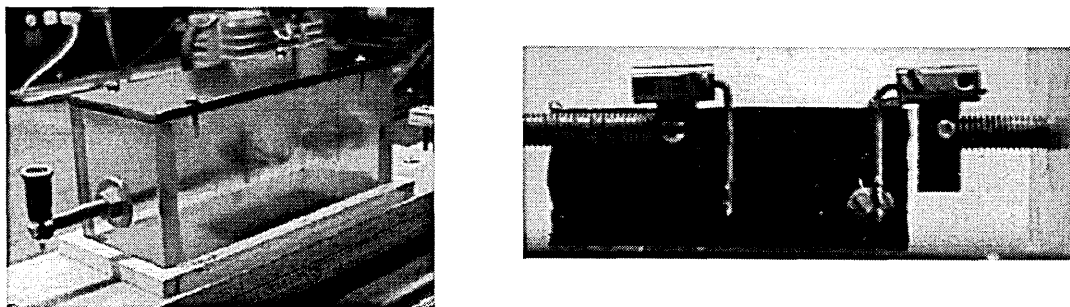


Figure 3.2. Experimental fuse cartridge ‘A’ (shown without filler) and fuse terminal post arrangement

3.3 Experimental Low Voltage Fuse Test Facility.

Figure 3.3 is a photograph of the test facility, which was specifically designed, constructed and commissioned to investigate disintegration of HBC conductive film substrate fuses. A induction motor driven dc generator/alternator set exists under the test bench.

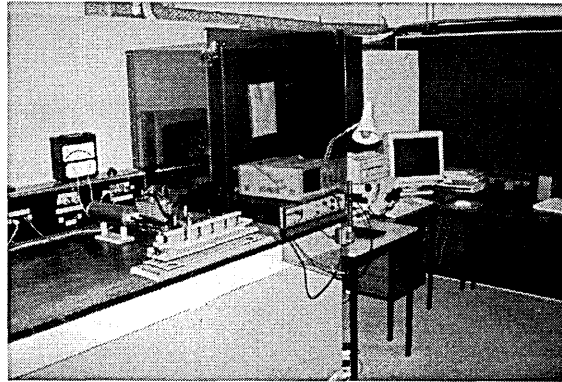


Figure 3.3 Experimental fuse test facility

A schematic diagram of the fuse test circuit is shown in Figure 3.4.

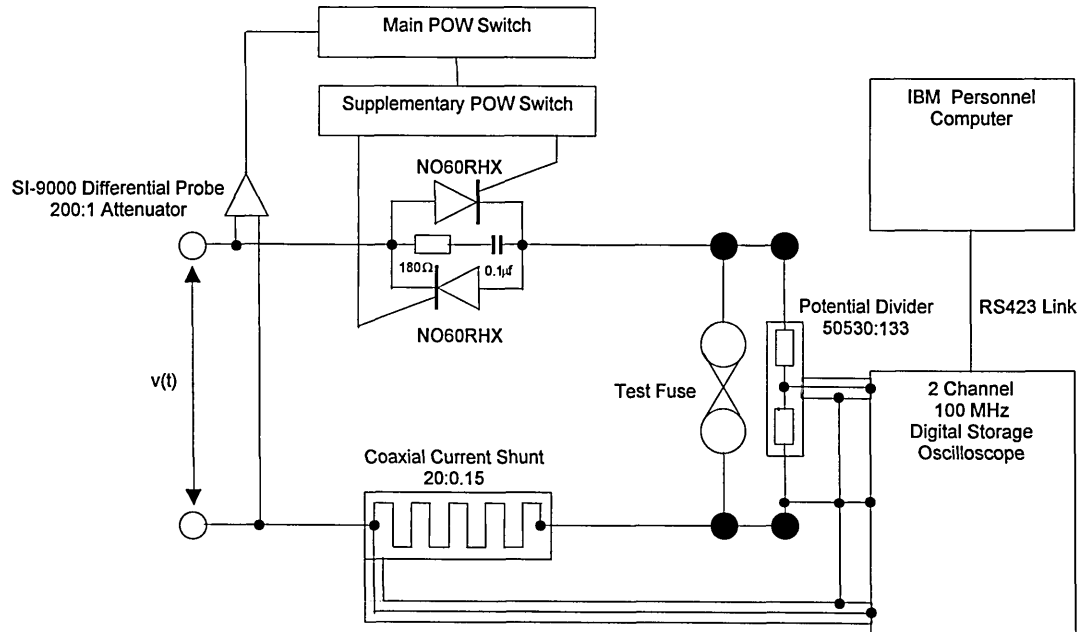


Figure 3.4 Experimental low voltage fuse test facility circuit schematic (excluding generator sets)

3.3.1 Energy Sources.

The experimental energy sources were derived from independent ac and dc generators. A three phase induction motor supplied from the university LV supply drove the generators. The supply frequency of the induction motor was 50 Hz. and the generator field windings were separately excited from a separate variable 200 volt dc supply. The generator supply voltage of the test circuit was pre-settable by rheostat adjustment of the field winding current.

The generated test circuit ac voltage was obtained from the single phase and neutral of the stator winding of the three phase star-connected generator. The generator was capable of supplying a maximum symmetrical voltage of 240 volts RMS. For the circuit shown in Figure 3.4, thyristor switching occurred at voltage zero, produced a peak asymmetrical current of 320 amps and the measured power factor ($\cos. \phi$) of the circuit was 0.1147.

The dc generator was rated at 200 volts. Thyristor switching this generator produced a current flow of 295 amps in the test circuit (Figure 3.4) of time constant 0.002968s.

Details on the energy sources and induction motor are given in Appendix 1.

3.3.2 Current Switching and Fault Application Control.

Current flow through the test fuse was accomplished by controlled switching of two inverse parallel connected thyristors. Matching thyristors of type NO60 RHX ($I_{T(RMS)} = 100A$) were used. This arrangement allowed multiple a.c. cycle fuse current conduction and hence, a means for investigation of long disintegration time periods. Thyristor switching was accomplished by applying thyristor gate pulses at specific time instances derived from a thyristor point-on-wave (POW) switch control unit.

When using the ac generator, switching of the thyristors was initiated relative to the test circuit supply voltage wave form. To achieve this the generator supply was monitored via a differential probe of ratio 200:1 and a reference point on the voltage wave form established using a zero crossing detector. Timing and pulse forming electronic circuitry were used to produce suitable thyristor firing pulses to initiate fuse current flow. These circuits were adjustable to enable fuse disintegration to occur at specific time delays relative to the rising supply voltage waveform zero crossing.

For the dc generator circuit supply, fuse current flow was initiated by switching the positive connected thyristor using a manually initiated pulse shaping circuit.

Details of the thyristors, differential probe and the point-on-wave switch control unit are presented in Appendices 2,3 and 4.

3.3.3 Accuracy of Current Switching

The fuse test facility was commissioned prior to investigations of fuse element disintegration to ensure the following,

- Good accuracy of current switching.
- The disintegration mode capabilities of the system.
- Good accuracy of fuse current and fuse voltage measurements.

Accuracy of current switching was good with the angular displacement between the required instant, and the actual instant of current flow initiation in the test circuit being within the limits of $\pm 2^\circ$. The repeatability of current switching within this limit was significantly high (> 95%).

3.3.4 Disintegration Capabilities of Fuse Test Facility .

Extensive commissioning trials were found to be necessary to determine the disintegration mode capability of the test facility.

The waveforms of fuse voltage captured during so called striated disintegration of wire fuse elements in filler were classical in shape [6] and the magnitude of the peak arc voltage measured across the terminals of the fuse, indicated that multiple arc ignitions could have occurred during disintegration [18][10]. The average peak voltage magnitude measured was 1125 volts and average time period of the voltage rise was 128 μ s

Physical examination of striated disintegration fuse filler remnants did not indicate that multiple arc ignitions in the form of dark and light shaded bands in the filler remnants (or fulgurites) [32] had occurred. This absence was put down to the size of the wires tested. However, reliability in the disintegration capabilities of the test facility was gained, by comparing experimental data with data obtained from an ASTA certified fuse test laboratory. In this case the fuse operation data was captured during short circuit tests (I2 BS-88) carried out on similarly constructed sample fuses. Post

operation X-Rays of these fuses exhibited dark and light banding and the character of the fuse voltage waveforms were similar to experimental facility waveforms. From these observations it was accepted that in the case of the experimental test facility, multiple fragmentation of the fuse element and multiple arcing phenomena did occur.

The commissioning trials imposed the following limits on element cross sectional area of wire to produce multiple arcing (Table 3.3). These limits were determined for ac conditions when fuse current flow was initiated at a supply voltage zero and disintegration initiation occurred near the instant of peak supply voltage consistent with the I2, most onerous arcing, short circuit test condition (BS 88, Part 1, 1988, IEC 269-1, 1986).

Material	Wire Diameter (mm)	Wire CSA (mm ²)	Wire Length (mm)	Cut Off Current (A)	Current Density (A/mm ²)
Silver	0.1143	0.0103	30	70	6796
Copper	0.0882	0.0061	30	73	11967

Table 3.3 Maximum wire diameters - disintegration initiated at voltage zero and occurs at the instant of peak supply voltage

3.3.5 Summary of Fuse Test Facility Capacity.

The facility and ASTA laboratory test results validated that striated element disintegration and multiple arc ignitions could be analysed using the facility from comparative observations of the steep voltage rise developed across the fuse terminals during disintegration and examination of the ASTA laboratory, after test fuse X-Rays. The peak value of the voltage was 1125 volts and the rate of rise was of the order 8.78 v/ μ s. The cross sectional areas of wire elements were too small to indicate classical fulgurite striated type disintegration patterns in the filler.

These results are consistent with the findings of Nasilowski, Hibner and Gomez [32][49][10] which indicated that the minimum diameter (d) and current density (J) that would produce striated fulgurites from disintegrating silver wire elements were $d=0.01\text{mm}$, $J>10\text{KA}/\text{mm}^2$ and for copper wires $d=0.2\text{mm}$, $J>13\text{KA}/\text{mm}^2$. The maximum wire element diameters and current densities obtainable from the facility during commissioning trials were smaller than these sizes.

The magnitude of the peak voltage measured across the fuse terminals during trials however did indicate the existence of multiple arc ignitions. Moreover, the rate of voltage rise and the time period from first arc ignition to the peak voltage instant supported this notion [10]. This was a difficulty, which influenced the approach to experimental investigations because the experimental strategy was to obtain data relating to element disintegration. The inability to determine the presence of arc ignitions from physical inspection of post fuse operation fulgurites, because of the limitations of the size of wire that could be tested using the facility, was a great disadvantage. Hence, it was necessary to develop new experimental techniques to overcome this difficulty and the integrity of the techniques had to be obtained from systematic commissioning trials. The analysis of the disintegration mechanism was therefore based on observed time event correlation. This is an important attribute of this investigation and will be addressed, comprehensively, in subsequent sections.

3.4 Element Disintegration and Arc Parameter Data Capture.

A sound understanding of how a system in a dynamic state develops in time can be obtained from visual observations. However, when an opaque medium encloses the system, these circumstances are impracticable. The HBC fuse, in being surrounded by filler, is such a case.

Many techniques to capture data relating to disintegration and fuse arcing in HBC fuses have been used by researchers [11][60][61][50] the most significant of which are briefly discussed under the headings, historical methods and transient methods.

3.4.1 Historical Methods of Fuse Data Capture.

Historical methods of fuse data capture are techniques where data relating to a transient event is obtained after the event has occurred. The transient development of the event is then judged from the historical data.

The several classifications of this methodology, can be grouped into two categories.

1. Physical examination of fuses, where the fuse has interrupted the circuit current. This methodology is referred to as, “examination of fully disintegrated fuses”.
2. Physical examination of fuses, where disintegration of the fuse has been terminated by commutation of the fuse current by a parallel device. This methodology is referred to as, “examination of commutated disintegration fuses”.

The usual methods of physical examination are by direct fulgurite inspection or by inspection of X-Rays of the fuse.

3.4.1.1 Examination of Fully Disintegrated Fuses

Examination of fully disintegrated fuses is a frequently used method. Data is readily available from inspection of fulgurites or wire remnants. Consequently the method has been used from the earliest current carrying conductor investigations [35][36] to the present day.

Nairne observed that after current interruption the conductor had disintegrated into hot balls. Many subsequent observations of wire remnants, by other researchers, noted the formation of unduloids and other forms of wire disintegration's [37][5][32]. Using post-operation observations, researchers proposed the transition from unduloid to spheroid was the primary disintegration mechanism [37]. Other observations noted fulgurites with dark and light rectangular shaped bands or alternatively rectangular shaped-segmented wire remnants [32]. Subsequently it was proposed that the striated mode of disintegration producing these post operation observations was different to unduloid type disintegration [32][52].

Post-operation observation of unduloid formations and striated fulgurites have produced formation modulus data based on separation distance between unduloids and the striated bands. Consequently, transient development of disintegration is accounted for from proposed element fragmentation producing these post operation observations. The number of fragments and, hence, arcs being the quotient of the element length and formation modulus.

3.4.1.2 Key Findings and Propositions - Examination of Fully Disintegrated Fuses.

Reliability of historical information obtained from fulgurites has been judged to be satisfactory in accounting for transient disintegration theories [10]. This perspective was adopted from circumstances where the mode of striated disintegration was believed to have occurred. Simulations of disintegration have subsequently been presented. The accuracy of the simulations is good, and hence confirm the integrity of the postulated disintegration theory and the method of data capture.

The reliability of historical data to predict the transient development of disintegration for the mode of unduloid disintegration has not been determined for fuse elements embedded in sand. Generally accepted unduloid disintegration postulations, based on historical data for elements suspended in air have been questioned [48].

The proposition that striated and unduloid modes of disintegration are different, is natural given the post-operation evidence. However, the proposition is based on two different temporal data sources as unduloid evidence is generally based on pre-arc ignition disintegration and striated evidence is based on post arc extinction disintegration. No reports presenting fulgurite evidence of arcing based on unduloid disintegration are known.

The method of data capture from inspection of post-operation striated fulgurites is satisfactory only if the disintegration event is capable of leaving visible evidence. It was not possible to use this method, when using the test facility for investigation of disintegration of fuse elements, because of the limitations of the wire diameters determined during commissioning trials. However, the deficiency posed some very basic questions on evidence and distinction between the commonly referred to “different modes of disintegration”.

3.4.1.3 Examination of Commutated Disintegration Fuses.

Commutated disintegration fuse examination is also a frequently used method. In this case data is obtained from direct inspection of fulgurites or inspection of X-Ray images of fuses, where fuse operation has been terminated by commutation of the fuse current. Disintegration commutation is accomplished by presenting a lower resistance

path to the fuse current at specific time instances during the disintegration period. Several forms of data can be obtained from inspection methods.

- A measure of non-eroded element material. This, reciprocally, can indicate the arc length at the instant of current commutation [25]. Subsequently, collective analysis of data obtained with different commutation times has been proposed to indicate the rate of element erosion [62] or, alternatively, arc elongation [11].
- A measure of cross sectional area of the cavity or lumen, within the fulgurite after arc extinction. Subsequent collective analysis of data could give an indication of the rate of arc expansion [25].
- The presence of fulgurite growth. This could indicate arc presence.[10][32][49].
- A measure of fulgurite growth. This could indicate expended arc energy in fusion of the filler, up to the commutation instant.

3.4.1.4 Key Findings and Propositions - Examination of Commutated Disintegration Fuses.

Reliability in the accuracy of data obtained from commutated fuse operation can be judged to be dependent on the measured parameters of the fulgurite lumen or wire remnants. The measurement parameters for the forms of data previously presented are different being; distance, mass or integer, respectively.

Considering the circumstances before the instant of fault current commutation, the element and filler will be in differing states of matter dependent on the time instant and condition of disintegration. Since a finite time period exists between the disintegration instant and that of a measurable instant, the physical state and displacement of the fuse remnants can alter. This is influenced by the orientation of the fuse, the state of matter and fuse materials and consequently this has a bearing in the accuracy of captured data.

The concern of this investigation was to study fuse element disintegration, which is evidenced only in some cases by fuse arcing. The investigation experimental requirement was to base measurements on time correlated data of disintegration.

Consequently, this reduced the need to capture accurate measurement data from historical commutated disintegration methods.

A fulgurite is physical evidence of the pre existence of an arc. Consequently, the capability to distinguish and count individual fulgurites is a reliable indicator of the number of burning arcs at some time instant [10]. Additionally, if an arc is supported between metallic electrodes then post commutation observation of non-eroded element material, bridged by fulgurite, also reliably supports the assumption of arc presence at some time instant [62]. Consequently, these two forms of the commutated disintegration data capturing technique were used in the investigation of element disintegration.

3.4.2 Transient Methods of Data Capture.

Transient methods of data capture are techniques where data is captured over the transient period of an event. Analysis of the data can then be time-correlated to the development of the event. Again many forms of this method exist which can be categorised under different headings of measurable fuse parameters. Consequently, discussion of data sensors, transmission of raw data, and data transducers will be presented in relevant sections as appropriate.

3.4.2.1 Fuse Voltage and Arc Voltage.

Recapitulating, the fuse voltage is the voltage potential measured between the two terminals supporting the fuse element. Alternatively, the parameter of arc voltage is the potential measured across the electrodes supporting individual arcs. For multiple arc element disintegration the fuse voltage at some time instant is the sum of the voltage potentials of individual arcs and interconnecting electrodes between the two fuse terminals.

Attributes of disintegration and arc models have been presented previously (Subsection 2.7~2.8). The primary motives of both model types were to simulate transient voltage development across the fuse terminals during element disintegration. Disintegration models accomplished this by time subdivision of the disintegration process and adoption of new conditions for each time period. Alternatively, arc models attempt to simulate the temporal development of individual arcs. Consequently, the voltage across the fuse terminals is the summation of numerous arc models.

The measurement of fuse terminal voltage during short circuit disruption would appear more related to investigation of element disintegration and, hence, fuse voltage waveforms captured during element disintegration have been analysed to account for temporal disintegration theories.

Early measurements of fuse voltage were captured by Baxter [5] using an analogue oscilloscope with slow time scans (10^{-2} secs). Silver wires were used as fuse elements, but filler medium was not stated. Photographs are presented of the oscillographic records, and the fuse voltage waveforms display a small number of successive dots during the period of element disintegration which is suggested by Baxter to indicate the sequential ignition of series arcs.

Subsequent oscillographs of fuse voltage were captured by Vermij [45], who used oscilloscopes with much faster scan rates (100 μ s). These results were obtained from fuses constructed with silver wires suspended in air. The waveforms appear uneven, similar to an increasing gradient of steps. The steps or discontinuities are interpreted as evidence of arc electrode fall establishment. Vermij, correlated the fuse voltage records with streak photographic evidence of wire disintegration, from which he proposes a theory of sequential fragmentation of wires suspended in air.

Direct measurement of arc voltage is more relevant for investigation of temporal development of the fuse arc. Data for this type of investigation has been captured using voltage probes penetrating the fuse cartridge [60][26]. In these cases the probes were equally spaced in line and orthogonal to the element axis and positioned close to the element to allow penetration of the advancing arc. The probe potentials were monitored using an oscilloscope. However, results using this method are suggested to be subject to inaccuracies [25] due to the erosion of probe tips and the heat transfer between the arc and probes.

3.4.2.2 Arc Light

Recapitulating, an electric arc sustained at atmospheric pressures and above has an intensely brilliant core [20]. This attribute has been used to study various parameters of the fuse arc. This parameter assists understanding of the temporal behaviour of the fuse arc. Alternatively, given that arcing occurs during disintegration of the fuse

element, detection of arc light could indicate the transient development of disintegration.

Spectroscopic observations of fuse arcs have been undertaken by Chikata *et al* [63], to determine the temporal intensity of selected arc spectra, electron density and arc temperature. Single notch, silver fuse elements surrounded by quartz and embedded in Pyrex™ tubes were used in these studies. Spectra data was obtained by a spectrograph aimed at the element notch. The results of the studies suggested that the fuse arc is mainly composed of SiO_2 vapour, which is consistent with the results of other workers [64][65].

Observations of the fuse arc were also obtained by Barrow *et al* [61][66] by first penetrating the fuse cartridge with optical fibres to investigate parameters of fuse element burn back and arc temperature. In this case single notch, silver elements packed in quartz were used as experimental fuses. Several optical fibres were used for burn-back investigations. The fibres were equally spaced, in line and orthogonal to the element axis, with the fibre tips positioned close to the element. Light from the arc was transmitted by the fibres to associated opto-couplers. The outputs of the opto-couplers were polled and data captured by oscilloscope and analysis of the results enabled a mathematical model of element burn back to be derived. For arc temperature investigations, a single fibre was used. This was aimed at the centre of the notch restriction. The light emanating from the fibre was monitored using a rapid scanning spectrometer and analysis of spectroscopic data enabled determination of arc temperature.

The method of monitoring the fuse arc using an optical fibre was extended by Cheim *et al* [67] where light emanating from the fibre was monitored by an opto-electronic system. The reported system was capable of monitoring two pre-selected arc radiation spectra. Using quantum mechanics and the ratio of the spectra intensities, enabled an estimation of the temperature of the arc to be determined.

Optical fibres were again used by Gomez [10] to monitor light radiating from the arc. In these studies captured data was used to account for the temporal disintegration of fuse elements. Five fibres were used. These were equally spaced along a wire fuse element embedded in quartz. Oscillographic results of fibre outputs, together with commutated disintegration X-Rays of fuses, were interpreted as evidence of sequential

disintegration of the element. A mechanism of disintegration was proposed, based upon the time periods between arc ignitions, indicated by fibre outputs and an empirically determined arc voltage limit.

Photographic techniques have been used to capture light radiation from disintegrating wires. A large proportion of visual evidence is presented of exploding wires, suspended in air [68][69]. For these investigations, disintegration generally occurs in the time period of 1~10 μ s [70][71], and is generally induced by discharging of capacitors. Inspecting the images, the absence of bright light sources indicating arc establishment is notable. Consequently, the range of light intensity captured in images is narrow and the resolution is good.

The opaque cartridge of the HBC fuse presents an obstruction to photograph disintegration of elements contained therein. This could account for the small amount of photographic evidence submitted. However, photographs of element disintegration, occurring over longer time periods, have been presented for elements suspended in air.

A single image proposed to display unduloid disintegration of a wire suspended in air has been presented by Baxter [5]. The resolution is poor, which is ascribed to the light intensity of established arcs.

Images of disintegrating wires suspended in air are presented by Vermij [45]. which were captured continuously using streak photography methods. Vermij proposes that the images display captured light emitted from arcs and from one image, in association with time-correlated fuse voltage records, suggests that the transient disintegration of the wire over a time period of 60 μ s is sequential.

Multiple images of element disintegration were captured using a high speed camera by Narancic *et al* [72]. In these studies sequential images are presented of disintegrating cadmium elements. The speed of the camera was 5000 f/s. and fuse elements were surrounded by sand, and packed in a Plexiglas tube. It is proposed that these attributes were close to those of HBC fuse construction. The fuses were tested under I1 and I2 tests duties (BS EN 602969). Narancic *et al* proposed that the images display arc development during both test types, however, image resolution is poor. Simultaneous arc ignition is proposed for test duty 2. Alternatively, sequential arc ignition is proposed for duty 1 but no correlation with oscillograph fuse voltage measurements is presented.

3.4.2.3 Fuse Material Density

X-Rays have been used extensively to inspect post-operation and post-commutated disintegration fuses. Generally, spatial material density information is obtained from these observations.

Further flash X-Ray techniques have been used where a short time duration beam of X-Rays is passed through the fuse element during the development of disintegration. Consequently, an image of element spatial material density is captured at some time instant during disintegration.

A series of X-Rays captured at different time instances during disintegration of silver wires suspended in air are presented by Arai [50]. The time period of disintegration measured by him was $\approx 60\mu\text{s}$. An X-Ray series comprised images of the disintegration of separate wires yet with similar attributes. The images were captured at different time instances and time-correlated to the fuse voltage wave form. Further images of separate disintegrating wires with different attributes, yet embedded in sand, are presented. The images clearly show the growth of deformation in separate but like wires. Deformation shape was contentious to that expected. Consequently, a different mode of disintegration is proposed to account for wire break-up. The images however, do not show growth of deformation in the same wire.

3.4.2.4 Key Findings and Propositions - Transient Data Capture.

Oscillographs of fuse voltage captured during disintegration of elements have been observed to indicate the ignition of arcs [45]. A discontinuity observed in the oscillograph can be interpreted as the establishment of the electrode fall region of an arc. To capture and distinguish individual discontinuities of arc ignitions the time scan of the oscilloscope must be fast [19]. In these circumstances, only part of long time period disintegrations will be captured which inhibits full determination of transient development of disintegration. Alternatively to capture long time period disintegrations, the speed of the oscilloscope becomes irrelevant and, in these circumstances, the voltage waveform appears smooth [10]. Correspondingly, high-speed capture of fuse voltage could aid determination of the nature of disintegration. Moreover, if this were possible, accurate measurements of fuse voltage would aid accurate disintegration simulations.

From all these findings, it was proposed to capture accurate fuse voltage at high resolution.

Light radiating from multiple arcs can be used to interpret the fragmentation of the fuse element during disintegration. This has been observed for disintegrating wires suspended in air [45]. The intensity of light radiation from arcs is very high. This presents a problem to photographic capture of the disintegration of the fuse element because of, for example, the wide range of light intensity radiating from the fuse. Fast cameras capable of capturing multiple images have to have fast shutter speeds. Film exposure times need to be small, consequently, the films must be very sensitive and given the high intensity of arc light, the lens apertures must be small. The resolution of the image, inevitably, will be poor as resolution quality is observed to vary proportionally with speed of disintegration or inversely with the occurrence of arcing.

Investigating the temporal development of disintegration from the start of arcing would be aided by visibly capturing fragmentation of the fuse element. An initial requirement of any capturing device to accomplish this, must be the capability to distinguish individual arcs in images. Previous images testify that the intensity of the arc light must be attenuated. Moreover, a prerequisite of the device to allow temporal analysis must be sequential multiple image capture. Technological advances and availability of video equipment now provides this capability.

The technique of penetrating the fuse cartridge with optical fibres would allow an image to be transmitted to a video camera. Yet, numerous fibres would have to be longitudinally aligned along the element. Moreover, arcing during element disintegration would destroy the fibre tips. These circumstances were anticipated to be time-consuming, prone to errors and financially unsound for this investigation. Additionally, the size of elements capable of multiple arc disintegration, using the experimental fuse test facilities, were small. Moreover, the ratio of element to available optical fibre diameters was considered detrimental to good image resolution.

Given the forgoing image capturing attributes, a new method to overcome the opaque cartridge of the HBC fuse to view disintegration was developed. Techniques used by other researchers to view disintegration and the experimental technique used in this investigation is addressed hereon.

3.4.3 Techniques to Observe HBC Fuse Element Disintegration.

Filler material, surrounding a HBC fuse element, is significant in the process of rapid element disintegration and current interruption [5][73] and the fundamental phenomena of element disintegration could be different for elements suspended in air than for elements bound in filler [5]. As element disintegration of HBC conductive film substrate fuses is one of the principal study areas of this investigation, measurement techniques to observe disintegration of filler bound elements are of considerable significance.

Spectroscopic observation of light radiating from arcs during disintegration of silver current-limiting fuse elements were made by Chikata *et al* [63]. The elements were surrounded by sand and packed in a Pyrex™ tube. No account is presented for the influence of the Pyrex™ tube on arc vapours or disintegration and its attributes as a arc-viewing medium.

Spectrum analysis of an ablation stabilised arc in ice was made by Cao *et al* [74] in which light radiation from arcs captured during disintegration of copper wires, was analysed. Temporal analysis of arc spectra over the period of element disintegration is attempted. This was of secondary importance to the primary aim of the investigation to establish arc diameter, arc column and vapour temperature, however, no account is presented for the influence of the ice on element disintegration.

A high voltage current-limiting fuse element was embedded in sand and packed in a Plexiglas tube by Narancic *et al* [72]. Sandwiched between the element and the tube wall was a thin layer of sand and multiple sequential images were captured of transient arc development. Visual capture methods can be judged from the poor resolution of the images, however no comparison between the performance of the Plexiglas fuses and standard fuses using like elements, to dispel the influence of the tube, were presented.

Use of a quartz slide to view element disintegration was suggested as a viable method by Turner and Turner[73]. In this arrangement one face of the element would be pressed against the slide and supported with filler on its opposite face, however, no images of element disintegration were presented. It is suggested that investigation of arcing is limited to its early stages. Moreover, the study of filler is limited due to the presence and subsequent destruction of the quartz slide.

3.4.3.1 Key Findings and Propositions - Techniques to Observe HBC Fuse Element Disintegration.

The method employed to view disintegration of the fuse element should not impose conditions on fuse construction, such that the transient development of disintegration deviates from that which occurs in a standard HBC fuse.

Pyrex™ and Plexiglas tubes present a satisfactory method to view disintegration. However, the effect on disintegration of the reduced amount of filler between the tube and the HBC fuse element is unreported. Circumstances with elements supported in ice are considered far removed from HBC fuse element construction.

An attribute of film substrate fuse construction presents an opportunity to the study of element disintegration. A transparent substrate would allow visual capture of element disintegration. It is suggested that minimal effect on element disintegration would be imposed in doing this and can be readily validated. Consequently, this method was used in this investigation.

3.5 Investigation Applied Experimental Techniques

Experimental techniques devised for investigation of the disintegration of HBC conductive film substrate fuses are presented in the concluding section of this Chapter. The section is subdivided as follows :

The first section presents the method used to view disintegration of HBC conductive film fuses. The attributes of the method present a subtle variation to the construction of experimental fuses presented in Subsection 3.2. Consequently, the approach of the investigation was changed from the analysis of the temporal phenomena of disintegration of HBC fuses to that of HBC conductive film substrate fuses.

The second subsection presents a methodology for capturing multi-source time correlated data relating to HBC conductive film substrate fuse element disintegration. It is proposed that the methodology will improve confirmation of transient phenomena of disintegration. Consequently, the techniques of capturing data from three separate data sources and the attributes of the techniques are described.

3.5.1 Method to View Disintegration of HBC Substrate Fuse Elements.

The applied experimental technique used to view disintegration of HBC conductive film substrate fuses was simple. A transparent substrate was used in the construction of the fuses. Incorporating the substrate in the wall of the fuse cartridge further modified the construction of the fuse. Consequently, disintegration of the fuse element could be viewed through the substrate

Similarity of the proposed applied experimental method to that presented by Turner and Turner [73], is acknowledged, moreover, the report describing the method came to the authors attention much later in the period of this investigation. However, it is proposed that the experimental sample fuses used in this investigation differ subtly from standard HBC fuses reported in the work of Turner and Turner and hence, the fuse type was labelled a 'HBC conductive film substrate fuse' for exactness. Therefore the construction of HBC conductive film substrate fuses is presented hitherto.

3.5.1.1 Experimental HBC Substrate Fuse Element Construction.

An example of a HBC conductive film substrate fuse element, used in experimental investigations, is shown (Figure 3.5).

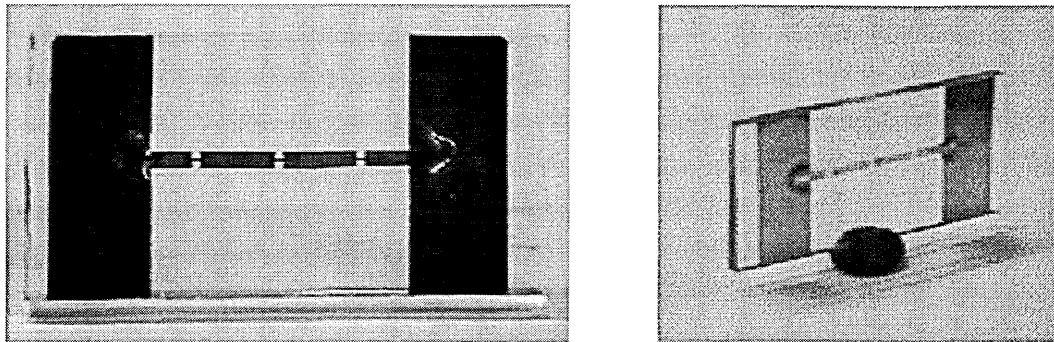


Figure 3.5 Example of HBC conductive film substrate fuse element used in experimental investigations

Various elements types were used in the construction of the experimental fuses investigated. The elements, the attributes of which were, previously presented in Subsection 3.2.1, were soldered using 60:40 solder, to the end caps. The end caps were fabricated from 25 mm (l) \times 10 mm (w) \times 0.15 mm (d) copper strip and bonded to the substrate. The narrow depth of the strip allowed close contact between the element and

the substrate. The element was pressed against the substrate by rear acting pressure of the compacted filler medium. The fillers and their compaction attributes are referred to in Subsection 3.2.2.

The two types of substrates used were commercial grade glass ‘type 1’, of size 50 mm (*l*) × 25 mm (*w*) × 3 mm (*d*) and commercial grade glass ‘type 2’ of size, 75 mm (*l*) × 25 mm (*w*) × 1 mm (*d*).

The chemical compositions of the substrates were,

Chemical Component	SiO ₂ %	Na ₂ O %	Al ₂ O ₃ %	K ₂ O %	MgO %	CaO %
Glass Type 1	73.01	13.61	1.17	0.56	3.68	7.86
Glass Type 2	72.83	14.25	1.21	0.97	4.27	6.34

Table 3.4 Primary chemical components and ratios of substrate materials.

The glass type 1 substrate was used in the construction of the majority of experimental fuses for financial reasons. The influencing attributes of the substrate types on element disintegration are discussed in Subsection 5.5.7.

3.5.1.2 Experimental Fuse Cartridge ‘B’

The fuse cartridge used to hold the substrate fuse elements is shown in Figure 3.6.

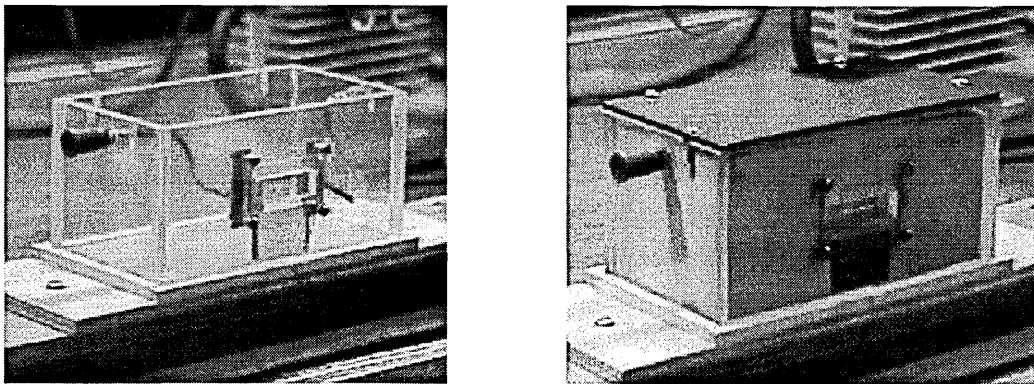


Figure 3.6 Fuse cartridge ‘B’ used to hold substrate fuse elements.

Cartridge ‘B’ had internal dimensions 153 mm (*l*) × 77 mm (*w*) × 77 mm (*d*). The cartridge had a removable lid to allow packing with filler. The lid was secured with

screws to seal the cartridge. Substrate fuse elements were clamped between two copper terminal posts and the side wall of the cartridge. The terminal posts were connected to circuit cables via standard connectors. A window in the cartridge wall allowed the fuse element to be seen through the transparent substrate. The window of dimensions 40 mm (l) \times 15 mm (w), was positioned centrally in the wall of the cartridge.

3.5.2 Methods of Data Capture

The lack of time correlation between data sources of previous element disintegration investigations has been referred to in earlier sections. To fully ascertain the temporal development of disintegration it was decided to use three independent data sources, namely :

- Fuse terminal data capture.
- Video image data
- Inspection of commutated disintegration fuse elements.

It is proposed that temporal development of disintegration would be identifiable from observation of events indicated by each data source and that the correlation of events would confirm observed phenomena of disintegration. Time correlation between all three data sources necessitate the establishment of a time datum.

The experimental data capture equipment, the integrity of captured data and time correlation techniques are addressed in the following sections

3.5.3 Fuse Terminal Data Capture.

Transient data relating to the parameters of fuse current and fuse voltage were captured. Current and voltage were monitored using standard voltage differential sensor methods. Transient measurements were taken, stored and initially analysed using digital storage oscilloscopes (DSO). Oscilloscope data was transferred to a personal computer. This provided a secure storage environment and means for later analysis.

3.5.3.1 Fuse Current.

Data relating to the magnitude of fuse current was obtained by monitoring the voltage difference across a double coaxial current shunt. The shunt was constructed from two matching 20:0.075 current shunts. The shunts were connected in series opposition side by side. This configuration was adopted to reduce measurement noise by

mutual field cancellation. Individual shunts were co-axially located within a copper screen housing and coaxial signal cables were used to connect the shunt to the DSO.

3.5.3.2. Fuse Voltage.

Data relating to the magnitude of fuse voltage was obtained by monitoring the voltage difference across one arm of a potential divider connected across the fuse terminals. The measuring arm comprised two resistors connected in series opposition for purposes of field cancellation and measurement noise reduction. The resistors were also enclosed in a conductive shielding screen and connected to the DSO using coaxial cable.

The potential divider resistors were of high power, high accuracy specifications. Calibration of the potential divider was undertaken using a wheatstone bridge network, accurate current source and galvanometer. The ratio of the potential divider was 50530:133.

3.5.3.3 Digital Storage Oscilloscopes - DSO

Oscilloscopes used in the investigation were of type Gould DSO 400. These provided two separate channels for capturing and analysing data. The maximum sample rate of the oscilloscopes was 100 MHz. This equates to an inter-sample time period of 10 ns on the minimum horizontal axis time base. The oscilloscopes were capable of storing 501 samples per channel. Capturing the 501 sample data window was able to be delayed from a time datum. The delay range was 20 ns to 5000s. A proportion of the sample window could also be captured before the time datum. The oscilloscopes were calibrated frequently using the internal calibrator that provided a 1 KHz, 1v peak to peak signal. Oscilloscope accuracy was frequently checked to ensure that they remained consistently within the stated tolerance limits. Details on the oscilloscope specifications are given in Appendix 5.

3.5.3.4 DSO - Personal Computer (PC) - Data Transfer and Data Conversion

Data was transferred from the DSO to an IBM compatible PC, via a RS432 link. Each DSO channel was transmitted and received independently. Channel data was

received in the PC in a stream format comprising channel identification, date, time, vertical volts per division, time base and raw digitised captured data.

Channel signal raw data was received in the form of the oscilloscope analogue to digital converter voltage levels. Before data conversion, the channel 0 (zero) volt digitised level had to be noted. Conversion of raw data to genuine signal levels was accomplished in the PC's MATLAB™ software environment. The precise (genuine) voltage level was 1/30th of the channel vertical volts per division. Actual fuse parameter levels were the product of the genuine voltage level and the shunt/potential divider ratios.

The channel time base equated to 50 sample periods. The quotient of these gave the time period between individual data points or the sampling interval.

3.5.3.5 Accuracy of Fuse Current and Voltage Measurements.

The accuracies of fuse current and fuse voltage measurements were found to be good.

The accuracy of fuse current measurement was checked using measured values of current in mathematical models [75][76] of the temperature rise of a wire fuse element. Model temperature predications were in the range of $\pm 1\%$ of values, determined by other researchers [3][4], who used separate values of current derived from separate data sources.

The accuracy of voltage measurement was established by first measuring the generator terminal voltage across a voltage divider, with a standard calibrated instrument and then comparing this value with that, measured by the DSO. The range of accuracy was $\pm 1\%$ (measuring 1.045v = generated 240v rms.). Furthermore, the value of peak voltage measured across the fuse terminals during disintegration of HBC wire element fuses, compared favourably with the value of peak voltage determined from an empirically derived relationship [12], which also supported the accuracy of voltage measurements.

3.5.4 Video Image Data.

Three separate video cameras were used in the investigation where the speed of data capture (frames/second f/s) was different for each camera. Cameras were selected

for use dependent on their frame speed and the time period of element disintegration being investigated. The cameras are speed categorised as slow, medium and fast. The slow and medium speed cameras were commercially available units. The fast camera, however, was designed, constructed, tested and commissioned by the author, specifically, for this investigation. Camera attributes and their significance, with respect to the time periods of disintegration are referred to in Subsections 3.5.4.1, 3.5.4.3 and 3.5.4.5.

3.5.4.1 Slow Speed Video Camera

The slow video camera was manufactured by Panasonic™ and was of type NV-G101B. The camera specifications are presented in Appendix 6, however the frame speed of the camera was 25 f/s which reciprocates to 1 frame every 40 ms. The shutter speed was variable, but for this investigation was set at 250 μ s. Light entered the camera via a standard optical lens system. The lens system focused the light on to a matrix of charged coupled devices (CCD). The output from one cell (pixel) of the CCD matrix is proportional to the light energy falling on the pixel in a finite exposure time period. Consequently, the pixel output is dependent on light intensity and exposure time. The electronically-conditioned pixel outputs were stored using conventional magnetic tape methods. These were later viewed using 625 line 50 field monitors. Selected static images were acquired using commercially available video-PC hardware and software image capture packages.

The frame speed of this camera is relatively slow for the tasks in hand. Appreciation of this can be gained when comparing the frame speed (40ms), with the time period of one cycle of power frequency current (20ms). Moreover, the time periods relative to the formation of unduloids in wires is 30~300ms [48][19], hence the range of the number of captured images is 1~7 depending on the time instant of capture of the initial image. Also, given a time period from the instant of unduloid formation to current interruption of the order of 500 μ s~3ms [48] only a single image may be captured of element disintegration.

3.5.4.2 Experimental Use and Event Time Correlation : Slow Speed Video Camera.

Given the speed limitation of the slow camera, it was only used to investigate disintegration of elements over long time periods ($>80\text{ms}$). The camera was mounted on a tripod and positioned to obtain maximum resolution of the viewed object, i.e. the fuse element, and the capturing of images was manually initiated. Direct synchronisation between the camera and the test facility supply voltage wave form was, therefore not feasible. Time correlation between the captured images and captured voltage and current oscillographs was achieved by visual indication of the instant of current switching in the captured images. The method incurs a range of time correlation between images and oscillographs in the range 0~40 ms. However, given the time periods of disintegration, this discrepancy was considered acceptable.

The camera provided accurate evidence of transient phenomena occurring from the instant of current injection to periods well beyond the instant of current interruption. Images and discussions of element disintegration, arising from the use of the camera, are presented in Subsection 4.3.

3.5.4.3 Medium Speed Video Camera.

The medium speed video camera was manufactured by Redlake Imaging Corporation, USA. The specifications for the camera of type, Motionscope®2000S are presented in Appendix 7, however the camera has a frame speed of 2000 f/s. which correlated to a frame every $500\mu\text{s}$. The shutter speed was variable, but for this investigation was set at $100\mu\text{s}$. Capturing of images was manually initiated and light to electrical current conversion was accomplished in a similar way to that of the slow video camera except that the medium speed camera stored the pixel outputs in a fast acquisition semiconductor memory. This allowed slower speed interrogation of the memory contents for visual analysis and magnetic tape storage of the images after the event. Images stored on magnetic tape were viewed using 625 line 50 field monitors. As with the slow camera, selected static images were acquired using commercially available video-PC hardware and software image capture packages.

The frame speed of the camera is an 800% improvement on the frame speed of the slow camera. Given the same example of disintegration, presented for time

appreciation of the slow camera, during the disintegration period ($500\mu\text{s}\sim 3\text{ms}$) 6 frames would be captured by the medium speed camera. This gave a considerable improvement over the single image captured by the slow camera

3.5.4.4 Experimental Use and Event Time Correlation: Medium Speed Video Camera

The speed of the camera allowed numerous sequential image analysis of element disintegrations over long time periods ($>30\text{ms}$). Moreover, the camera provided sequential images that allowed adequate analysis of fast element disintegrations during very short time periods ($<1\text{ms}$).

Figure 3.7 shows the camera, mounted on a tripod positioned to obtain maximum resolution in captured images.



Figure 3.7 Medium speed video camera experimental arrangement.

Due to the limitation of the combined camera frame rate (2000 f/s) and shutter speed ($100\mu\text{s}$), the object resolution was poor and appeared very dark under normal lighting conditions. To overcome this, external high intensity light sources were used to direct light on to the object.

Similar to the slow video camera, direct time correlation between the medium speed video camera and a reference point on the test facility supply voltage wave form was not feasible with the equipment. However, the same method of capturing a visual indication of the instant of element current flow initiation in the images was used. With this feature, the range of time correlation between captured images and captured voltage and current oscillographs of $0\sim 500\mu\text{s}$ was achievable.

Images captured by the medium speed video camera were used to corroborate those captured by the slow camera for the disintegration of elements within similar time periods. Furthermore, images were used to investigate temporal arc development during fast disintegration time periods to corroborate the images captured by the fast video camera. In these cases a filter, with a luminous transmittance in the range of 0.16%max~0.023%min and spectral response 350nm~780nm (BS-EN169), was used to attenuate the intensity of the light radiated from the arcs. The filter and camera arrangements are shown in Figure 3.8.

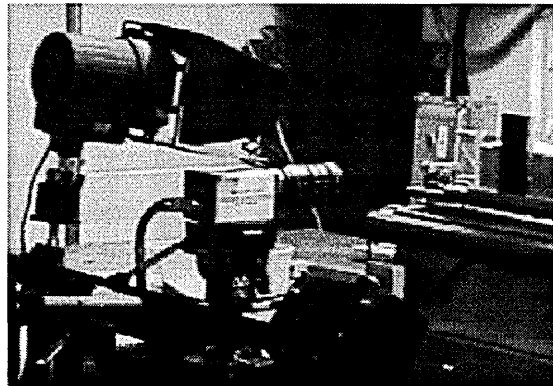


Figure 3.8 Medium speed video camera and filter arrangement.

3.5.4.5 Fast Speed Video Camera

A photograph of the fast speed video camera, designed, constructed, tested and commissioned specifically for investigation of fast time period element disintegration, is shown in Figure 3.9



Figure 3.9 Fast speed video camera arrangement consisting of optical system, control electronics and DSO image capturing facilities

The integrity of the images captured by the camera was an important design consideration. A systematic program of development, testing and commissioning was, therefore, necessary to confirm and provide repeatable evidence of the camera integrity. Consequently, the construction and operation of the camera will be elaborated in some detail, hitherto. Moreover, results obtained in commissioning and testing of the camera will be presented as validation evidence of the integrity of the images subsequently presented in Chapters 4 and 5.

Light Sensor

The sensor used to capture light radiating from the fuse element was manufactured by Texas Instruments, USA, and of type TSL 1401. The sensor measured 10.9mm (l) \times 8.25mm 9 (w) and comprised of 128 pixels, contained in an 8 pin DIL package. A photograph of the sensor is shown in Figure 3.10.

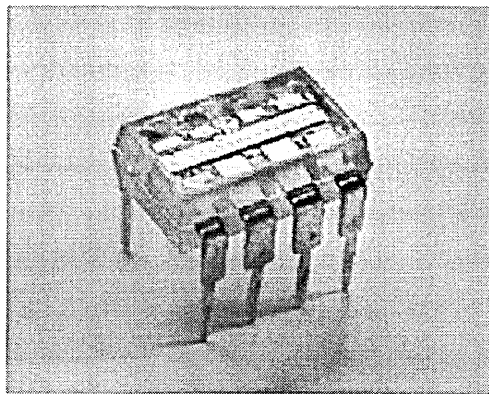


Figure 3.10 Fast video camera, light sensor, TSL 1401

Each pixel contains a photo diode, associated charge amplifier and pixel data hold circuitry. Light energy falling on a photo diode gives rise to the generation of photo current. The current is then integrated by the active integration circuitry associated with each photo diode. The pixel data hold function provided simultaneous start integration and stop times for all pixels.

During the integration period a sampling capacitor is connected to the output of the integrator through an analogue switch. The amount of charge accumulated in each pixel is directly proportional to the light intensity of the source and the integration time.

The output and reset of the pixel integrators, is controlled by a 128 bit shift register and reset logic. An output cycle is initiated by the application of a serial input pulse (SI). This causes all 128 sampling capacitors to be disconnected from their respective integrators and initiates an integrator reset period. The integrator reset period ends 18 clock cycles after the SI pulse clocks in. The device uses a 2MHz clock (CLK) for this purpose, consequently the integrator reset period equates to $9\mu\text{s}$. Following integrator reset, the next integration time period begins. As the SI pulse is clocked through the shift register, the charge held in each pixel is sequentially connected to a charge coupled output amplifier. This generates a voltage at the output of the sensor (AO). The nominal range of pixel output is 0 volts for no light and 2 volts for nominal full scale output. The sensor's nominal spectral response is in the range of 300nm~700nm.

The above sensor operating parameters, in essence, illustrates that the maximum frame capture speed of the camera is 1 frame every $64.5\mu\text{s}$. This correlates to a camera speed of 15,504f/s.

Optical System

The optical system comprising lens, beam splitter and two light sensors were embodied in an opaque box (Figure 3.11). A high quality planar convex lens was used to converge light radiating from the fuse onto two light sensors after

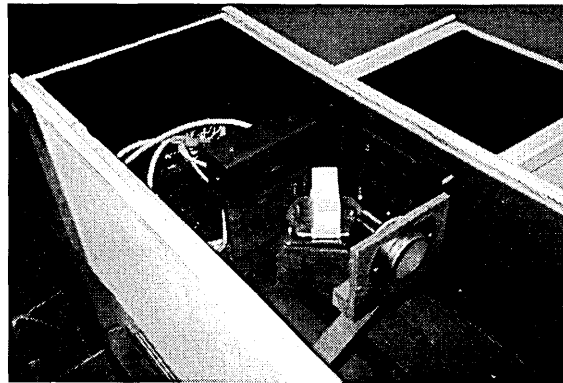


Figure 3.11 Fast speed camera optical system.

passing through a beam splitter. The rationale for using the beam splitter was to increase the capture speed of the camera. This was achieved by applying independent SI pulses to both sensors at different time instances. It was anticipated that the increased number of multiple images captured by the sensors would allow for better interpretation of temporal element disintegration. Unfortunately, when the sensors were exposed to the same intensity light source for the same integration time periods, extreme difficulty was encountered matching the magnitude of sensor outputs so that temporal analysis could be conducted with a very short time period between independent SI pulses ($10\sim 20\mu\text{s}$).

However, the presence of individual light sources were corroborated from comparison of two images captured at the same time instance and the transient development of light sources was established with a long time period between independent SI pulses (30~40 μ s).

Camera Control

Sensor output sequences were initiated by the application of serial input pulses. The pulses were derived from electronic circuitry, specifically designed and constructed to control the capture of images by the camera. Sensor analogue outputs were captured at specific time instances using 100 MHz digital storage oscilloscopes. The oscilloscopes were of the same type, described in Subsection 3.5.3.4.. Figure 3.12 shows

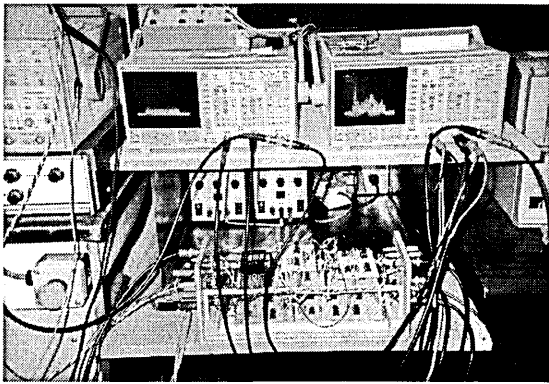


Figure 3.12 Fast video camera control electronics and sensor output capture oscilloscopes.

the camera control electronics and oscilloscope arrangement.

Figure 3.13 shows a simplified schematic diagram of the camera and the interconnections between the fuse test facility, the optical system, the camera control electronics and the oscilloscopes.

The fuse voltage is applied, via an isolation buffer amplifier, to the

input of a fast precision comparator. The comparator reference could be manually adjusted. The output of the comparator is latched to stop multiple transitions of the comparator output occurring. The latch could be manually reset and the latch output was used to trigger an 'event' monostable circuit. The monostable provided a time delay period between the instant of comparator latching to a desired time instant after latching. On expiry of the delay time period, a second monostable was triggered to provided a pulse of suitable duration (400ns). This pulse was applied to the light sensor, as the serial input (SI) pulse. Parallel sets of 'event' and 'SI' monostables were OR'd together to provide a series of SI pulses. The series of pulses are manually set by adjustment of the event monostable time periods and structured to initiate multiple output sequences of the sensor as illustrated in the time event diagram in Figure 3.14.

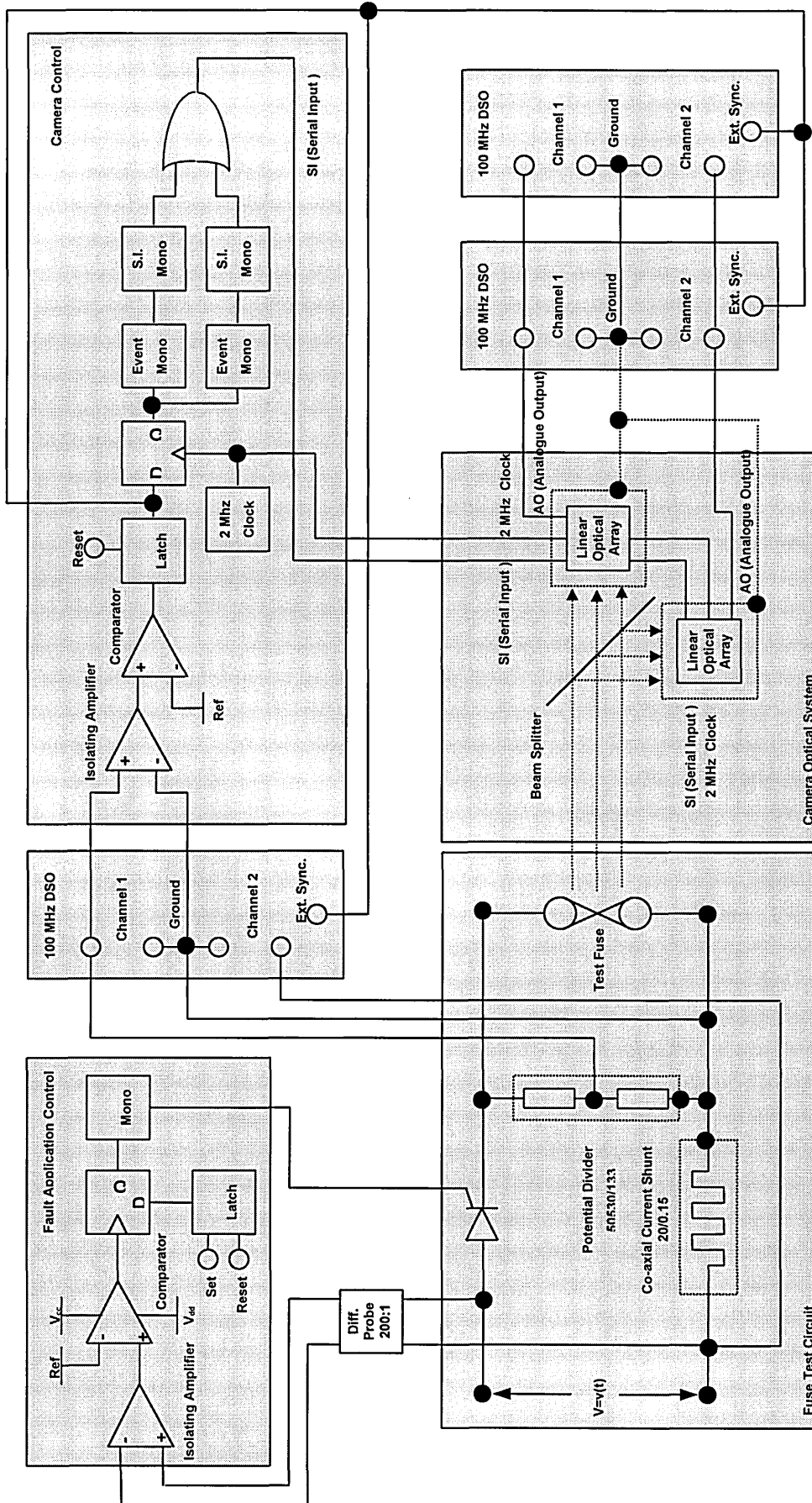


Figure 3.13 Fast speed video camera control, optical system, fuse test facility and OSA interconnection diagram

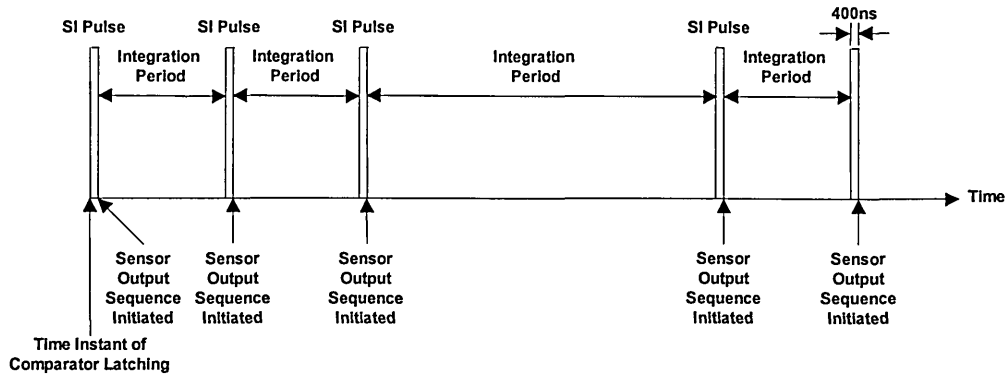


Figure 3.14 Structured timing sequence of serial input (SI) pulses

From the following diagram (Figure 3.15), it may be seen that the output sequences are initiated at required time instances with respect to the comparator latch time instant and the comparator latch triggers the oscilloscopes so that the oscilloscopes could be set to capture sensor output data at specific time instances. It is important for temporal analysis of element disintegration that the sensor integration time periods are equal for oscilloscope captured images.

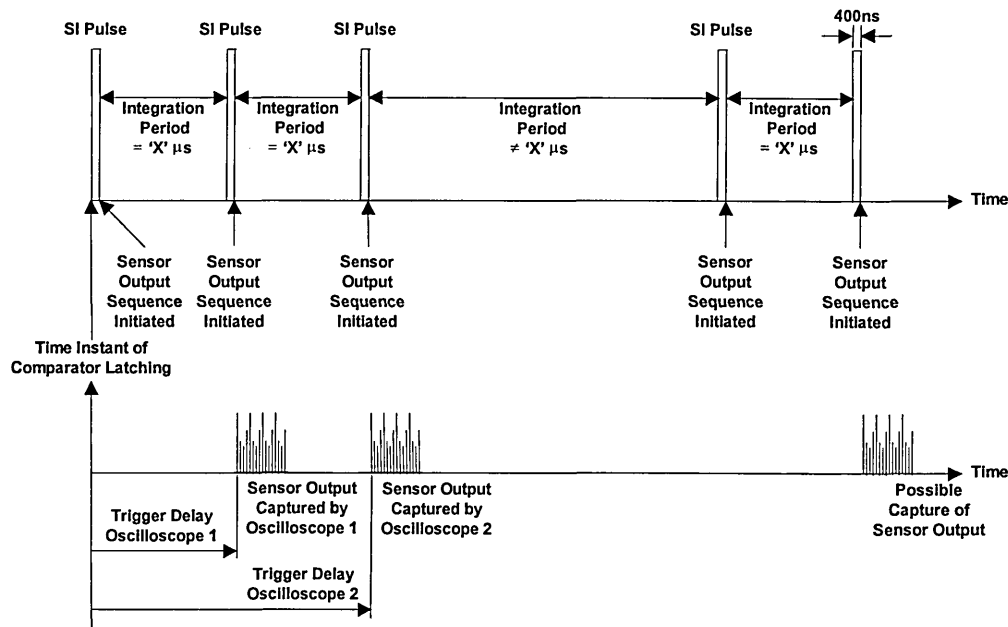


Figure 3.15 Structured oscilloscope capture sequence of sensor outputs.

Camera Testing

A camera testing procedure was devised to determine the camera attributes and collate the images captured by the camera as evidence of its validity to capture images of fast disintegration of fuse elements. To accomplish this an attempt was made to simulate the proposed disintegration light patterns of wire fuse elements. To do this an homogenous light source was constructed as shown in Figure 3.16, comprising a high powered light source (650W) and light box.

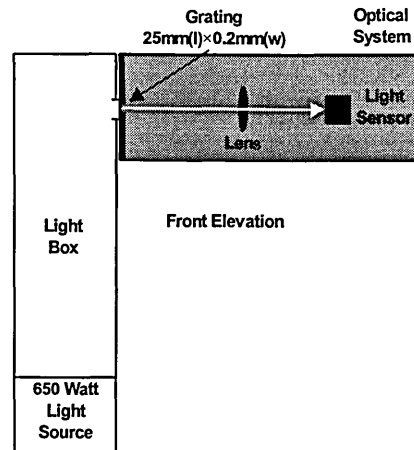


Figure 3.16 Alignment arrangements of optical system and homogenous light source

Light radiating from the source was directed upwards into the columnar light box where a small opening (hole) on one side of the box allowed light to exit the box. The hole was positioned on the same horizontal axis to the light aperture of the camera. Light entered the camera through a 25mm (l) \times 0.2mm (w) grating and was focused on to the two light sensors.

A electronic ramp generator was constructed to simulate the fast transient rise of the fuse voltage. This signal was injected into the camera control electronics. By setting the comparator reference voltage, equal to a voltage magnitude, which would latch the comparator near the start of the voltage ramp, an SI pulse was generated and applied to the sensor. The SI pulse initiated an output sequence from the sensor and subsequently started a new integration time period. The length of the integration time period was manually set, as previously described.

Using this test method, the output of the sensors were monitored and their positions adjusted relative to the horizontal axis of the optical system. This was carried out until the responses of all pixel outputs were within a range of ± 0.1 volts of each other (3% nominal fsd). Additionally, by positioning a 0.5mm diameter rod perpendicular to the horizontal axis, and through the vertical axis of the optical system, the sensor positions were axially aligned so that the center pixels of the pixel array lay either side of the vertical axis.

The results from a series of tests which are presented in Appendix 8, confirmed that the relationship between pixel voltage output and integration time was linear.

To confirm the transient performance of the camera necessitated designing a series of patterned encoded wheels. Such a wheel is shown in Figure 3.17. The wheels were designed to be positioned directly in front of the camera aperture grating with the horizontal axis of the wheel in line with the horizontal axis of the optical system and rotated, at a speed of 12000 rpm. A basic wheel was pattern

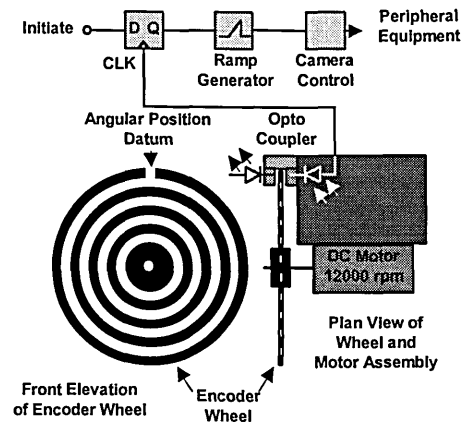


Figure 3.17 Patterned encoded wheel and simplified block diagram of camera test arrangements.

encoded with 25 alternating transparent and opaque rings. The centre ring of a wheel was positioned in line with the vertical axis of the optical system. An angular position datum was established on each wheel by a transparent window in the opaque outer ring. This was detected by an opto coupler, which triggered the ramp generator when camera data capture was initiated.

Wheels with varying encoded patterns were used to validate the transient response of the camera, an example of which is shown in Figure 3.18 with the corresponding normalised sensor output shown in Figure 3.19. Further examples of patterned encoded wheels and sensor outputs are presented in Appendix 8.



Figure 3.18 Patterned encoded wheel, designed to simulate sequential arc ignition

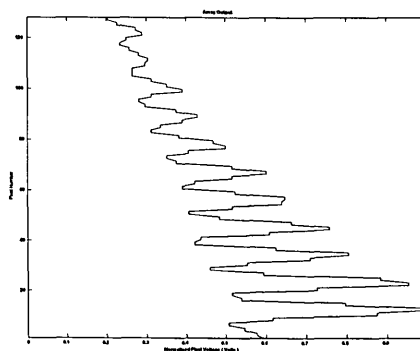


Figure 3.19 Normalised sensor output integration time = 1.5ms

Camera Commissioning

Before commissioning the camera, a 'fuse holder' was constructed. This is shown in Figures 3.20 and 3.21.

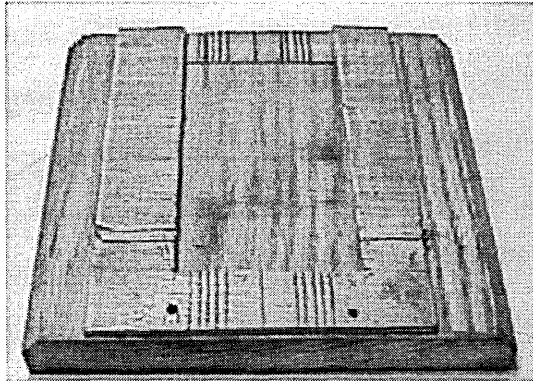


Figure 3.20 HBC conductive film substrate fuse holder with horizontal and vertical datum's for accurate positioning of fuse elements indicated.

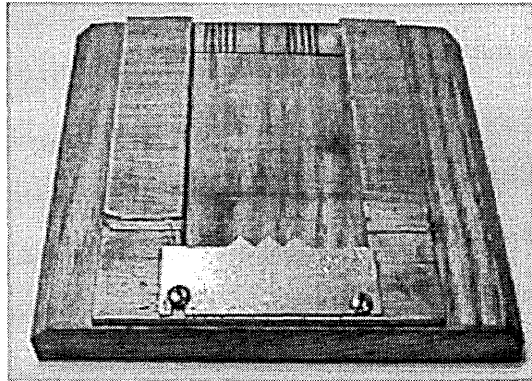


Figure 3.21 HBC conductive film substrate holder with additional substrate clamping plate with vertical alignment datum's indicated.

The holder was used to aid the construction of HBC conductive film substrate fuse elements. By using the holder, a near homogenous series of sample substrate elements could be constructed by first fixing the fuse substrate relative to a horizontal datum and then positioning and soldering the element between the end caps, relative to the datum. The distance between the datum and the horizontal axis of the element was set which ensured consistent alignment of fuse elements with the horizontal axis of the camera optical system. Similarly, during construction, fuse elements were also positioned relative to a vertical datum, which consistently ensured the alignment of fuse elements was central to the vertical axis of the camera optical system. Commissioning of the camera was carried out using copper wire fuse elements $0.2\text{mm } \varnothing \times 25 \text{ mm (l)}$.

To confirm the noise immunity of the camera, the optical system was first sealed to stop entry of light from ambient sources. Wire fuses mounted close to the camera were then ruptured to first ascertain the magnitude of the voltage level measured across the fuse terminals at the assumed instant of element disintegration. Measurements of voltage were captured and the camera comparator was set to latch at this level of voltage. Comparator latching initiated a sensor integration period as previously described and the length of the integration period was set at $100 \mu\text{s}$. This time period was chosen to be comparable to the time period of element disintegration and arc ignition which was assumed to be indicated in oscillographic records by the fast rising

fuse voltage. After expiry of the time period, the sensor outputs were captured by oscilloscopes. Analysis of the results confirmed excellent noise immunity of the camera. The results of the sensor outputs obtained for confirmation of camera noise immunity are presented in Appendix 9.

Final camera commissioning tests were conducted to set the range of the sensor output (0~2volts) within the range of the maximum light intensity radiated from the fuse element during disintegration, on the basis that the intensity of light radiated from the fuse is assumed to be greatest during element disintegration and the period of arc ignition. Consequently, the light sensor integration time was set to the allowed minimum (65.5 μ s), to provide the maximum image capture rate. Wire element HBC conductive film substrate fuses were ruptured and the light, radiated from the fuses during disintegration, was captured by the sensor opto-couplers. Analysis of the oscillographs of sensor outputs indicated the sensor pixels had reached saturation level (nominally 3.5 Volts). Therefore a light attenuator was positioned in front of the sensor to reduce the detected light intensity. Fuse ruptures, output analysis and light attenuation adjustment was carried out systematically until the sensor outputs did not saturate. The luminous transmittance of the light attenuator after this procedure was 0.12%max~0.061%min with a spectral light range of 350nm~780nm (BS-EN196). The results from these tests are presented in Appendix 9

Time correlation between the capture of light sensor data and fuse terminal data was validated at the assumed time instant of element disintegration. A range of time correlation of $\pm 2 \mu$ s, was established from analysis of the oscillographs of many repeatable measurements of the fuse voltage and comparator latch.

Systematic testing and commissioning of the fast video camera enabled a satisfactory performance specification to be determined which is presented together with the camera schematic wiring diagrams in Appendix 10.

3.5.5 Techniques to Terminate Disintegration of HBC Substrate Fuse Elements

Recapitulating, termination of disintegration in fuse elements is accomplished by presenting a lower by-pass resistance path to the fuse current at specific time instances. Consequently, the state of matter of the fuse is 'frozen', subject to factors referred to earlier, at the time instant of current commutation. Post commutation examination of a

fuse can, therefore, capture data relating to disintegration at the time instant of current commutation. Two techniques were used in this investigation to divert the fuse current and consequently terminate disintegration.

3.5.5.1 Commutation Relative to Fuse Voltage.

A ‘crow bar’ thyristor was connected across the fuse terminals. Additionally, a variable resistor was connected between the anode and gate of the thyristor as shown in Figure 3.22.

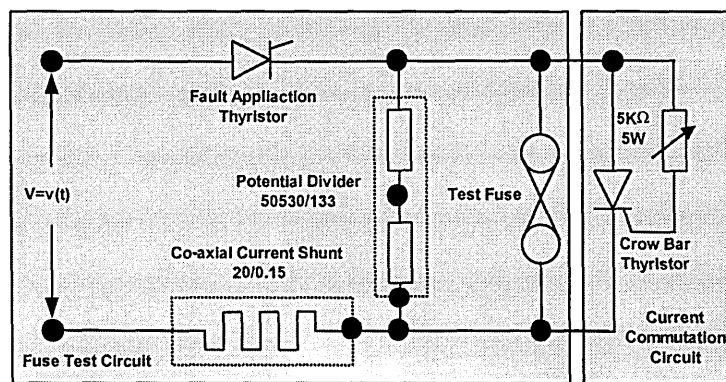


Figure 3.22 Fuse test circuit with additional crowbar thyristor, variable resistor arrangement, which allowed for commutated disintegration of fuse elements relative to fuse voltage

Incremental adjustment of the variable resistor enabled different thyristor triggering time delays, depending on the fuse voltage and the thyristor triggering current level. Consequently current commutation and disintegration in fuses was terminated relative to the fuse voltage.

3.5.5.2 Commutation Relative to Fast Video Camera Comparator Latch.

A crowbar thyristor was also used to commute fuse current, relative to the latching of the fast video camera comparator involving a different thyristor triggering technique. This arrangement is shown in Figure 3.23 and explained on the following page.

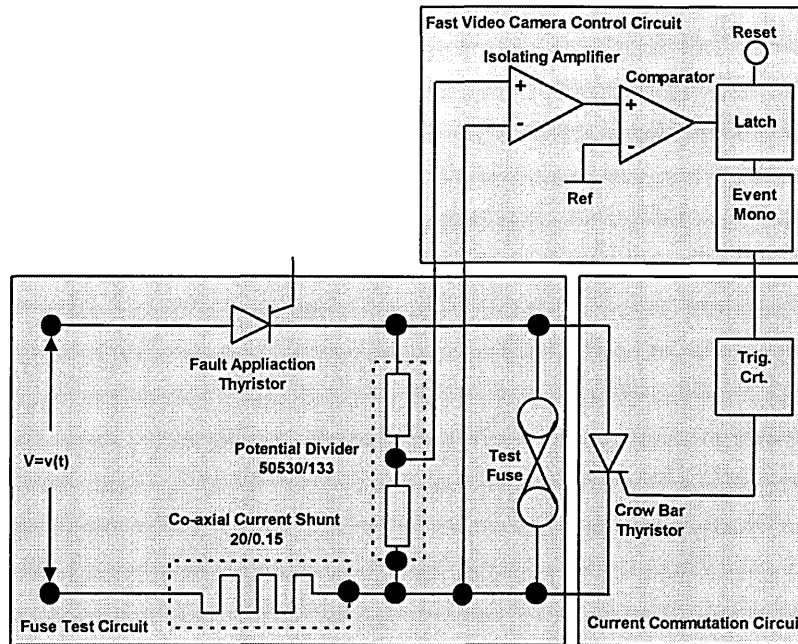


Figure 3.23 Fuse test circuit and additional crowbar thyristor arrangement, which allowed commutated disintegration of fuse elements relative to fast video camera comparator latching.

In this arrangement, upon the latching of the fast video camera comparator, the time delay of a selected 'event' mono stable circuit is initiated. Expiry of the time delay is then arranged to trigger the crowbar thyristor and consequently commutate the fuse current and hence terminate disintegration relative to the comparator latching.

3.6 Chapter Summary and Propositions

The main objective of this investigation was to investigate the disintegration of conductive film HBC substrate fuses. The fundamental nature of the investigation required a fundamental approach to the construction of the fuses and measurements. The parameters of fuse construction have been identified and their attributes presented. Fuse constructions were purposely developed to permit visual investigation of disintegration. An experimental test facility has been designed, constructed, tested and commissioned to fulfil the investigation objectives and commissioning tests validated the accuracy and scope of the fuse test facility.

A comprehensive treatment has also been presented of the significant experimental data capturing techniques used by other researchers to investigate the parameters of HBC fuse disintegration. These methods have been categorised and the

attributes of the techniques analysed, from which key attributes of the required techniques for the investigation have been proposed and subsequently used for capturing data relating to the disintegration of HBC conductive film substrate fuses. A procedure to analyse the data captured from three separate data sources has been proposed and implemented in hardware. Using event time correlation of data captured from separate data sources, it has been shown that the transient phenomena associated with disintegration in fuses can be observed and validated.

The proposed experimental techniques involving three separate data capturing techniques, therefore, have been justified as an appropriate methodology for investigating disintegration. The techniques of terminal measurement and video camera image capture have also been implemented as transient data capturing methods. Validation of disintegration by inspecting commutated disintegrated fuses is categorised as a historical data capturing method with inherent limitations. Systematic testing and commissioning of the transient data capturing sources was carried out to confirm their integrity and to provide evidence to validate the results of temporal disintegration investigations using time event correlation. Time event correlation between the three separate data sources has finally been reviewed and hardware solutions have been implemented

In summary, this Chapter has addressed the attributes of the available experimental techniques for capturing data relating to the disintegration of HBC conductive film substrate fuses and proposed methodologies and hardware solutions. The results obtained using these experimental data capturing techniques to examine disintegration of HBC conductive film substrate fuses and subsequent analysis of disintegration phenomena are the subject of the following Chapter.

Chapter 4

Experimental Observations of the Causation Phenomena of Fuse Element Disintegration

4.1 Introduction

This Chapter presents the results of experimental investigations into the causation phenomena of fuse element disintegration, which focus on the observations of the classical ‘unduloid’ and ‘striated’ classifications of disintegration for different fuse fillers.

4.2 Experimental Approach and Chapter Format

Because the fundamental investigations were examining, principally, the unduloid and striated disintegration of wire fuse elements, the observations were considered, primarily, in two distinct pre-arcing time periods, referred to hereon as the ‘long’ (80ms~200ms) and ‘very short’ (3ms~20ms) time domains. Fuse behaviour was examined, subsequently in the time periods (20~80ms), and referred to as the short time domain. The ‘long’ and ‘very short’ time domains also featured in the investigations of the experimental conductive substrate fuse element samples, compacted in silica quartz and encapsulated resin fillers. Consequently, the disintegration phenomena of the fuse elements could be proposed for similar current densities and compared. Moreover, the different compaction density of the fillers that influence the causation and subsequent fragmentation of the element, could also be investigated in the same time domains.

The Chapter presents a temporal description of observed disintegration phenomena for each element type, starting in real time from the instant of fault current application and beyond the instant of current interruption. Subsequently, analyses of the observed phenomena are presented and the key points summarised for each class of fuse in these two time domains, which inform the concluding discussion.

4.3 Investigation of Disintegration in the Long Time Domain

The experimental investigations commenced with classical unduloid formation in silver wire elements suspended in air as this form of disintegration had been investigated extensively by previous researchers [32][44]. These investigations assisted the establishment of the application of time domain classification, from the instant of

fault application to the occurrence of element disintegration, within the capacity of the experimental test facilities. Recapitulating, the time period associated with unduloid formation was classified as 'long'. Furthermore it was demonstrated in Chapter 3, that the phenomena of disintegration in this long time domain could be reliably examined within the capture time rates of experimental equipment (Subsection 3.5).

4.3.1 Description of Temporal Observations of Wire Disintegration in Air.

Fuse Element Longitudinal Deformation.

Virtually immediately following initiation of fault current conduction in the wires suspended horizontally between two terminals, pronounced longitudinal deformation of the fuse element was observed using video cameras, which took the form of wave motion (Figure 4.13ii). This 'wave' motion tended to subside after ≈ 50 ms leaving the element in a smooth 'catenary' shape. In most cases the element catenary settled below its original horizontal position, although, the element's disposition was also observed, occasionally, to settle above the horizontal plane (Figure 4.1). This motion is analysed in section 4.3.2 and Appendix 11.



(i) Catenary shaped element disposition below the horizontal origin ≈ 50 ms after current initiation. Element = $O.2032\varnothing$ mm/60mm silver wire.



(ii) Catenary shaped element disposition above the horizontal origin ≈ 50 ms after current initiation. Element = $O.2032\varnothing$ mm/60mm silver wire.

Figure 4.1 Images of 'catenary' shaped element disposition. (Medium speed video camera images)

Fuse Element Axial Deformation.

Axial element deformation in the wire was observed in the form of classical unduloids. Observations showed that the temporal evolution of unduloids is sequential and their initial formations were seen to occur around the instant of disintegration. The formation time, from that of the pristine wire to unduloid shape, was observed to be of the order of 6ms. Figure 4.2, indicates the case where unduloids formed just prior to the onset of element disintegration.

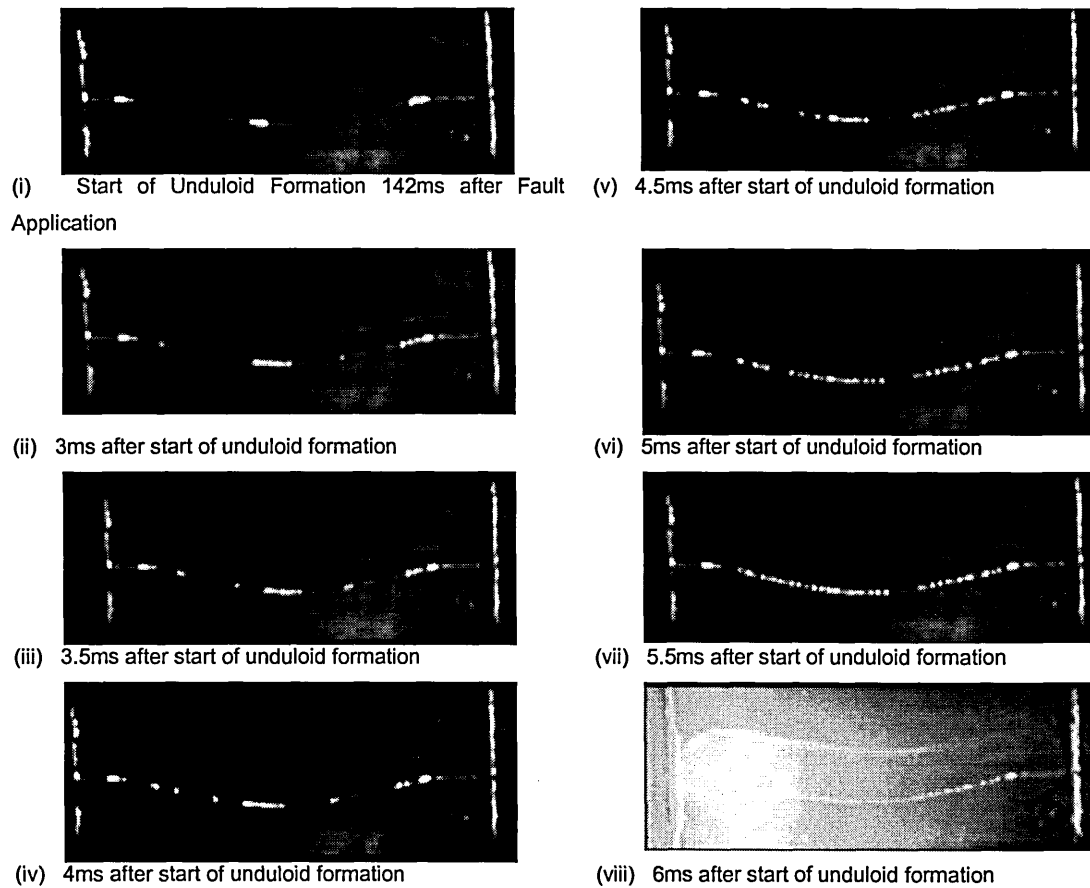


Figure 4.2 Sequenced images displaying temporal development of unduloid formation in a 0.2032 \varnothing mm/60mm silver wire element, (Medium speed video camera images)

It was also observed, from the video images of elements captured during fault current conduction, that minimal axial element deformation occurred, physically, in the vicinity of the element terminal connections (Figure 4.3).

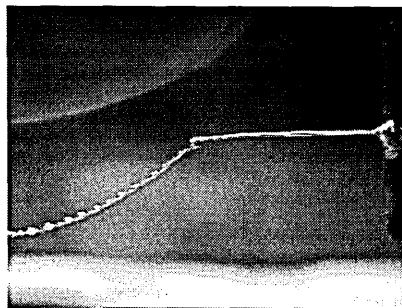


Figure 4.3 Close up image of the connection between end cap and a 0.2032 \varnothing mm/60mm silver wire element about 40ms after the instant of disintegration (Slow speed video image)

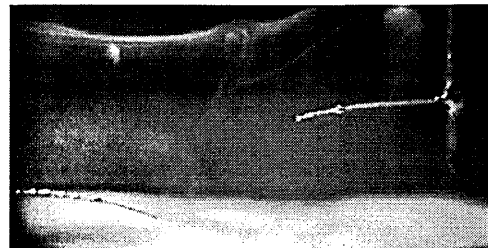
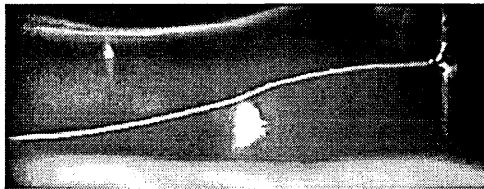
Fuse Element Disintegration.

Initial disintegration of the element was most frequently observed (>85% of cases) to initiate in the vicinity of one of the terminals (Figure 4.4).



Figure 4.4 Image of a 0.2032Ømm/60mm silver wire element with disintegration initiating in the vicinity of an element end cap connection point. (Medium speed video image)

More significantly, the onset of disintegration of the element was observed to initiate both before and after the formation of unduloids (Figures 4.5~4.6)



(i) Image near the instant of disintegration of 0.2032Ømm silver wire element (Time $t_{pa} \approx 155\text{ms}$) (ii) Image 40ms after the disintegration instant (i) (Time = $t_{pa}+40\text{ms}$)

Figure 4.5 Sequenced images displaying the onset of disintegration of a 0.2032Ømm/60mm wire element before the formation of unduloids (Slow speed video camera images)



(i) Image prior to the disintegration of a 0.2032Ømm/60mm silver wire element (Time $t_{pa} \approx 155\text{ms}$) (ii) Image 2ms after the disintegration instant (i) (Time = $t_{pa}+2\text{ms}$)

Figure 4.6 Sequenced images displaying the formation of unduloids before the onset of disintegration of a 0.2032Ømm/60mm wire element (Medium speed video camera images)

Following the initiation of disintegration, fragmentation of the element was observed to continue on, with detached multi-unduloid remnants being violently expelled from the initial point of arc ignition (Figure 4.7). These observations have particular implication for the use of Nasilowski's unduloid empirical formulas in determining the magnitude of the peak arc voltage, discussed in Subsection 4.3.2.

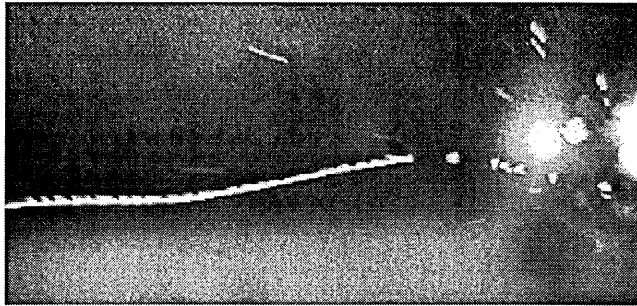


Figure 4.7 Image of 0.2032Ømm/60mm silver wire element remnants expelled away from the point of arc ignition (Slow speed video camera image)

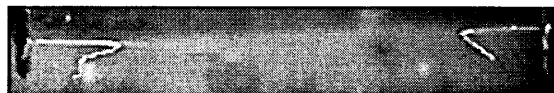
Furthermore, the parts of the element, which did not become detached during fragmentation, were seen to 'fly' back in a whip-like action from the break point in the element. In the case of a single break, the remaining attached parts of the element were seen to 'pivot' about a fulcrum point in the non-deformed section of the element close to one of the terminals (Figure 4.8).



(i) Image of the attached element pivoting about the non-deformed section of the element remnants. (Medium speed video image)



(iii) Close-up image of the 'whipped' back element remnants. (Slow speed video image)



(ii) Image of the attached remnants of the element having 'whipped' back around the 'pivot' point. (Slow speed video image)

Figure 4.8 Images of the 'whip lash' action of attached remnants of an 0.2032Ømm/60mm silver wire element around a 'pivot' point in the vicinity of an element terminal.

Fuse Voltage Magnitude and Fuse Operation.

During disintegration of the fuse element in a 50~100 v rms ac test circuit the number of undulations exceeded 50 (wire length $l = 60\text{mm}$) but the number of arcs was always between 1 and 3 (Figure 4.9). This finding conflicts with the conventional understanding of unduloid operation where it is, generally, understood that an arc ignites between each unduloid.



- (i) Disintegration of a 0.2032 \varnothing mm/60mm sliver wire element with a single arc ignition in the vicinity of the element terminal.
- (ii) Disintegration of a 0.2032 \varnothing mm/60mm sliver wire element with two arc ignitions (Fuse 131)
- (iii) Disintegration of a 0.2032 \varnothing mm/60mm sliver wire element with three arc ignitions, with one in the vicinity of a element terminal.

Figure 4.9 Images indicating the number of arc ignitions observed during the disintegration of a 0.2032 \varnothing mm/60mm silver wire element (Medium speed video camera images)

The number of observed arcs correlated with the fuse voltage oscillograms (Figure 4.10) where the peak arc voltage was typically in the range 50~80 volts and the rate of voltage rise was $\approx 0.0174\text{v}/\mu\text{s}$.

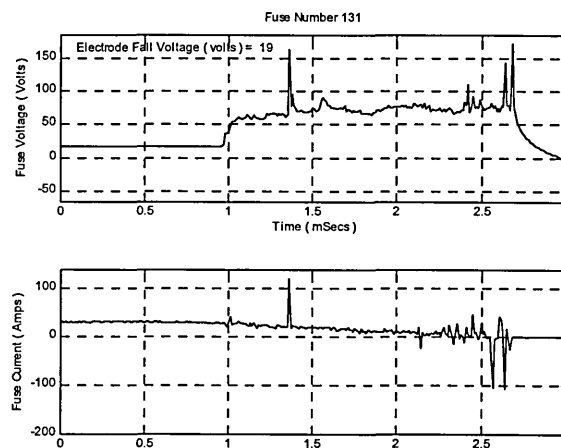


Figure 4.10 Fuse voltage and current waveforms during the time period of disintegration of a 0.2032 \varnothing mm/60mm silver wire in air.

Furthermore the temporal development of disintegration evidenced by evolution of the arc ignitions seen in video images was found to be sequential (Figure 4.11).

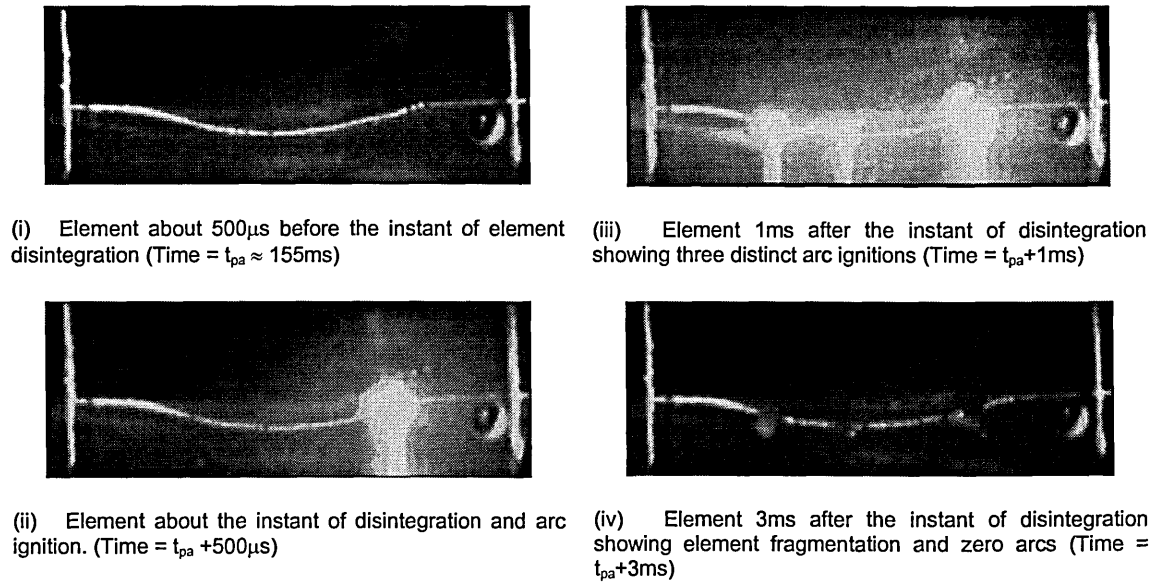


Figure 4.11 Sequenced images displaying the sequential ignition of arcs evidential of sequential disintegration of a 0.2032 \varnothing mm/60mm silver wire element (Medium speed video camera images)

Disintegration of the fuse typically occurred, predominantly, at the instant at or about the a.c. peak fault current (Figure 4.12).

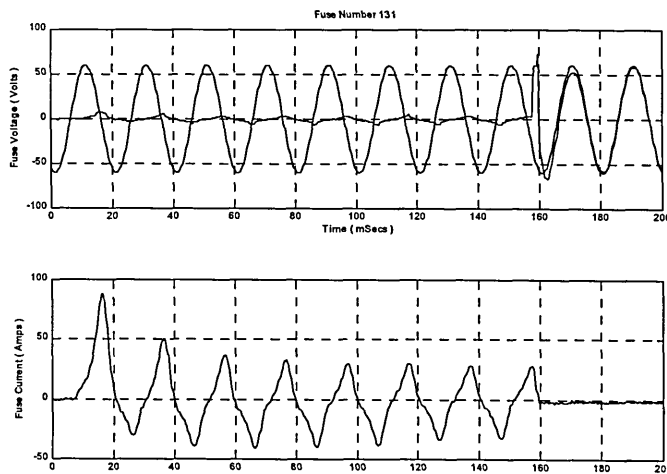


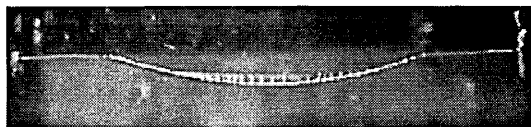
Figure 4.12 Fuse voltage and current waveforms during the long time domain for fault current conduction in a 0.2032 \varnothing mm/60mm silver wire element in air.

4.3.2 Issues and Propositions Originating from Temporal Observations

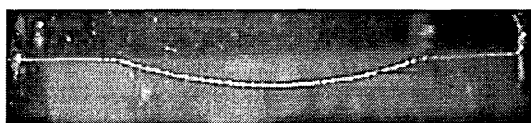
Prior to the application of fault current it is well known that the axial dimensions of the element cannot be absolutely uniform, nor can the elements longitudinal disposition be truly horizontal along its length. Upon application of the current the longitudinal element deformation increases by thermal expansion of the element due to Joulean heating. The physical barriers presented by the end terminals are, therefore the only restriction to the element's full lateral expansion. It follows logically, and by analysis (Appendix 11) that the profile of a uniform section conductor, fixed at its ends, will take the form of the observed catenary of the wires tested in air. The air surrounding the element is considered, therefore, to constitute a negligible physical barrier to free movement of the element and hence could be described as a medium of minimum confinement next to a vacuum. This minimal confinement notion applies



(i) Current carrying element forming catenary shape about 40ms after current application



(ii) Element with unduloid formations about the instant of current commutation.



(iii) Non current carrying element starting to contract about 40ms after current commutation



(iv) Non current carrying element about 120ms after current commutation.

Figure 4.13 Images of the thermal contraction of a 0.2032 \varnothing mm/60mm silver element after current commutation (Slow speed video camera images)

equally to any disturbance stimuli to the wire caused by the effects of a.c. current wave shape, as indicated in the analysis of the dynamic behaviour of current-carrying wires. Thus, it is proposed that the observed 'kinetic wave motion', (Figure 4.13), is a consequence of the a.c. wave shape and the associated differential thermal expansion of the wire suspended in a medium confined only at its ends.

After the subsidence of the wave motion and lateral expansion, the observations indicated that the final disposition of the element above and below the initial horizontal plane is random. It follows that the force of a uniform section element pushing against the terminals will be compressive and will be diminished, in un-constricted media, by the element deforming

uniformly along its length, i.e. parabolically. The opposing forces would be those due to gravity, air friction and wire momentum as indicated in the appended analysis of the dynamic behaviour of wires. The interplay between thermal expansion of the wire and the height of the catenary when current is momentarily crow-barred is evidence by the captured time sequenced images (Figure 4.13).

Figure 4.14 shows the classical uniform formation of unduloids along a section of the wire's length.



Figure 4.14 Unduloid formations observed in the remnants of a 0.2032Ømm/60mm silver wire element, following current commutation 160ms after current initiation.

The observations of fully formed unduloids correlated with the geometrical disposition, shape and number observed by Nasilowski [44], hence, the observed unduloid formation modulus (λ) complied with his empirical relationship for the number of unduloids formed along the length of the wires (Eq. 2.6). It is clear from the captured images that unduloids do not form along the whole length of the wire because

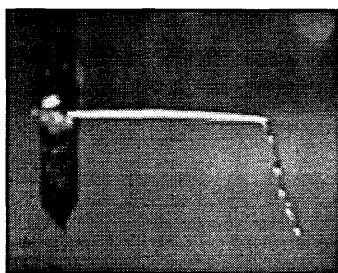


Figure 4.15 Image of fuse remnants indicating the location of a large temperature gradient (Slow speed video camera image).

of the cooling effect of the terminals (Figure 4.15). Logically, it is clear that when the main mass of the wire is close to melting the wire section close to the terminals, in being at a lower temperature, will be more solid. Given the physical difference in the state near the ends of the wire and the axial movement of the wire under the action of the sheer force component of the trapped compressive

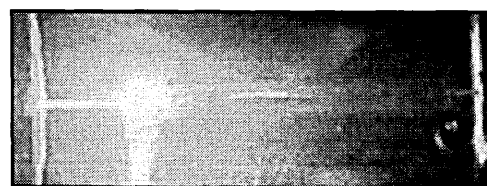
force (Appendix 11), the wire will, theoretically, sheer at the point of maximum stress and minimum weakness, as observed. The concentration of the stress at the semi-molten solid interface was confirmed by FE CAD techniques [77] (Appendix 12).

Following the sheering of the wire, the axial component of the compressive force will convert to an axial tensile force and the wire will move away from the terminal. The fall in the temperature of the wire, due to the fall in current, will cause the wire to contract rapidly as evidenced by the change in height of the catenary over a period of 40ms. Figure 4.13iii and 4.13iv. The combined contraction and tensile forces act on the unfixed ends of the wire to pull the wire apart and, therefore, to increase the rate the gap in the broken section of the wire increases. This increase in the rate is observed as a whip-like action that causes the longer end of the wire to fly past the terminal, (Figure 4.8).

In the samples studied the number of arc ignitions observed was significantly smaller than the number of unduloids. Consequently a relationship for the magnitude of fuse arc voltage based on empirical formulas for unduloid formation modulus [32] and element length are considered to be unsubstantiated for wire disrupted by current in air.

4.3.3 Additional Observations of the Influences of Component Forces acting about the Locations of Element Disintegration

Further indications of the strength and influence of gravitational force were obtained from the study of vertically-oriented wires in air. These observations indicated, (Figure 4.16), that element fragmentation and arc ignition still initiate close to terminals where large temperature gradients exist (Figure 4.16). Moreover, the longitudinal deformation of the element was observed still to be a highly symmetrical catenary (Figure 4.16i). It is considered, therefore, that the relegation of gravity as of second or third rank influence is justified.



(i) Initiation of disintegration at the bottom of the element (ii) Initiation of disintegration at the top of the element

Figure 4.16 Images of random element end cap connection location of disintegration in a vertically orientated 0.2032 \varnothing mm/60mm silver element (Camera rotated through 90°) (Medium speed video camera images)

It is of interest to note that the influence of gravitational force on the disruption mechanism although weak for straight short wires, became apparent from crow-bar

current observations of ‘ Ω ’ shaped wires, (Figure 4.17), as the gravitational force is sufficient to cause longer ‘ Ω ’ shaped wires to flip rapidly to ‘inverted Ω ’ shapes, before disruption occurs. The offered explanation, without proof, is that the gravitational force is significant but of a much lower order than the combined shear and tensile forces and, hence, influence on the disintegration of the wire. It is clear that the shape of the wire during heating is affected by gravity where wires are long and peculiarly shaped.

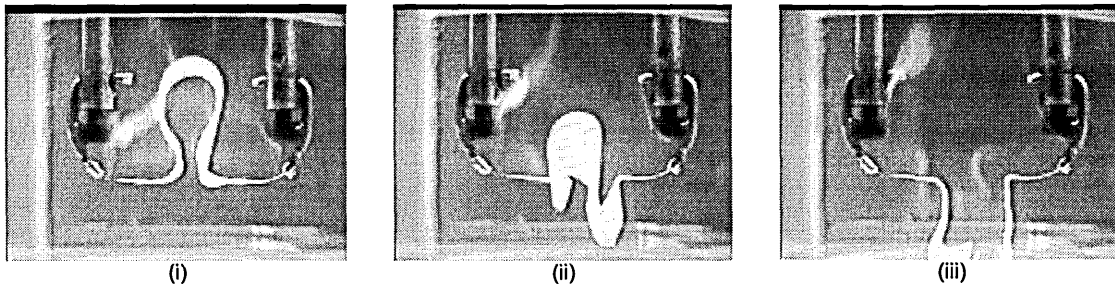
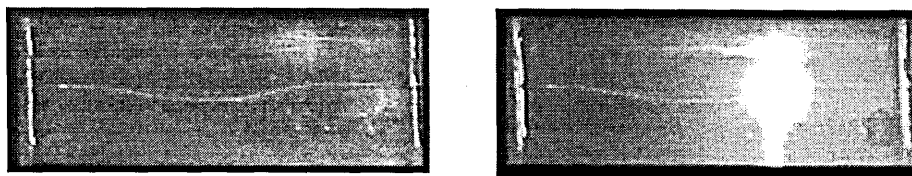


Figure 4.17 Images of axial movement of a 0.2032mm silver wire element indicating shear forces acting in the vicinity of the end cap element connection. (Slow speed video camera images)

4.3.4 Additional Observations of Proposed Influencing Phenomena on the Formation of Unduloids.

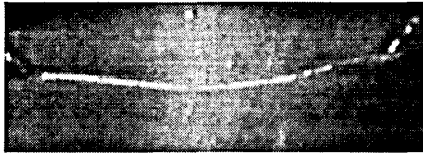
No unduloids were ever observed to form during investigations within the long time domain for copper wires in air or for copper or silver wires in water. However the location of the onset of disintegration without unduloids for the above conductor in air/water recurred towards the wire terminals and disintegration action remained ‘whip-like’ (Figures 4.18~1.19).



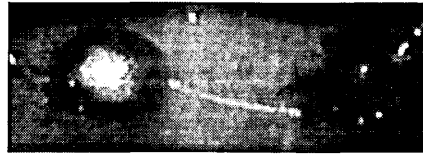
(i) Current carrying ‘catenary shaped’ element about 130ms after current application (Time =t)

(ii) Current carrying element with disintegration initiated in the vicinity of the element terminal (Time=t+1ms)

Figure 4.18 Sequenced images of the disintegration of a 0.2mm/60mm Copper wire suspended in air (Medium speed video camera images)



(i) Current carrying 'catenary shaped' element about 120ms after current application (Time = t)



(ii) Current carrying element with disintegration initiated in the vicinities of the connections to the element terminals (Time = t+1ms)

Figure 4.19 Sequenced images of the disintegration of a 0.2032Ømm/30mm Silver wire suspended in water (Medium speed video camera images)

The observations of continued evolution of unduloids, following the current in the wire being forced to zero, (Figure 4.5 and 4.30), were considered to be of significance, simply because they demonstrate that the electromagnetic pinch forces can play no role in the physical formation of unduloids and the necking of the space between for these test conditions and, hence, it would appear that the electromagnetic pinch forces have no effect on the disintegration of the current carrying wire. However, it is considered along with other research workers [45][37] that surface tension forces are dominant in the mechanism of unduloid formation but, again, electromagnetic forces are at most second rank. This contention is based on the observations of the influence of electromagnetic pinch forces of current carrying parallel wires (Figure 4.20~4.21) which indicated that only minimal attraction existed between parallel current carrying wires (Axial wire separation = 3mm) since longitudinal deformation of the wires initially occurred in the same direction and were subsequently seen to 'cross over'.



(i) Longitudinal deformation of current carrying parallel elements due to thermal expansion. No attraction of elements due to electromagnetic influence is indicated. (Slow video image about 40ms after current application)



(iii) Current carrying elements shown 'interweaving' about 120ms after current application.



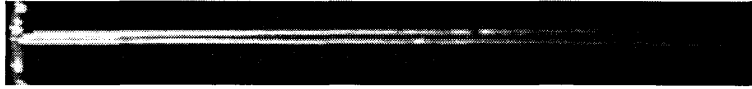
(ii) Current carrying elements shown 'interweaving' about 80ms after current application.



(iv) Fused elements after disintegration.

Figure 4.20 Sequenced images of parallel 0.2032Ømm/60mm silver wire elements (Axial element separation = 3mm) indicating the weak influence of electromagnetic forces and the dominance of thermal expansion forces (Slow speed video camera images)

Attraction between parallel elements was only observed when the elements were mounted with a minimal axial separation (<1mm). Subsequently the elements fused together, were catenary shaped and disintegrated towards one terminal.



(i) Parallel elements before current application (Axial element separation = 1mm)



(ii) Fused parallel elements indicating longitudinal element deformation due to thermal expansion about 120ms after current application



(iii) Fused parallel elements after disintegration

Figure 4.21 Sequenced images of parallel 0.2032 \varnothing mm/60mm silver wire elements (Axial element separation = 1mm) indicating the fusion of elements and familiar disintegration pattern (Slow speed video camera images)

4.3.5 Key Findings in the Investigation of Unduloid Formation in Wires Suspended in Unconfined Media.

- Vibrations in wires can be induced by periodic current waveforms.
- Longitudinal deformation of wires suspended in air is a significant phenomenon in the long time domain disintegration.
- Thermal expansion forces are considered to be significant in the causation of longitudinal deformation of the fuse element.
- Air, with the exception of a vacuum is proposed to allow maximum freedom of movement of the element and hence, minimal confinement of forces induced in the element due to thermal expansion.
- The time period for the formation of unduloids ($\approx 6\text{ms}$) is considered to be short when compared with the pre-disintegration time period ($\approx 150\text{ms}$).

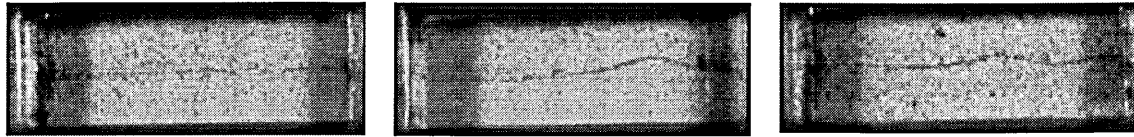
- Surface tension forces are indicated to be dominant and electromagnetic forces are at most considered second rank in the mechanism of unduloid formation.
- Axial element deformation, due to the formation of unduloids, has been observed to occur after the onset of element disintegration.
- The evolution of unduloids have been observed to continue after current zero, consequently observations of unduloid formations in fuse remnants challenges the postulation that element disintegration is a consequence of unduloid formation.
- Kinetic movement of the wire due to tensile forces and wire cooling after the perturbation of initial wire fragmentation is considered to be significant in progressing further wire fragmentation.
- Fragmentation and subsequent arc ignitions have been observed to be sequential.
- Identical 'whip-like' disintegration can occur in wires that do and do not produce unduloids Therefore, it is considered that the existence of unduloids in wires depends on the material type and the surrounding media, and hence formations are inconsistent.
- Nasilowski's empirical formulas for determining the magnitude of the peak arc voltage of wires in weakly confined surrounding media, based on the wire length and length of unduloid module has been shown to be not capable of substantiation.

4.3.6 Description of Temporal Observations of Disintegration of Conductive Film Substrate Fuses Immersed in Sand.

Fuse Element Longitudinal Deformation.

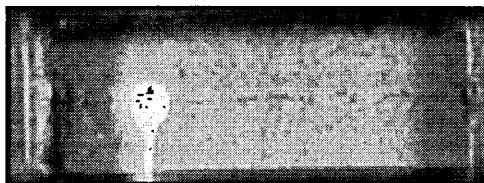
Virtually immediately following initiation of fault current conduction, longitudinal deformation of the wire was observed and subsequently seen to subside

within approximately ≈ 50 ms. In specific circumstances, longitudinal deformation of the element was observed to be random in shape (Figure 4.22).

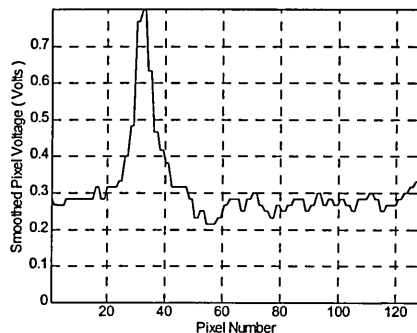


Current carrying 0.2032 \varnothing mm/25mm silver wire elements ≈ 50 ms after initiation of current conduction.

Figure 4.22 Images, captured during long time domain disintegration of conductive film substrate fuses, indicating the random shape of element longitudinal deformation (Medium speed video camera images)



(i) Current carrying 0.2032 \varnothing mm/25mm silver wire element embedded in fine quartz ≈ 93 ms after initiation of current conduction. (Medium speed video camera image)



(ii) Current carrying 0.2 \varnothing mm/25mm copper wire element embedded in fine quartz ≈ 90 ms after initiation of current conduction. (Fast speed video camera image) (Pixel pitch = 0.195mm)

Figure 4.23 Images, captured during long time domain disintegration of conductive film substrate fuses indicating the location of initial fragmentation of the fuse element.

Fuse Element Axial Deformation.

In most cases, no axial deformation of silver or copper wires was observed up to the onset of disintegration.

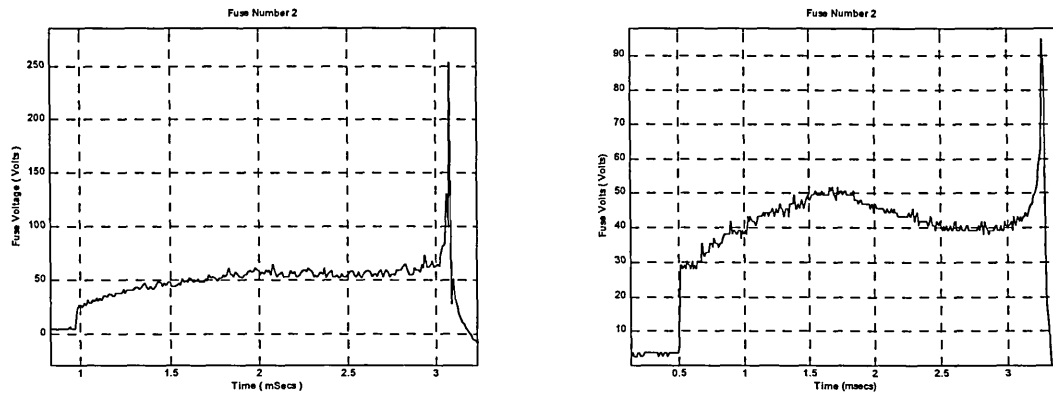
Fuse Element Disintegration.

Disintegration of the fuse element was most regularly ($>87\%$ of cases) observed to initiate in the vicinity of one of the wire terminals (Figure 4.23).

Following the onset of disintegration, no significant movement of the wire was observed.

Fuse Voltage Magnitude and Fuse Operation

The ignition of a single arc was observed in video images. This correlated with the fuse voltage oscillograms (Figure 4.24) which indicated a typical peak voltage of 50~60 volts with a rate of voltage rise ≈ 0.0146 v/ μ s.



(i) 0.2032Ømm/25 silver wire element. ($t_{pa} = 93.85\text{ms}$) (ii) 0.2Ømm/25mm copper wire element. ($t_{pa} = 89.8\text{ms}$)

Figure 4.24 Typical oscillograms of fuse voltage captured at the fragmentation instant of conductive film substrate fuse elements (Long time domain disintegration investigation)

The onset of wire disintegration occurred mainly at the instant at or about the peak a.c. fault current (Figure 4.25).

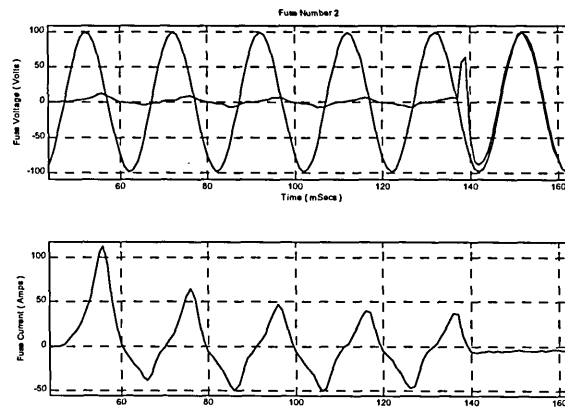


Figure 4.25 Typical oscillograms of fuse voltage and fuse current captured during long time domain fault current conduction Element: 0.2032Ømm/25mm silver wire, Filler: fine quartz.

4.3.7. Issues and Propositions Originating from Temporal Observations of Element Disintegration

From the observations of longitudinal deformation of wires immersed in sand, it is logical to propose in accordance with the postulations for wires in air and by analysis (Appendix 11), that the longitudinal deformation of the wire increases by thermal expansion due to Joulean heating. Similarly in this case, the full lateral expansion of the

wire is restricted by the physical barriers presented by the fuse end terminals, however, the surrounding sand filler additionally restricts the full expansion of the wire. Given that the compaction density of the sand and the size of the sand granules are not absolutely uniform, the sand, can, therefore be considered to be an inhomogeneous medium to free movement of the wire, and is referred to hereon as a confining medium. Therefore, it follows logically that the observed final random disposition of the wire is principally due to the differing degree of confinement provided by the sand filler along the length of the wire. Furthermore, as a consequence, the acute longitudinal deformation of the wire, due to thermal expansion, will occur at a location where the confining forces of the sand are weakest.

It is important to note that no axial deformation of the wires was temporally observed before the onset of disintegration. However, from observations of wire remnants slight axial deformation with propensity to spheroids at random locations along the wire length were seen. In most cases, however, the wire remnants were fragmented only at a single location where an indication of arcing was evident from fulgurite remains. Furthermore, observations were made of sand granules uniformly embedded in the surfaces of the wires, predominantly along the length of the wires except in the vicinities of the wire terminals. In these regions the wires remained in a pristine condition indicating little evidence of the effects of heating or deformation.

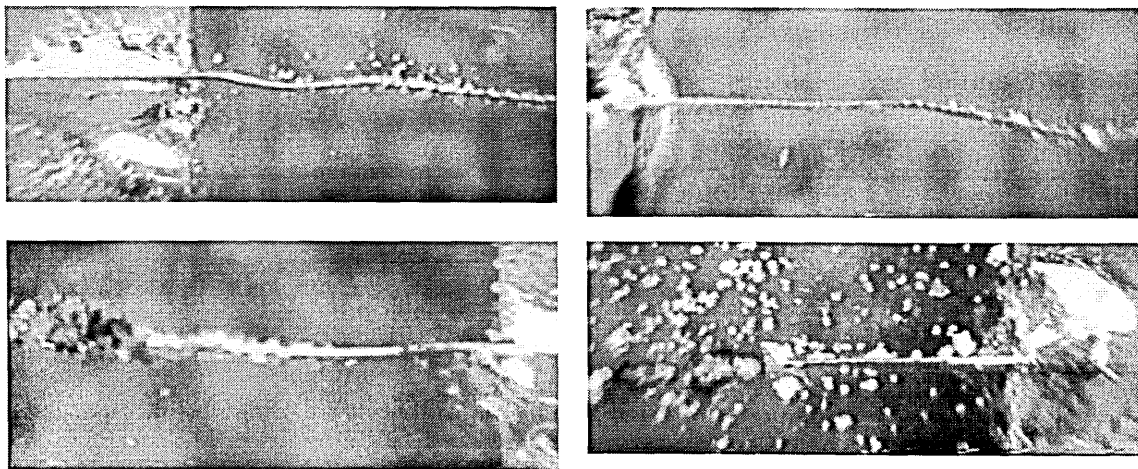


Figure 4.26 Images of element remnants indicating uniformly embedded quartz granules, minimal axial deformation of the element in the vicinity of the wire terminals and the location of arc ignition.

The observations clearly indicated the cooling effect of the wire terminals and it follows the existence of a large temperature gradient in this region. Logically the

wire should fracture at its weakest point, and therefore given the physical states of the wire and the trapped compressive stress in the wire, it is sensible to propose that this will occur close to a wire terminal, as observed.

Given that kinetic motions occur due to the transformation of compressive forces to tensile forces at the instant of disintegration were fundamental in the subsequent fragmentation of wires in air, it is therefore proposed that the confining force of the filler is responsible for the minimal fragmentation of the wire in this case. Moreover, the analysis of the force acting on a wire in a confined space (Appendix 11.6) indicates that the magnitude of the forces and trapped compressive stress are much greater than those for wires in an un-confined medium for similar current carrying conditions. This corresponds with the results of the experiments, which indicated that, for wires in sand the onset of disintegration occurred earlier in the heating process.

4.3.8 Key Findings in the Investigation of Disintegration of Wires Immersed in Confined Media.

- Longitudinal deformation of wires was evident in the long time domain disintegration of conductive film substrate fuses immersed in compacted sand.
- Thermal expansion forces are considered to be fundamental in the causation of longitudinal deformation and hence of disintegration.
- Sand fuse filler is proposed to restrict free movement of the element, and in doing so increases thermal expansion forces and hence increases the trapped compressive stress in fuse elements.
- The small longitudinal deformation of wires in compacted sand is probably due to the differential compaction density of the sand and the size of the sand granules.
- Since, prior to disintegration only historical evidence of unduloid tendency was observed, it is proposed that unduloid formations can occur but they are considered at most second rank to other above phenomena in the causation of element disintegration.

- The onset of disintegration was most frequently observed to initiate in the region of one of the wire terminals, where it is evidential that large temperature gradients existed.
- After the onset of disintegration it is proposed that the confining forces of the sand filler restrict physical movement of the element.
- The rate of increase in fuse voltage during the pre-peak arc voltage period was slow compared with the corresponding values for wires in air.

4.4 Conclusions of Disintegration in the Long Time Domain.

The formations of unduloids was found to be inconsistent since very precise control of the Joulean energy released into the element was required to obtain them. For wires suspended in air, incremental adjustment of the energy about the point where positive temporal observation of unduloids occurred, resulted in either element disintegration with no unduloid formations and minimal element fragmentation or alternatively element disintegration with increased fragmentation and the evolution of spheroids. It is argued that these observations support the proposition that the onset of disintegration is a consequence of thermal expansion forces and high trapped compressive stresses acting on wires at locations close to the fuse terminals. Since in this case confining forces are minimal, subsequent wire fragmentation, after the onset of disintegration, is a consequence of kinetic motion of the wire produced by tensile forces and wire cooling.

Over long time periods no temporal observations were made of unduloid formations in conductive film substrate fuses immersed in sand. Therefore it is proposed that a confining medium is significant in this respect and consequently unduloid formations are not significant in the disintegration of this type of fuse in this time domain. However, the mechanism of disintegration is still similar to that of wires in air, since the onset of disintegration always occurred in similar locations.

In conclusion all observations of disintegration in the long time domain support the proposition that the forces of thermal expansion are fundamental to the onset of disintegration for both types of fuse. Furthermore, kinetic movement of the wire after the onset of disintegration is fundamental to subsequent fragmentation of an unconfined wire.

4.5 Investigation of Disintegration in the Very Short Time Domain.

This study was designed to investigate the disintegration phenomena of wires subjected to short circuit fault currents where operation occurs typically between 3~20ms. From previous discussions (Subsection 2.2) of the classifications of disintegration, for this time domain the observed disintegration phenomena were expected to conform to the ‘striated’ arc formation classification. Therefore, multiple wire fragmentation and subsequent arcing were anticipated and since a significant improvement in fuse performance was expected this investigation was considered highly significant to the central objectives of the thesis.

In these studies wires were subjected to prospective currents (i_p) in the range 270~320 amps and for applied voltages in the range 200~240 volts. Forced current ‘crow bar’ commutation techniques were employed to study the disintegration prior to and following the onset of disintegration.

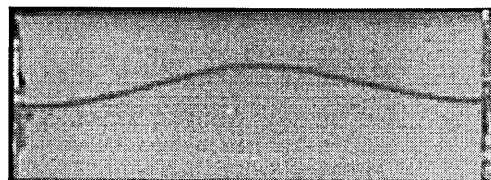
4.5.1 Temporal Observations of the Disintegration of Wires in Air

Fuse Element Longitudinal Deformation.

Virtually immediately following initiation of fault current conduction, longitudinal deformation of the wire was observed in all circumstances, and continued up to the onset of wire disintegration. Longitudinal deformation tended to be catenary in shape, as previously referred to and wire disposition with reference to the horizontal plane was observed to be random in direction (Figure 4.27).



(i) Catenary shaped current carrying 0.2032Ømm/30mm silver wire element with longitudinal disposition below the horizontal origin \approx 6.5ms after current initiation. ($I_p=320A$)



(ii) Catenary shaped current carrying 0.2032Ømm/30mm silver wire element with longitudinal disposition above the horizontal origin \approx 6.5ms after initiation of current conduction.

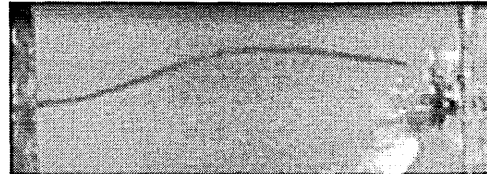
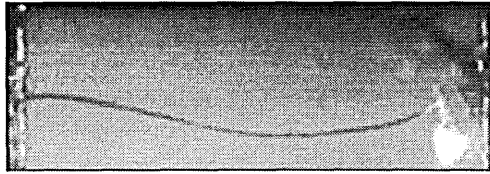
4.27 Images, captured during very short time domain disintegration for wires in air, indicating the random disposition of catenary shaped wires. (Medium speed video camera images)

Fuse Element Axial Deformation.

In most cases no axial deformation of the wires was observed up to the onset of disintegration of the wire.

Fuse Element Disintegration.

Disintegration of the wire was most frequently (>81% of cases) observed to initiate in the vicinities of the wire terminals (Figure 4.28).

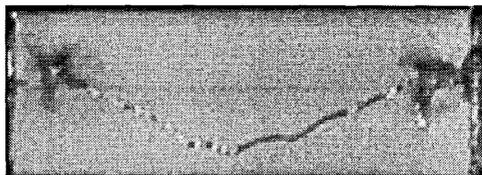


(i) Non current carrying 0.2032Ømm/30mm silver wire element. Current commutated about the onset of disintegration \approx 6.6ms after initiation of current conduction

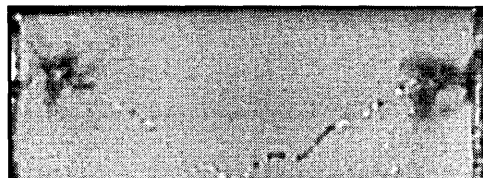
(ii) Non current carrying 0.2Ømm/30mm copper wire element. Current commutated about the onset of disintegration \approx 6.6ms after initiation of current conduction.

4.28 Images captured during very short time domain disintegration of wires in air showing the location of initial fragmentation of the fuse wire. (Medium speed video camera images)

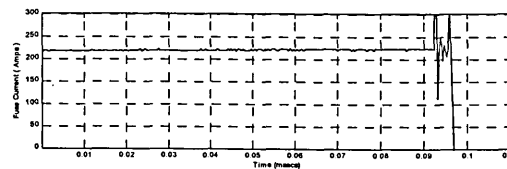
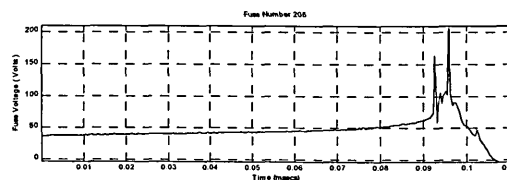
Following the onset of disintegration and subsequent immediate ‘crow-bar’ current commutation, the remnants of silver wires were observed to continue to fragment into a series of non-uniform segments.



(i) Non current carrying 0.2032Ømm/30mm silver wire element about 500µs after current commutation



(ii) Non current carrying 0.2032Ømm/30mm silver wire about 1ms after current commutation



(iii) Fuse voltage and current oscillogram

Figure 4.29 Sequenced images indicating continued wire fragmentation after forced current commutation and correlated fuse voltage and current oscillograms captured during very short time domain disintegration of wires in air. (Medium speed video camera images)

The remnants of copper wires were observed to evolve into spheroids (Figure 4.30).

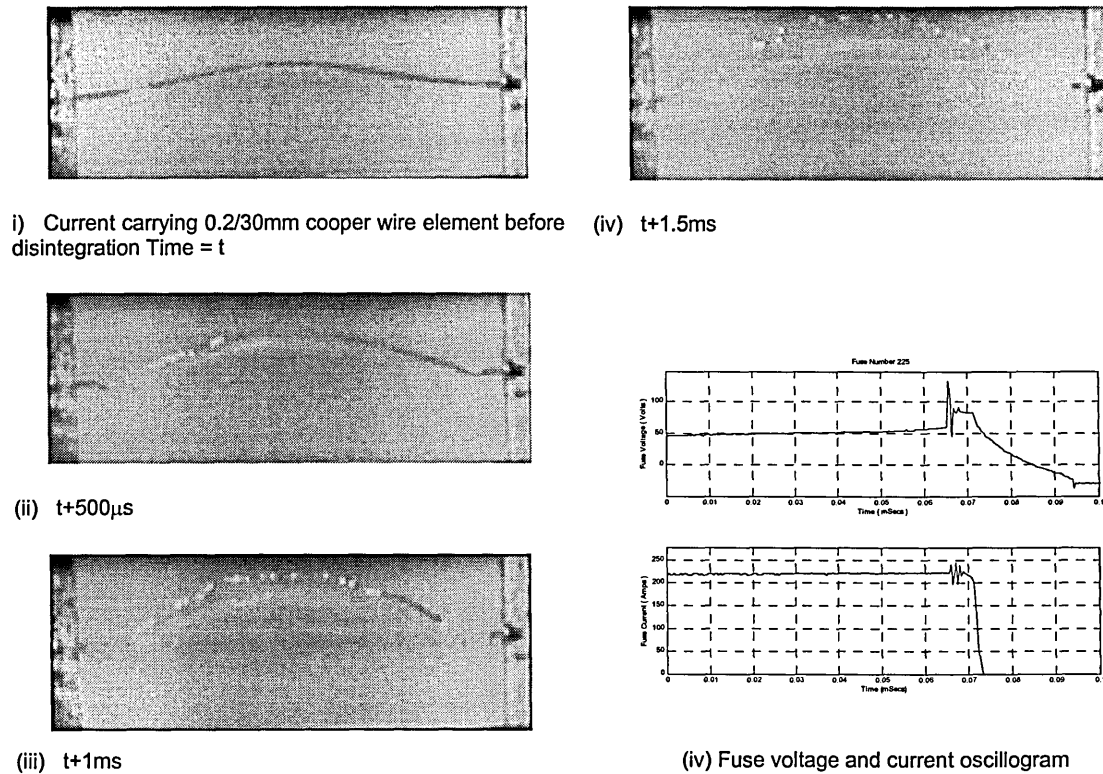


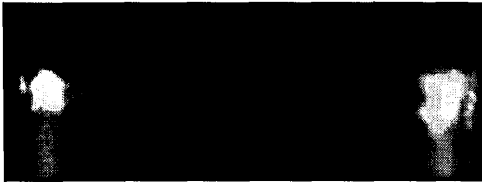
Figure 4.30 Sequenced images captured during very short time domain disintegration for wires in air, indicating the evolution of spheroids in non-current carrying copper wire remnants after forced current commutation (Medium speed video camera images).

These observations (Figure 4.29~4.30) are significant, and further support the propositions presented in Subsection 4.3.2, that unduloid formations are second rank in the mechanism of wire disintegration.

Fuse Voltage Magnitude and Fuse Operation.

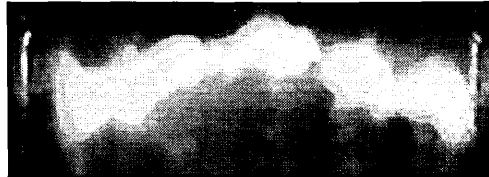
Observations of multiple sequential arc ignitions were indicated in video images (Figure 4.31i~iv), which correlated with fuse voltage oscillograms (Figure 4.31v~vi), and were consistent with the previous temporal observations of wire fragmentation. The number of arc ignitions was indeterminable from video images, however voltage oscillograms indicated the number to be in the range 8~12 from identification of electrode fall voltage discontinuities. The pre-peak arc voltage time period was typically $\approx 1\text{ms}$ and the rate of voltage rise $\approx 0.166\text{v}/\mu\text{s}$.

Fuse Number 148



(i) Time = t, Arc ignition in the location of the wire terminals (0.2032Ømm/60mm silver wire element, medium speed video camera images using optical attenuator)

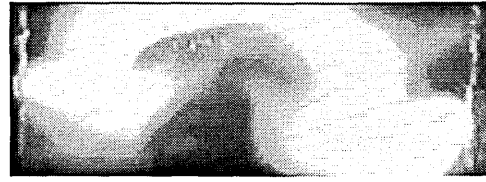
Fuse Number 150



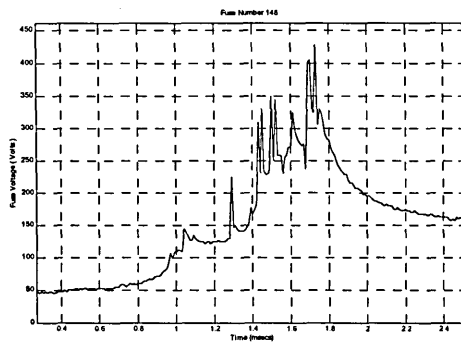
(iii) Time = t, Image indicating a series of short arcs. (0.2032Ømm/60mm silver wire element, medium speed video camera images using optical attenuator)



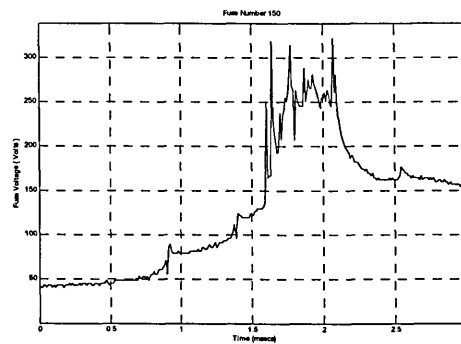
(ii) t+500µs



(iv) t+500µs



(v) Fuse voltage oscillogram

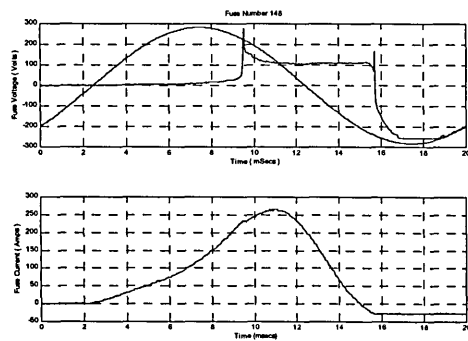


(vi) Fuse voltage oscillogram

Figure 4.31 Sequenced images of arcing and correlated fuse voltage and current oscillograms captured during very short time domain disintegration for wires in air, indicating sequential wire fragmentation and arc ignition

Given the number of series arcs and the time instant of the onset of disintegration, the effects of the current limiting action of the fuse is evident from the oscillograms (Figure 4.32).

Fuse Number 148



Fuse Number 150

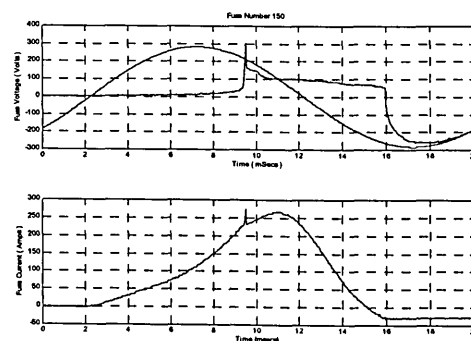


Figure 4.32 Oscillograms of fuse voltage and current captured during very short time domain disintegration of wires in air.

4.5.2 Issues and Propositions Originating from Temporal Observations of Element Disintegration.

It has been proposed that the forces of gravity and the confining medium are insignificant in the long time domain disintegration of wires in air. Observation of the random disposition of the wire above the horizontal origin and the catenary shaped longitudinal deformation in this investigation again support these notions and therefore it follows logically and from the analysis of the dynamic behaviour of current carrying wires up to the melting temperature (Appendix 11) that longitudinal deformation is a consequence of thermal expansion of the wire due to Joulean heating.

Significantly, no axial deformation of the wires was observed up to the onset of disintegration and historical observations of wire remnants indicated no evidence of axial deformation or the effects of heating in the vicinities of the wire terminals (Figure 4.33). Furthermore, in separate circumstances, sequential fragmentation of the wires was observed both during arcing and after current zero due to crow-barring of the current and notably unduloids were seen to form after current zero.

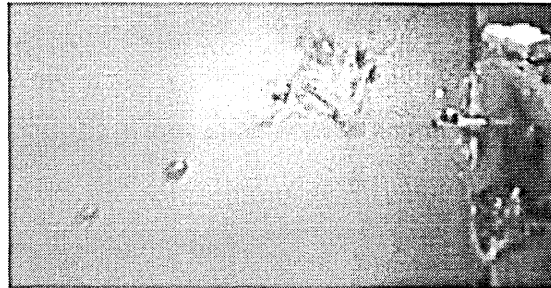


Figure 4.33 Image of fuse remnants indicating the minimal axial deformation of the wire in the vicinity of the end cap, the location of arc ignition, and wire fragmentation.

The observations again clearly indicate the cooling effect of the wire terminals and the temperature of the wire during disintegration and therefore in the vicinity of the wire terminals a large temperature gradient can again, reliably, be assumed to exist.

Axial motion of the wire induced by thermal expansion was observed up to the onset of disintegration, which was confirmed by FE CAD analysis of the displacement of a uniform conductor in the very short time domain (Appendix 12). Consequently, given the stress distribution in the wire and the temperature profile along the wire, it logically follows that disintegration will still occur in the vicinity of the wire terminal, which agrees with experimental observations.

Following the onset of disintegration, subsequent sequential fragmentation of the wire was observed during arcing and after current zero. Moreover, non current carrying wire remnants were regularly seen to fragment into non-uniform segments and then subsequently evolve into spheroids which indicate that surface tension force is a second rank phenomena in the mechanism of wire fragmentation. Therefore it is sensible to propose from observations and analysis that axial 'wave motion' emanating from rapid lateral expansion of the wire is fundamental in fragmentation of the wire.

4.5.3 Investigation Key Findings for Wires in Unconfined Media.

- Longitudinal deformation of the wire is evident in the very short time domain disintegration of wires in un-confined media.
- Thermal expansion forces are considered to be significant in the causation of longitudinal deformation of the wire.
- No significant observations were made of axial deformation of the wire prior to the onset of disintegration.
- Axial kinetic motion of the wire was evident up to the onset of disintegration and during wire fragmentation.
- The onset of disintegration was regularly observed to initiate in the location of one of the wire terminals, where a large temperature gradient is logically assumed to exist.
- Wire fragmentation and subsequent ignition of short arcs were sequential.
- Surface tension force is considered to be a second rank phenomenon in the very short time domain mechanism of wire fragmentation.

4.5.4 Temporal Observations of the Disintegration of Conductive Film Substrate Fuses Immersed in Sand

Fuse Element Longitudinal Deformation

Wire longitudinal deformation was observed immediately following application of fault current and continued up to the onset of wire disintegration. As with long time

domain disintegration of wires surrounded by sand, the observed shapes of deformation were random (Figure 4.34)



Current carrying 0.2032Ømm/25mm silver wire elements \approx 7.3ms after initiation of current conduction

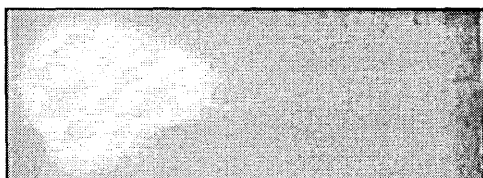
Figure 4.34 Images captured during very short time domain disintegration of conductive film substrate fuses, indicating the random shape of wire longitudinal deformation (Medium speed video camera images).

Fuse Element Axial Deformation.

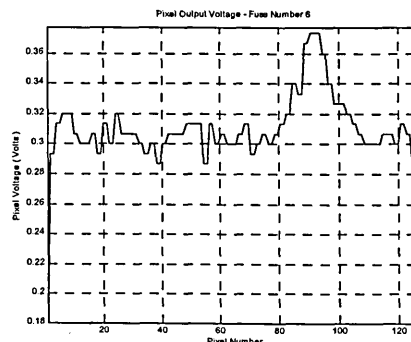
In many observations no axial deformation of silver or copper wires was observed before the onset of disintegration.

Fuse Element Disintegration.

Similar to previous observations, the onset of wire disintegration was most frequently (>70% of cases) observed to initiate towards one end of the wire (Figure 4.35).



Current carrying 0.2032Ømm/25mm silver wire element embedded in fine quartz \approx 7.4ms after initiation of current conduction (Medium speed video camera image)

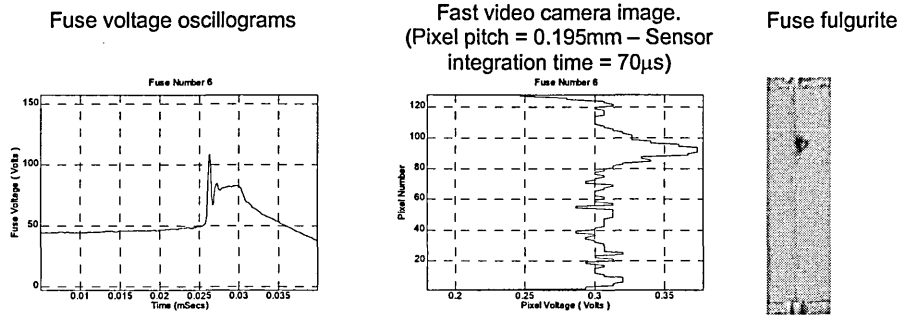


Current carrying 0.2Ømm/25mm copper wire element embedded in fine quartz \approx 7.4ms after initiation of current conduction (Fast speed video camera image) (Pixel pitch = 0.195mm)

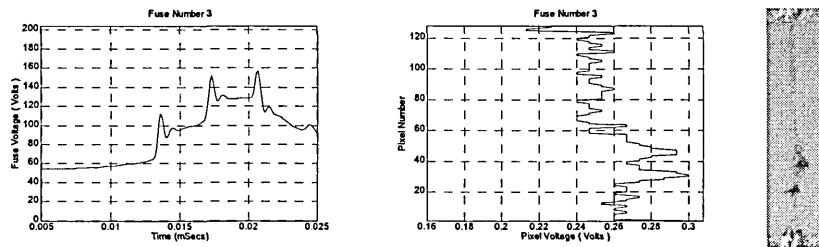
Figure 4.35 Images captured during very short time domain disintegration of conductive film substrate fuses indicating the location of initial fragmentation of the fuse wire.

Following the onset of disintegration, sequential fragmentation of the wire continued which was evidenced by the sequential ignition of a series of short arcs

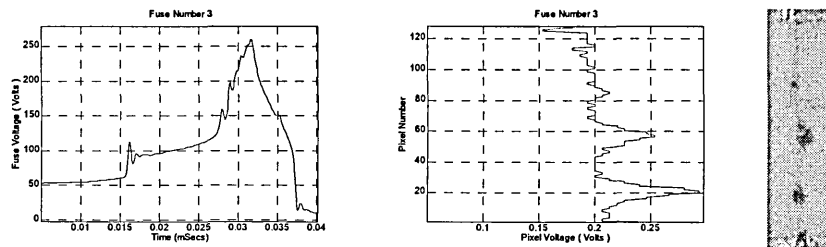
observed in video images. This was confirmed by correlation with fuse voltage oscillograms and commutated disintegration fulgurite evidence (Figure 4.36).



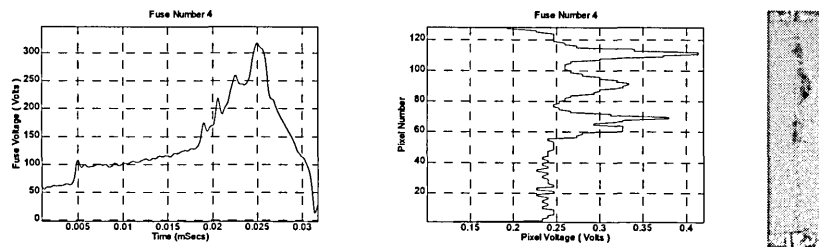
(i) Image indicating a single arc ignition in 0.2Ømm/25mm copper wire element



(ii) Image indicating two arc ignitions



(iii) Image indicating three arc ignitions

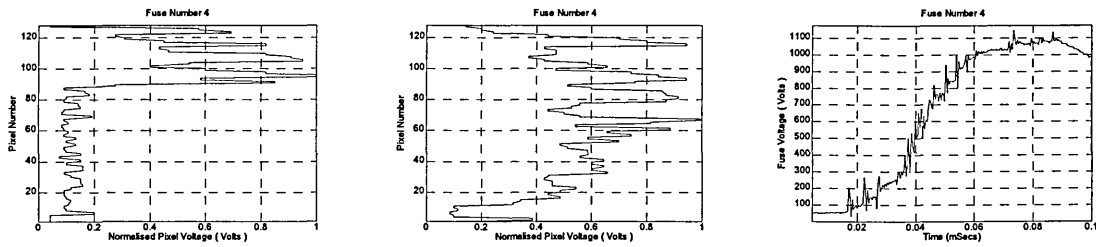


(iv) Image indicating four arc ignitions

Figure 4.36 Correlated video images, voltage oscillograms and images of fuse fulgurites which evidence wire fragmentation by sequential arc ignition during very short time domain disintegration of conductive film substrate fuses

Fuse Voltage Magnitude and Fuse Operation.

Further studies on the same wires were undertaken without the current commutation. In this case the observations indicated a series of short arc ignitions along the length of the wire (Figure 4.37).



- (i) Fast speed video image indicating sequential short arc ignitions taken about the onset of wire fragmentation. (Time = t)
- (ii) Fast speed video image indicating the temporal development of wire fragmentation evidenced by further short arc ignitions. (Time = t+30 μ s)
- (iii) Fuse voltage oscillogram, Element = 0.2 \varnothing mm/25mm copper wire, Filler = fine quartz.

Figure 4.37 Sequenced images and correlated voltage oscillographs indicating temporal development of wire fragmentation evidenced by the ignitions of a series of short arcs along the length of the wire.

Delayed current commutation was also employed to examine the progression of arc formation. In the case when the current was commutated about the instant of the peak arc voltage, inspection of fulgurites indicated that the whole of the wire had been consumed by arcing phenomena in the time period of arc ignition.

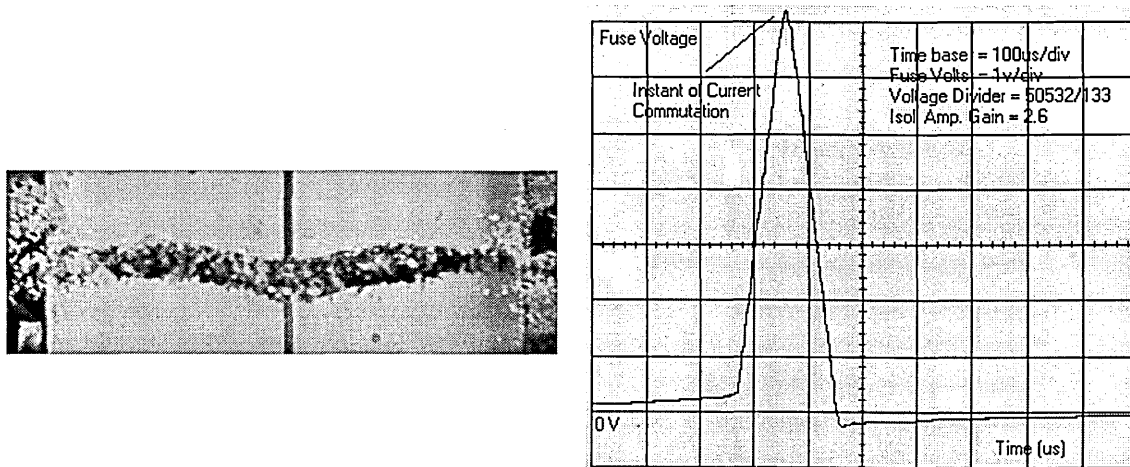


Figure 4.38 Image of fuse fulgurite and voltage oscillogram indicating the total dispersion of the fuse wire by arcing phenomena during the period of arc ignition, Element = 0.2 \varnothing mm/25mm copper wire, Filler = fine quartz.

A precise number of arc ignitions could not be determined from video images, voltage oscillograms or fulgurites. However, the peak arc voltage generally attained a value in the range 1000~1100 volts in a time period of $\approx 70\mu\text{s}$ (rate of voltage rise $\approx 15\text{v}/\mu\text{s}$), which would indicate an increased number of arcs relative to the corresponding tests on wires in air and given similar electrode fall phenomena. Therefore, fuse operation was observed to be significantly better in this case and the current limiting action of the fuse was clearly identifiable in oscillograms (Figure 4.39).

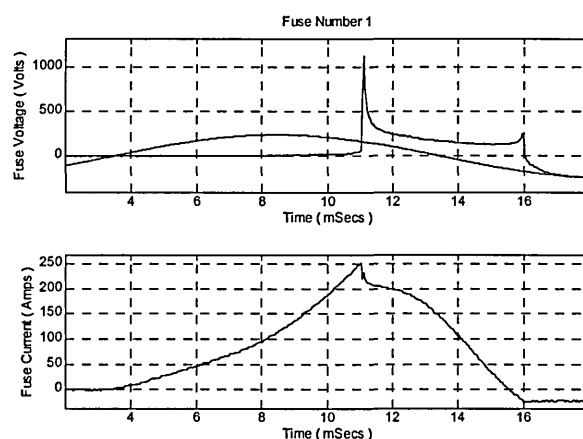
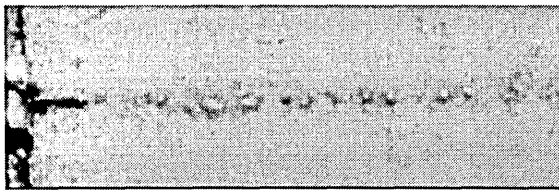


Figure 4.39 Typical oscillogram of conductive film substrate fuse voltage and current during very short time domain fault conditions, Element: 0.2 \varnothing mm/25mm copper wire, Filler: fine quartz.

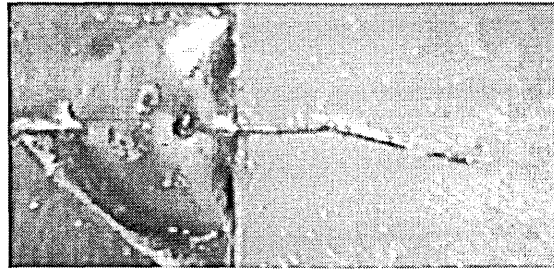
4.5.5 Issues and Propositions Originating from Temporal Observations of Wire Disintegration.

In accordance with the previous discussions of longitudinal deformation of the wire, the observations in this investigation still support the propositions that thermal expansion is fundamentally the causation of wire deformation and that the non uniform filler confining forces are the causation of the observed random shape of deformation.

Similar to the very short time domain case of wires in air, no transient axial deformation of the wire was observed before the onset of disintegration. However, after crow-barred commutation of the current, wire remnants were observed to comprise a series of spheroids or segments positioned along the former length of the wire except in the vicinities of the terminals where pristine wire 'stubs' remained indicating little evidence of deformation or melting.



(i) Spheroid remnants of 0.2Ømm/25mm copper wire



(ii) Segmented remnants of 0.2032Ømm/25mm silver wire

Figure 4.40 Images of spheroids and segmented sections of wire remnants and wire 'stubs' after current diversion

From the observations shown in Figure 4.40 the cooling influence of the wire terminals is still clearly identifiable and hence the observations of spheroids and segments of wires, the temperature profile of the wire can be reliably assumed. Consequently, this rationally indicates the location of a large temperature gradient in the vicinity of the wire terminal where the onset of disintegration was regularly observed to occur.

Following the onset of disintegration, the wire was observed to sequentially fragment. Since, surface tension forces have been identified as second rank in the very short time domain mechanism of the fragmentation of wires in air, then logically, this must be the case for wires in confined media, since the time period of wire disintegration has been observed to be shorter. Furthermore, due to the constricting medium it is logical that axial kinetic wave motion of the wire, which is proposed to be the causation phenomena for fragmentation of wires in un-confined media, would in this case be suppressed. Hence, at this point the causation phenomena for the fragmentation of a constricted wire remains undetermined.

4.5.6 Investigation Key Findings for Wires in Confined Media

- Longitudinal deformation of the wire was still observable in the very short time domain disintegration of conductive film substrate fuses immersed in sand.
- Thermal expansion forces are considered to be significant in the causation of longitudinal deformation of the wire.

- No significant observations were made of axial deformation of the wire before the onset of disintegration.
- Disintegration was regularly observed to initiate in the location of one of the wire terminals, where it is evident that a large temperature gradient exists.
- Wire fragmentation and subsequent ignition of short arcs were sequential.
- The rate of rise of fuse voltage was faster than for disintegration of wires in air.
- During the time period of arc ignition it was indicated that the whole of the fuse wire had been dispersed by arcing phenomena.

4.6 Conclusions of Very Short Time Domain Investigations of Disintegration.

Observations for both types of fuse have indicated that in the very short time domain the onset of disintegration regularly initiated in the location of a large temperature gradient towards one of the wire terminals. Therefore it is proposed that the forces of thermal expansion are fundamental to this phenomena and it is concluded that the very short time domain mechanism for the onset of disintegration for both types of fuse is similar.

For wires in unconfined media, kinetic wave motions have been observed to follow the onset of disintegration and hence it is concluded that this phenomenon is fundamental to subsequent wire fragmentation. However, for wires in a confined medium this phenomenon remains as yet undetermined.

Segmented disintegration of wires was observed and therefore it has been proposed that surface tension forces are at most a secondary phenomena in the mechanism of disintegration. Observations of classical striated 'banding' in fuse fulgurites were never obtained in these investigations for reasons given later, however it is reasonable to conclude that striated type disintegration occurred in these investigations and that in other circumstances, observations of fulgurite 'banding' could be a consequence of wave motion and subsequent prolonged arcing.

4.7 Chapter Conclusions.

Disintegration of the fuse wire and ignitions of short arcs have been observed in the pre-peak arc voltage time period for un-confined wire element fuses and wire element conductive film substrate fuses immersed in a confined medium. It is proposed on the basis of the observations and analysis that,

- Fundamentally, the mechanism for the onset of wire disintegration is similar in the time domains and for the types of fuses investigated.
- Rapid thermal expansion of the fuse wire element is considered to be a principal causation phenomenon of disintegration.
- Kinetic motion is a significant phenomenon in the subsequent fragmentation of un-confined wires after the onset of disintegration which is considered to be attributable to tensile forces, wire cooling, arc ignition forces and throw-off forces.

Chapter 5

Review and Evaluation of Further Experimental Observations of Fuse Element Disintegration and Arcing Phenomena, Project Summary and Conclusions.

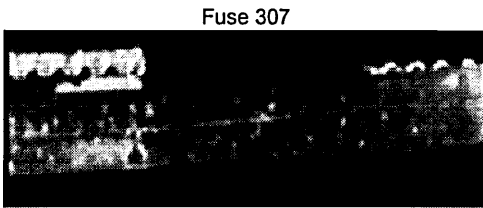
5.1 Introduction.

The special techniques and equipment developed to investigate the causation phenomena of fuse element disintegration, enabled further experimental investigations to be carried out to determine and quantify other fuse operation phenomena. Reviews and evaluations of these investigations are presented in this Chapter which together with a summary of the project, the recommendations and conclusions of the project, form the final Chapter of this Thesis.

5.2 Review of Observations to Determine the Causation Phenomena of Fuse Element Fragmentation in Confined Media in the Very Short Time Domain.

In an attempt to determine the causation phenomena of wire fragmentation in confined media, observations were made in the very short time domain (3ms~20ms) of the disintegration of wires encapsulated in epoxy resin. In this case it is proposed that the resin approaches a homogenous confining medium inhibiting longitudinal or axial deformation of the wire considerably in excess of that of compacted sand. This proposition was confirmed from the observations of the wire up to the onset of disintegration and arc ignition (Figures 5.1i and 5.1iv).

Following the initiation of disintegration and immediate crow-bar commutation of the current, the wire was observed to fragment into a series of segments (Figures 5.1ii and 5.1v) The wire remnants were then seen to rapidly move along the tube towards the initial location of disintegration and arc ignition and subsequently to evolve into spheroids within the remaining tube cast in the resin. It is interesting to note that the physical geometry of the spheroids appeared to be smaller than those observed in the remnants of similar wires immersed in sand.



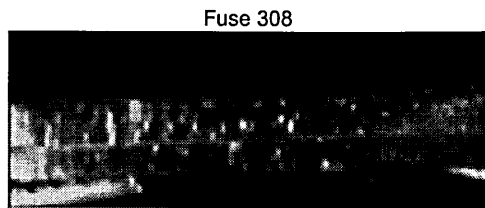
(i) Current carrying 0.2032Ømm/40mm Silver wire element embedded in epoxy resin (Time = t)



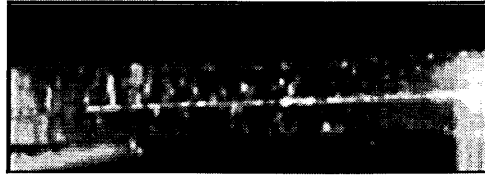
(ii) Current carrying wire about the instant of disintegration (Time = t+500µs)



(iii) Non current carrying wire after current diversion (Time = t+1ms)



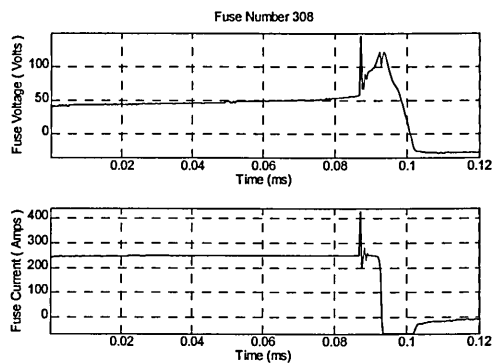
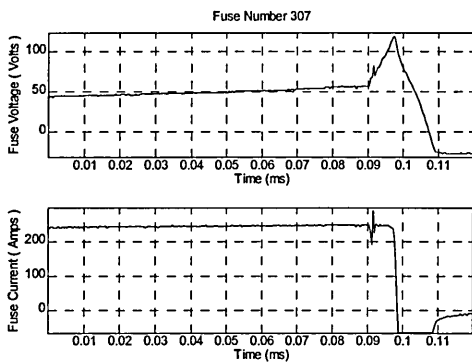
(iv) Current carrying 0.2032Ømm/40mm Silver wire element embedded in epoxy resin (Time = t)



(v) Current carrying wire about the instant of disintegration (Time = t+500µs)



(vi) Non current carrying wire after current diversion (Time = t+1ms)



(vii) Fuse voltage and current oscillograms

Figure 5.1 Sequenced video images and correlated voltage and current oscillograms which evidence temporal segmented fragmentation of a wire fuse element embedded in epoxy resin

5.2.1 Issues and Propositions Originating from Observations.

From the appended analysis of the dynamic behaviour of current carrying wires and Figures 5.1i~5.iv, it is argued that during Joule heating of the wire, the previously observed thermal expansion of the wire in this case will be much more constrained by the confining forces of the encapsulating epoxy resin filler and the fuse terminals. The compressive stresses in the wire have been shown by analysis (Appendix 11.6) to be

much increased for an encapsulated wire. However, it follows logically, that the confining forces of the encapsulating resin cannot be truly uniform along the length of the wire and totally restrict lateral expansion of the wire. Therefore, given a degree of lateral wire movement it is consistent to suggest that, at the instant of a discontinuity, the wires compressive stresses will be released. Consequently, at this instant kinetic movement of the wire will be initiated, as observed.

5.2.2 Key Findings of the Investigation of Very Short Time Domain Disintegration of Encapsulated Wires

- No observations were made of longitudinal or axial deformation of the wire before the onset of disintegration.
- Kinetic movement of the wire was observed after the onset of disintegration.
- The spherical remnants of the wire were physically smaller than those observed in the remnants of similar wires, which were immersed in sand.

5.2.3 Evaluation of the Phenomena of Wire Fragmentation in Confined Media in the Very Short Time Domain.

The previous investigation into the disintegration of encapsulated wires was carried out to aid evaluation of the causation phenomena of the fragmentation of wires immersed in confined media in the very short time domain. For resin encapsulated wires, observations were made of kinetic movement of the wire remnants after the onset of disintegration, therefore it is reasonable to assume that a similar phenomena occurs for wires immersed in sand and since spheroids were observed, which gives an indication of the physical state of the wire after the onset of disintegration, it is possible that a thermo-viscous kinetic wave could be responsible for the fragmentation of the wire. However, it is very important to indicate that notions of the phenomena of wire fragmentation is not firmly established from these observations due to the speed of data capturing equipment (frame speed = 500 μ s). These observations are addressed in later sections.

5.3 Review of Observations of the Extent of Fuse Element Fragmentation and Arcing due to the Forces of Wire Confinement.

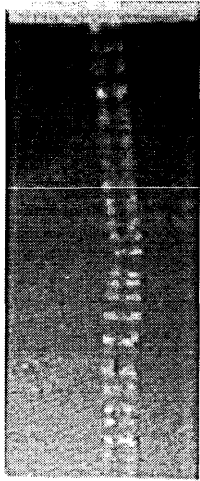
It is evident from the temporal observations of wire disintegration that the forces acting on a wire influence the extent of wire fragmentation and subsequent ignition of short arcs. From observations of the disintegration of wires in air, minimum element fragmentation occurred in the long time domain but considerable fragmentation of similar wires was observed in the very short time domain.

Increased fragmentation of encapsulated wires has been observed in the very short time domain. Although the extent of fragmentation was not quantifiable from observations, it was evident that the geometry of the fragments (spheroids) were physically smaller compared to the spheroids/unduloids observed in the remnants of corresponding disintegrated wires in un-confined media. From analysis (Appendix 13), it can be shown that the extent of fragmentation would differ for the two media, however, it is important to recall that surface tension force is second rank in the mechanism of wire fragmentation and consequently the observations could be misleading due to the speed of the data capturing equipment (frame speed = 500 μ s).

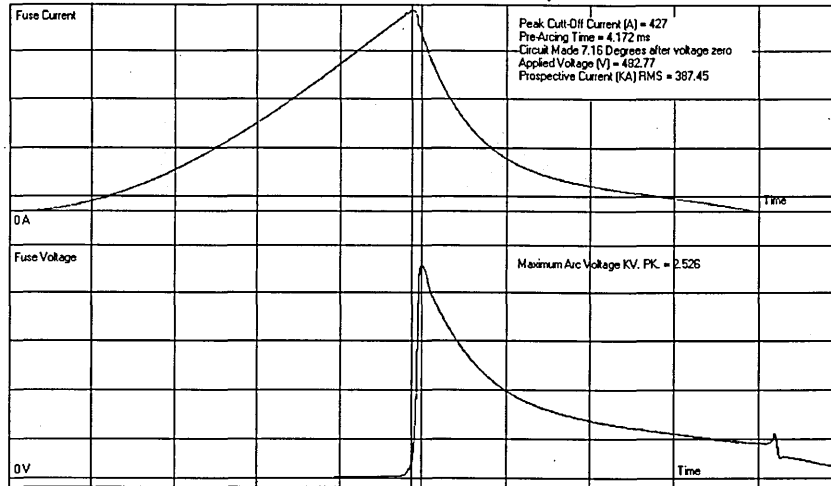
Similarly, for each filler medium, the number of short arc ignitions has been observed to increase between the two time domains and, in the same time domain, for it to increase for un-confined and confined media. Therefore, all the observations indicate that the extent of wire fragmentation and arcing is directly related to the degree of wire confinement and hence, it would be expected that the number of indicated arc ignitions in fulgurites would be greater for fuses constructed with quartz sand fillers of different compaction densities.

Figure 5.42 displays fuse voltage and current oscillograms and striated fulgurite X-rays of fuse remnants which were constructed with a 0.254 \varnothing mm/50mm single silver wire embedded in fine quartz and also in a hydrographically bonded fine quartz filler. The data was obtained from tests undertaken at an ASTA certified fuse test station where the fuses were operated under equivalent (I2 BS-88) test duties. The fuse fulgurites for these tests show that the number of indicated arc ignitions are similar for both fuse types, but in the case of the fuse with bonded filler the measured peak arc voltage was approximately double that of the fuse with non-bonded filler.

Circumstance 1. 0.254 \varnothing mm/50mm silver element embedded in fine quartz filler

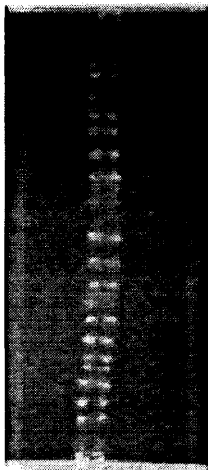


(i) X-ray of fuse remnants indicating \approx 26 short arc ignitions

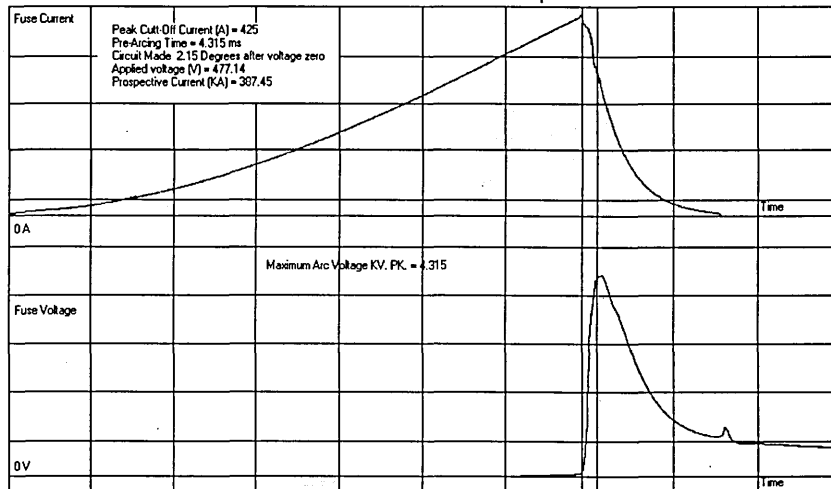


(ii) Fuse current and voltage oscillographs

Circumstance 2. 0.254 \varnothing mm/50mm silver element bonded in fine quartz filler



(iii) X-ray of fuse remnants indicating \approx 27 short arc ignitions



(iv) Fuse current and voltage oscillographs

Figure 5.2 X-rays of fuse remnants and correlated fuse current and voltage oscillograms for fuses constructed with fillers of different compaction density.

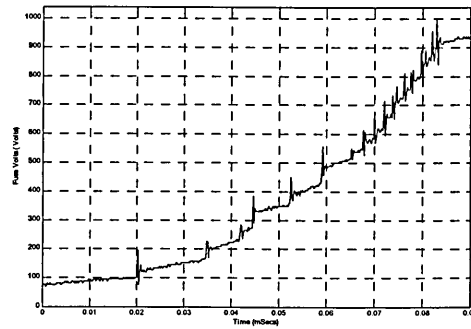
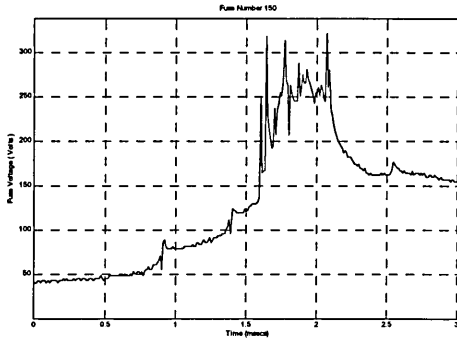
5.3.1 Evaluation of the Observations of the Extent of Wire Fragmentation and Arcing due to the Forces of Wire Confinement.

From the ASTA test results it is confirmed that the difference in the fuse voltages is primarily due to an increase in arc electrode fall voltage as these results correspond with and support the work of Gomez [10], who determined the number of arcs by experiment and simulated the fuse arc ignition process by primarily justifying different values of electrode fall voltage for different fillers.

The contention between the observations of this project and the ASTA test results, are, however perplexing. In the very short time domain for a confined wire, from analysis and observations it would be logical to suggest that, if the magnitude of the wire's trapped stresses greatly exceed the strength of the wire, an explosion, and hence, a shock wave type disruption of the wire would occur. If so, prior to disruption maximum forces would exert at the anti-nodes of the standing wave, and on disintegration the wire would fragment at these points producing striated pattern type disruption as observed in the ASTA tests fulgurites. Logically, the frequency of the standing wave is directly related to the magnitude of the trapped stresses in the wire and therefore an increased number of indicated arcs would have been expected. Therefore, it is concluded that some other factor must have a bearing on the extent of fragmentation and arcing in wires immersed in sand. The factor is shock wave and hence frequency and pattern related and therefore to conclude this discussion it has been suggested by the director of this project Professor Peter M. McEwan that a granular filler, irrespective of compaction density, attenuates the frequency dependent mechanism of striation whereas encapsulated (elastic type medium) appears to amplify it.

5.4 Review of Observations of the Rate of Rise of Fuse Arc Ignition Voltage due to the Forces of Wire Confinement.

The rate of rise of fuse voltage has been observed to increase relative to the forces of confinement. Furthermore, the appearance of the voltage waveforms during the pre-peak arc voltage time periods for the very short time domain investigations, were characteristically, 'S' shaped and indicated that element fragmentation evidenced by arc electrode fall discontinuities could follow a regular pattern. The time periods between the initial arc ignitions were relatively long compared with the shorter equal time periods between subsequent arc ignitions (Figure 5.43).



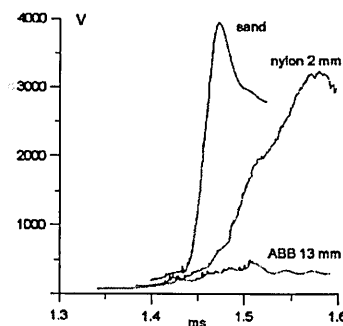
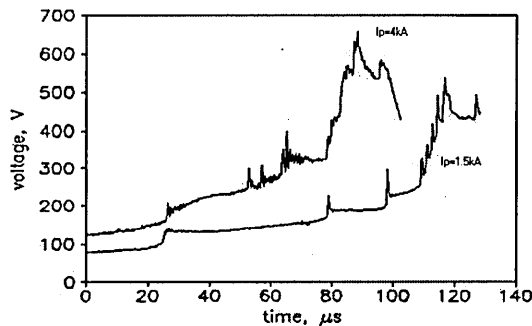
- (i) 0.2032 \varnothing mm/60mm silver wire element suspended in air (ii) 0.1524 \varnothing mm/30mm silver wire element embedded in fine quartz

Figure 5.3 Fuse voltage oscillograms inditing the characteristic 'S' shaped pattern of disintegration

5.4.1 Evaluation of the observations of the Rate of Rise of Fuse Arc Ignition Voltage due to the Forces of Wire Confinement.

Gomez [10], in his investigation of arcing mechanisms assumed that the time period between sequential arc ignitions was constant. However, the fuse voltage oscillograms (Figure 5.3) indicate this proposition to be at best approximate. The sequential ignition of arcs has been confirmed for some test samples and reported in this investigation (Subsection 4.3.1 and 4.5.4).

The effect of confinement on the rate of rise of fuse arc ignition voltage was also investigated by Wolny [78] who concluded that the shape of the voltage waveform is related to arc pressure and deformation of the fuse element, which is associated with the rising temperature of the element segments within the confining medium (Figure 5.4).



- (i) Variance of the rate of rise of fuse voltage relative to current density – Element = 0.36 \varnothing mm/50mm copper wire-filler = 13 \varnothing mm ABB tube. (ii) Variance of the rate of rise of fuse voltage relative to element confinement. Element = 0.36 \varnothing mm/50mm copper wire $I_p=2.2kA$

Figure 5.4 Fuse voltage oscillograms presented by Wolny[19][78] indicating the variance of the rate of rise of fuse voltage relative to current density and element confinement during the disintegration of wire fuse elements.

Similar notions were also presented by Lipski [52] who suggested that the striated fulgurite ‘banding’ evidence of the fuse arc ignition process is accountable to arc ignition forces balanced by electromagnetic pinch forces.

Observations from this investigation however suggest that the shape of the voltage waveform could be related to a shock wave or kinetic wave motion of the wire after the onset of disintegration. Therefore, it logically follows from observations and analysis that the rate of fuse voltage rise is related to the magnitude of the trapped stresses in the wire at the discontinuity of initial disintegration, which is fundamentally related to confining forces.

5.5 Review of Experimental Observations of the Temporal Development of Disintegration and Arcing in Conductive Film Substrate Fuses.

Classical notions of the temporal development of arcing in HBC fuses are based on the shape of the fuse voltage waveform. For short circuit fault current levels it is proposed that a series of multiple short arc ignitions occur during the initial phase of fuse element disintegration. This phenomena has previously been confirmed in these investigations and consequently the steep voltage rise of the fuse waveform has been accounted for.

However, following the instant of the peak arc voltage the temporal development of disintegration and arcing during the post-peak arc voltage period remains undetermined. During this period the fuse voltage for an effective fuse reduces, initially very quickly before slowing down in the latter part. Classically, it is accepted that merging of adjacent short arcs occur and that the falling voltage is fundamentally due to the loss of electrode fall voltage components and arc elongation.

This section of the Chapter presents observations from the investigation of the temporal development of arcing during the post-peak arc voltage period, which was carried out with the intention to confirm the phenomena accountable for the reducing fuse voltage waveform.

5.5.1 Observations of Arcing Phenomena about the Peak Arc Voltage Instant.

Previous observations of arcing in wire element conductive film substrate fuses immersed in sand during the pre-peak arc voltage period, have shown, that at the time instant of the peak arc voltage, a fulgurite has formed along the entire former length of the fuse wire element (Figure 4.37). Logically, this indicates that the whole of the fuse

element has been consumed by arcing phenomena in this time period which is also confirmed by observations of arcing in short and medium notch elements of conductive film substrate fuses immersed in sand.

Circumstance 1

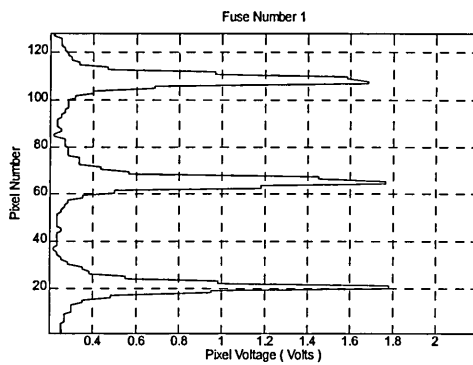


(Fig 5.5i) Short notch element embedded in fine quartz about 500 μ s after the instant of arc ignition (Time = t1) (Fast speed video images)

Circumstance 2



(Fig 5.5vi) Medium notch element embedded in fine quartz about 500 μ s after the instant of arc ignition (Time = t1) (Medium speed video images)

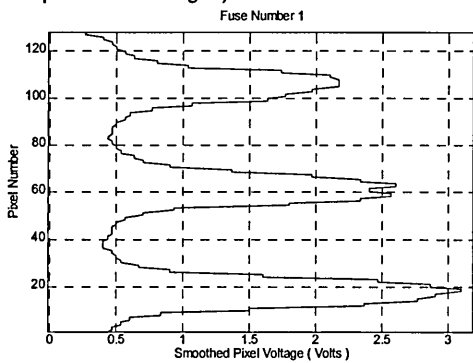


(Fig 5.5ii) Time t2 = t1+500 μ s

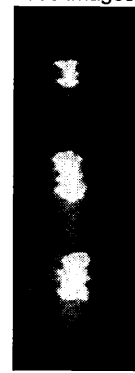


(Fig 5.5vii) Time t2 = t1+500 μ s

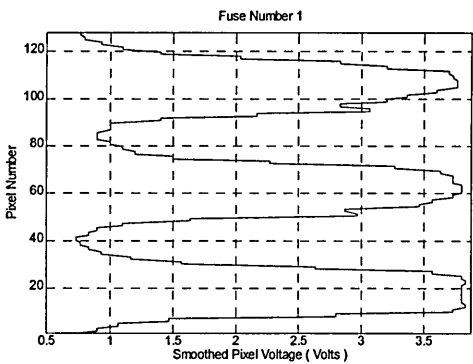


(Fig 5.5iii) Time t3 = t1+1ms

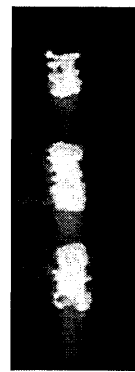


(Fig 5.5viii) Time t3 = t1+1ms

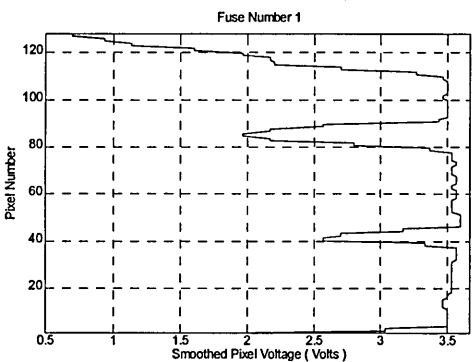


(Fig 5.5iv) Time t4 = t1+1.5ms



(Fig 5.5ix) Time t4 = t1+1.5ms

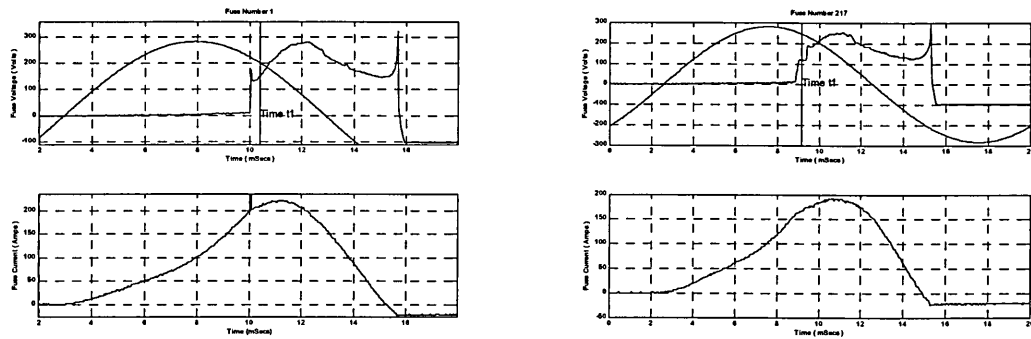


(Fig 5.5ix) Fuse voltage and current oscillograms

Figure 5.5 Sequenced images indicating the development of arcing during the pre-peak arc voltage period and correlated fuse voltage and current oscillograms captured during disintegration in short notch element conductive film substrate fuses.

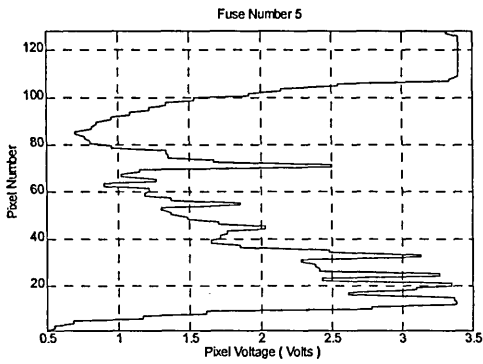
From these observations of arcing phenomena up to the instant of the peak arc voltage begs the question, **at the instant the element material separating adjacent arcs is eroded, do two arcs merge to form one longer arc?**

Classical notions suggest the arcs merge and therefore the following investigations were carried out in an attempt to confirm whether this happens during the very short time domain disintegration of conductive film substrate fuses.

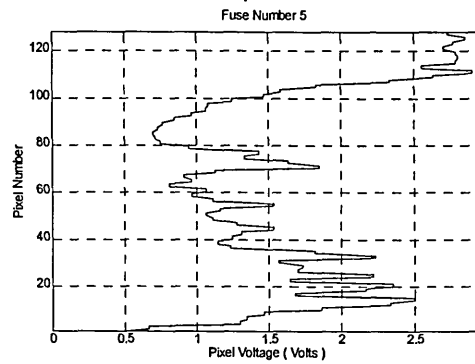
5.5.2 Observations of Post-Peak Arc Voltage Period Arcing Phenomena

To investigate the phenomena of arc merger the fast speed video camera was used to capture sequenced images immediately after the peak arc voltage instant during the disintegration of wire element fuses immersed in sand. It was expected that arc merger would be indicated by the observation of adjacent peaks in foremost images continuing to form a single peak in a subsequent images. Figure 5.6 displays typical images captured 100 μ s and 200 μ s after the peak arc voltage instant.

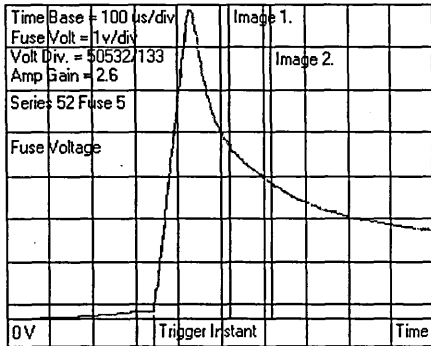
Circumstance 1 – 0.2mm \varnothing /25mm copper element embedded in fine quartz filler



(i) Image captured 100 μ s after the instant of the peak arc voltage

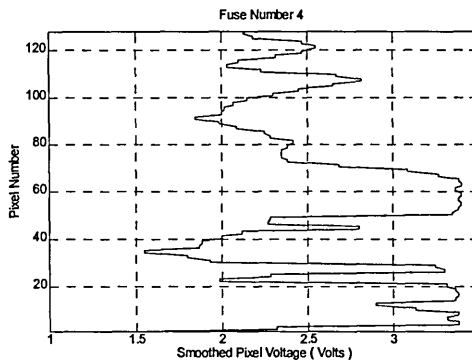


(ii) Image captured 200 μ s after the instant of the peak arc voltage

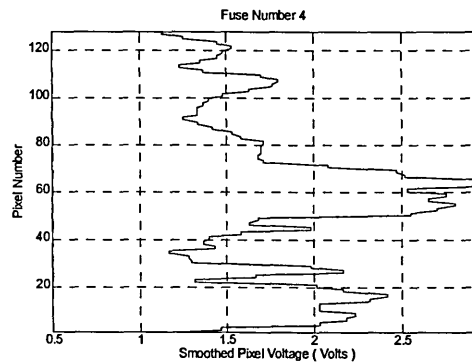


(iii) Circumstance 1 : Fuse voltage oscillogram

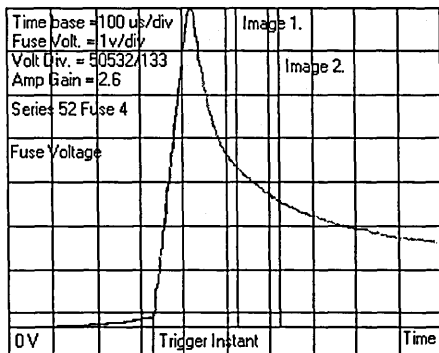
Circumstance 2 – 0.2 \varnothing /25mm copper element embedded in fine quartz filler



(iv) Image captured 100 μ s after the instant of the peak arc voltage



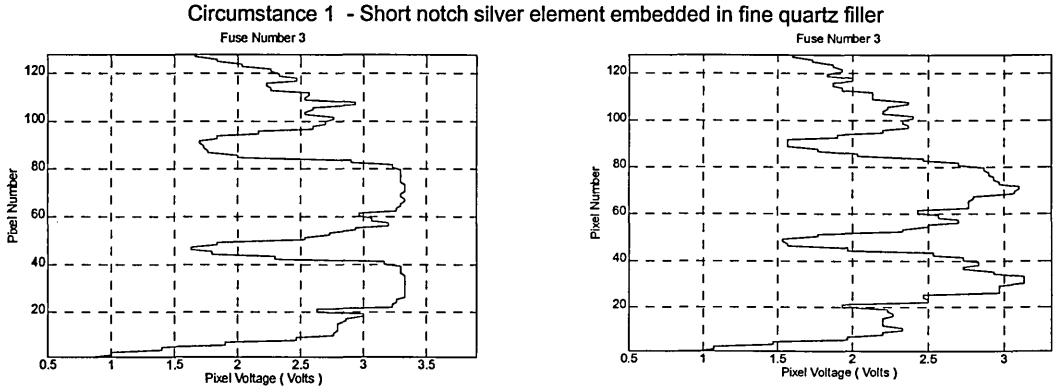
(v) Image captured 200 μ s after the instant of the peak arc voltage



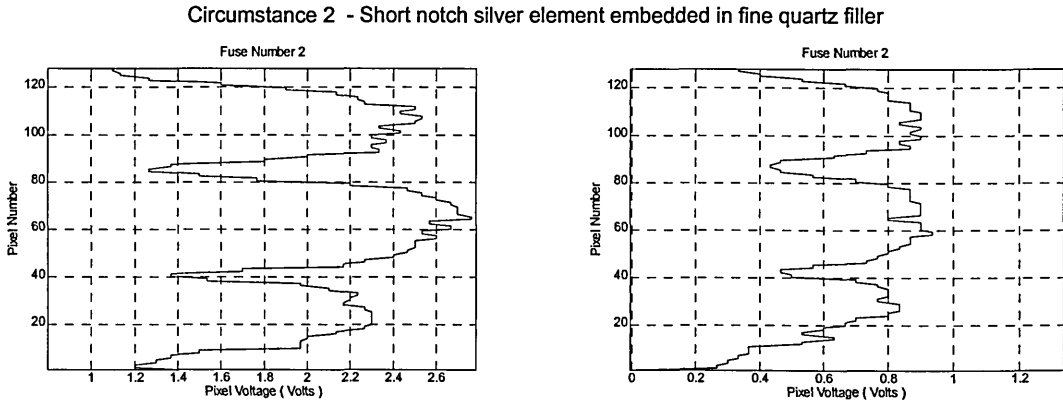
(vi) Circumstance 2 : Fuse voltage oscillogram

Figure 5.6 Sequenced images indicating arcing phenomena in the post-peak arc voltage period and correlated fuse voltage oscillographs captured during disintegration in wire element conductive film substrate fuses

Observations from many repeated tests were similar to those of Figure 5.6, and indicated no transient longitudinal displacement of light sources in the captured images, which was contrary to expectations. It was noticed that, latter images always appeared strikingly similar to the preceding image. However, a reduction in the sensor pixel output voltage indicative of reduced radiating light energy was always observed. Similar observations were also obtained from images captured during the post-peak arc voltage period of short-notched element fuse disintegration.



(i) Image captured about the peak arc voltage (Time = t) (ii) Image captured 1ms after the peak arc voltage (Time = t + 1ms)



(iii) Image captured 2ms after the peak arc voltage (Time = t + 2ms) (iv) Image captured 3ms after the peak arc voltage (Time = t + 3ms)

Figure 5.7 Sequenced images indicating arcing phenomena in the post-peak arc voltage period of disintegration in short notched conductive film substrate fuses

5.5.3 Issues Originating from Post-Peak Arc Voltage Period Observations

The observations of arcing during the post-peak arc voltage period would suggest that the phenomenon of arc merger does not occur. Furthermore fast speed high resolution fuse voltage oscillographs also support this proposition, since negative going discontinuities were never observed during this time period which logically would indicate the loss of an electrode fall voltage component and arc merger, just as the observation of a positive going discontinuity indicates the confirmed new arc ignition in the pre-peak arc voltage time period..

These observations are contrary to all previous studies and notions of arcing since they suggest that multiple arcs burn continuously during the post peak arc voltage time period and, if this were the case, to comply with the captured voltage oscillograms the average arc voltage component must reduce to a level below that previously determined to support an arc [20]. Consequently, these results generated in-depth analysis of the experimental techniques used to obtain the images.

It was considered that several phenomena could have inadvertently been the cause of the previous observations, viz:

- Image phenomena - The luminescence of the background fulgurite or the deterioration of the foreground substrate may be masking the light radiating from the arc.
- Electronic hardware phenomena - The charge retention of data by sensor pixels between sample windows was not valid.
- Fuse construction phenomena - The possibility that the substrate commutates the fault current during fuse operation.

Subsequently, systematic investigations were carried out to evaluate the effects of each phenomenon on the data capturing techniques, which are briefly discussed in the next section.

5.5.4 Image Phenomena.

In this investigation, arcing phenomena in conductive film fuses immersed in water were observed (Figure 5.8), again using the fast speed video camera. Logically in these circumstances the effects of fulgurite luminescence would be eliminated.

The captured images indicated that in this case, the phenomena of arc merger could occur since in the transition between in Figure 5.8i to 5.8ii the central light source obviously disappears. This perspective is further supported by observations of negative going discontinuities in the correlated fuse voltage oscillogram (Figure 5.8iii). Significantly, successive images captured in the latter part of the arcing period (Figure 5.8vi and 5.8vii) indicated differences in the location of light radiating from the fuse relative to the longitudinal axis which would suggest arc elongation, contrary to sand-filled fuse observations.

Circumstance 1

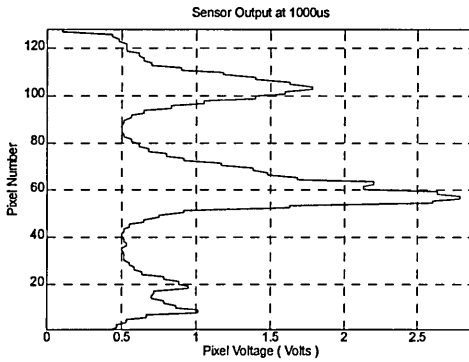


(Fig 5.8i) Image indicating the presence of 3 arcs (Image captured about 1ms after the onset of disintegration) (Time = t1)

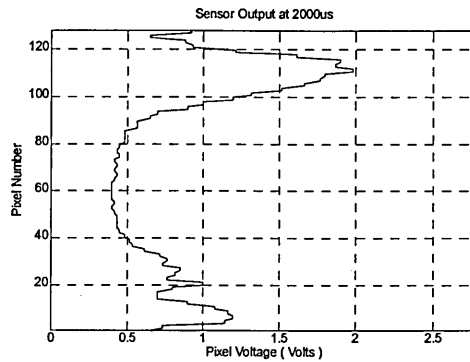


(Fig 5.8ii) Image indicating a reduction in the number of arcs (Time = t1+ 1ms)

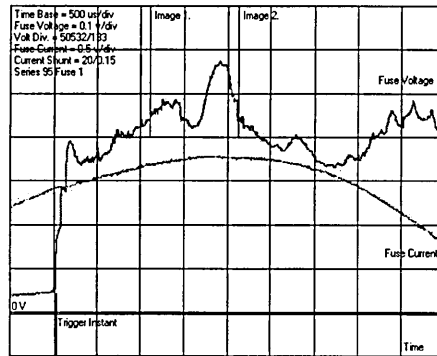


(Fig 5.8iii) Fuse voltage oscillogram

Circumstance 2

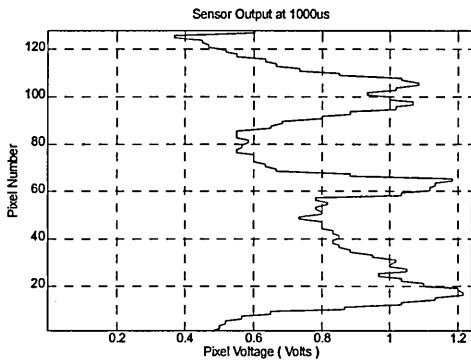


(Fig 5.8iv) Image indicating the presence of 2 arcs (Image captured about 1ms after the onset of disintegration) (Time = t2)

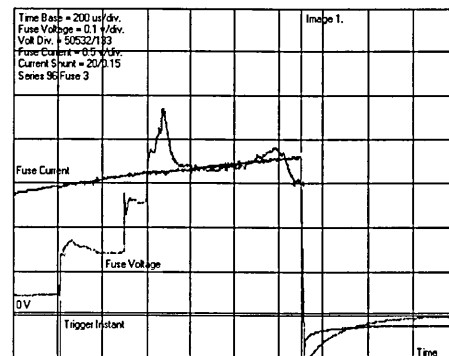


(Fig 5.8v) Fuse voltage oscillogram

Circumstance 3

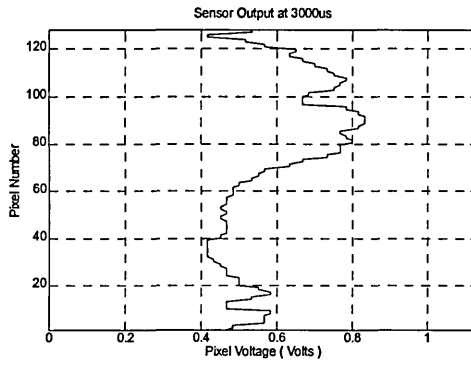


(Fig 5.8vi) Image indicating long arc activity between element 'stubs'. (Image captured about 3ms after the onset of disintegration) (Time = t 3)

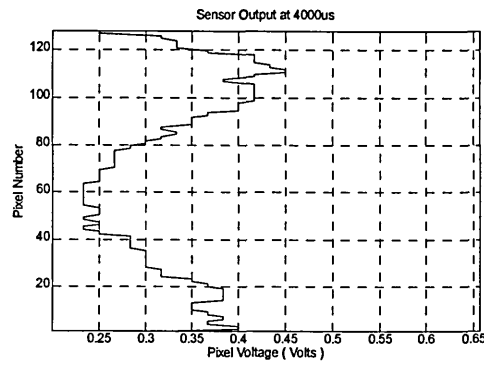


(Fig 5.8vii) Image indicating continued long arc activity between element 'stubs'. arcs (Image captured about 4ms after the onset of disintegration) (Time = t3+1ms)

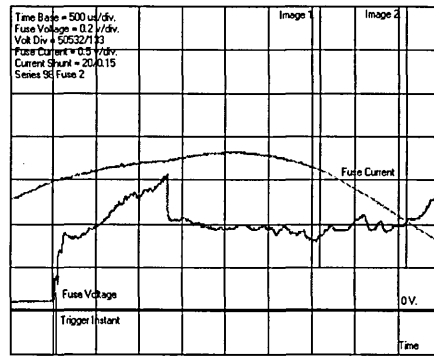


(Fig 5.8viii) Fuse voltage oscillogram

Figure 5.8 Sequenced images indicating arcing phenomena and correlated voltage oscillograms of disintegration in short notch conductive film substrate fuse elements suspended in water.

In conclusion, since arc merging is possibly indicated, both in images and in voltage oscillograms, it was thought rational to eliminate the deterioration of the substrate as a viewing medium and the causation of image phenomena. Furthermore, the integrity of the images captured transiently during the latter part of the arcing period are partially confirmed by this investigation. However, elimination of fulgurite luminescence as the causation of the previous puzzling observations of arcing in sand could not be discounted simply because of the different filler media.

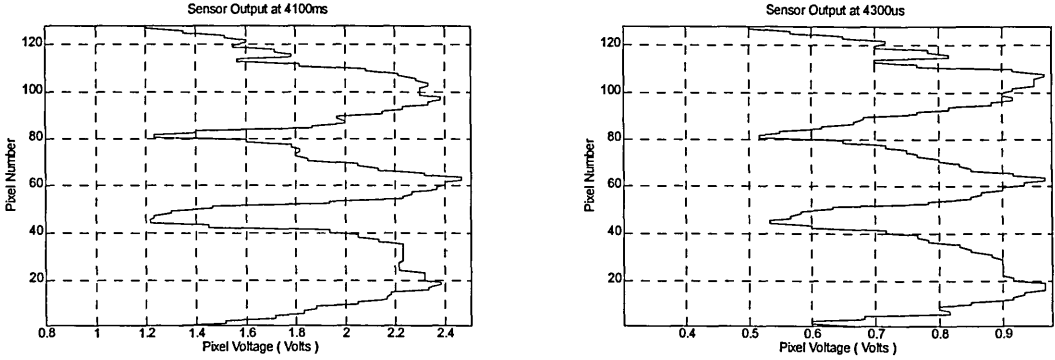
5.5.5 Arc Light Hysteresis.

A supplementary investigation to the latter was carried out to establish the significance of fulgurite luminescence in captured sequential images of arcing in sand. Fundamentally, a rate of decay of light radiation was established which hereon is referred to as 'arc light hysteresis'. The investigation involved capturing two images

either side of an instant of crow-barred fault current diversion in the post-peak arc voltage period. Consequently, it was reasonable to assume that arcing phenomena would be ongoing at the time of the first image, whilst in the second image post arcing phenomena would be indicated.

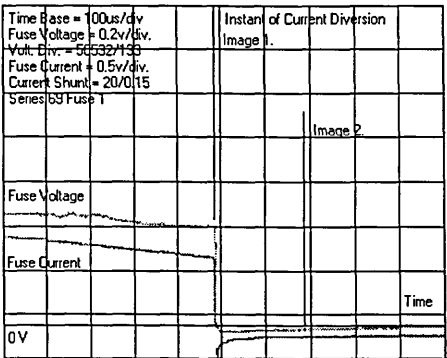
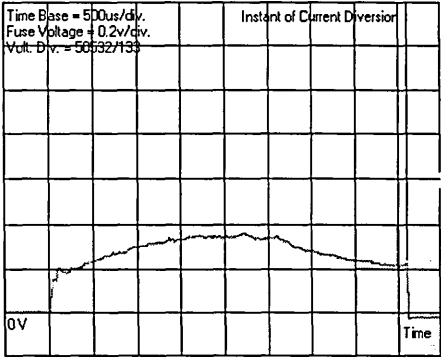
The ratio of light radiation between successive images of equal sample period about the instant of current diversion was generally <0.5 .

Current diversion initiated at 4.1ms after the onset on disintegration - Short notch silver element – Fine quartz filler



(i) Image captured about 4.1ms after the onset of disintegration (Time = t)

(ii) Image captured about 4.3ms after the onset of disintegration (Time = t+200μs)



(iii) Fuse voltage and current oscillograms

Figure 5.9 Sequenced images indicating the light radiating from a short notch conductive film substrate fuse and correlated fuse voltage and current oscillogram captured about the instant of fault current diversion.

These observations initially indicated that light radiating from fuse components i.e. the sand filler could be significant and that observation of arcing phenomena was not possible with the image data capturing equipment.

However, in circumstances where the fault current was not crow-barred, images captured with the same sample period and at the same time instant in the period of disintegration of similar fuses, indicated that the ratio of light radiation was typically \approx

0.8. The difference in the decay of light radiation (0.8~0.5) could rationally be accounted for in the crow-bar tests due to the absence of liberated arc energy at the capture time of the second image and consequently fulgurite luminescence could present a solution to the previous puzzling observations of arcing phenomena. However, even if fulgurite luminescence was a significant factor, the initial observations of arcing phenomena were still baffling since, to comply with classical notions of post peak arc voltage arcing phenomena some longitudinal displacement of light sources in the fulgurite should have been indicated in successive images. Moreover, because of the observations of negative going discontinuities in fuse voltage oscillograms for the circumstances of arcing in water it is reasonable to question why these were not observed in voltage oscillograms captured during the operation of sand filled fuses. Therefore, it was sensible at this stage to conclude that arcing phenomena in sand in the post-peak arc voltage period remained unconfirmed.

5.5.6 Electronic Hardware Phenomena.

To establish if captured images retained some degree of trapped data from preceding capture windows, an investigation was carried out using pattern-encoded wheels, similar to the arrangements used in commissioning tests of the fast speed video camera (Subsection 3.5.4.5). A degree of ‘image lag’ was determined by capturing two data samples of equal time duration . The first sample was captured during a patterned light sequence and immediately following this, a second sample was captured during a period of darkness. A typical sample sequence is shown in Figure 5.10.

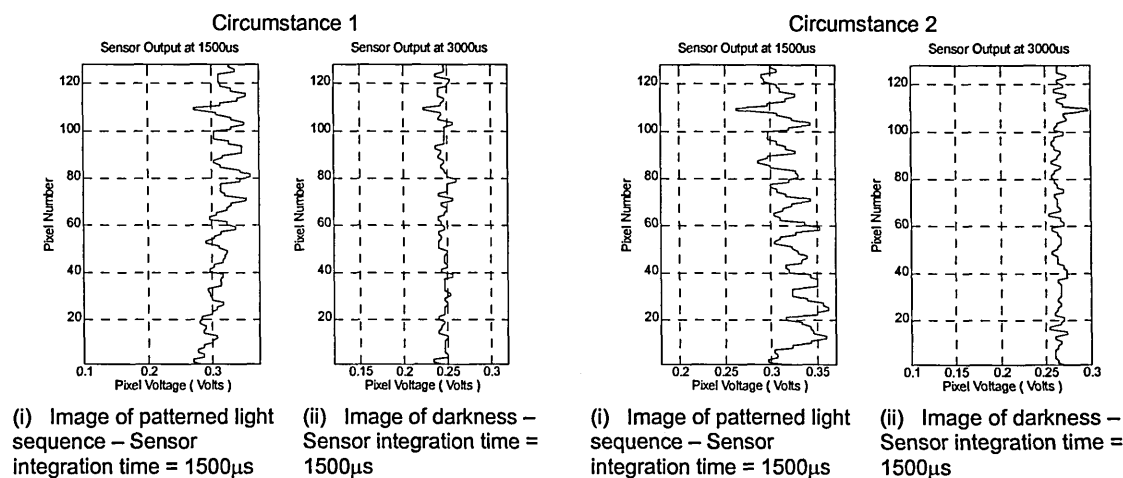


Figure 5.10 Sequenced images of patterned light /darkness captured during the investigation to establish the degree of image lag for the fast video camera.

It was established that the degree of image lag was small and in the region of 5% [79] and therefore justifiable to eliminate this phenomena as the causation of the perplexing observations of arcing phenomena in conductive film substrate fuses immersed in sand.

5.5.7 Fuse Construction Phenomena.

It was a concern of the arcing phenomena investigation, that during fuse operation the substrate may commutate the fault current and hence transform the phenomena of fuse operation. To evaluate this, additional sample fuses were used with the wire totally embedded in sand to compare operational circumstances.

The fuse voltage and current oscillograms (Figure 5.11), indicated only very slight differences for the two fuse types which, in essence, were that the arc ignition current was marginally higher and the pre-peak arc voltage period marginally shorter for the conductive film substrate fuse.

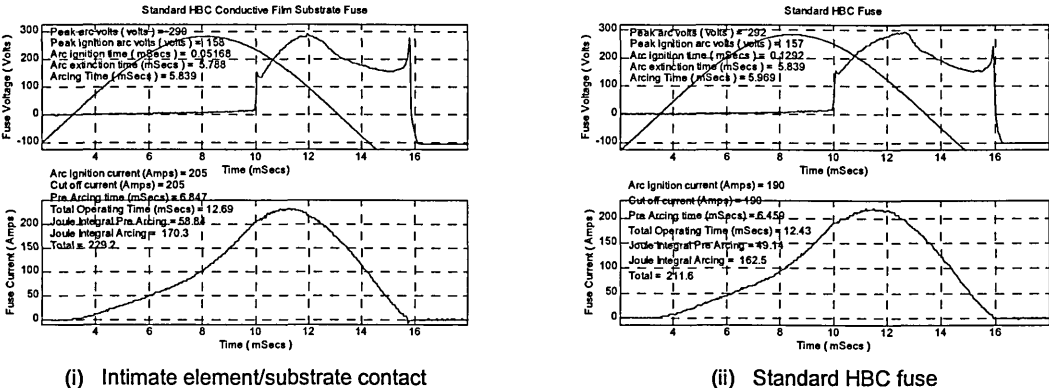


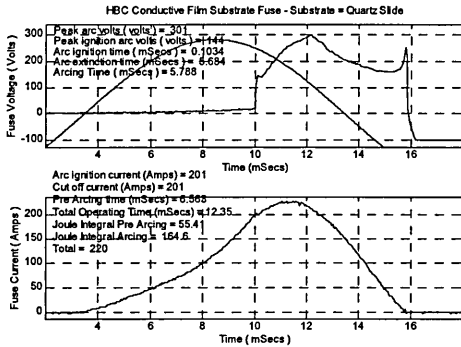
Figure 5.11 Fuse voltage and current oscillograms captured during the investigation of the substrate influence on arcing phenomena in the post-peak arc voltage time period.

From these observations it is reasonable to eliminate substrate commutation of the fault current, during the pre-arcing period only, due to the very low electrical conductivity of the substrates used and from comparison of the oscillograms, given that they were very similar in this time region. Moreover, it was rationally assumed that the slight differences in arcing indicated were due to the cooling influence (higher arc ignition current) and constraint of arc axial expansion (shorter pre-peak arc voltage period) by the substrate for the conductive film substrate fuse type.

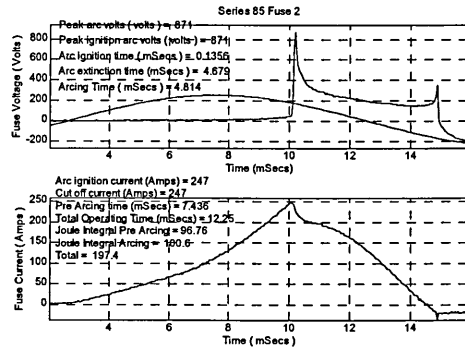
Despite the forgoing justifications, the observations do not discount the possibility that the substrate commutated the fault current during the arcing period. To

aid evaluation of this phenomena a separate series of tests were carried out using ‘type 2 glass’ as the substrate. The oscillograms captured for these fuse samples were similar to those of the fuses constructed with ‘type 1’ glass substrate. Furthermore, the sequential images of arcing phenomena similarly indicated no difference in light radiating from the fuse relative to the longitudinal axis and also similarly indicated a reduction in sensor output voltages between successive images.

Circumstance 1. Short notch silver element –Type 2 glass substrate – fine quartz filler



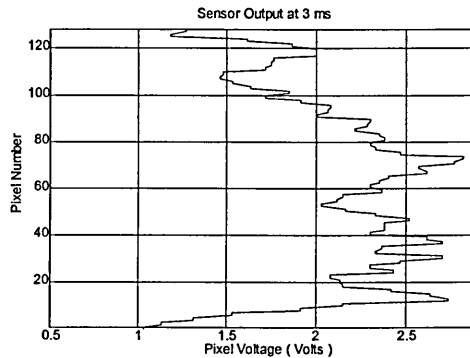
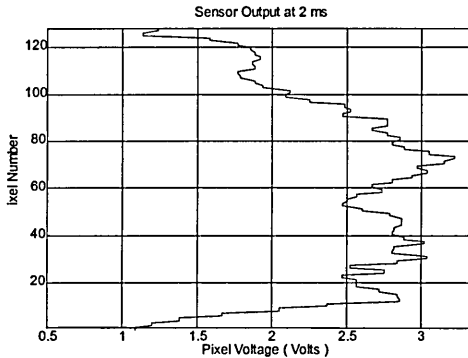
Circumstance 2. 0.2mmØ/25mm Copper wire element – Type 2 glass substrate – fine quartz filler



(i) Fuse voltage and current oscillograms

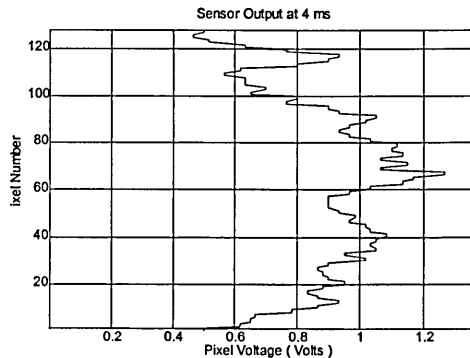
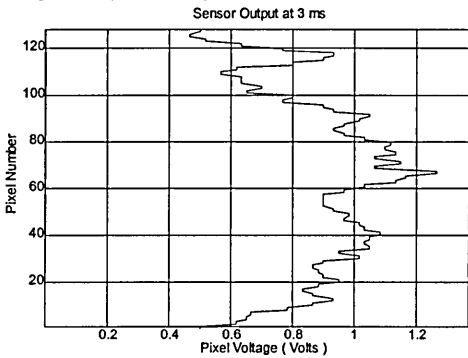
(ii) Fuse voltage and current oscillograms

Circumstance 2. 0.2mmØ/25mm Copper wire element –Type 2 glass substrate – fine quartz filler



(iii) Image captured about 2ms after the onset of disintegration (Time = t1)

(iv) Image captured about 3ms after the onset of disintegration (Time = t1+1000us)



(v) Image captured about 3ms after the onset of disintegration (Time = t2)

(vi) Image captured about 4ms after the onset of disintegration (Time = t2+1000us)

Figure 5.12 Sequenced images indicating arcing phenomena and correlated fuse voltage and current oscillograms captured during the post-peak arc voltage period of disintegration in conductive film substrate fuses (Type 2 glass substrate).

In conclusion the results from this supplementary investigation were also considered inconclusive to eliminate the phenomena of substrate conduction during the arcing period because of their similarity to the 'type 1' glass substrate observations.

5.5.8 Proposition of Fault Current Commutation by Fuse Fulgurites.

The observations of arcing phenomena in filler were still highly perplexing, and therefore an original concept was proposed by the projects Director, Professor P.M. McEwan, namely that:

- The substrate, but more significantly the quartz fulgurite commutates the fault current during the post-peak arcing period.

It was proposed that this phenomenon could present a plausible explanation for the perplexing observations, since this would account equally for the even longitudinal reduction in sensor pixel output voltages between successive images, and the absence of negative voltage discontinuities in oscillographs. To investigate this unique possibility the component wavelengths of the fuse 'arc' light or 'spectra' were analysed using optical spectroscopy techniques.

5.5.9 Spectroscopic Analysis of Arcing in Conductive Film Substrate Fuses.

The spectroscopic analysis of arcing in conductive film substrate fuses was carried out from separate investigations of the arc light components captured in the pre-peak and post peak arc voltage time periods. The fundamental aim of this investigation was to establish:

1. In the pre-peak arc voltage time period whether the arc light spectrum comprised mainly of spectra of fuse element material wavelengths.
2. In the post-peak arc voltage time period whether the arc light spectrum comprised mainly of spectra of fuse filler material wavelengths.

It was considered that if the spectra captured during the pre-peak arc voltage time period conformed with the first proposition, this would confirm the notions of arc elongation due to element burn back and the arc being supported between element electrodes. However, if the spectra in the post peak arc voltage period conformed with the second proposition then the notions of fulgurite commutation of the fault current would be reasonable.

5.5.10 Spectroscopic Analysis Experimental Arrangements.

Spectroscopic analysis of arcing phenomena was carried using a 6800 Series Optical Spectrum Analyser (OSA), manufactured by Rees Instruments Limited. A block diagram of the OSA configuration interfaced to the fuse test facility is shown in Figure 5.13 and a photograph of the experimental arrangements is shown in Figure 5.14.

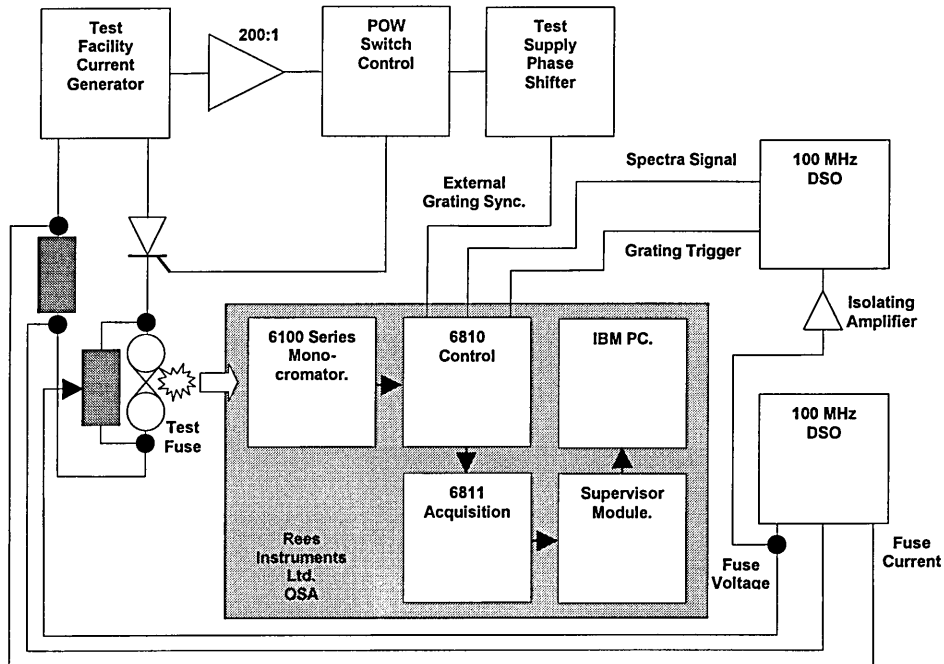


Figure 5.13 Diagram of optical spectrum analyser interfaced to the fuse test facility



Figure 5.14 Experimental arrangement used in the spectroscopic analysis of HBC conductive film substrate fuse arcing phenomena.

The 6100 monochromator comprised a rotating grating and Si(6111) photo detector with a bandwidth of 200nm~900nm. The 6810 control module controlled the scanning speed of the monochromator, signal gain of the photo detector and the sampling interval. For this investigation the monochromator was controlled externally to enable synchronisation between the disintegration of the fuse and the sampling window of the OSA. This was accomplished by first monitoring and then phase shifting the test facility ac generated voltage waveform, to supply the monochromator and control the speed, which basically controls the angular position of the OSA grating. The schematic wiring diagrams for the electronic circuits to achieve this are presented in Appendix 14. The difference in test facility supply frequency and OSA local supply frequency was established as <2% and therefore the calibration of the spectra wavelengths was upheld.

Sample fuses were embodied in an opaque box with a small aperture located exactly in the forefront of the fuse element. The aperture was then accurately positioned so that the horizontal and vertical axis of the fuse element and the OSA grating were in precise alignment (Figure 5.15).

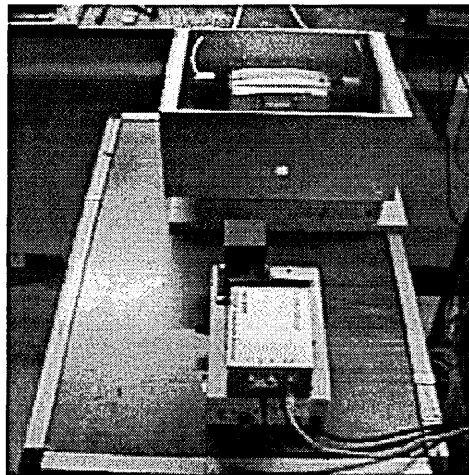


Figure 5.15 Experimental arrangement of OSA and fuse enclosure (Shown without top cover and opaque shroud)

A nominal distance between the fuse and the OSA was experimentally established to eliminate saturation of the photo detector output by the high intensity arc light and to allow analysis of the relative intensity of spectra. The apparatus containing the fuse and the OSA were finally enclosed in an opaque shroud to prevent ingress of light from ambient sources.

Two separate digital storage oscilloscopes (DSO) of the same type as those previously used, were used to capture fuse voltage and current data, and a grating trigger signal and light spectra data. Both oscilloscopes were triggered relative to the onset of fuse element disintegration, to enable specific light spectra to be correlated to a time instant in the disintegration period.

5.5.11 Analysis of Post-peak Arc Voltage Time Period Arc Light Spectra

Analysis of the arc light spectra in the post-peak arc voltage period was carried out using conductive film substrate fuses immersed in both quartz sand and water. Moreover, both silver and copper elements were used to aid comparison of disintegration phenomena and to distinguish between specific spectra. Figure 5.16, displays a typical arc light spectrum and correlated fuse voltage oscillogram captured during the disintegration of a short notch silver element embedded in quartz.

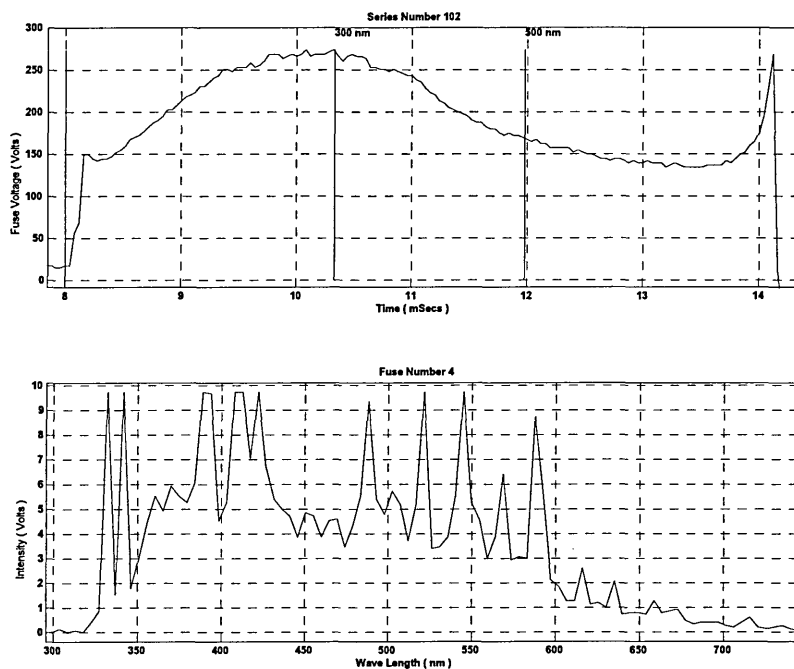


Figure 5.16 Typical arc light spectrum and correlated fuse voltage oscillogram captured during the post-peak arc voltage time period of disintegration in a short notch silver HBC conductive film substrate fuse

Many samples of arc light spectrum were captured for each type of fuse construction (≈ 15) to permit averaging and noise elimination. One sample of these results are shown in Figures 5.17~5.20.

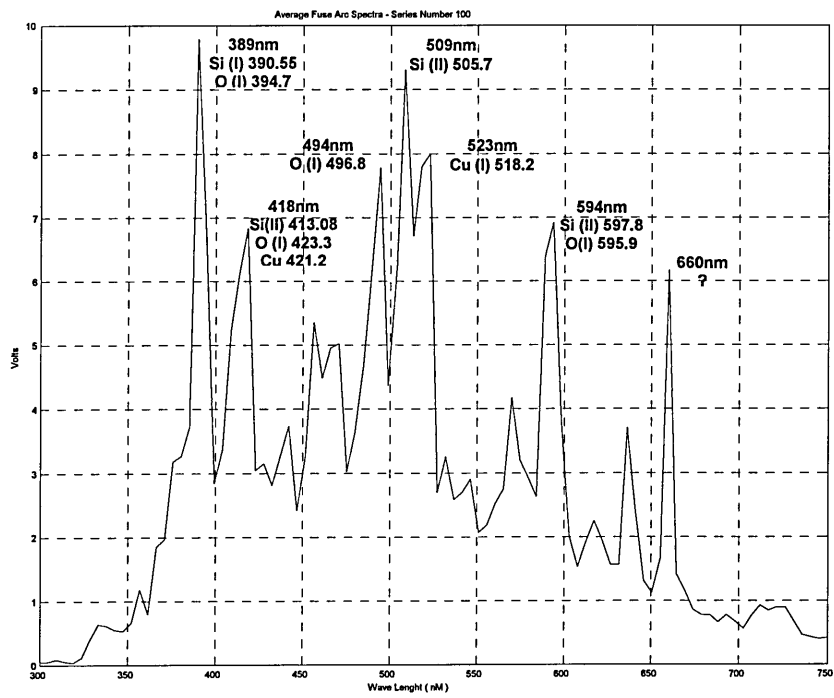


Figure 5.17 Mean arc light spectrum captured during the post peak arc voltage time period in the disintegration of a conductive film substrate fuse with a 0.2mm/25mm copper wire element embedded in fine quartz.

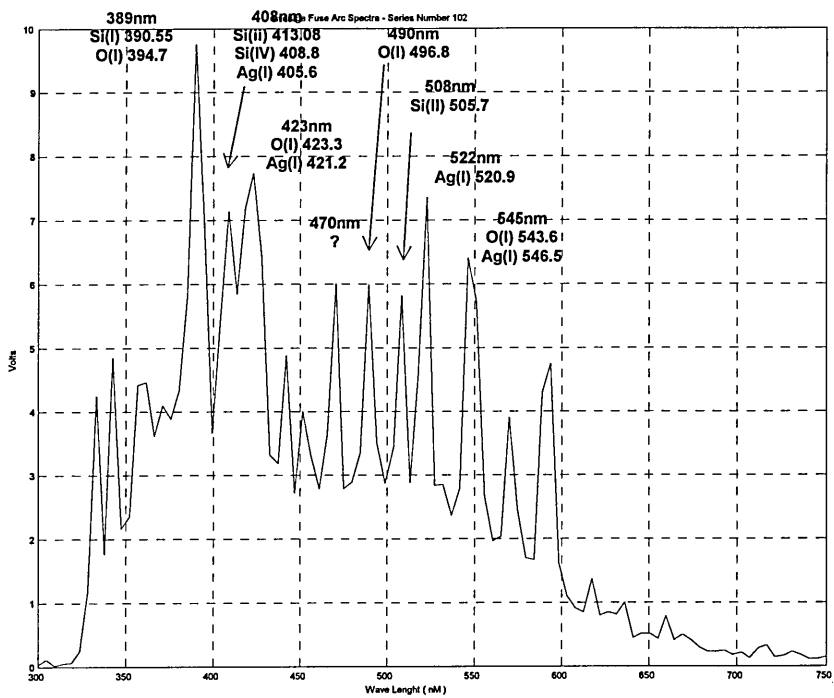


Figure 5.18 Mean arc light spectrum captured during the post peak arc voltage time period in the disintegration of a conductive film substrate fuse with a short notch silver element embedded in fine quartz.

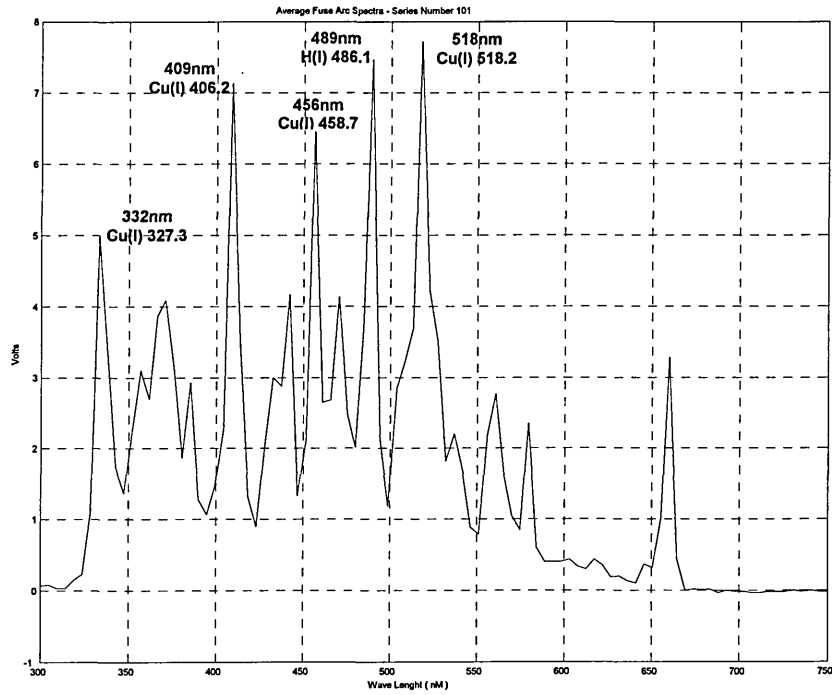


Figure 5.19 Mean arc light spectrum captured during the post peak arc voltage period in the disintegration of a conductive film substrate fuse with a 0.2Ømm/25mm copper wire element suspended in water.

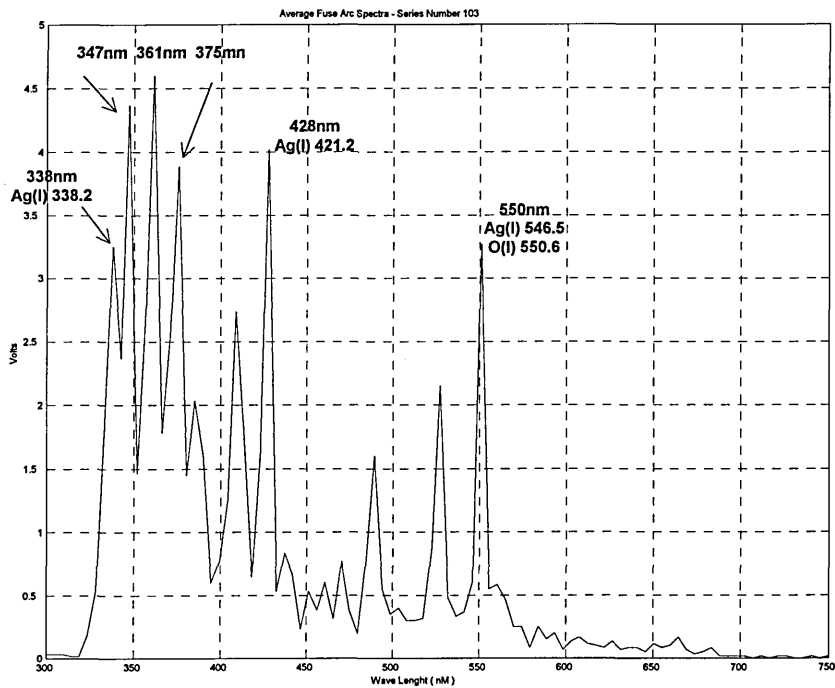


Figure 5.20 Mean arc light spectrum captured during the post peak arc voltage period in the disintegration of a conductive film substrate fuse with a short notch silver element suspended in water.

Interpretation of Arc Light Spectrum.

Interpretation of the arc spectra proved to be difficult due to the intimacy of wavelengths for specific material spectra and the sampling rate of the data capturing equipment. This can be adjudged in consideration of Figures 5.17~5.20, where the wavelengths of specific spectra have been determined and are presented with wavelengths of possible material spectra.

Despite the above shortcomings, when comparing the spectrums, it is rational to propose that spectra for fuse element materials are present in all of the spectrums. However, when comparing the spectrums for the same element materials but different filler materials (Figures 5.17 ⇒5.19 or 5.18⇒5.20) it is suggested that in the case of quartz, the filler spectra are dominant and their intensity are significantly greater. Alternatively, in the case of water, the fuse element material spectra are dominant and their intensities are greatest. These observations are also supported when the spectrums for like filler materials, but different element materials, are compared (Figures 5.17⇒5.18 or 5.19⇒5.20).

5.5.12 Analysis of Pre-peak Arc Voltage Time Period Arc Light Spectra.

For consistency in the investigation, the analysis of arc light spectra emitted from a fuse immersed in sand during the pre-peak arc voltage period was carried out using conductive film fuses constructed with short notch silver elements. This type of fuse design was also used because it produced long pre-peak arc voltage time periods (Figure 5.5v) as opposed to wire elements which, at a similar stage during disintegration produce a very short pre-peak arc voltage time period. Consequently, for short notch elements it was proposed that arcing would be supported on the shoulders of the fuse element during the pre-peak arc voltage time period to correspond with Figures 5.1i~5.1iv. Figure 5.21 displays a typical arc light spectrum captured during this time period that correlated with the fuse voltage oscillograms.

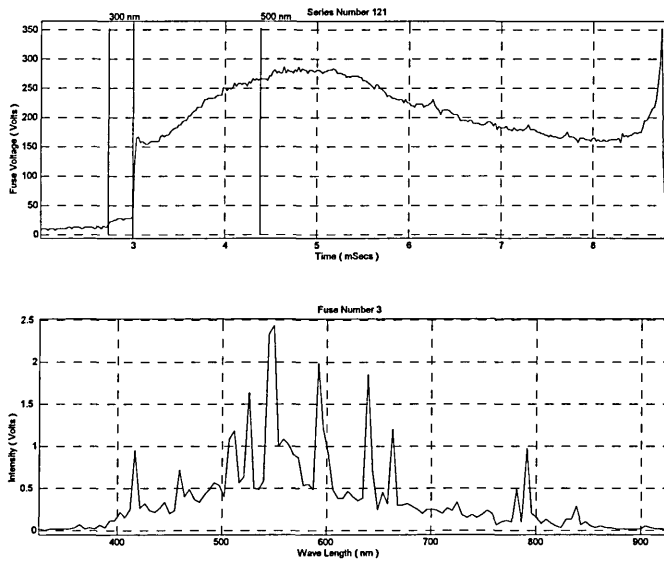


Figure 5.21 Typical arc light spectrum and correlated fuse voltage oscillogram captured during the pre-peak arc voltage time period of disintegration in a short notch silver HBC conductive film substrate fuse

A similar practice of capturing many arc light spectrum samples was carried out during the pre-peak arc voltage time period (≈ 15), to again permit averaging and to provide some degree of noise filtering. The result of these tests is shown in Figure 5.22.

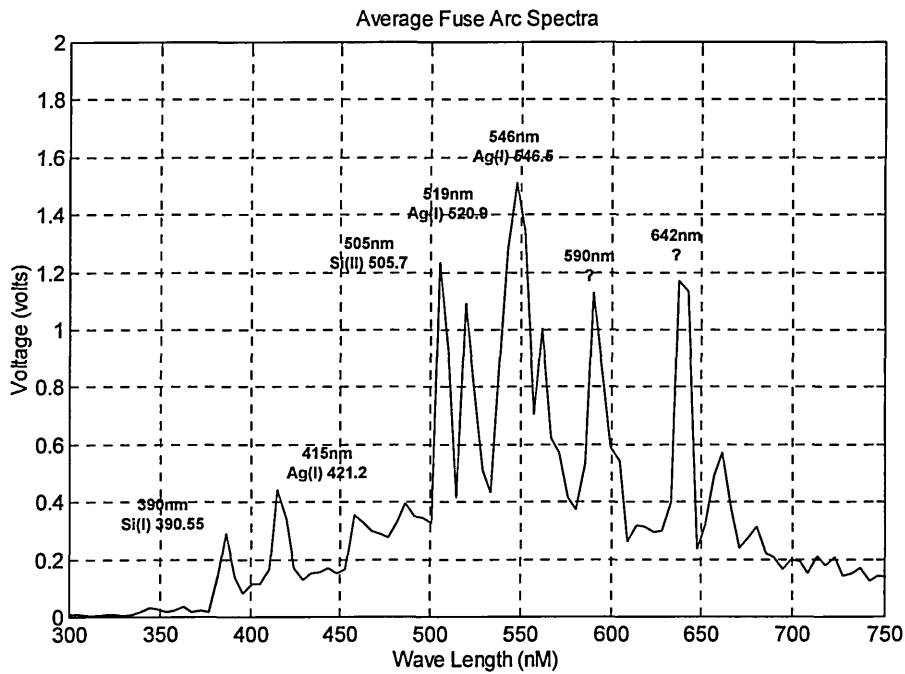


Figure 5.22 Mean arc light spectrum captured during the pre-peak arc voltage time period of the disintegration of a conductive film substrate fuse with a short notch silver element embedded in fine quartz.

Interpretation of Arc Light Spectrum.

Despite the difficulties of identifying specific spectra and data capturing time rates, the mean arc light spectrum of the pre-peak arc voltage period indicates the presence of both element material and filler material spectra. However, it is noticeable that the relative intensity of fuse element spectra are greater than those of filler spectra, and also the element material spectra are dominant in the spectrum.

5.5.13 Comparison of Arc Light Spectrum Captured during Separate Periods of Fuse Element Disintegration.

For the purposes of comparison, the mean arc light spectrums captured during both time periods of element disintegration of short notch silver element conductive film substrate fuses, immersed in sand, are reproduced in Figure 5.23, from which it is clearly evident that the distribution of spectra is markedly different. Moreover, from that for the pre-peak arc voltage period accepting the previous interpretations for the components of the spectra, it is clear that the dominance and intensity of element and filler spectra transpose between the two time regions.

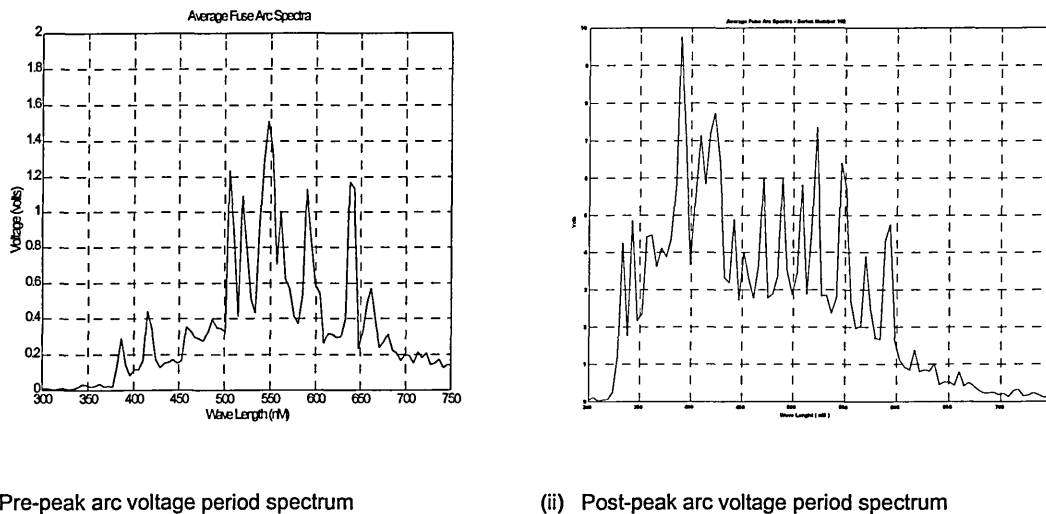


Figure 5.23 Arc light spectrums captured during the disintegration of short notch silver element conductive film substrate fuses immersed in sand.

5.5.14 Evaluation of Spectroscopic Studies of Fuse Arcing.

Chikata *et al* [63], presented observations from spectroscopic studies of fuse arcing phenomena in sand and proposed that arcing persists in SiO_2 vapour. This

conclusion has also been confirmed from other investigations [64][65][74]. The sample fuses of Chikata *et al* were constructed with a single restriction and a spectrum of arc light was captured continuously, which indicated high intensity spectra of both sand and fuse element materials. Additionally, continuous data for specific spectra was captured independently that indicated that fuse element and silica spectra appear at the onset of arcing. Moreover, Chikata observed that some silica spectra (doubly ionised *Si(II)* wavelengths) held high intensities for most of the arcing period whereas the monitored element spectra and that of the silica spectra *Si(I)* (390.5nm) quickly decayed.

Cheim *et al* [67], following previous researcher's conclusions of arcing in *SiO₂* vapours, attempted to determine arc plasma temperature by monitoring silica spectra, *Si(II)* and *Si(III)*, and similarly observed their presence during the whole of the arcing period.

Cao *et al* [74], investigated an ablation-stabilised arc in ice whereby they initiated arcing by disintegrating thin copper wires. Arc spectrums were captured at various instances after the onset of the fault current which indicated that copper spectra were present and dominated in the spectrums captured at long time instances after the onset of arcing (3~5ms for a 0.07Ømm wire and 9ms for a 0.35Ømm wire).

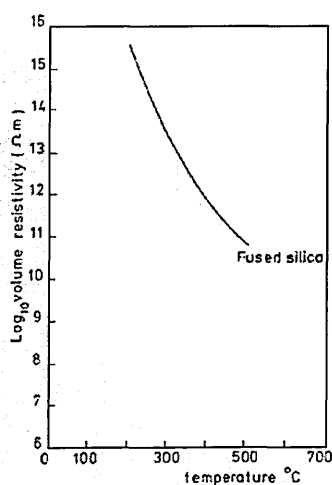
The spectroscopic observations made by these researchers correspond with the findings of this project. The spectrums for example, presented by Cao *et al* are very similar to the spectrum presented in Figure 5.19. and consequently, in the case of water or ice being used as a filler medium, they support the notion that arcing persists in element vapours. Moreover the spectrums also support the rationale previously given for the non-deterioration of the glass substrate and elimination of image phenomena in captured images of arcing in water in this project.

Significantly, the spectrum presented by Chikata *et al* is very similar to the spectrum presented in Figure 5.17 but, unfortunately the spectrum of Chikata *et al* is not correlated to the fuse voltage waveform. However, Chikata's observations of the intensity of specific spectra are time resolved to fuse voltage waveforms and correspond with the associated spectra in the spectrums of both arcing periods captured in this project. Moreover, the intensities of *Si(II)* spectra were observed by Chikata *et al* to decay in the post peak arc voltage period which was also the case in the observations of Cheim *et al*. These observations correspond with the reduction in sensor pixel output voltage observed in sequenced images of arcing captured in this project.

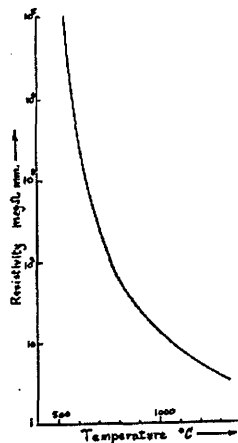
In summary, it is reasonable to propose from the spectroscopic observations that, in the pre-peak arc voltage period, arcing persists in metallic vapours which corresponds with the observations of element burn back and arc elongation of Figure 5.5i~5.5iv. Moreover, in the post-peak arc voltage period all the spectroscopic observations of arcing phenomena in quartz support the conclusion, that arcing persists in SiO_2 vapour. However, in other spectroscopic investigations image and fuse construction phenomena, i.e. the influence of the arc viewing medium and fulgurite luminescence, have not been identified or addressed, and therefore the observations equally support the notion of fault current conduction by the fulgurite. In conclusion, all spectroscopic evaluations of arcing phenomena in sand indicate that ‘silica’ spectra are significant in the latter stages of the arcing period.

5.6 Evaluation of the Electrical Conductivity of Silica

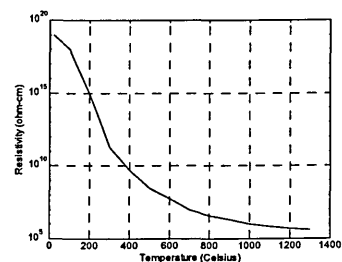
The concept of fulgurite conductance of the fault current during fuse operation has been previously raised [80][8][9] and some indication of its dynamic nature has been determined during the recovery voltage time period [73]. It is very well known that the conductance of quartz is steeply dependent on temperature and can vary several orders of magnitude. Three independent sources of data, which indicate this characteristic are presented in Figure 5.24.



(i) Data source : Glasses and its applications [81]



(ii) Data source : Turner and Turner [73]



(iii) Data source : International reference tables [82]

Figure 5.24 Independent data sources indicating the electrical resistivity of silica quartz as a function of temperature

The temperature of the proposed arc column has been assessed to be in the range of 3000°K~7000°K [61] but more extensively as high as 20000°K [67][63]. Logically, it follows that the electrical conductivity of the fulgurite during arcing must be lower than the lowest values given in the above characteristics and therefore the notion of current commutation to the fulgurite is therefore, highly plausible.

It is also important to note that, the resistance temperature characteristics for most types of glass are generally lower than quartz and therefore the possibility of current commutation through the glass substrate is also plausible. Finally, it is interesting to indicate that at glass melting temperatures $\approx 1500^{\circ}\text{C}$ the electrical conductivity of glass is only a few *ohm.m* and low enough to melt glass electrically by Joule heating, which is now a common glass manufacturing technique [81].

5.7 Key Findings of the Experimental Observations of the Temporal Development of Disintegration and Arcing in Conductive Film Substrate Fuses.

- During the post-peak arc voltage time period in the disintegration of conductive film substrate fuses immersed in sand, no longitudinal displacement of light sources were observed in captured images of arcing phenomena, which was contrary to the case of fuses immersed in water.
- During the post-peak arc voltage time period in the disintegration of conductive film substrate fuses immersed in sand, no negative discontinuities in the arc voltage were observed, which was contrary to the case of fuses immersed in a water medium.
- During the post-peak arc voltage time period, light radiating from fulgurites in quartz filled fuses is significant.
- Spectroscopic investigations of arcing in quartz filled fuses viewed through a silica based medium, indicate the presence of fuse element and fuse filler spectra in both arcing time periods. However, the intensity and the dominance of each type of spectra transpose for the two time periods.
- The electrical conductivity of fused silica and most types of glass is very low at assessed arc temperatures.

5.8 Project Summary, Evaluation, Recommendations and Conclusions.

5.8.1 Summary.

My Ph.D. study was aimed at enhancing the knowledge of the most fundamental mechanism of fuse operation, this being the causation phenomena which initially breaks the electrical circuit in which a fuse is connected and subsequently the phenomena which interrupts the flow of fault current. Experimental-specific diagnostic test equipment and fuse construction techniques have been developed to enable the investigation of fuse operation to take place. Consequently, comprehensive images captured by video cameras of the disintegration of wires in un-confined and confined media in two time domains and subsequent arcing have been presented which were correlated with captured fuse voltage oscillograms over a wide range of time.

The emphasis, however, was placed on investigating the phenomena occurring during the pre-peak arc voltage period, since this was considered to be of considerable significance to the understanding of fuse operation, as briefly evaluated later. The observations have indicated the causation phenomena for the onset of disintegration which were in agreement with theoretical analysis. Moreover, the subsequent phenomena of fuse element fragmentation has been observed and identified for elements suspended in an un-confined medium and also logically deduced for confined fuse elements but not completely substantiated experimentally in the very short time domain.

Furthermore, an attempt was made to corroborate the occurrence of arc merger in sand filled fuses using visual image methods which, have possibly uncovered a new post peak arc voltage period phenomenon, i.e. fulgurite commutation of the fault current. This phenomenon was investigated using spectroscopic techniques, the results of which were in agreement with other spectroscopic investigations of arcing and which indicated that the radical proposition of fulgurite current commutation is feasible. However, the results of both visual and spectroscopic experimental methods are subject to uncovered flaws in experimental techniques in observing arcing phenomena. Hence, current commutation from the arc to surrounding sand filler, as opposed to arc merger, as a mechanism for causing the reduction of the arc voltage in the post peak arc voltage period has not been established, conclusively in this project

5.8.2 Evaluation of Study.

This study has demonstrated experimentally that,

- The phenomena of fuse element disintegration can be investigated using video image capturing techniques.
- The onset of disintegration of a fuse element immersed in a confining medium can be viewed through a transparent substrate or encapsulating resin.
- Evaluation of disintegration in different time domains can be accomplished by precise control of the Joulean energy released into fuse wire elements.
- Fuse operation and significantly the disintegration of the fuse element and arcing can be quickly interrupted by the commutation of the fault current from the fuse by a parallel crowbar thyristor.
- When using discrete experimental test equipment, the time period between data capture instances should be at least half that of the time period of the monitored event.
- By introducing a foreign body (glass substrate) into an enclosed system (HBC fuse), the dynamic behaviour of the original enclosed system could be modified. Consequently, the captured data relating to the dynamic performance of the modified system should be scrutinised before the dynamic performance of the original system is proposed.

5.8.3 Recommendations for Future Work.

The research field and understanding of the phenomena of electrical conductor disintegrations is broad and well established. However, in order to further the knowledge of the disintegration of fuses, it is suggested that the following investigations could be pursued further.

- A series of investigations in similar disintegration time domains as those presented could be carried out, but alternatively, using dc fault currents. Consequently, due to the absence of natural current zeros the extent of fuse element fragmentation due to the forces of arcing during the most onerous of conditions can be identified. Moreover, the extent of short arc ignitions could be established in the time domains.

- A thorough analysis and investigation into the effect of fuse element vibrations and deformation due to shape of the fault current waveform could be undertaken. Consequently, the phenomena of a fuse element breaking before the element reaches melting temperature due to trapped stresses could be established which challenges classical research findings.
- A series of investigations could be conducted precisely controlling the disintegration of identical wires immersed in a confining medium of the same type but of differing compaction densities. This investigation could establish more accurately a relationship between the forces of confinement and the frequency of the standing wave, if, as proposed, is induced in the wire by thermal expansion.

5.8.4 Recommendations of the Project to the Operation of Fuses.

In accordance with classical fuse operation theory, the rise of the fault current has been observed to be reduced due to the multiple ignitions of short arcs. This phenomenon has been identified to be fundamentally due to the influence of the confining medium. Since the fuse element is observed to be wholly dispersed by arcing phenomena during the pre-peak arc voltage period and that it has been revealed that the filler producing fulgurite, could conduct the fault current, it is reasonable to conclude that understanding of this phenomenon to control the pre-peak arc voltage time period is of considerable significance to fuse operation.

5.8.5 Recommendations for the Construction of Practical HBC Conductive Film Substrate Fuses.

The scope of this project was to utilise the infinite geometrical variations of fuse element designs supported by film substrate fuse technology to control fuse arcing, hence it is reasonable to conclude this Thesis, by proposing recommendations to the design of practical HBC conductive film substrate fuses, given the project findings.

- Since, thermal expansion of the fuse element and the confinement of it by the environment surrounding the fuse element are significant in the mechanism of disintegration, bonding of the fuse element to a solid substrate benefits fuse arcing and the current limiting capabilities of a fuse due to the increased extent of element fragmentation

- Where it is necessary to limit the peak arc voltage, it is suggested that the restrictions in an otherwise uniform conductor are located in very close proximity to each other, so that at the instant trapped stresses in the element are released by the onset of disintegration in one of the restrictions, other restrictions benefit from the induced forces of disintegration.
- Given that the substrate could commutate the fault current during the arcing period, it follows logically that the electro-thermal characteristics of possible substrate materials should be addressed at very high temperatures before selection.

5.8.6 Contributions to Knowledge.

The following, is a list of the main contributions to knowledge resulting from the work reported in this thesis:

- Visual documentation of the phenomena of fuse element disintegration.
- Identification of thermal expansion as a fundamental mechanism of disintegration of fuse wire elements suspended in an un-confined medium or immersed in a constricting medium in the time domains investigated.
- The apportionment of the influence of phenomenological forces for the onset of disintegration of fuse wire elements ([1] thermal expansion [2] Surface tension [3] Electromagnetic)
- Confirmation that the mechanism of fuse wire fragmentation is sequential in the time domains investigated.
- An evaluation of electrical current conduction in quartz filled fuses during the arcing period of fuse operation.

5.8.7 Publications.

The following paper has so far been presented and published

Unduloid formation and the Causation of Current Interruption in Current-Carrying Wires.

Brown R.E, McEwan P.M.

Sixth International Conference of Electric Fuses and their Applications, Turin, Italy, 20-22 September 1999

References

- [1] *A Safety Device.*
Edison, T.A.
Patent No.227226, May 4, 1880
- [2] *Electrical Review 5,*
Turner, H.W., Turner, C.
Nov 1971
- [3] *Theoretisches und Praktisches uber Abschmelzsicherungen*
Meyer, G.J.,
Elektrotechnische Zeitschrift Hefte , Vol. .28, 1907, p 430-435.
- [4] *Rating of Conductors for Short Duration Currents.*
Morgan, V.T.,
Proc. IEE, Vol. 118, No. 3/4, March/April 1971, p555-570
- [5] *Electric Fuses*
Baxter, H.W.
Publisher : Edward Arnold, London April 1950, *also* ERA Report GT/224, ERA
Technology Limited, Cleeve Road, Leatherhead, Surrey. KT22 75A
- [6] *Electric Fuses*
Wright, A., Newbery, P.G.,
IEE Power Engineering Series 2, Peter Peregrinus Ltd., London, UK, 1982
- [7] *A New Fuse Phenomena*
Metcalf, A.W.,
BEAMA Journal 44, p109, 151, 1939.
- [8] *Phenomena occurring During the Extinction of Arcs in Fuses.*
Turner, H.W., Turner, C.
Conference Proceedings, 2nd International Symposium on Switching Arc
Phenomena, Lodz, Poland, September 1977, p 293-299.
- [9] *Electrical Conductivity of Arc Extinguishing Media for Low Voltage Fuses*
Paukert, J.
Conference Proceedings, International Conference on Electrical Fuses and their
Applications, Trondheim, Norway 13-15 June 1984, p 70-75.
- [10] *HBC Fuse Models Based on Fundamental Arcing Mechanisms*
Gomez, J.C.
Ph.D. Thesis, Sheffield Hallam University, Sept.1994.
- [11] *Calculation of the Course of the Current and Voltage of a Current Limiting Fuse*
Dolegowski, M.
International Conference on Electric Fuses and their Applications, Liverpool
U.K., April 1976, p218.

- [12] *Calculation of the Over Voltage Peak Values when breaking Short Circuits by means of Multi Strip Fuses.*
Hibner, J.
 Conference Proceedings, 2nd International Symposium on Switching Arc Phenomena, Lodz, Poland, September 1973, p 269-274.
- [13] *Numerical Predication of the Pre-arcing Performance of HRC Fuses.*
McEwan, P.M.
 Ph.D. Thesis, Liverpool Polytechnic, October 1975.
- [14] *Over Current Protection of High Power Semiconductor Devices.*
Fontaine, M.J.
 IEE, Discussion Meeting, Elec.Times, 1972.
- [15] *Nonlinear Thermal Effects in Metal/Non-metal Systems*
De Cogan, D.
 4th Int. Workshop on the Electronic Properties of Metal/Non-metal Microsystems, Sheffield Hallam University, Sheffield, UK, Sept.1993, p459-466
- [16] *Exploding Wires: Introduction.*
Chase, W. G.
 Exploding Wires, Edited by Chase W.G. and Moore H.K., New York USA, Plenum Press, Vol. 2, 1962, p1.
- [17] *High Temperature Exploding Wires.*
Bennett, F.W.
 Progress in High Temperature Physics and Chemistry, Vol.2, Pergamon Press 1966.
- [18] *Calculations of the Arc Ignition Voltage on Single Disruption of Uniform Fuse Element by its Independent Disintegration in H.B.C. Fuses.*
Hibner, J.
 Conference Proceedings, 5th International Symposium on Switching Arc Phenomena, Lodz, Poland. 1985. p 368-371.
- [19] *Fuse to Varistor Current Commutation.*
Wolny, A.
 Elektryka No.76, 1994, p15.
- [20] *Gaseous Conductors*
Cobine, J.D.,
 McGraw Hill, 1941.
- [21] *Analysis of High Breaking Capacity Fuse Link Arcing Phenomena.*
Wright, A., Beaumont, K.J.,
 Proceedings of the Institute of Electrical Engineers, Vol. 123, No. 3 March 1976.

- [22] *Introduction to the Arc*
Somerville, J.M.
An Introduction to Discharge and Plasma Physics, Edited by Haydon S.G., The University of New England, Armidale 1964.
- [23] *The Current Limiting Fuse, Discrimination and Braking Capacity.*
Lerstrup, K.
Ingenioren, International Edition, Vol. 2, No. 1, 1958.
- [24] *The Voltage of Single Disrupt in a Chain of Arc Intervals by Short Circuit Disintegration of Strip Fuse Elements of Fuses.*
Hibner, J.
Conference Proceedings, 1st International Symposium on Switching Arc Phenomena, Lodz, Poland, Sept. 1970, p226-231.
- [25] *Dynamic Modelling of the Operation of Current Limiting Fuses.*
Gnanalingam, S
Ph.D. Thesis, Liverpool Polytechnic, 1979.
- [26] *Arcing Phenomena in High Voltage Fuses.*
Daalder, J.E., Schreurs, E.F.,
EUT Report 83-E-137, Department of Electrical Engineering, Eindhoven University of Technology, 1983.
- [27] *Analysis of High Rupturing Capacity Fuse Link Pre-arcing Phenomena.*
Leach, J.G., Newbery, P.G., Wright, A.
Proc. IEE, 120(9), p252-260.
- [28] *Electro-Mechanical Analysis of Thin-Film Substrate Fuses*
Wilniewicz, M.P.,
Ph.D. Thesis, Sheffield Hallam University 1999.
- [29] *A Semiconductor Fuse Link on a Ceramic Substrate*
Takahashi, H., Hirose, K.
Conference Proceedings, 4th International Conference on Electrical Fuses and their Applications, Nottingham, U.K., September 1991, p92-95.
- [30] *Fuse to Varistor Current Commutation.*
Wolny, A.
Elektryka No.76, 1994.
- [31] *Stan badani mechanizmow zaplonu I gaszenia luku w bezpiecznikach*
Lipski, T.
Elektryka, 1970, Vol. 46, No. 11, p 472.
- [32] *Unduloids and Striated Disintegration of Wires.*
Nasilowski, J.,
Exploding Wires Vol. 3, Planum Press, New York U.S.A., 1964, p 295-313

- [33] *Arcing Characteristics of Fuses with Small Over Currents (DC and AC).*
Baxter, H.W.
 The British Electrical and Allied Industries Research Association, Report G/T 228, 24 March 1950.
- [34] *Test Procedures and Arcing Phenomena in HV Fuse Links near the Minimum Breaking Current.*
Aslak Ofte, Rondeel, W.
 Conference Proceedings, International Conference on Electrical Fuses and their Applications, Trondheim, Norway 13-15 June 1984, p 190-195.
- [35] *Electrical Experiments by Mr. Edward Nairne.*
Nairne, E.
 Phil. Transactions, Royal Society (London) 1774.
- [36] *Mr. Edward Nairne FRS - Discoverer of the Electrical Fuse ?*
McEwan, P.M.,
 Prospects of Developments of Current Breaking Techniques, PTWPiS, Gdansk, 1996.
- [37] *Über den Durchgang der Elektrizität durch metallische Haardrahte.*
Kleen, W.
 Ann.Phys., Band 11, 1931, Vol. 5, p579 - 605.
- [38] *Über die Umwandlung eines flüchtigen Zylinders in gesonderte Klugeln.*
Plateau, F.
 Ann. Phys. 1867, Vol. 132, p 654.
- [39] *A Mechanism for the Fuse Pre-Arcing Period*
Carne, E.B.
 A.I.E.E. Transactions, Vol. 72, 2 March 1953, p 593 - 599.
- [40] *Scientific Papers (Book)*
Lord Rayleigh.
 Cambridge University Press, London, England. Vols. 1-3, 1899-1902.
- [41] *Why Unduloids Do Not Always Appear*
Lipski, T.
 Conference Proceedings, 3rd International Symposium on Switching Arc Phenomena, Lodz, Poland. 1977. p 305-309
- [42] *Appearance of Unduloids in Exploding Wire Phenomenon*
Bisaria, A.K.
 Indian Journal of Pure and Applied Physics, Vol. 11, September 1973.
- [43] *Use of Capillary and Pinch Instability for Dendritic Crystal Growing*
Meyer, E., Rinderer, L.
 Journal of Crystal Growth, Vol.28,1975, p199-208.

- [44] *New Observations on the Formation of Unduloids on Wires.*
Lipski, T., Furdal, A.
 Proceedings of the I.E.E. Vol. 117, No. 12 December 1970.
- [45] *The Voltage across a Fuse during the Current Interruption Process*
Vermij, L.,
 IEEE Transactions on Plasma Science, Vol. PS-8, No. 4, Dec. 1980, p460-468.
- [46] *Electrical Behaviour of Fuse Elements.*
Vermij, L.
 Ph.D. Thesis, Department of Electrical Engineering, Eindhoven University of Technology, 1969.
- [47] *On the Magneto Thermo Viscous Elastic Mechanism of Unduloids Formation on Wires.*
Zimny, P.
 Conference Proceedings, 2nd International Symposium on Switching Arc Phenomena, Lodz, Poland, September 1973, p 241-246
- [48] *Unduloid Formation and the Causation of Current Interruption in Current Carrying Wires.*
Brown, R.E., McEwan, P.M.,
 International Conference on Electrical Fuses and Their Applications, Turin, Italy, Sept. 1999, p 101-104
- [49] *The Number of Arcs Initiated during Striated Disintegration of the Uniform Strip H.B.C. Fuse Elements at AC Short Circuit Current Interruption.*
Hibner, J.
 International Conference on Electric Fuses and Their Applications, Trondheim Norway, 13-15 June 1984, p 60 - 69.
- [50] *Deformation and Disruption of Silver Wires*
Arai, S.
 Conference Proceedings, International Conference on Electrical Fuses and their Applications, Liverpool, U.K., April 1976, p50-58.
- [51] *Theory of Thermal Plasma and Application to Observed Phenomena.*
Maecker, H.
 An Introduction to Discharge and Plasma Physics, Edited by Haydon S.G., The University of New England, Armidale 1964, p264-265.
- [52] *On the Theory of the Striated Fuse Wire Disintegration*
Lipski, T.
 IEEE Transactions on Plasma Science, Vol. PS-10, No. 4, December 1982
- [53] *Application of the Arc-Pinch Force Interaction Theory to the Calculation of Striation Modulus of the Strip H.B.C. Fuses*
Lipski, T.
 Conference Proceedings, International Conference on Electrical Fuses and their Applications, Trondheim, Norway 13-15 June 1984, p 52

- [54] *Proba teoretycznego wyjaśnienia mechanizmu rozpadu przewodów poddanych działaniu uderów prądowych o wielkiej strömosci*
Hrynczuk, J.
 D.Sc. Thesis 1966, Politechnika Gdanska, Wydział Elektryczny.
- [55] *Electrothermal Fuse Element Disintegrating Mechanism by Short Circuit Currents.*
Jakubiuk, K.
 Conference Proceedings, 4th International Conference on Electrical Fuses and their Applications, Nottingham UK, Sept. 1991, p226-230.
- [56] *The Calculation of Over-voltage Characteristics of HBC Fuses.*
Hibner, J.
 Conference Proceedings, International Conference on Electrical Fuses and their Applications, Liverpool, U.K., 1976, p70.
- [57] *The Operation Joule Integral Calculation of Current Limiting Fuses by the Resistance Method.*
Hibner, J.
 Conference Proceedings, 3rd International Symposium on Switching Arc Phenomena, Lodz, Poland, September 1977, p 293-299.
- [58] *Experimental Investigation of Wall Stabilised Arc Mechanisms of Wires in Fuse Filler.*
Gomez, J.C., McEwan, P.M.
 International Conference on Electrical Fuses and their Applications, Ilmenau, Germany, September 1995 p243-250
- [59] *Calculation of the Course of the Current and Voltage of a Current Limiting Fuse*
Dolegowski, M.
 International Conference on Electric Fuses and their Applications, Liverpool U.K., April 1976, p218.
- [60] *Der Lichtbogen an Schmelzleitern in Sand.*
Kroemer, H.
 Archiv Fur Electrotechnik, 36 Band, 8 Heft 1942, p455-471
- [61] *The use of Optical Spectroscopy in the Analysis of Electrical Fuse Arcing.*
Barrow, D.R., Howe, A.F.
 Conference Proceedings, 4th International Conference on Electrical Fuses and their Applications, Nottingham, U.K., September 1991, p221-225.
- [62] *Digital Simulation of Fuse Breaking Tests.*
Gnanalingam, S., Wilkins, R.
 I.E.E. Proceedings, Vol. 127, Pt. C. No. 6, November 1980.

- [63] *Spectroscopic Observations of Arcs in Current Limiting Fuse through Sand.*
Chikata, T., Ueda, Y., Murai, Y., Miyamota, T.
 Conference Proceedings, International Conference on Electrical Fuses and their Applications, Liverpool, U.K., 1976, p 114-121.
- [64] *Characteristics of Arc in Melting Fuse Element Filled with Quartz Sand*
Bizjak, M., Zunko, P., Poberaj, S.
 IEEE, 6th Medit. Elec. Conf., Ljubljana, 1991, p1493-1496
- [65] *The Calculation of the Parameters of the Plasma of the Arc in a Fuse*
Frenckel, Z.
 Conference Proceedings, 4th International Conference on Electrical Fuses and their Applications, Nottingham, U.K., 1991, p 235-240.
- [66] *A Comparison of the Computer Modelling of Electric Fuse Arcing and their Real Life Performance.*
Barrow, D.R., Howe, A.F.
 Conference Proceedings, 4th International Conference on Electrical Fuses and their Applications, Nottingham, U.K., September 1991, p231-234.
- [67] *Spectroscopic Observations of High Breaking Capacity Fuse Arcs.*
Cheim, L.A.V., Howe, A.F.,
 IEE Proc.-Sci. Meas. Technol., Vol. 141, No. 2, March 1994, p 123-128.
- [68] *Behaviour of Exploding Gold Wires*
Tucker, T.J.
 Journal of Applied Physics, Vol. 32, No. 10, Oct. 1961.
- [69] *Liquid Behaviour of Exploding Wires.*
Chase, W.G.,
 The Physics of Fluids, Vol. 2, No. 2, March-April 1959, p230-235.
- [70] *Correlated X-Ray and Optical Streak Photographs of Exploding Wires.*
Fansler, K.S., Shear, D.D.
 Exploding Wires, Edited by Chase W.G. and Moore H.K., New York USA, Plenum Press, Vol. 4, 1968, p185-193.
- [71] *Studies of Exploding Wire Phenomenon by use of Kerr Cell Schlieren Photography.*
Muller, W.
 Exploding Wires, Edited by Chase W.G. and Moore H.K., New York USA, Plenum Press, Vol. 1, 1959, p186-208.
- [72] *Arc Energy and Critical Tests for HV Current Limiting Fuses.*
Narancic, V.N., Fecteau, G.
 Conference Proceedings, International Conference on Electrical Fuses and their Applications, Trondheim, Norway 13-15 June 1984, p 236-251.

- [73] *The Role of Fuse Filler in Circuit Protection*
Turner, H.W., Turner, C.,
 International Conference on Electric Fuses and their Applications., Liverpool
 U.K., April 1976, p80-88.
- [74] *Spectrum Analysis of an Ablation Stabilised Arc in Ice.*
Cao, L.J., Stokes, A.D.
 Conference Proceedings, 4th International Conference on Electrical Fuses and
 their Applications, Nottingham, U.K., September 1991, p27-32.
- [75] *Synthetic Resonant Fuse Test Circuit.*
Lang, T.,
 Diplomarbeit, Technische Universitat Ilmenau, 1996.
- [76] *Numerical and Analytical Solution of the Transient Adiabatic Joulean Heat
 Equation for Common Electrical Conductors*
Reichelt, T.,
 Diplomarbeit, Technische Universitat Ilmenau, 1997.
- [77] *FE CAD Predication of Stress and Displacement Distribution in a Uniform
 Conductor*
Wilniewicz, M.P.
 Private Communication.
- [78] *Effect of Fuse Element Confinement on the Rate of Rise of Fuse Arc ignition
 Voltage*
Wolny, A.
 International Conference on Electrical Fuses and Their Applications, Turin,
 Italy, Sept. 1999, p 135-139.
- [79] *Data Sheet - TSL 1401 128x1 Linear Sensor Array With Hold.*
 Texas Instruments Inc., Dallas Texas, USA, November 1996
- [80] *A Simple Method to Calculate the Maximum Voltage that Arises When a Fuse
 Link Breaks a DC Short Circuit Current.*
Rex, H.
 Conference Proceedings, 6th International Symposium on Switching Arc
 Phenomena, Lodz, Poland. 1989.
- [81] *Glasses and their Applications.*
Rawson, H.
 The Institute of Metals, London, 1991
- [82] *International Reference Tables of Numerical Data, Physics, Chemistry and
 Technology.*
 Vol. 6, McGraw Hill 1929
- [83] *Thermal Studies of Thin-Film Fuses.*
Inameti, E.E.
 Ph.D. Thesis, University of Nottingham, UK, August 1988

Appendices

Appendix 1

Fuse Test Facility, Energy Sources and Induction Motor Specifications.

A1.1 Induction Motor

Manufacture	Brush
Motor Number	9423640
Frame	RJ4
Power	26 HP
Speed	1430 RPM
Phase	3
Frequency	50 Cycles
Voltage	200/415
Star	36/72
Rating	CMR
R Voltage	340 V
R Current	34 A
Reference Number	337521

A1.2 DC Generator

Manufacture	Brush
Contract Number	337511
Machine Number	F81A6900
Power	8 kW
Speed	1430 RPM
Voltage	200 V
Current	40 A
Spec. BSS	4613
Winding	COMPD
Rating	CMR
Date	Nov. 56

A1.3 AC Generator

Manufacture	Higgs
Type	AG
Frame	32Y
Power Factor	5 KVA
Speed	1500 RPM
Frequency	50 Cycles
Phase	3
Rated Current	14.5 A
Rated Voltage	240 V RMS

Appendix 2

Fuse Test Facility, Thyristor Specifications

A2.1 Thyristor Type – NO60R.

V_{DRM} V_{RRM} - Range	200-1500	V
$I_{T(AV)}$ at T case	63	A
	85	$^{\circ}C$
$I_{T(RMS)}$	100	A
I_T	100	A
$I_{TSM(1)}$ 10 ms $V_R \leq 60\% V_{RRM}$	1000	A
$I_{TSM(2)}$ 10 ms $V_R \leq 10V$	1100	A
$I^2t_{(2)}$	6613	A^2S
di/dt non-Rep/Rep	400/200	$A/\mu s$
I_{GT}/V_{GT}	100/3	mA/V
I_{DRM} I_{RRM}	10	mA
I_H	160	mA
Rthj-c dc&180 $^{\circ}$ sine	0.35	K/W
Rthj-c 120 $^{\circ}$ rect	0.40	K/W
Rthc-s	0.1	K/W
V_o	0.89	V
r	6.1	$m\Omega$
V_{TM} at I_{TM} T_J 125 $^{\circ}C$	2.1/195	V A

Appendix 3

Fuse Test Facility, Differential Probe Specifications

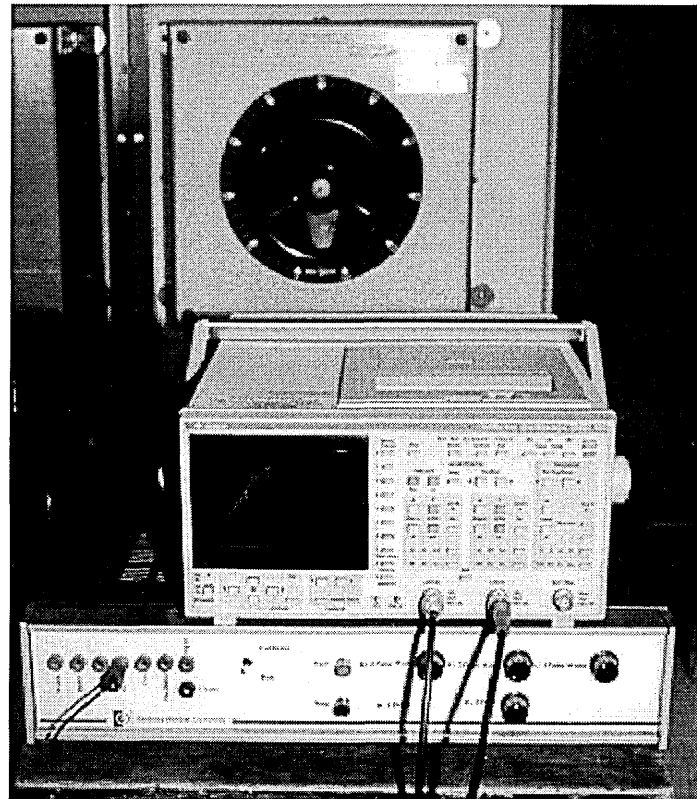
A3.1 Differential Probe Type, SI-9000

Manufacturer :	Hollidyne Electronics Limited,
Bandwidth :	DC to 15MHz (-3dB)
Rise Time :	24nS
Input Configuration :	Balanced Differential
Input Attenuator :	Switch Ratios of 200:1 and 20:1
Accuracy :	±2% at +18°C to +28°C excluding offset and noise.
Input R and C :	2MΩ and 2.5pF each input to ground
Input Voltage :	All voltages refer to each input lead and are referenced to oscilloscope ground. Differential max: ±700 V (dc+Peak ac) at 200:1 attenuation ±70 V (dc+Peak ac) at 20:1 attenuation Common Mode max : ±700 V (dc+Peak ac) at 200:1or 20:1 attenuation Absolute max : ±1000 V (dc+Peak ac) Exceeding this limit may damage the probe.
Common Mode rejection (typical) :	50 Hz : -80dB, 1KHz : -70dB, 100KHz : -59 dB, 1MHz : -47 dB
Output Voltage :	Amplitude : ± 3.5V (dc+Peak ac) max Offset : < ±5mV typical (-10°C to +40°C) Noise : 2mV typical Source impedance :1Ω typical at 1 kHz, 8Ω typical at 1 MHz
Ambient Temperature :	Operating : -10°C to +40°C Storage : -30°C to +70°C
Power Requirements :	Four internal 1.5V or 1.2V AA size Batteries or external ac to 6V mains adapter. Automatic power shutdown when battery voltage falls below 4V
External Connections :	Signal Input: red and black 4mm plugs with retractable shrouds on red and black leads of approx. 1m length. Signal Output : 1m coaxial cable with BNC connector. Power Input : recessed jack socket with positive polarity inner connection.

Appendix A4

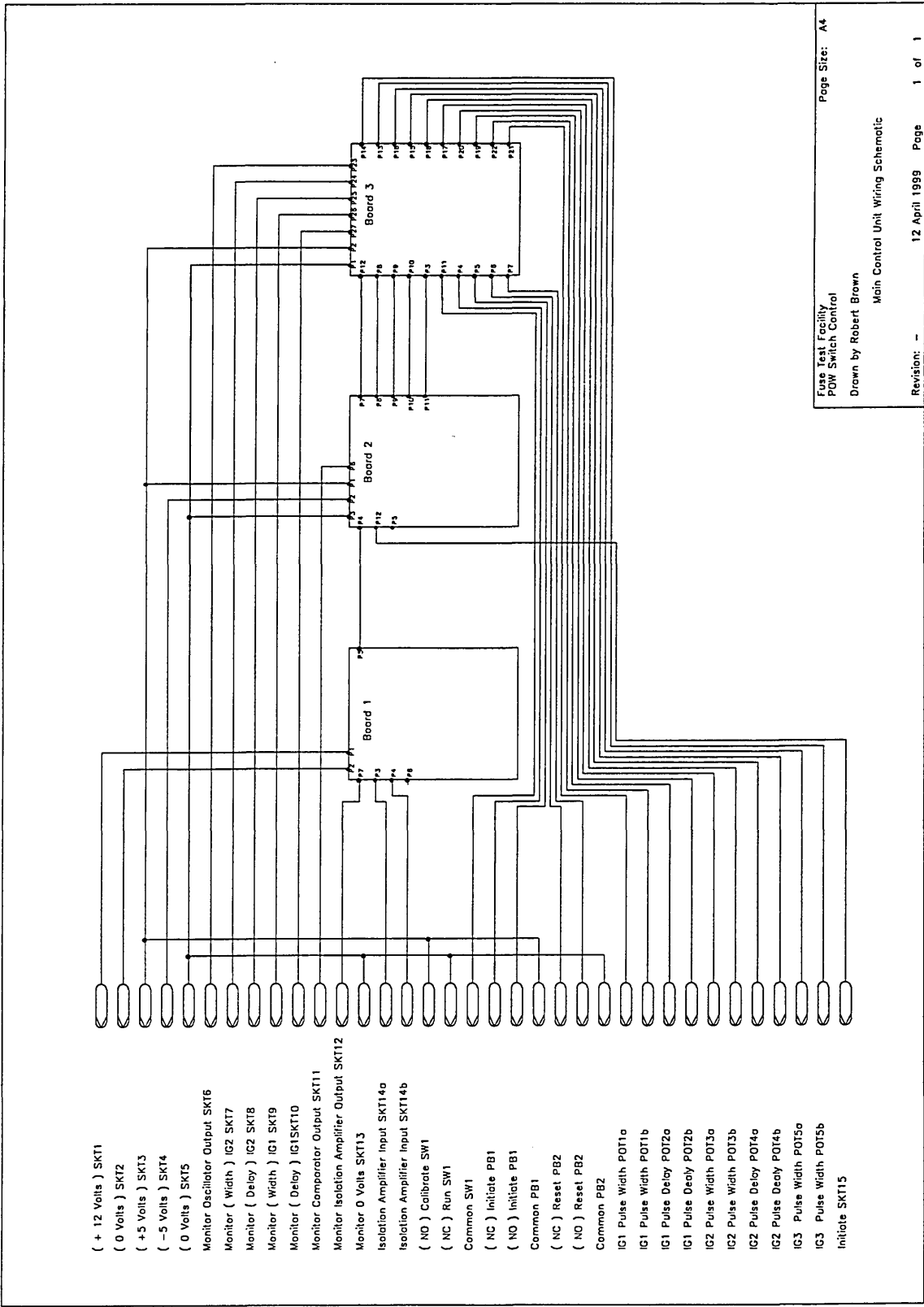
Fuse Test Facility: Point on Wave Switch Control Unit - Schematic Diagrams

The following pages, present the schematic diagrams of the circuits, which comprised the point on wave switch control unit shown in Figure A4.1, which was used in this project. The overall control unit was made of two separate units, which are referred to in the diagrams as the main and supplementary units.



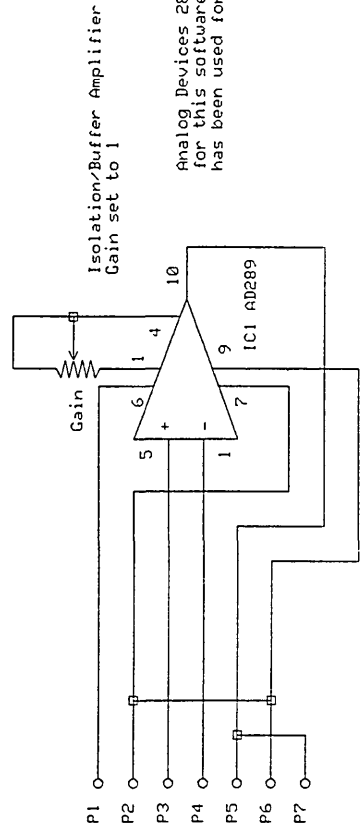
Point on wave
switch control
unit

Figure A4.1 Fuse Test Facility: Point on wave switch control unit. (Shown with digital storage oscilloscope and manual generator field current reostat)

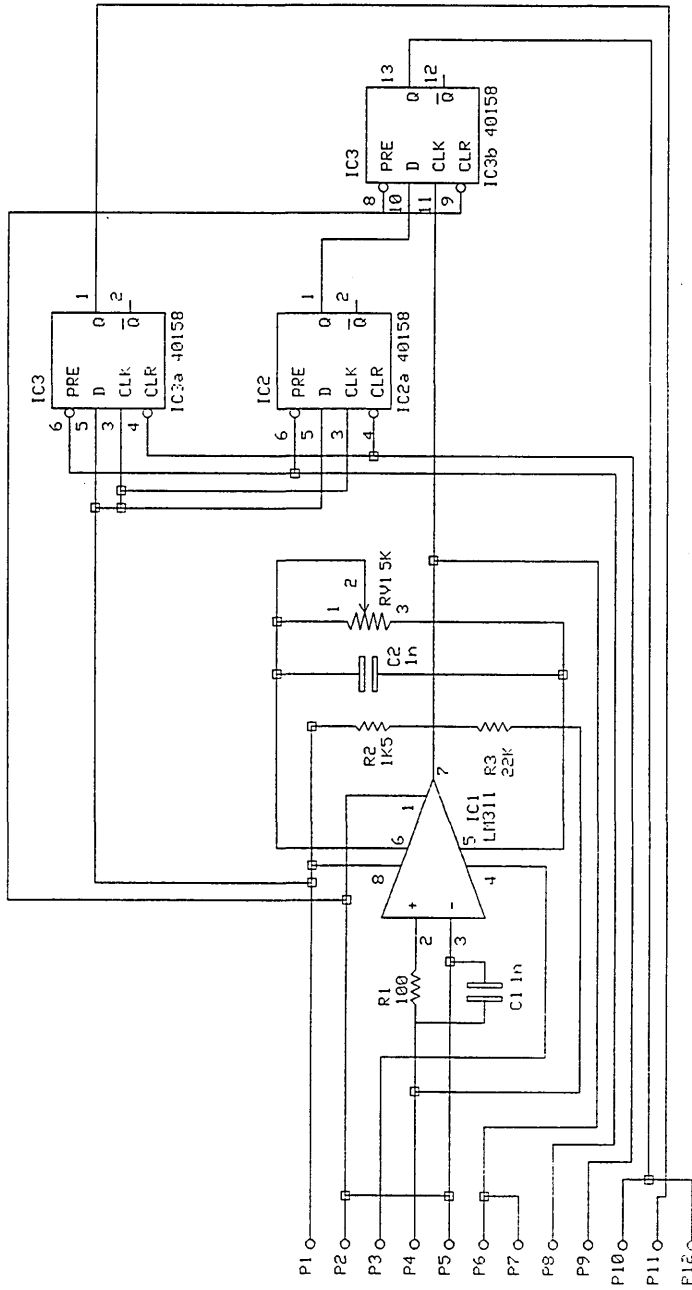


Fuse Test Facility
 POW Switch Control
 Drawn by Robert Brown
 Main Control Unit Wiring Schematic
 Revision: -- 12 April 1999 Page 1 of 1
 Page Size: A4

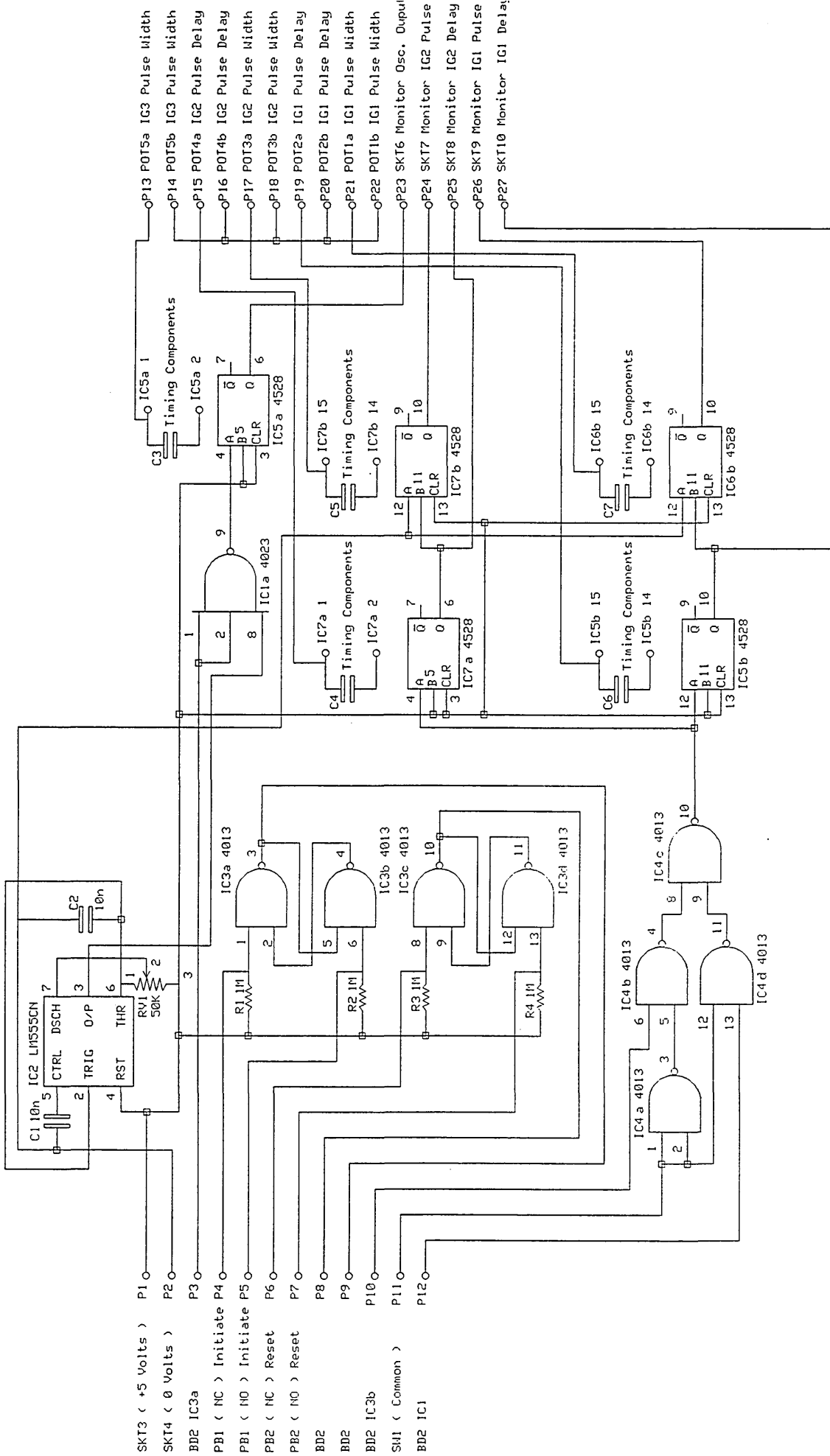
SKT1 (+12 Volts)
 SKT2 (0 Volts)
 SKT14a Isolation Amplifier Input
 SKT14b Isolation Amplifier Input
 BD2 IC1
 Isolation Amplifier Common
 SKT12 Monitor Isolation Amplifier



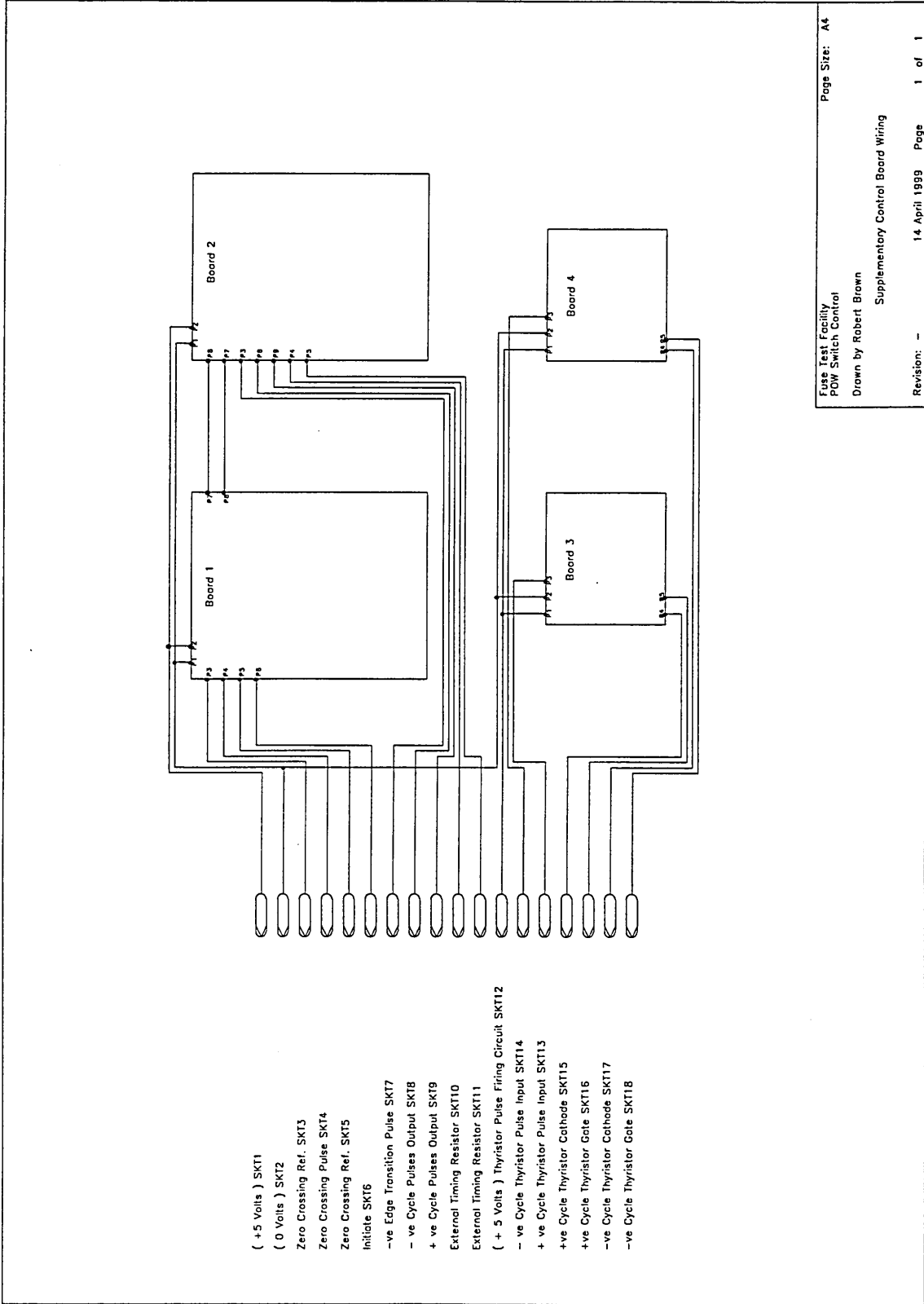
Analog Devices 289 is a non standard device package for this software. A standard Op amp package has been used for this schematic diagram.

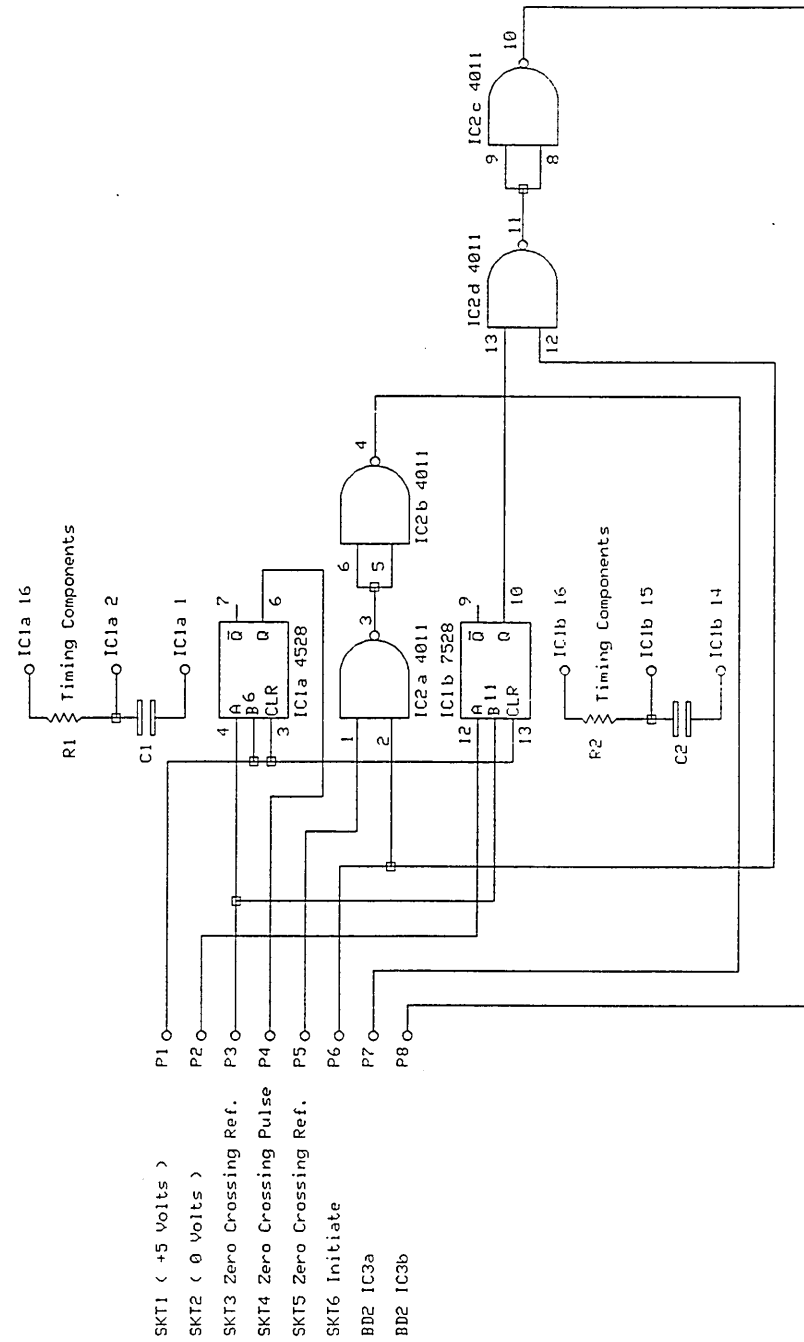


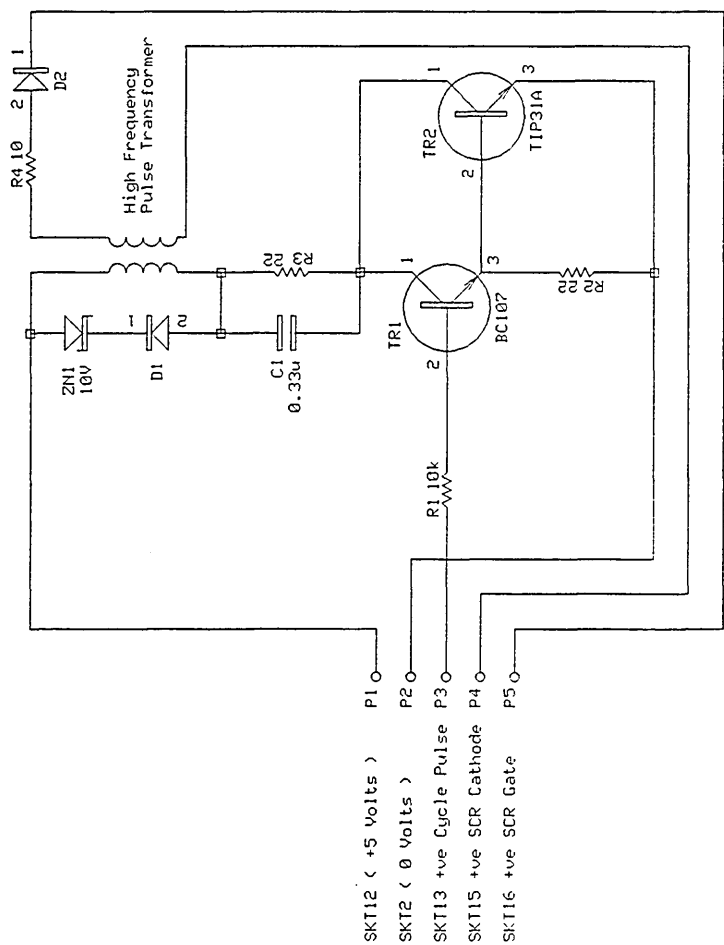
- SKT3 (+5 Volts)
- SKT4 (0 Volts)
- SKT5 (-5 Volts)
- BD1 IC1
- Reference
- SKT11 Monitor Comp. Output
- BD3 IC4d
- BD3 IC3a
- BD3 IC3c
- BD3 IC4b
- BD3 IC1a
- SKT15 Initiate



P04 Switch Control
 Wiring Schematic
 Board 3
 Sheffield Hallam University
 School of Engineering
 Drawn by R.E. Brown
 Date : 29/March/1999
 Page 3 of 3

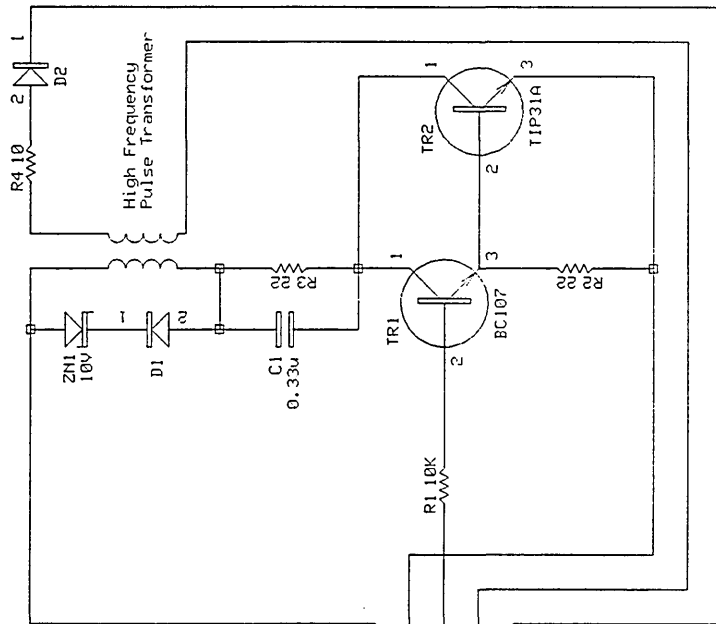






PDM Switch Control
 Wiring Schematic
 Supplementary Board 3
 Sheffield Hallam University
 School of Engineering
 Drawn by R.E. Brown
 Date : 29 March 1999
 Page 3 of 4

SKT12 (+5 Volts) P1 O
 SKT2 (0 Volts) P2 O
 SKT14 -ve Cycle Pulse P3 O
 SKT17 -ve SCR Cathode P4 O
 SKT18 -ve SCR Gate P5 O



Appendix 5

Fuse Test Facility, Digital Storage Oscilloscope Specifications

Digital Storage Oscilloscope - Type 400

Manufacturer: Gould Instrument Systems Ltd.,
Roebuck Road, Hainault, Ilford, Essex. IG6 3 EU

Display :	
CRT :	5-inch diagonal screen. Raster scan, Vertically scanned.
Graticule :	Electronically generated 8 × 10 divisions with 0.2 subdivisions.
Intensity :	Separate controls for traces, Graticules and Alphnumerics
Vertical System :	Two identical channels, CH1 and CH2. Inputs via BNC connectors
Sensitivity :	2mV/div to 5mV/div in 1-2-5 sequence.
Accuracy :	±2.5% of reading ±1 digitising level (1/30th of a division)
Variable Sensitivity :	> 2.5:1 range allowing continuous adjustment of sensitivity between ranges.
Input Impedance :	1MΩ/28pF
Input Coupling :	DC-GND-AC
Bandwidth :	0-20 MHz (-3dB)
Input Protection :	400V dc or Peak AC. (10KHz or less on all ranges below 0.2V/div.)
Expansion :	Post storage × 0.062 to 4.00
Horizontal System :	
Sweep rate :	27 ranges in 1-2-5 sequence
Transient capture :	500 ns/div to 50s/div
Repetitive Sampling :	200 and 100 ns/div
Sample accuracy :	±0.01% of sample time
Expansion :	× 10 with linear dot interpolation
Trigger Delay	
Trigger delay range :	20ns to 5000s
Trigger delay accuracy :	±0.015, ±1ns
Pre trigger :	0 to 98% of sweep in 0.45 steps
Resolution :	25 of time/div, 20 ns min.
Trigger System :	Variable level control with Auto/Normal facility, resolution of less than 0.1 div.
Auto/Normal Mode :	In Auto the time base free runs when insufficient signal (20 Hz - 20, 50 or 100 MHz) is present or when the selected level is outside the range of the input signal.
Source :	CH1, CH2, External or Line
Coupling :	DC, AC, High frequency reject filter.
Slope :	+ve or -ve

Sensitivity :	Internal DC Coupled <0.3 div DC to 2 MHz <1.5 div 2 MHz to 20 MHz Internal AC Coupled <0.3 div 10 Hz to 2 MHz <1.5 div 4 Hz to 20 MHz External DC Coupled <150 mV DC to 2 MHz <600 mV 10 Hz to 2 MHz External AC Coupled <150 mV 10 Hz to 2 MHz <600 mV 4 Hz to 2 MHz
Range :	Internal ± 10 divisions External $\pm 3V$.
External Input Impedance :	100k Ω /10 pF.
External Input Protection :	250V DC or peak AC
Trigger Jitter, non ETS Ranges :	(50 s/Div to 500 ns/Div), ± 25 of time /div (un expanded), ± 2 ns
Trigger Jitter ETS Ranges	± 2 ns

Display Modes :

Refreshed:	Stored data and display updated by triggered sweep
Roll :	Stored data and display updated continuously for time bases 50ms/div to 50sec/div. Trigger stops the updating process. Refresh and roll operate as repetitive single shot for time base ranges faster than 50ms/div.
Dot Join :	Dots are joined by vertical raster lines. Linear dot interpolation is provided when the trace is horizontally magnified (using Mag).
X-Y :	X-Y display is 8 \times 8 divisions. Stored data and display are updated by triggered sweep. There is no dot joining, $\times 10$ expansion or cursor in this mode. CH1 is used as the X (8 bit resolution 25 steps/div) and CH2 as the Y (7 bit resolution 15 levels/div) deflection.
Single trace :	CH1 or CH2
Dual trace :	CH1 and CH2
Add :	CH1 and CH2 can be added to give the algebraic sum of the two channels. Addition is pre-storage.
Invert :	Both channels may be independently inverted.
Single Shot :	Freezes store at the end of a single triggered sweep.
Display trace hold : (all)	Freezes the display immediately.
Channel 1 Trace hold	Freezes channel 1 display immediately.
Channel 2 Trace hold :	Freezes channel 2 display immediately
Reference trace :	One reference trace can be displayed in addition to the two input channels. This can display a waveform memory of a trace copied from CH1 or CH2.

Acquisition System	
Maximum sample rate	100 mega samples/sec simultaneously on each channel.
Vertical resolution :	8 Bits (1 in 256) 30 levels per division.
Record length :	501 points per channel.

Acquisition Modes

Normal Mode :	Transient and repetitive signal capture. (Repetitive capture is only on time base ranges faster than 200 ns/div. This gives an equivalent sample rate of 2ns/sample on the 100 ns/div range.
X - Y Mode :	Bandwidth 20, 50 or 100 MHz (-3 dB) depending on the instrument type. Phase difference $<3^\circ$ at 1/200 of the bandwidth. Acquisition rate dependent on the time base range.
Averaging :	Averages can be set from 2 to 256 in binary sequence, selected from the menu system. Averaging operates continuously or, using single shot for the set number of acquisitions, (weighted range).
Peak detection :	Minimum pulse width 1 μ s. 100% probability of capture. Operates on time base range 100 μ s/div or slower.

On Screen

Measurements

Accuracy :	Voltage $\pm 2.5\%$ of reading, ± 1 digitising level (1/30 of a division) Time $\pm 0.01\%$ of reading ± 1 digit.
Resolution ;	Voltage 0.4% of FSD. Time 0.2% of FSD.

RS423 Interface

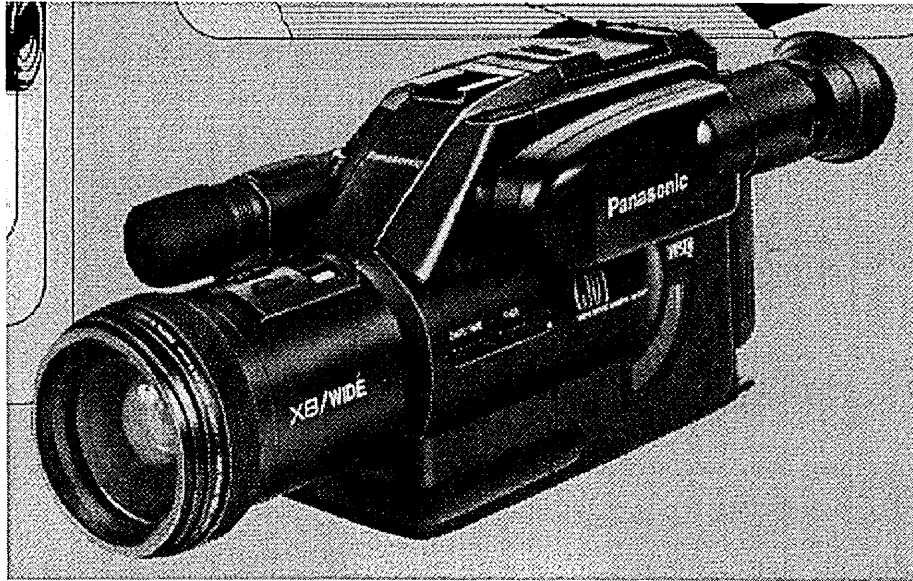
	Serial interface port for bi-directional waveform data and associated range parameter transfer.
Baud rate:	75, 150, 300, 600, 1200, 2400, 4800, 9600.
Data bits :	8.
Parity :	None.
Start-stop :	Fixed : one start, one stop bit.

Appendix 6

Slow Speed Video Camera Specifications

Type: Panasonic NV-G101B

Manufacturer: Matsushita Electric Industrial Co. Ltd., Osaka, Japan



Specifications.

Video Recording System	4 Rotary heads, helical scanning system
Tape Speed	23.39mm/s
Tape Format	VHS-c
Recording/Playback Time	45min. with NV-EC45E
Video	
Television System	CCIR; 625 lines, 50 fields PAL colour signal
Modulation System	Luminance; FM azimuth recording
Output Level	Video out (Phono) 1.0 v p-p
Image Sensor	1/3 inch CCD image sensor
Lens	8:1 2speed power zoom lens with digital AI auto focus. F1.4 Auto iris Filter diameter 49mm
Viewfinder	2/3 inch electronic viewfinder
Standard Illumination	1,400 lux
Minimum Required Illumination	3 lux
Video Horizontal Resolution Colour	VHS; more than 230 lines
Signal to Noise Ratio	Vide; more than 40dB

Appendix 7

Medium Speed Video Camera Specifications

Type: Motionscope® 2000S

Manufacturer: Redlake Imaging Corporation, California, USA.



Specifications

Sensor Resolution Up to 480×420 8-bit pixels per frame, depending on the frame rate.

Sensor Array	656×496 Pixels
Recording Rates	(50 PAL), 60,125,250,500,1000,2000.
Exposure Rates	Electronic shutter operates at the rates of 1× to 20× of set recording rates. Ranges from 1/60 th sec. To 1/80,000 th sec.
Frame Storage	16384 Frames, standard memory.
Lens	Standard C-mount
Size	Camera head 6.2cm (H)×6.2cm (W)×10cm (L)

Appendix 8

Fast Speed Video Camera Testing Results.

A8.1 Examples of Encoder Wheels Designed to Simulate Fuse Element Fragmentation and Arc Ignition and Results of Sensor Outputs.



Figure A8.1 Encoder wheel designed to simulate sequential fragmentation and arc ignition initiated at one end of the fuse element

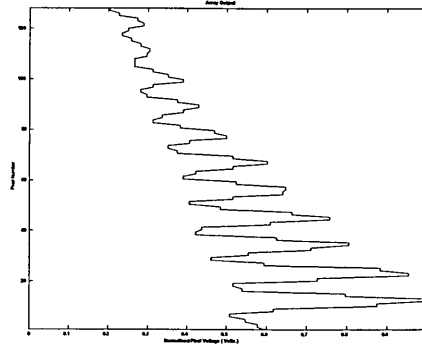


Figure A8.2 Normalised sensor output - sensor integration time = 1.5 ms



Figure A8.3 Encoder wheel designed to simulate sequential fragmentation and arc ignition initiated at one end of the fuse element

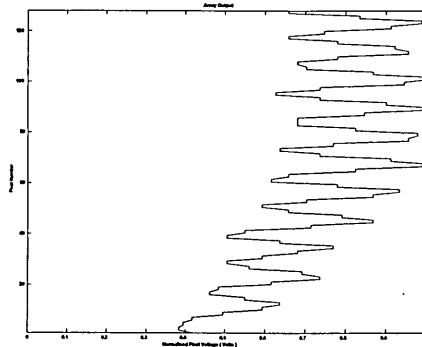


Figure A8.4 Normalised sensor output - sensor integration time = 1.5 ms



Figure A8.5 Encoder wheel designed to simulate sequential fragmentation and arc ignition initiated in the centre of the fuse element

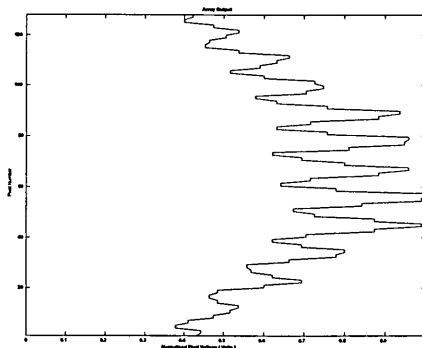


Figure A8.6 Normalised sensor output - sensor integration time = 1.5 ms

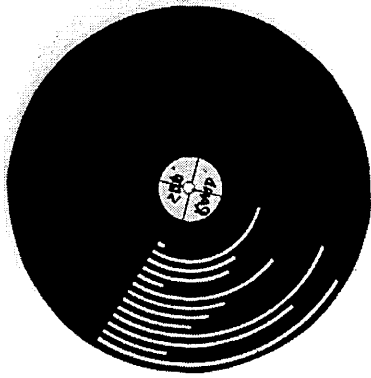


Figure A8.7 Encoder wheel designed to simulate random sequential fragmentation and arc ignition

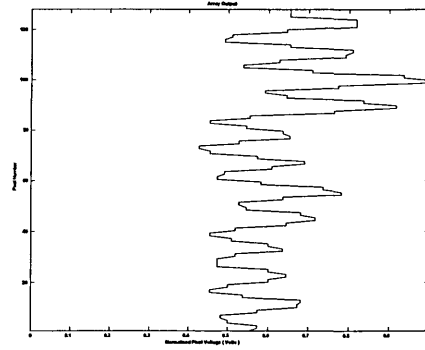


Figure A8.8 Normalised sensor output - sensor integration time = 1.5 ms



Figure A8.9 Encoder wheel designed to simulate sequential fragmentation and arc ignition and subsequently arc expansion

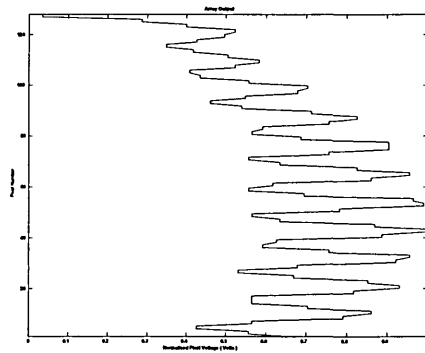


Figure A8.10 Normalised sensor output - sensor integration time = 1.5 ms

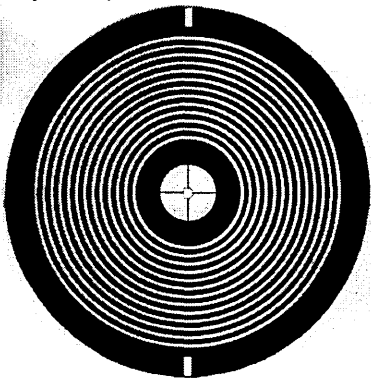


Figure A8.11 Encoder wheel designed to simulate simultaneous fragmentation and arc ignition of the whole element

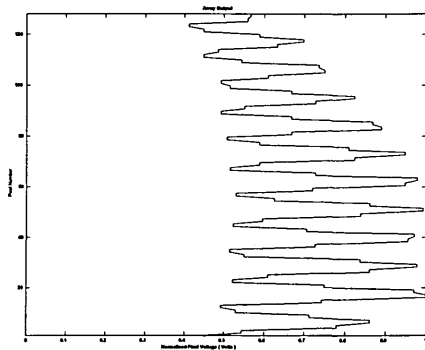


Figure A8.12 Normalised sensor output - sensor integration time = 1.5 ms

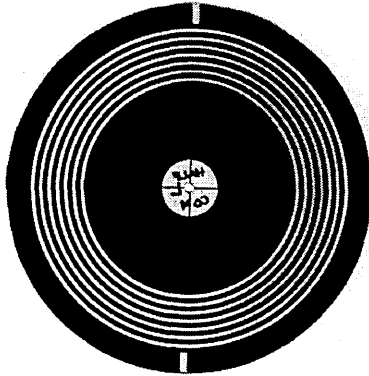


Figure A8.13...Encoder wheel designed to simulate simultaneous element fragmentation and arc ignition initiated at one end of the fuse element

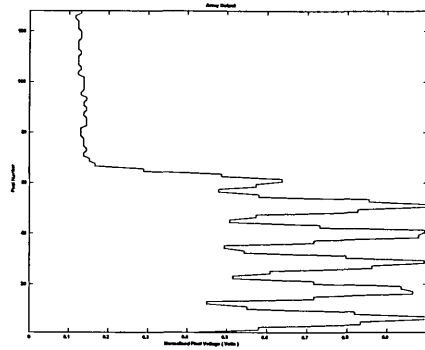


Figure A8.14 Normalised sensor output - sensor integration time = 1.5 ms

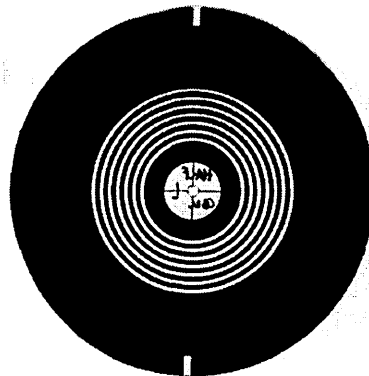


Figure A8.15 Encoder wheel designed to simulate simultaneous element fragmentation and arc ignition initiated at one end of the fuse element

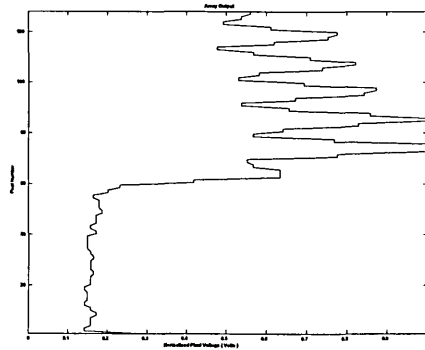


Figure A8.16 Normalised sensor output - sensor integration time = 1.5 ms

A8.2 Results of Sensor Output Monitoring Exercise

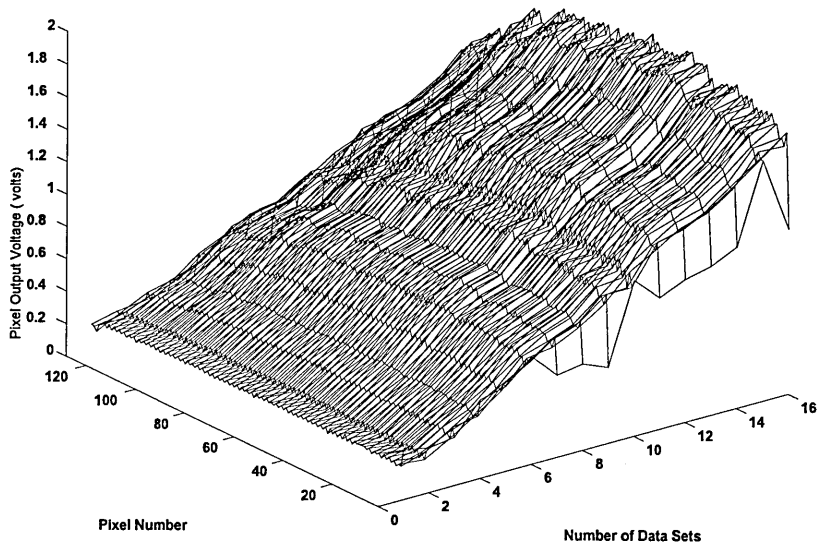


Figure A8.17 Mesh plot of sensor pixel output voltage against integration time (data set 1 = 100 us, set 15 = 1 500us)

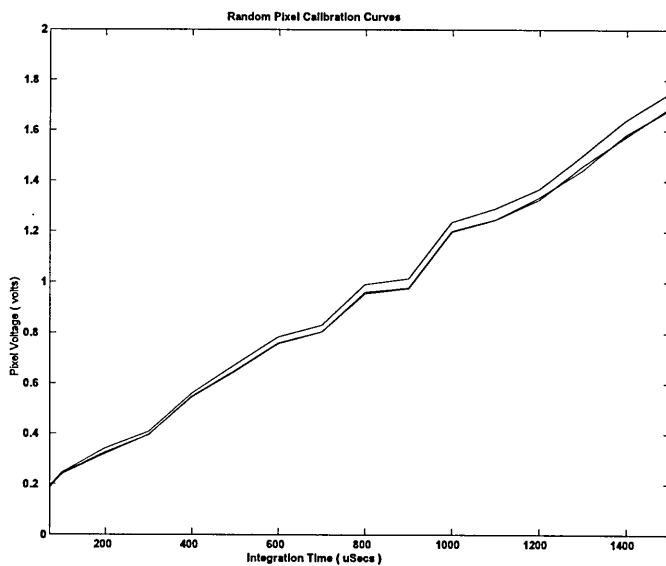


Figure A8.18 Plot of pixel output voltage against integration time (Random pixels selected)

Appendix 9

Fast Speed Video Camera Commissioning Results.

A9.1 Results of Sensor Light Intensity Range Tests

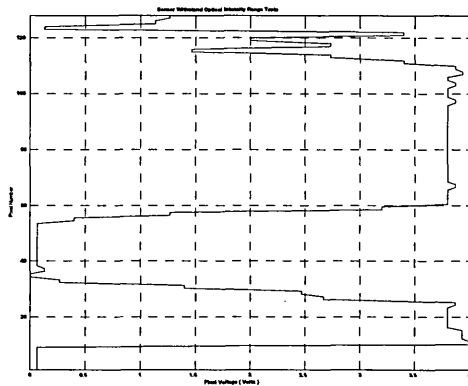


Figure A9.1 Sensor Output, Integration time = 65.5µs, No Filter

Fuse and Test Specifications

Element = Copper
Size = 0.2mm Ø/25mm (I)
Filler = Fine Quartz
Supply Voltage = 240 volts rms 50 Hz
Prospective Current = 320 Amps
Fault Application = Voltage Zero
Pre arcing Time ≈7ms

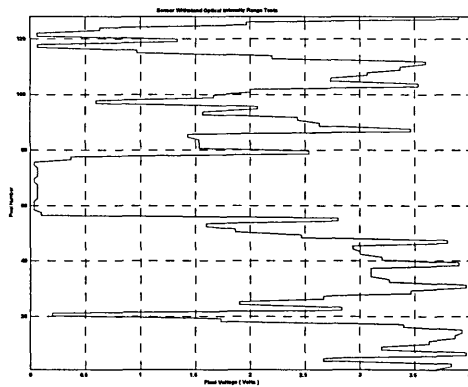


Figure A9.2 Sensor Output, Integration time = 65.5µs, Luminance transmittance 0.16% max. - 0.061% min

Fuse and Test Specifications

Element = Copper
Size = 0.2mm Ø/25mm (I)
Filler = Fine Quartz
Supply Voltage = 240 volts rms 50 Hz
Prospective Current = 320 Amps
Fault Application = Voltage Zero
Pre arcing Time ≈7ms

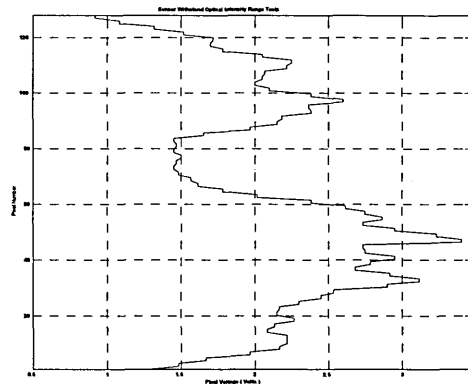


Figure A9.3 Sensor Output, Integration time = 65.5µs, Filter Luminance transmittance 0.061% max. - 0.023% min

Fuse and Test Specifications

Element = Copper
Size = 0.2mm Ø/25mm (I)
Filler = Fine Quartz
Supply Voltage = 240 volts rms 50 Hz
Prospective Current = 320 Amps
Fault Application = Voltage Zero
Pre arcing Time ≈7ms

A9.2 Results of Noise Immunity Tests

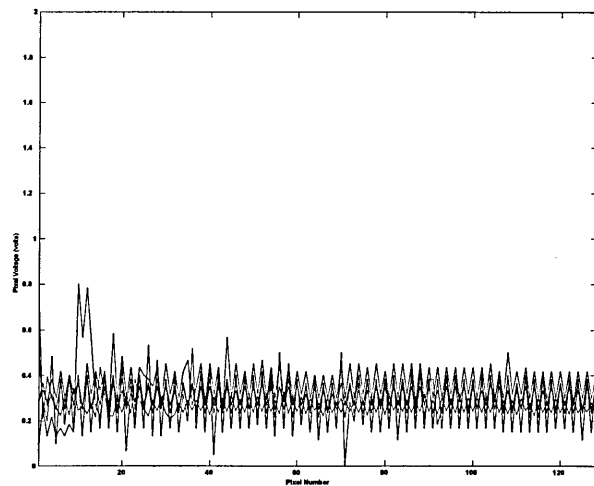


Figure A9.4 Fast speed video camera commissioning. - Noise immunity test results. – Camera image of homogenous light source when separately triggered by fuse disintegration.

Appendix 10

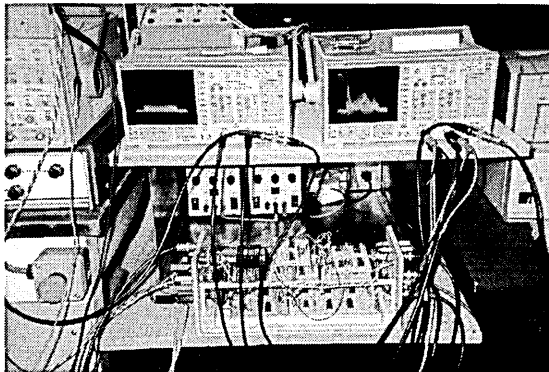
Fast Speed Video Camera Specifications

A10.1 Performance Specifications.

Accuracy	$\pm 1\%$ fsd fsd = 2volts/1.5ms integration time
Clock frequency	5kHz min – 2MHz max
Image Lag	<5% [79]
Output noise voltage	$\approx 3\text{mVrms}$ [79]
Pixel response non-uniformity	1%min - 10%max
Repeatability	>95%
Resolution	16.6 mV/div
Set up time – serial input SI	20ns [79]
Sensor Integration time	65.5 μs min – 100ms max
Sensor Output Range	0-2 Volts nominal 0-3 Volts max Sensor integration time = 65.5 μs , Filter luminance transmittance = 0.16%max 0.061%min
Spectral Response	300nm – 700nm [79]

A10.2 Schematic Wiring Diagrams.

The following pages present the interconnecting wiring diagrams and the schematic diagrams of the circuits, which comprised the fast speed video camera control unit (Figure A10.1) and the internal wiring of the camera (Figure A10.2). The camera control unit was made up of seven separate boards and consequently the boards are referred to numerically.



A10.1 Fast speed video camera control unit.

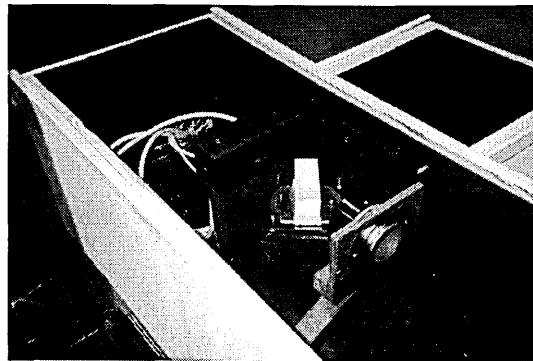
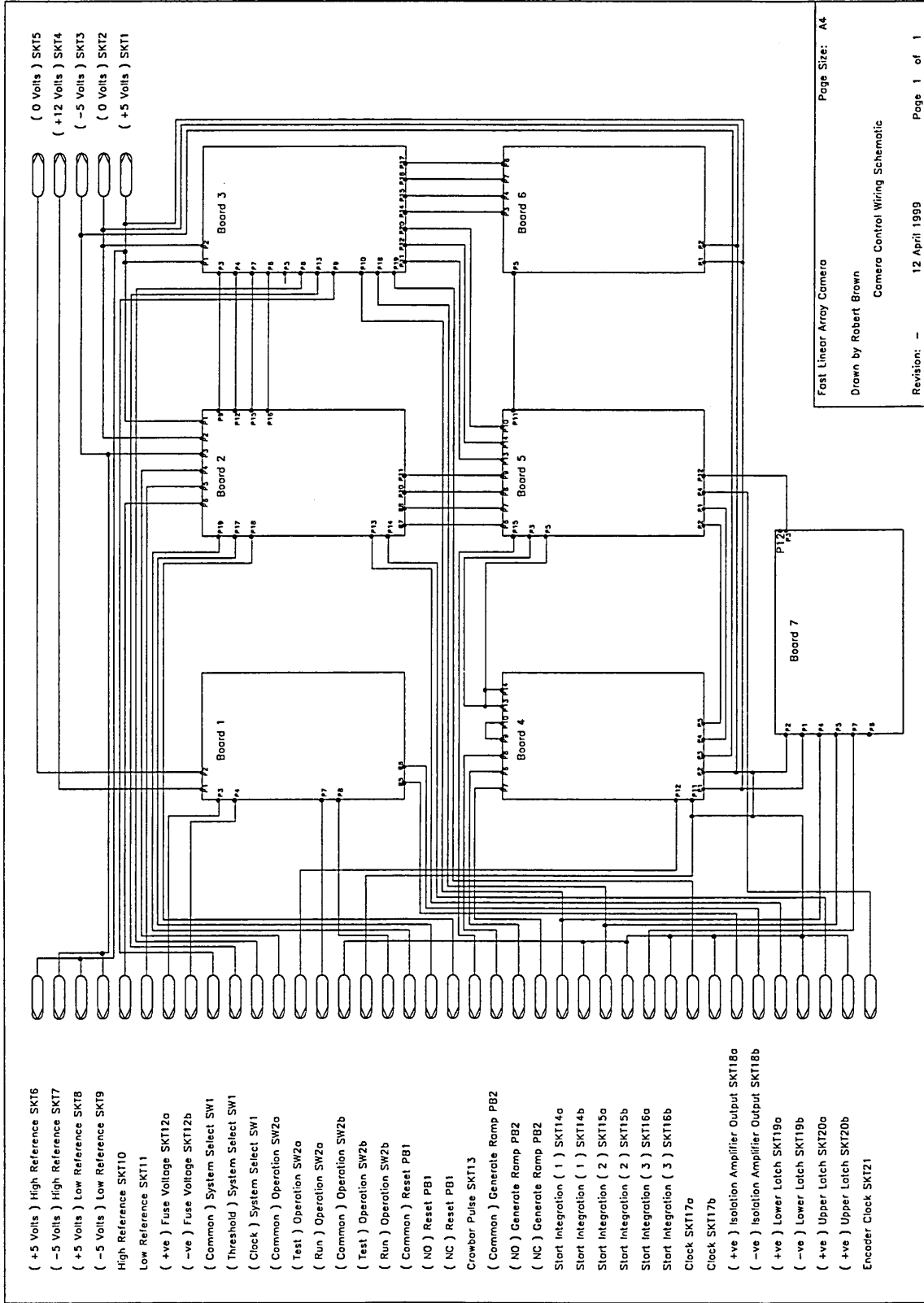
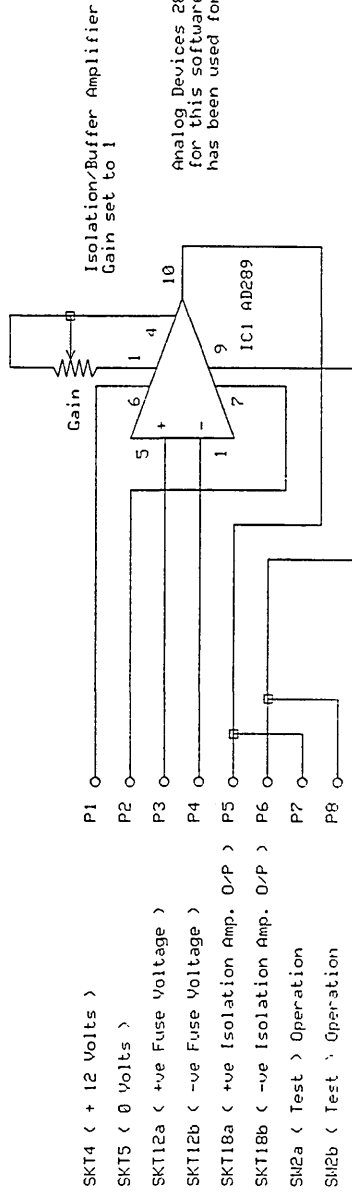
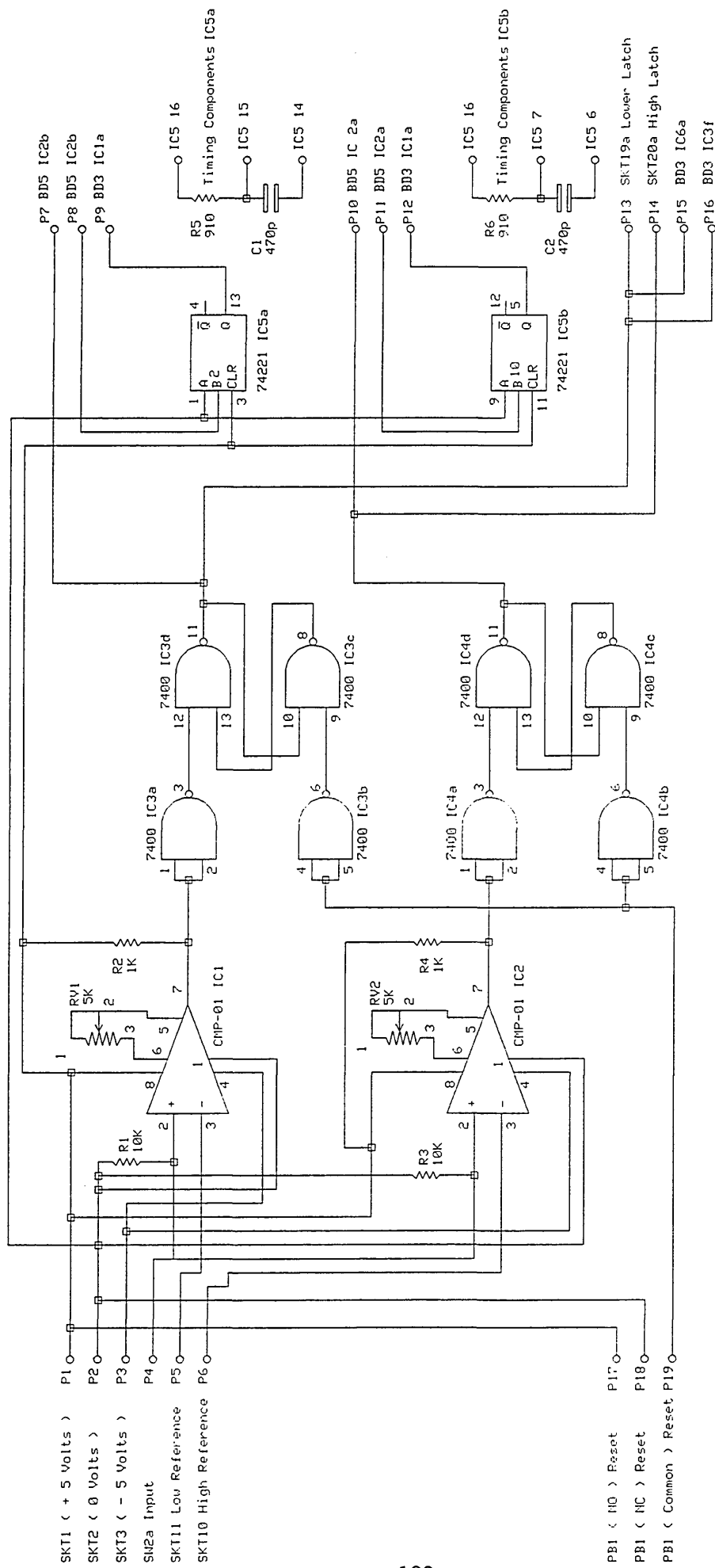


Figure A10.2 Fast speed video camera

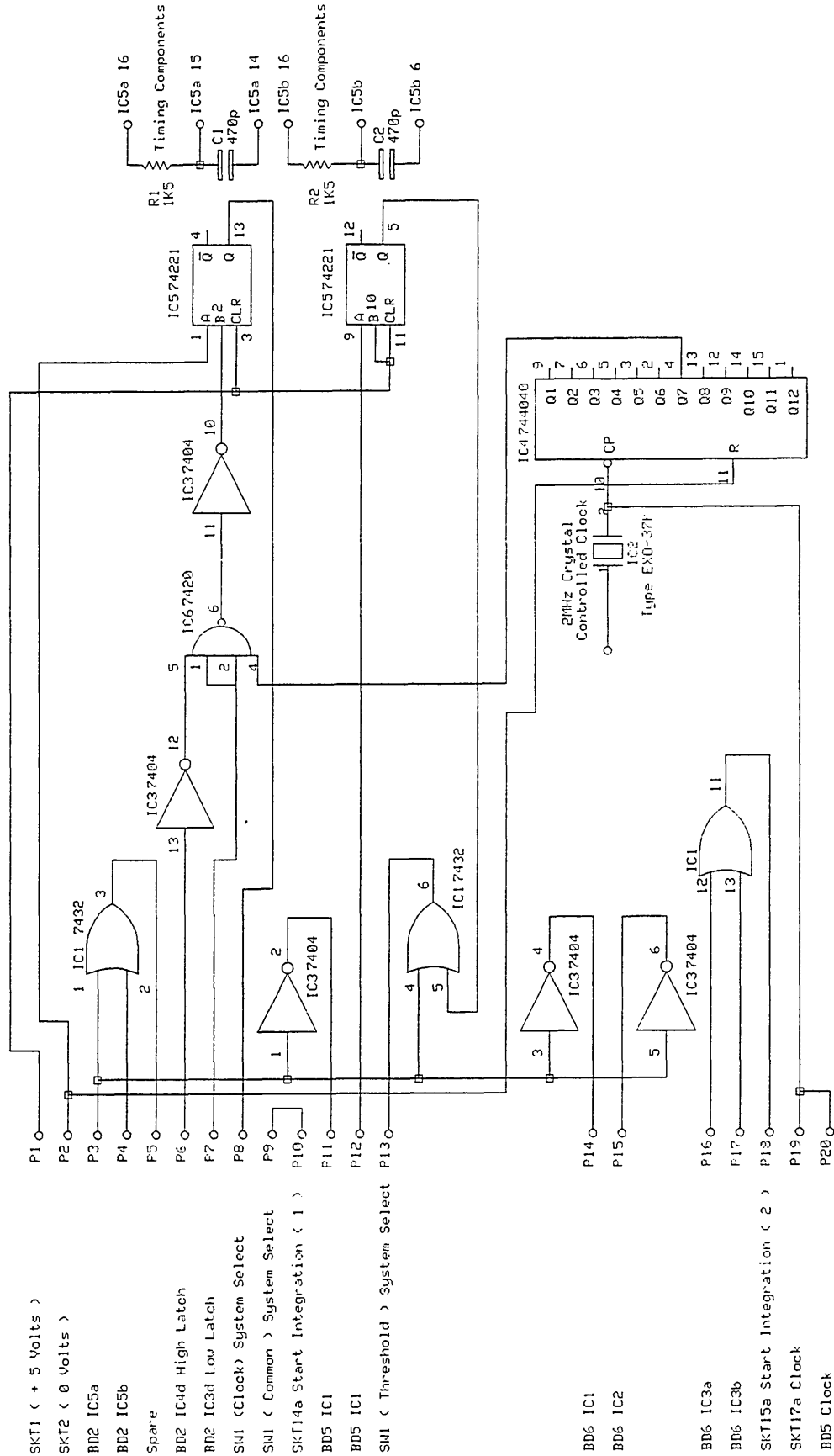




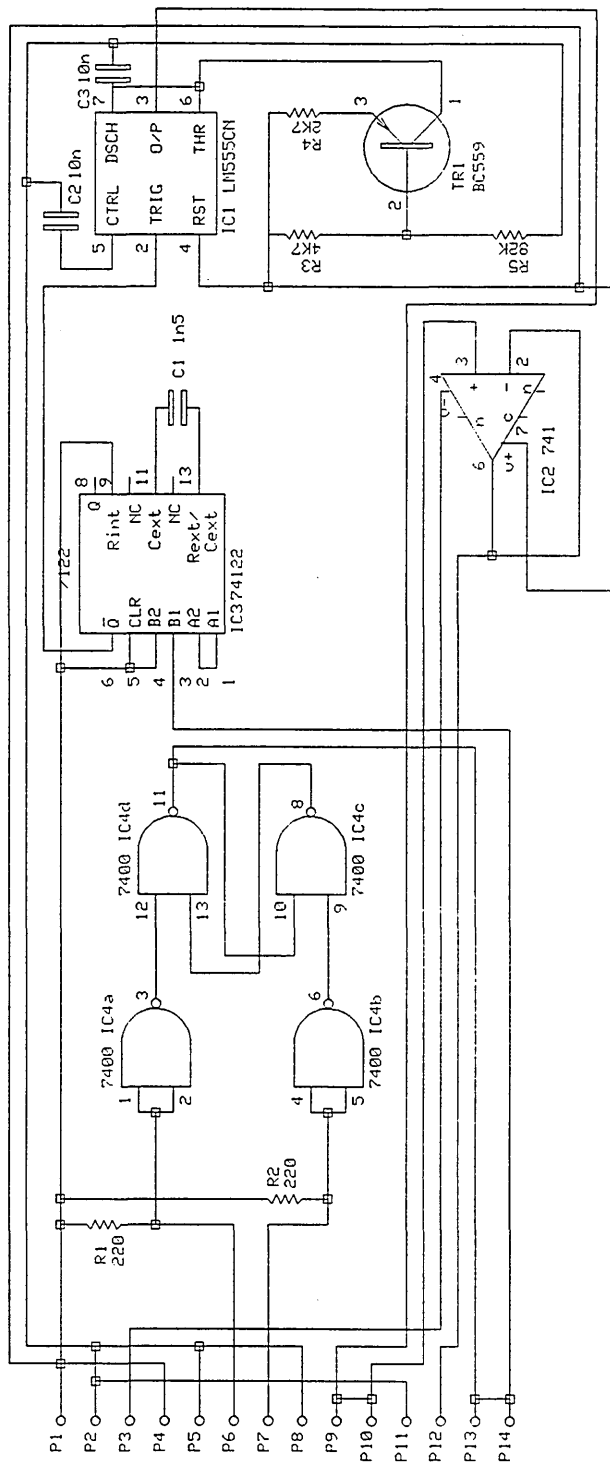
Analog Devices 289 is a non standard device package for this software. A standard Op amp package has been used for this schematic diagram.



Fast Linear Array Camera
 Wiring Schematic
 Board 2
 Sheffield Hallam University
 School of Engineering
 Drawn by R.E. Brown
 Date : 29:March:1999
 Page 2 of 7

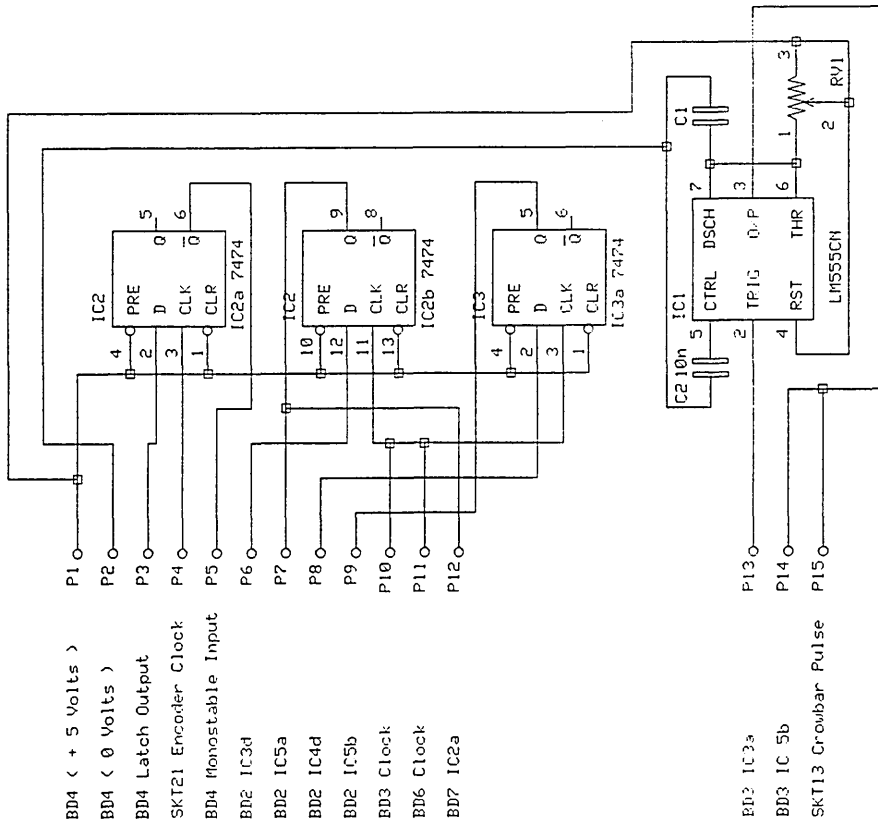


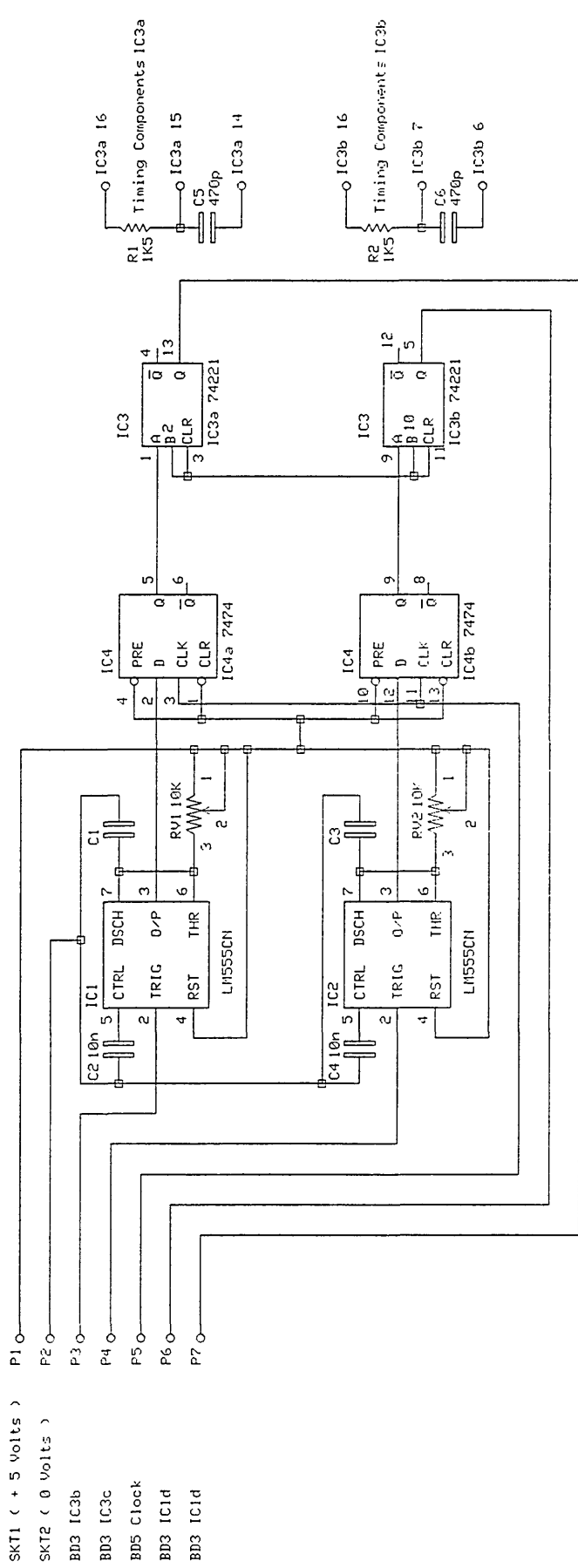
Fast Linear Array Camera
 Wiring Schematic
 Board 3
 Sheffield Hallam University
 School of Engineering
 Drawn by R.E. Brown
 Date : 29:March:1999
 Page 3 of 7



- SKT1 < + 5 Volts >
- SKT2 < 0 Volts >
- SKT3 < - 5 Volts >
- BD5 < + 5 Volts >
- BD5 < 0 Volts >
- PB2 < IN > Generate Ramp
- PB2 < IN > Generate Ramp
- PB2 < Common > Generate Ramp
- Ramp Generator Output
- Buffer Amplifier Input
- SH2b < Test > Operation
- SH2a < Test > Operation
- Latch Output
- Monostable Input

Fast Linear Array Camera
 Wiring Schematic
 Board 4
 Sheffield Hallam University
 School of Engineering
 Drawn by R.E. Brown
 Date : 29 March 1999
 Page 4 of 7



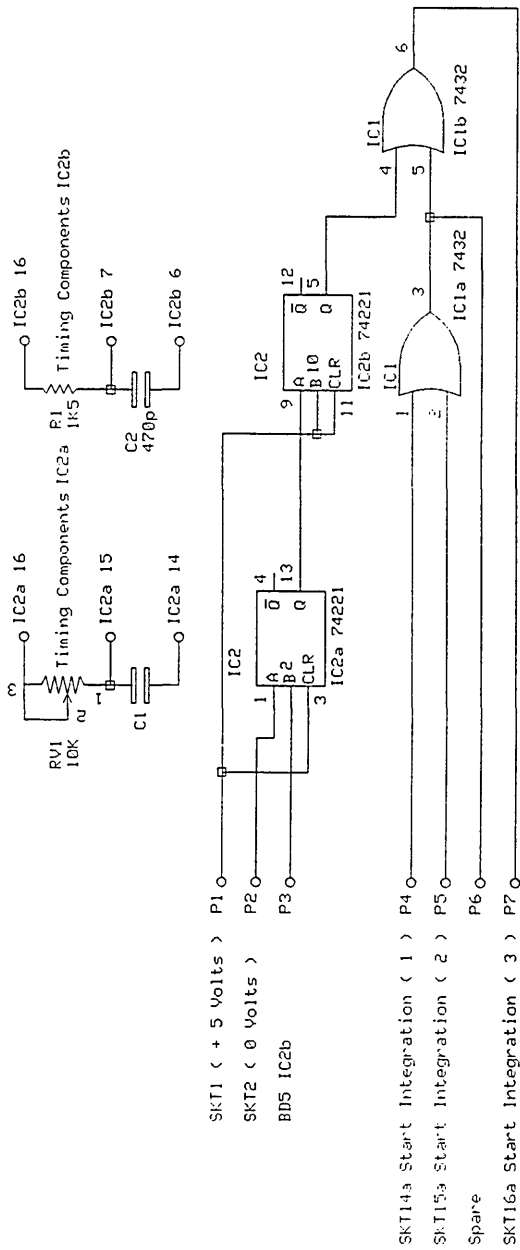


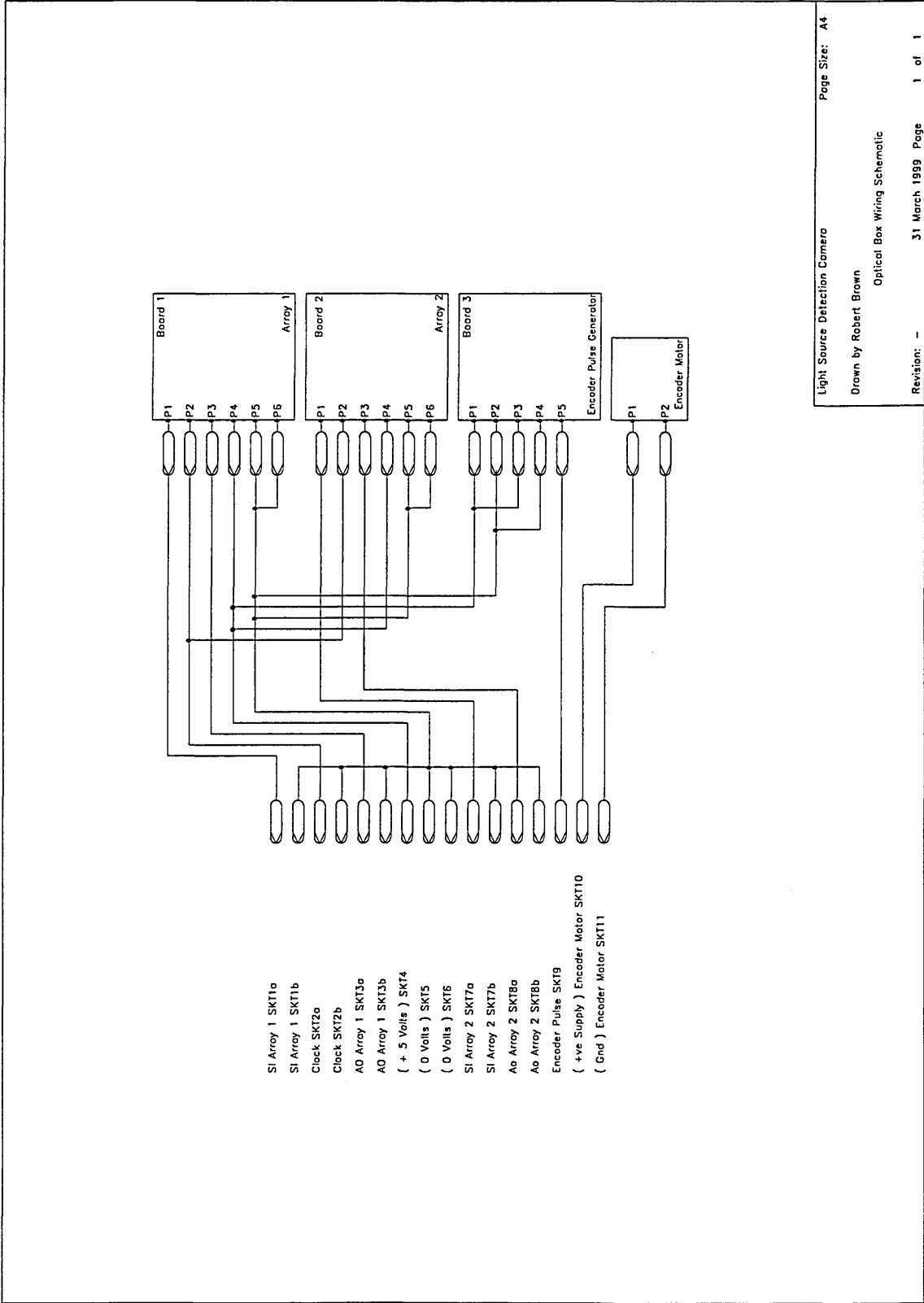
SKT1 (+ 5 Volts)
 SKT2 (0 Volts)
 BD3 IC3b
 BD3 IC3c
 BD5 Clock
 BD3 IC1d
 BD3 IC1d

IC3a 16
 Timing Components IC3a
 IC3a 15
 C5
 470p
 IC3a 14

IC3b 16
 Timing Components IC3b
 IC3b 7
 C6
 470p
 IC3b 6

Fast Linear Array Camera
 Wiring Schematic
 Board 6
 Sheffield Hallam University
 School of Engineering
 Drawn by R.E. Brown
 Date : 29:March:1999
 Page 6 of 7





Appendix 11

Analysis of the Dynamic Behaviour of Current Carrying Wires up to Melting Temperature.

The energy conservation equations for transient current carrying wires up to the melting temperature is given by Equation A11.1.

$$\begin{array}{l} \text{Electrical input} \\ \text{energy} \end{array} = \begin{array}{l} \text{Heat required to} \\ \text{raise the wire to} \\ \text{melting} \\ \text{temperature} \end{array} + \begin{array}{l} \text{Heat lost} \\ \end{array} + \begin{array}{l} \text{Kinetic Energy} \end{array} \quad \text{Eq. A11.1}$$

For simplicity, it is reasonable to assume that the heat losses from the wire are negligible if $l \gg d$. Consequently, the energy conservation equation becomes,

$$\int_0^{t_{pa}} i^2 \frac{\rho l}{S} = \int_0^{T_{melt}(t=t_{pa})} mTCdT + \int_{l(t=0)}^{l(t=t_{pa})} Wdl + F_r \int v^2 dv + m \int vdv \quad \text{Eq. A11.2}$$

The temperature rise of the wire $T(t)$ is given by Equation A11.3 [4][13].

$$T(t) = \int \frac{\rho_o}{S_o^2 C_o \gamma_o} i_o^2 \frac{[1 + \alpha T(t) + \zeta T^2(t)]}{[1 + \beta T(t) + \eta T^2(t)][1 + \delta T(t) + \xi T^2(t)]} dt \quad \text{Eq. A11.3}$$

In the following solution, Equation A11.3 was solved exactly using MathCad (Figures A11.2 – A11.33). For the purposes of this analysis the equation approximates to the following relationship.

$$T(t) \approx \frac{\rho_o}{S_o^2 C_o \gamma_o} \int i^2 dt \quad \text{Eq. A11.4}$$

The increase in length of the wire $l(T)$ is given by Equation A11.5,

$$l(T) = l_o (1 + \delta T(t) + \xi T^2(t)) \quad \text{Eq. A11.5}$$

$$l(T) \approx l_o (1 + \delta T(t)) \quad \text{Eq. A11.6}$$

Consequently, the incremental increase in length of the wire is

$$\Delta l(T) = l(T) - l_o \approx l_o \delta T(t) \quad \text{Eq. A11.7}$$

A11.1 Analysis of the Velocity of Wire Vibration due to Symmetrical AC Current.

The current waveform is given by Equation A11.8,

$$i(t) = \hat{I} \sin \omega t \quad \text{Eq. A11.8}$$

therefore the temperature rise $T(t)$ of the wire is,

$$T(t) \approx \frac{\rho_o}{S_o^2 C_o \gamma_o} \int \hat{I}^2 \sin^2 \omega t \, dt \approx \frac{\rho_o}{S_o^2 C_o \gamma_o} \int \left(\frac{1 - \cos 2\omega t}{2} \right) dt \quad \text{Eq. A11.9}$$

and the increase in the length $l(T)$ of the wire follows as,

$$\Delta l = \frac{l_o \delta \rho_o}{S_o^2 C_o \gamma_o} \int \left(\frac{1 - \cos 2\omega t}{2} \right) dt \quad \text{Eq. A11.10}$$

The velocity of increase in wire length $\frac{dl}{dt}$ is given by,

$$v = \frac{dl}{dt} = \frac{l_o \delta \rho_o}{S_o^2 C_o \gamma_o} \left(\frac{1 - \cos 2\omega t}{2} \right) \quad \text{Eq. A11.11}$$

And the acceleration $\frac{d^2 l}{dt^2}$ by,

$$a = \frac{d^2 l}{dt^2} = \frac{\omega l_o \delta \rho_o}{S_o^2 C_o \gamma_o} \sin(2\omega t) \quad \text{Eq. A11.12}$$

Consequently, an acceleration force exists given by,

$$= S_o l_o \gamma_o \times \frac{\omega l_o \delta \rho_o}{S_o^2 C_o \gamma_o} \sin(2\omega t) = \frac{l_o^2 \omega \delta \rho_o}{S_o C_o} \sin(2\omega t) \quad \text{Eq. A11.13}$$

Waveforms indicating the time varying nature of Equations A11.11,A11.12 and A11.13 are shown in Figure A11.1

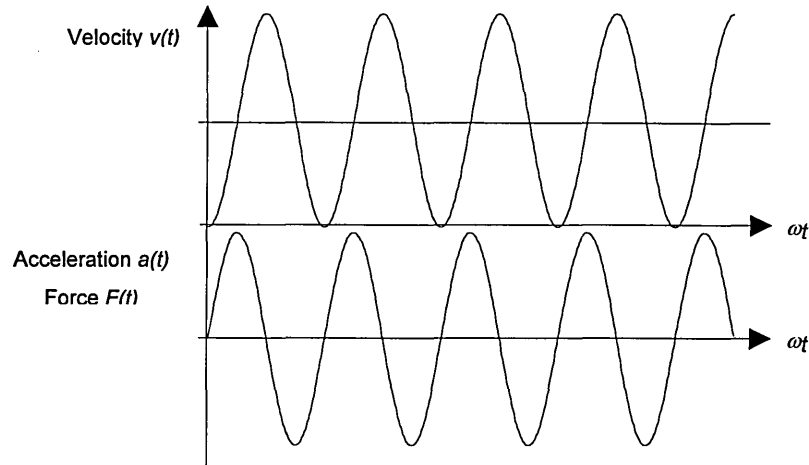


Figure A11.1 Normalised waveforms of wire velocity, acceleration and force at fixed temperature.

A11.2 Consideration of MathCad Solution in the Long, Short and Very Short Time Domains.

Long Time Domain.

For wire melting in the long time domain ($80\text{ms} < t < 200\text{ms}$) wires will be subject to between 8 and 20 oscillations of diminishing amplitude with increase in oscillation number. The effect of the vibrations is therefore considered to be least for this time domain.

On a general point, the amplitude of the oscillations is considered to be temperature dependent, since metals, particularly silver, are very soft at their half-melting temperature. It is reasonable to conject that vibrations due to ac current wave shape will be observable over the period 80ms~200ms but they will also be highly damped by the change in physical state of the wire when its temperature is above half its melting value (Figure A11.33).

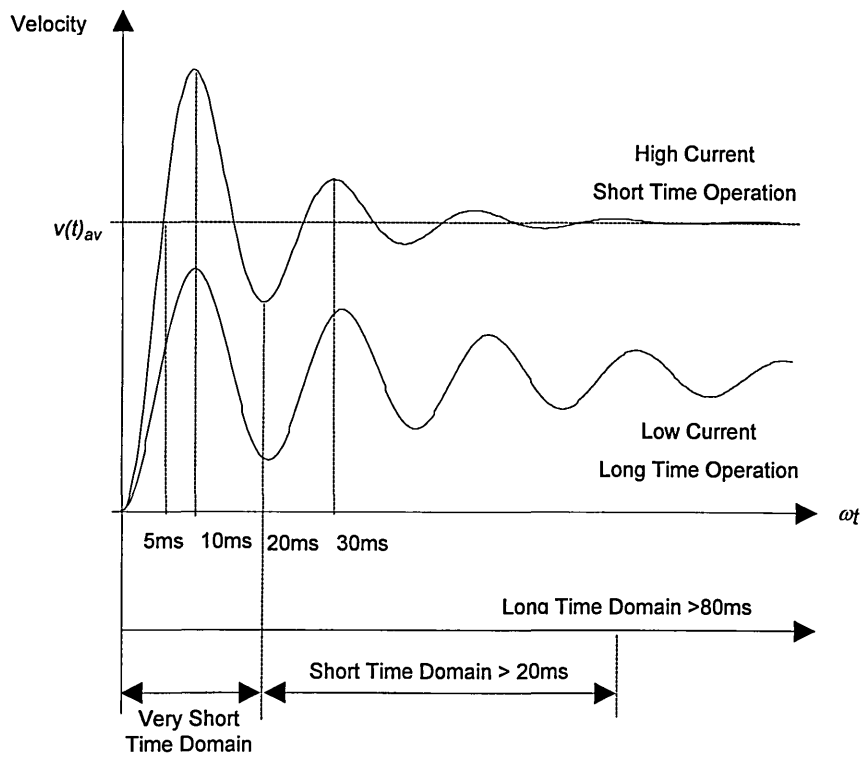
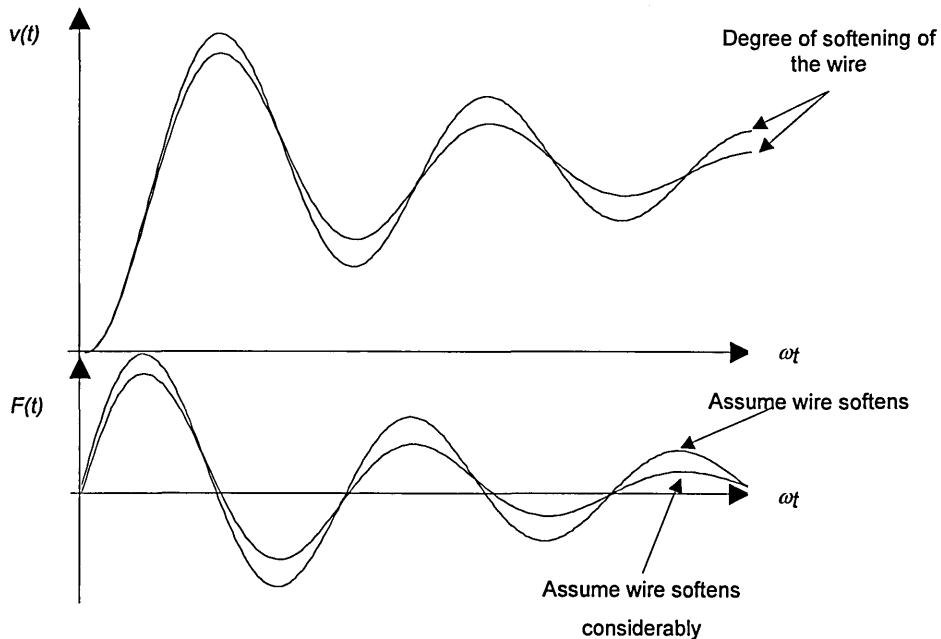


Figure A11.33 Diagram indicating the damping of current waveform induced wire vibrations by softening of the wire.

Short Time Domain.

The vibrational force although affected by the softening of the wire will exist nevertheless, and hence will, assist in breaking the wire close to/or at the end terminal (solid/molten interface).



A11.34 Diagram indicating the assumed degree of wire softening in the short time domain.

Very Short Time Domain.

No vibrations occur in the very short time domain due to the wave shape. The analysis, however, demonstrates that the force due to thermal expansion of wires is significant in the very short time domain.

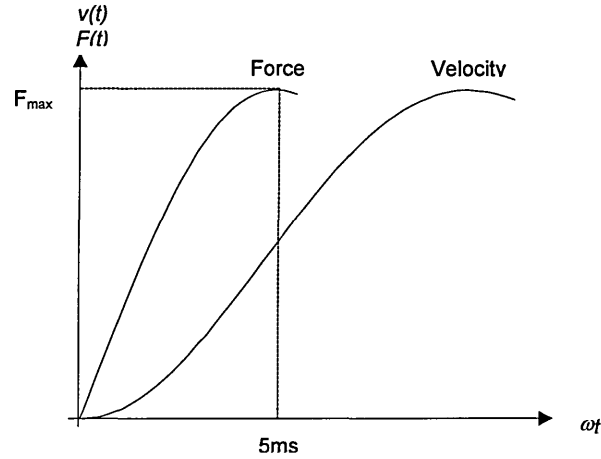


Figure A11.35 Diagram indicating the significant forces induced by waveform shape in the very short time domain

A11.3 Analysis of the Velocity of Wire Vibration due to DC Current.

The current in a dc inductive circuit is given by Equation A11.14,

$$i(t) = I \left(1 - e^{-\frac{t}{\tau}} \right) \quad \text{Eq. A11.14}$$

from which,

$$\int i^2 dt = I^2 \tau \left(\frac{t}{\tau} - \frac{3}{2} - 2e^{-\frac{t}{\tau}} + \frac{1}{2}e^{-\frac{2t}{\tau}} \right) \quad \text{Eq. A11.15}$$

A11.4 Consideration of DC Current MathCad Solutions in the Long, Short and Very Short Time Domains.

Very Short Time Domain

Assuming a practical time constant for a fuse of 20ms in Equation A11.15, operation in the very short time domain $t_{pa}=5\text{ms}$ gives,

$$\int i^2 dt \approx I^2 t \quad \text{Eq. A11.16}$$

The temperature rise $T(t)$ in the dc case,

$$T(t) = \int \frac{\rho_o}{S_o^2 C_o \gamma_o} i^2 \frac{[1 + \alpha T(t) + \zeta T^2(t)]}{[1 + \beta T(t) + \eta T^2(t)][1 + \delta T(t) + \xi T^2(t)]} dt \quad \text{Eq. A11.17}$$

The MathCad solution of this equation (Figure A11.32), for dc current in the very short time domain, shows that $l(t)$ approximates to $l_0 \alpha t^2$, hence $\frac{dl}{dt} \propto t$ and $\frac{d^2 l}{dt^2} = \text{constant}$. It follows from this that, the acceleration force acting on the wire will be a constant and hence no vibrations will occur.

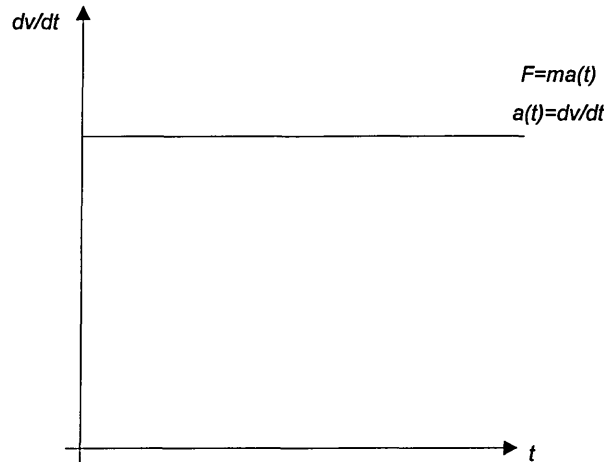


Figure A11.36 Diagram indicating the constant force and acceleration in wire length during very short time domain operation.

Short and Long Time Domains.

The waveforms of $i^2 dt$, $T(t)$, $l(t)$, $v(t)$ $a(t)$, and $F(t)$ are characteristically similar for all three time domains. Hence it follows that the change in the length of the wire with time is due solely to the thermo-physical temperature-dependent parameters for dc current carrying wires.

A11.5 Evaluation of the Height of a Catenary Shaped Deformed Wire.

For mathematical simplicity the catenary is assumed to be semi-circular.

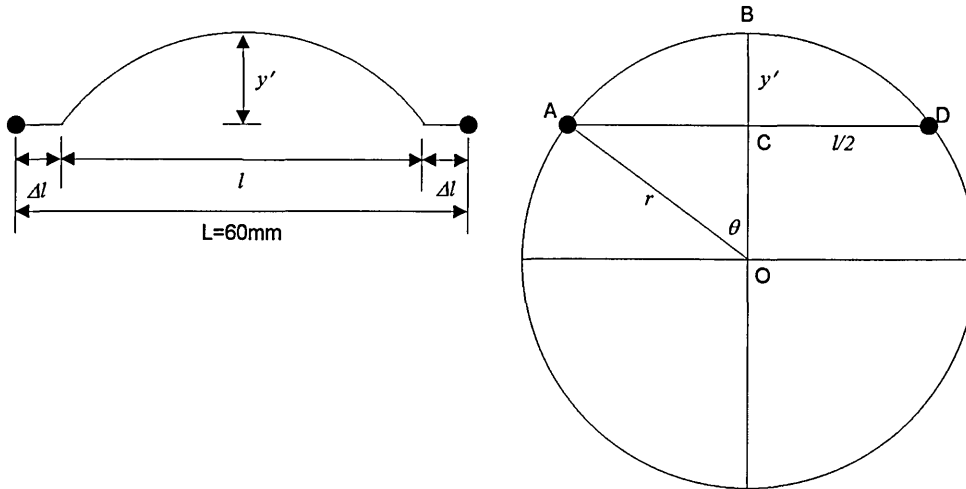


Figure A11.37 Geometrical notation for the evaluation of the height of a catenary shaped deformed wire.

$$\text{Arc } AB = r\theta = 1.023 \times \frac{l}{2} \quad \text{Eq. A11.18}$$

(from computation Figure A11.21)

$$\text{Chord } AO = r = \frac{\text{Chord } AC}{\sin \theta} = \frac{l}{2} \frac{1}{\sin \theta} \quad \text{Eq. A11.19}$$

Substitute Equation A11.19 into Equation A11.18

$$\frac{l}{2} \frac{\theta}{\sin \theta} = 1.023 \frac{l}{2} \quad \text{Eq. A11.20}$$

$$\therefore \theta = 1.023 \sin \theta \quad \text{Eq. A11.21}$$

Solution of Equation A11.21

$$\theta = 0.36652 \text{ rads } (21^\circ) \quad \text{Eq. A11.22}$$

Substituting Equation A11.21 into Equation A11.18

$$r = \frac{1.023l}{2 \times 0.36652} = 1.397l \quad \text{Eq. A11.23}$$

Determination of y'

$$y' = r(1 - \cos \theta) = 1.397l(1 - \cos(21^\circ)) = 0.0928 l \quad \text{Eq. A11.24}$$

Assuming $\Delta l = 5\text{mm}$, and $l = 50\text{mm}$

$$y' = 4.64\text{mm} \quad \text{Eq. A11.25}$$

A11.6 Determination of Force Acting on a Wire in a Confined Space.

For this case the wire's movement Δy will be less than y' , but it is assumed that in constricted media, $v(t) = \frac{dl}{dt} \approx 0$ and $a(t) = \frac{dv}{dt} \approx 0$. Therefore the only component of force would be obtained from the work done (WD), is that required to raise an unconstrained wire a distance Δy . It is also assumed that the energy expended in expanding the wire remains constant. Hence,

$$WD = F\Delta y \quad \text{Eq. A11.26}$$

Assuming this energy is constant, it follows that the force F acting on the wire is inversely proportional to the average distance the wire is displaced from the horizontal plane, e.g.

$$F = \frac{1}{\Delta y} \quad \text{Eq. A11.27}$$

The average displacement of the wire, Δy within a constricted media such as quartz sand filler will be much less than y' the displacement for wires in air, and will be even less for a wire encapsulated in resin. Consequently, the trapped force will act as a compressive stress (E) in the wire i.e.,

$$E = \frac{F}{S} \text{ per unit length} \quad \text{Eq. A11.28}$$

and hence from Equation A11.27,

$$E \propto \frac{1}{\Delta y} \quad \text{Eq. A11.29}$$

Given this analysis it is plain that constricted wires will be subject to greater stress due to restricted thermal expansion the more compacted the surrounding media. (Figures A11.38 and A11.39).

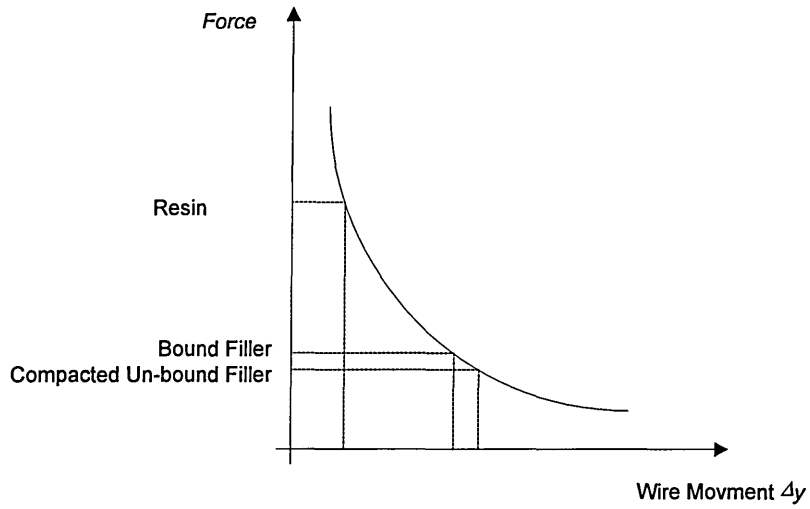


Figure A11.38 Graph indicating the relationship between wire movement and force exerted by thermal expansion for different surrounding media.

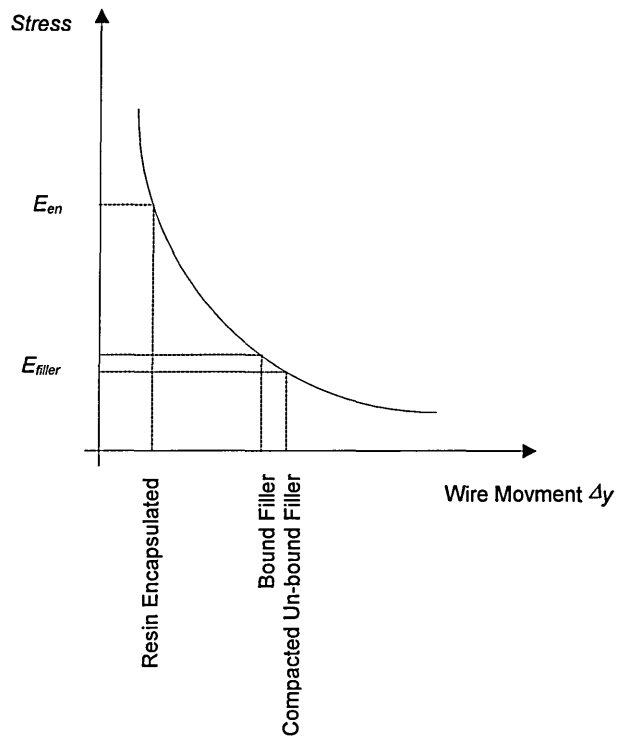


Figure A11.39 Graph indicating the relationship between wire movement and trapped wire stress for different surrounding media.

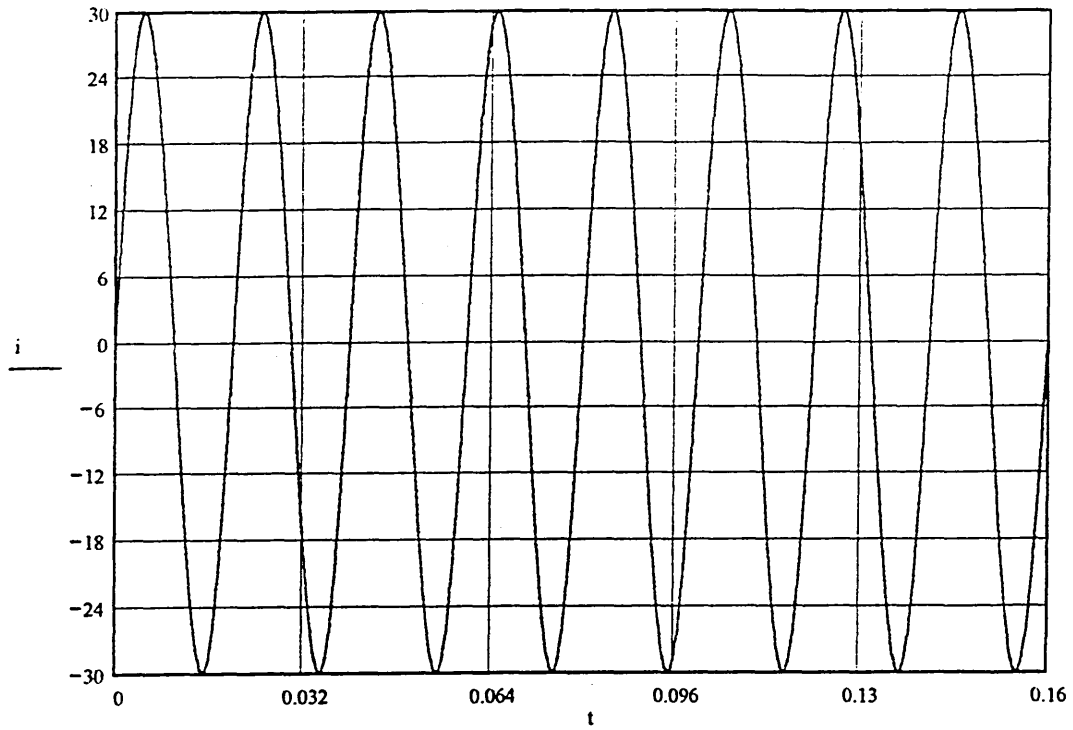


Figure A11.2 Symmetrical ac current case :Long time domain wire current×time (axis : time(ms), current (A))

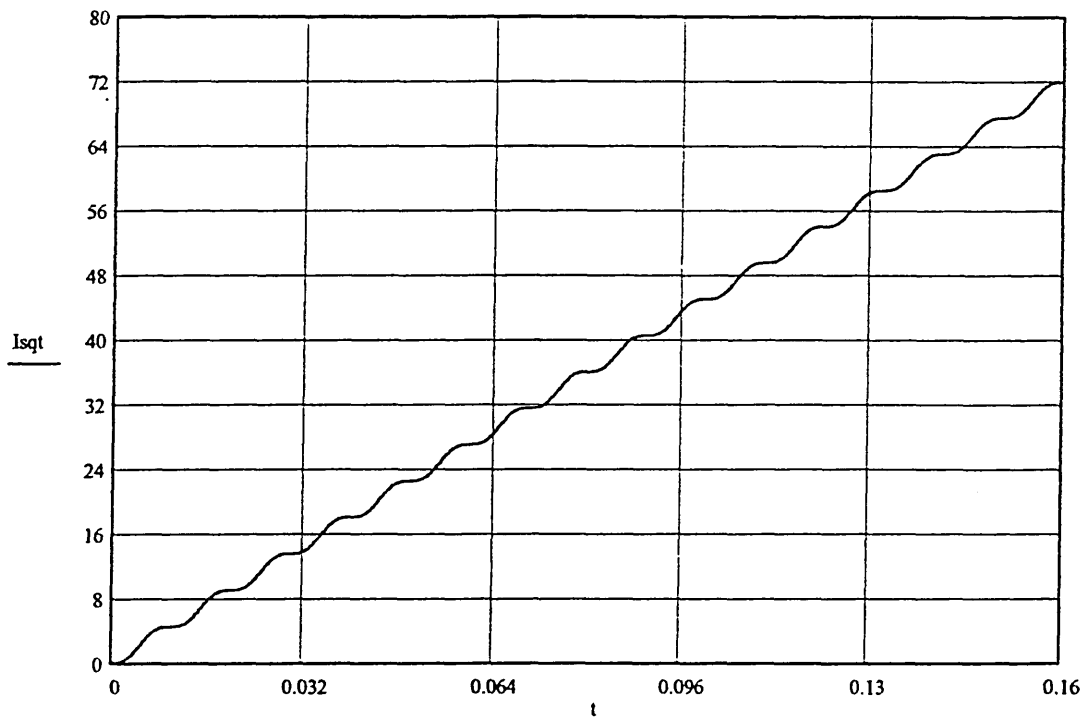


Figure A11.3 Symmetrical ac current case : long time domain : wire I^2t ×time (axis :time(ms), $I^2t(A^2s/m^4 \times S_e^2)$)

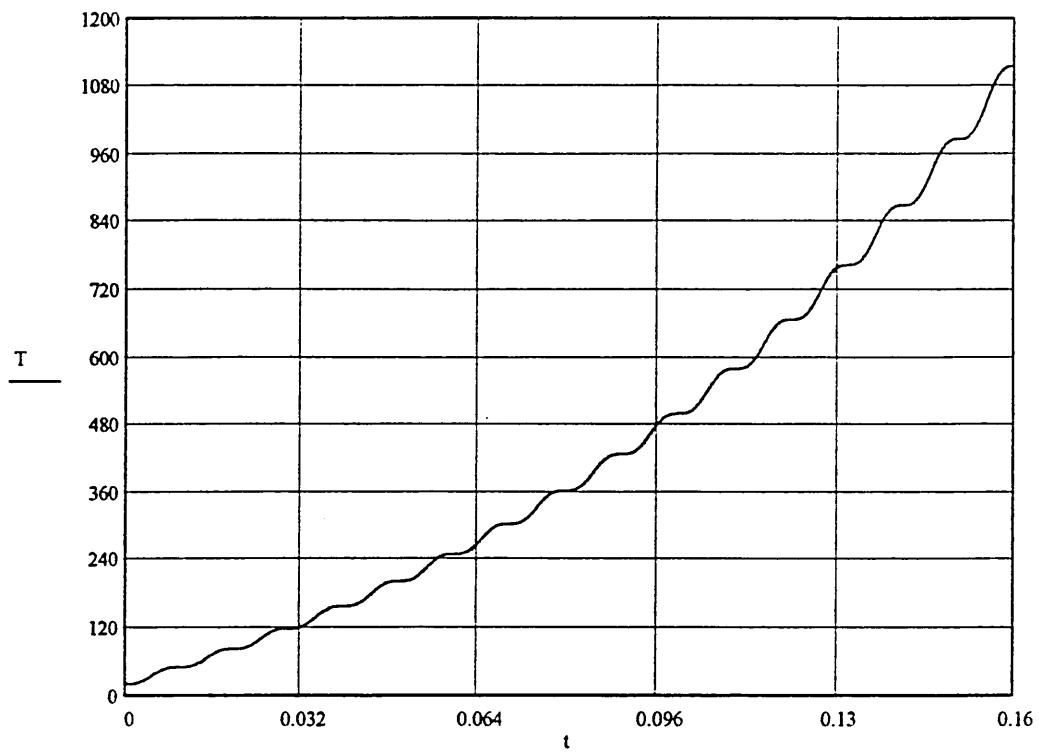


Figure A11.4 Symmetrical ac current case : long time domain : wire temperature×time (axis : time(ms), temperature (°C))

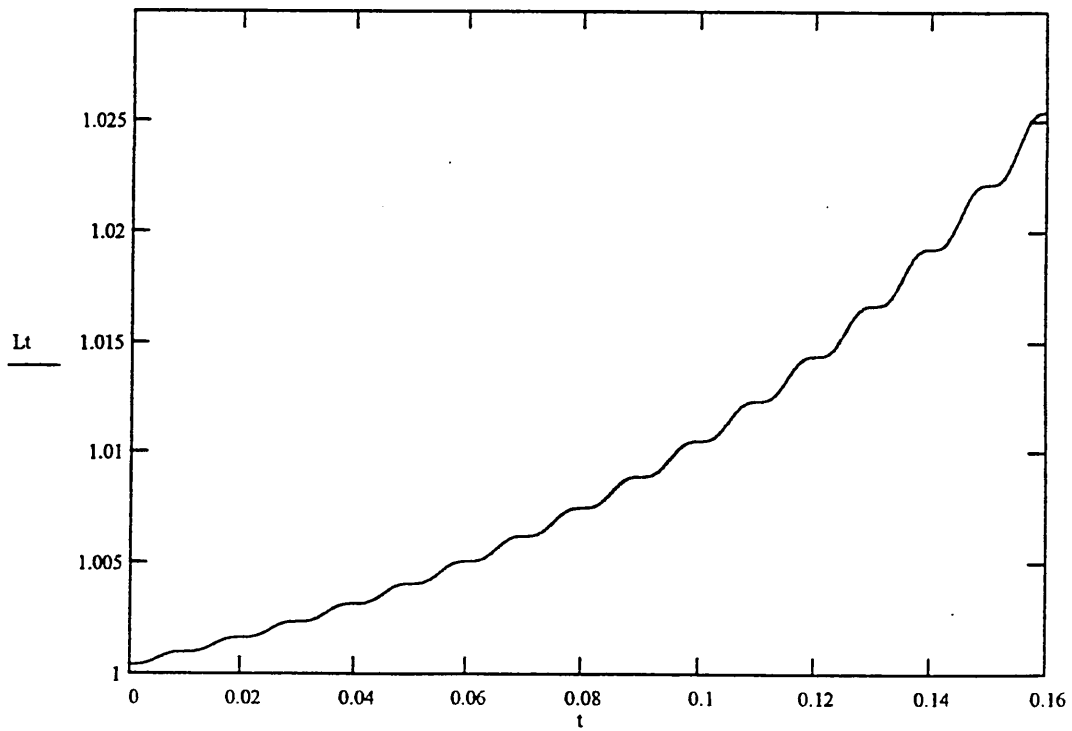


Figure A11.5 Symmetrical ac current case : long time domain : wire length×time (axis : time(ms), length ($l_0 + \Delta l/l_0$))

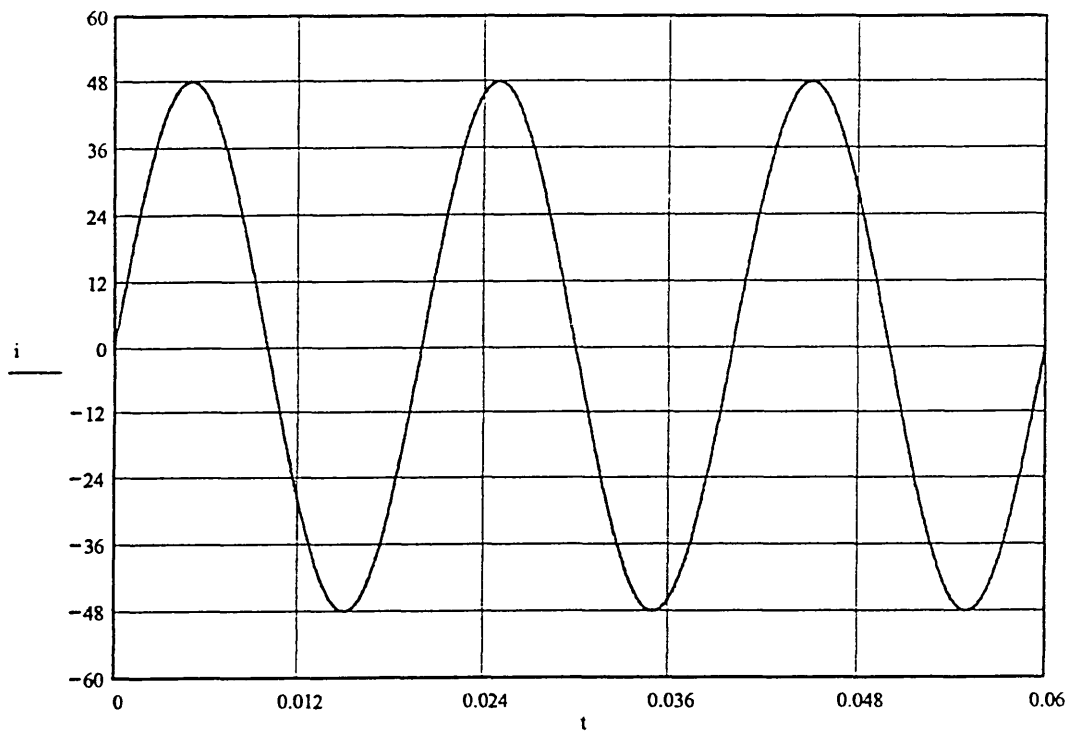


Figure A11.6 Symmetrical ac current case : short time domain wire current×time (axis : time(ms), current (A))

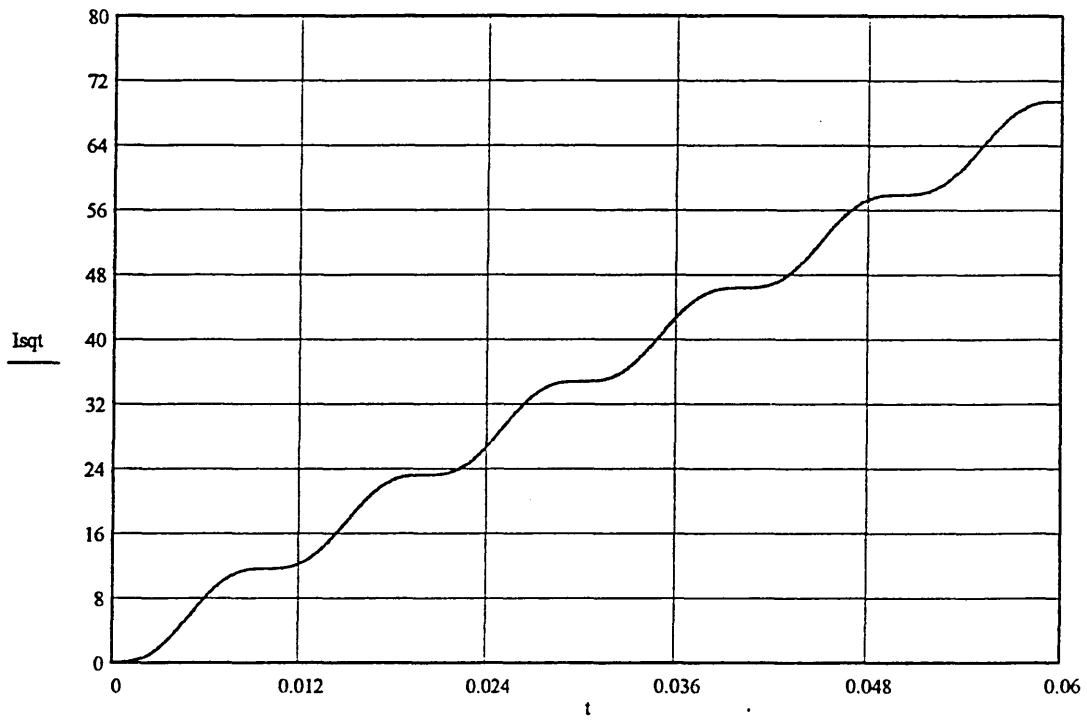


Figure A11.7 Symmetrical.ac current case : short time domain : wire $I^2 t \times \text{time}$ (axis : time(ms), $I^2 t (A^2 s / m^4 \times S_o^2)$)

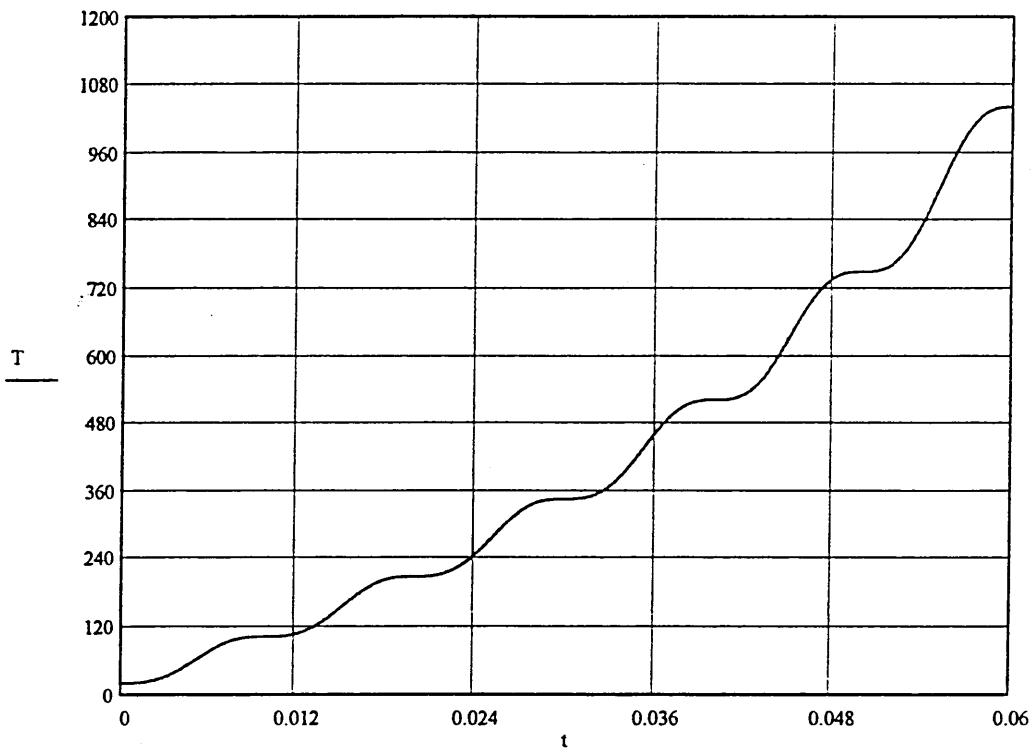


Figure A11.8 Symmetrical ac current case : short time domain : wire temperature×time (axis : time(ms), temp (°C))

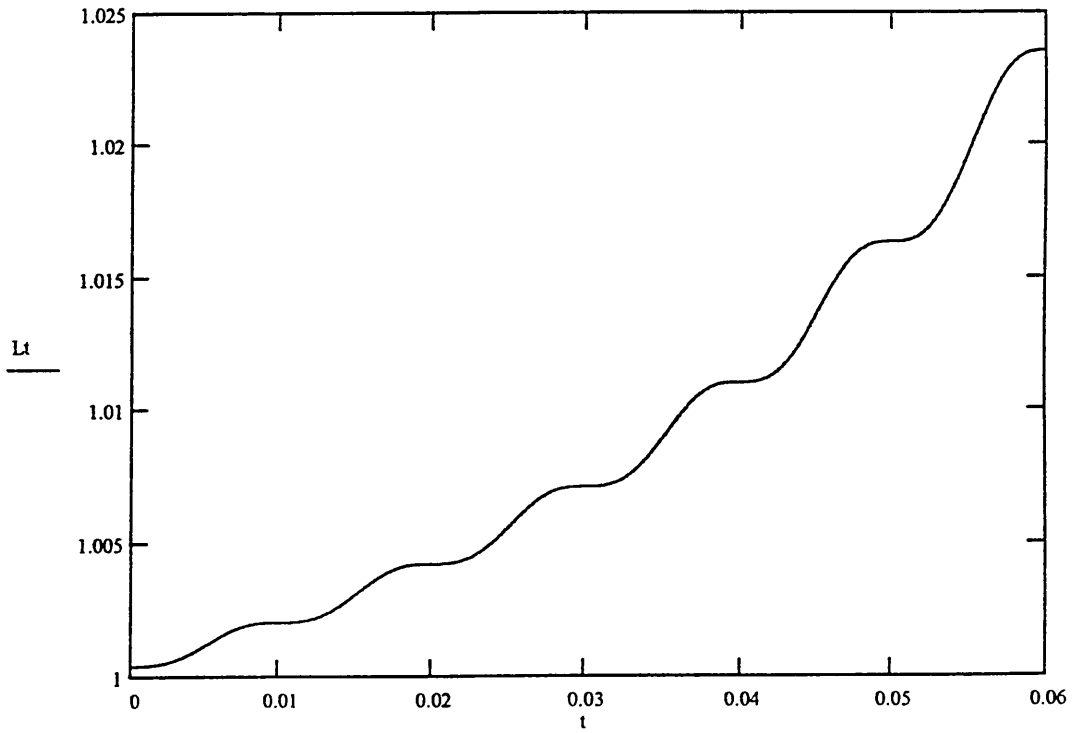


Figure A11.9 Symmetrical ac current case : short time domain : wire length×time (axis : time(ms), length ($l_0 + \Delta l/l_0$))

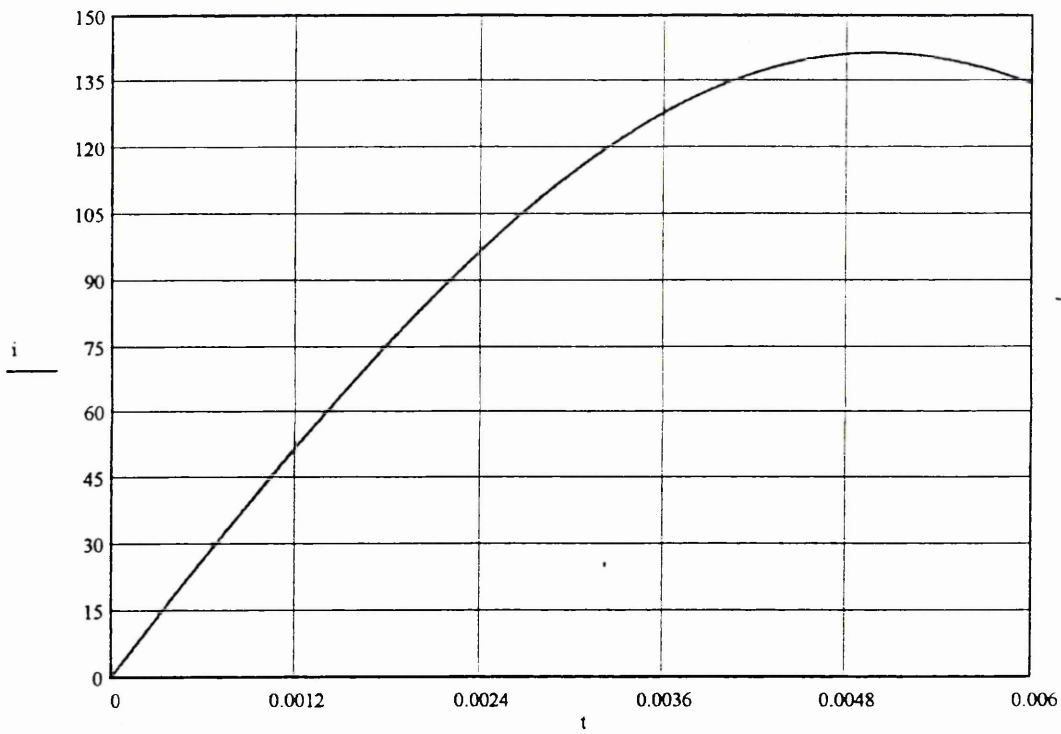


Figure A11.10 Symmetrical ac current case : very short time domain wire current×time (axis : time(ms), current (A))

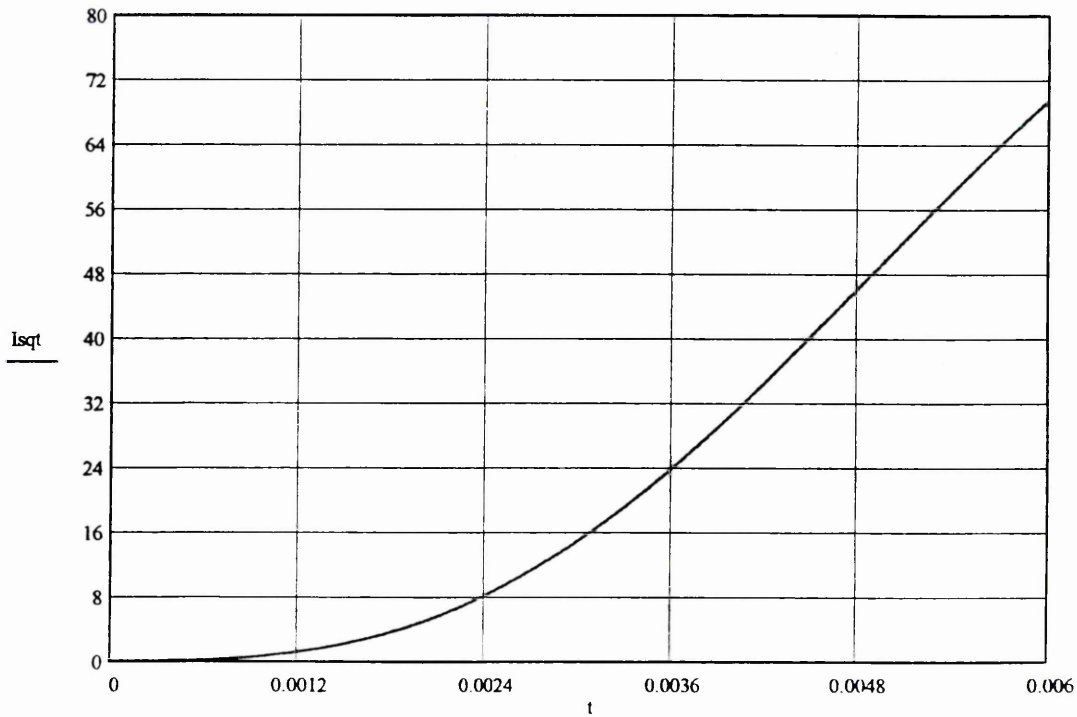


Figure A11.11 Symmetrical ac current case : very short time domain : wire I²t×time (axis : time(ms), I²t(A²/s/m⁴ × s²))

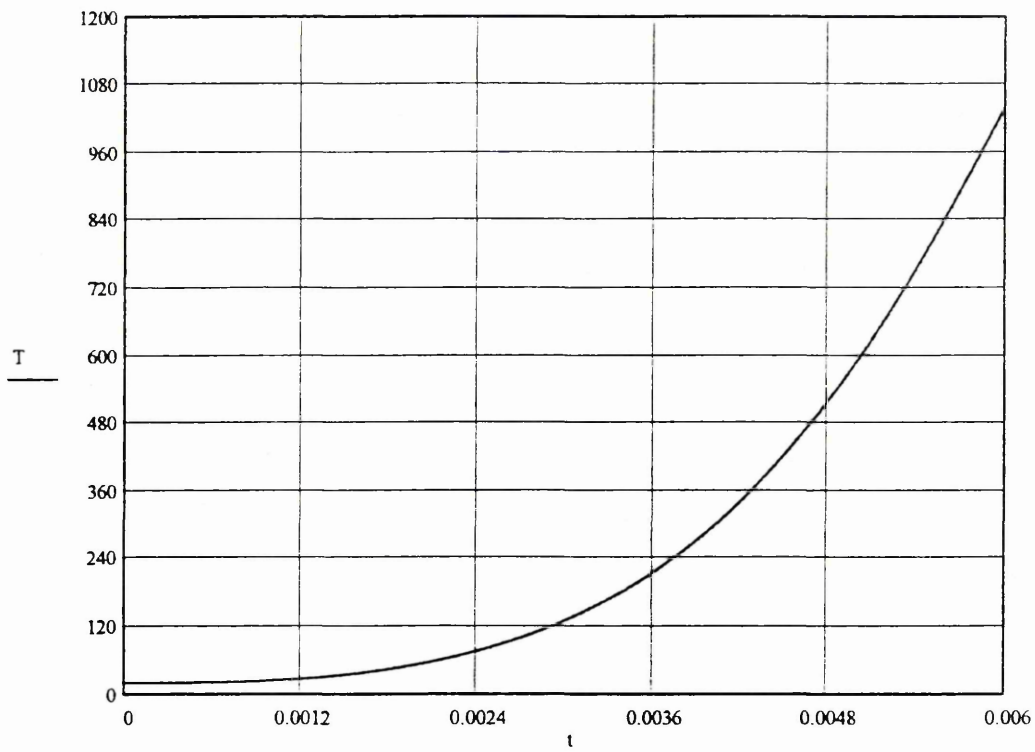


Figure A11.12 Symmetrical ac current case : very short time domain : wire temperature×time (axis : time(ms), temp (°C))

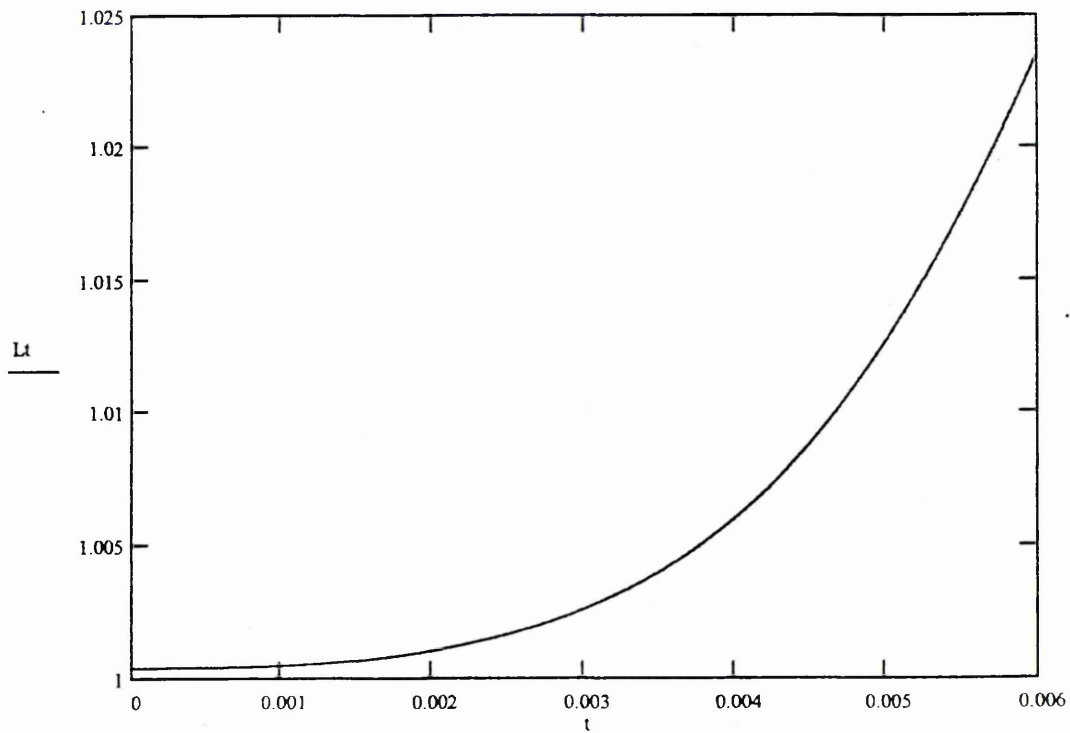


Figure A11.13 Symmetrical ac current case : very short time domain : wire length×time (axis : time(ms), length ($l_0 + \Delta l/l_0$))

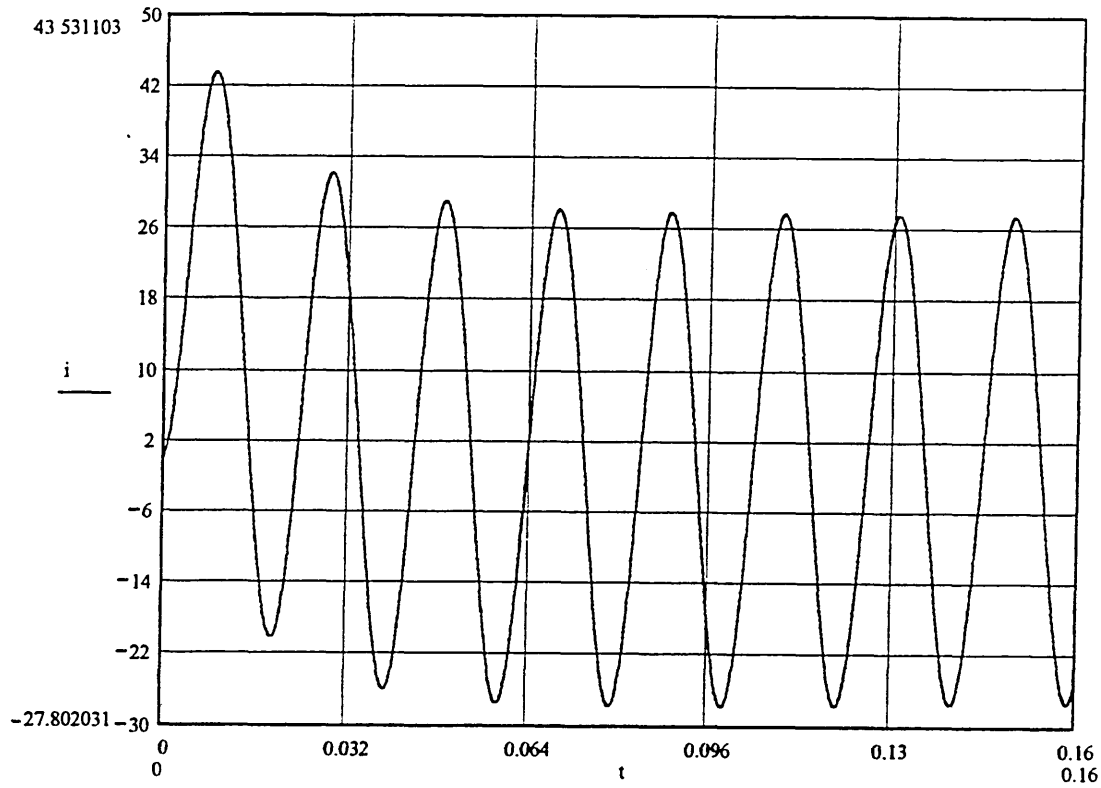


Figure A11.14 Conventional Asymmetrical ac current case : long time domain wire current×time (axis : time(ms), current (A))

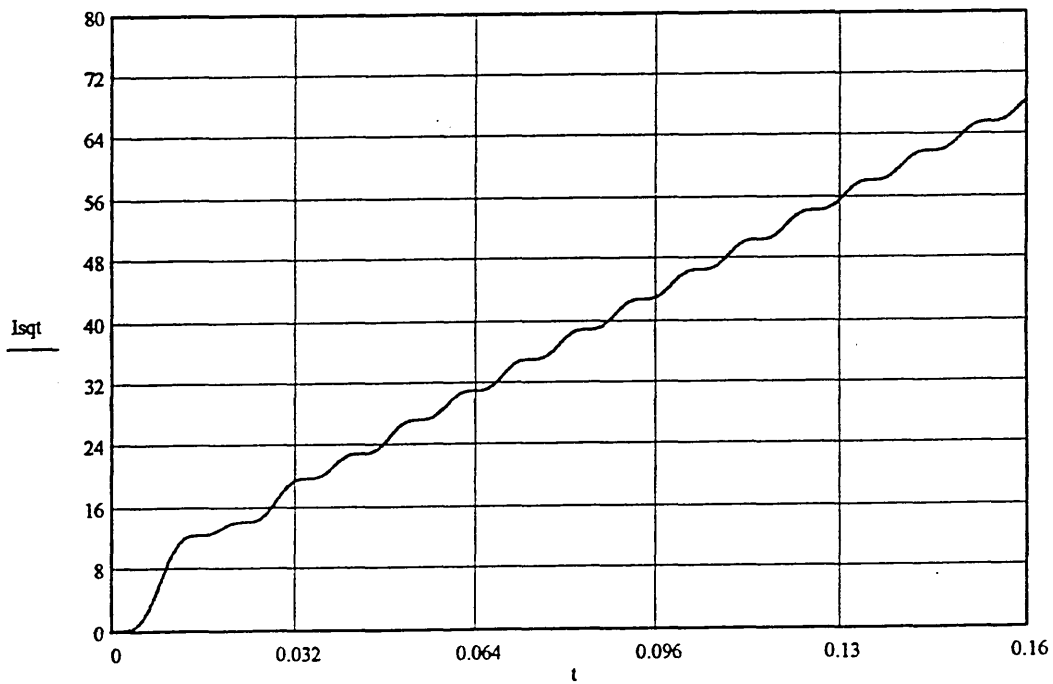


Figure A11.15 Conventional Asymmetrical ac current case : long time domain : wire $I^2 \times \text{time}$ (axis : time(ms), $I^2(A^2/s/m^4 \times S_o^2)$)

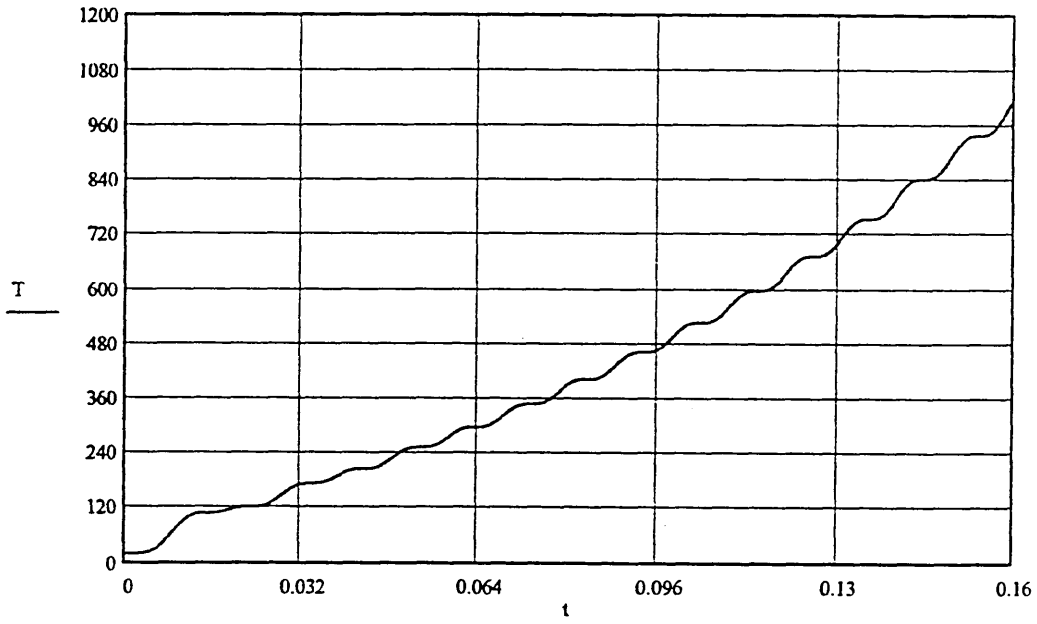


Figure A11.16 Conventional Asymmetrical ac current case : long time domain : wire temperature×time (axis : time(ms), temp (°C))

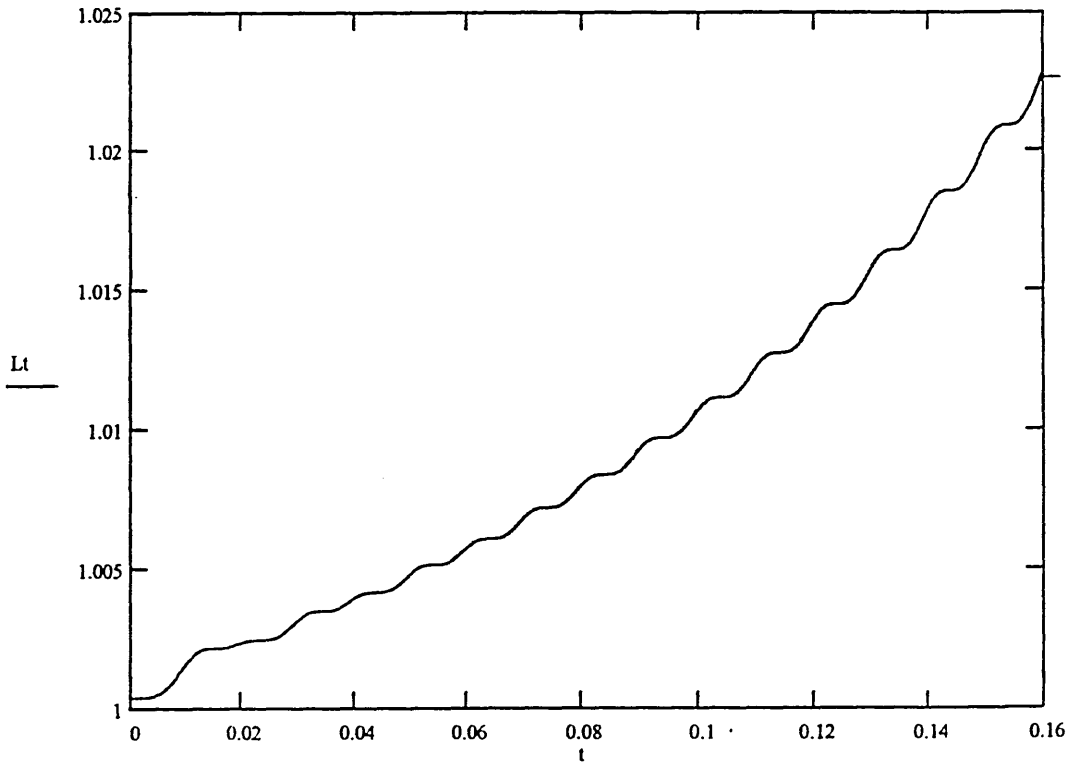


Figure A11.17 Conventional Asymmetrical ac current case : long time domain : wire length×time (axis : time(ms), length (l₀+Δl/l₀))

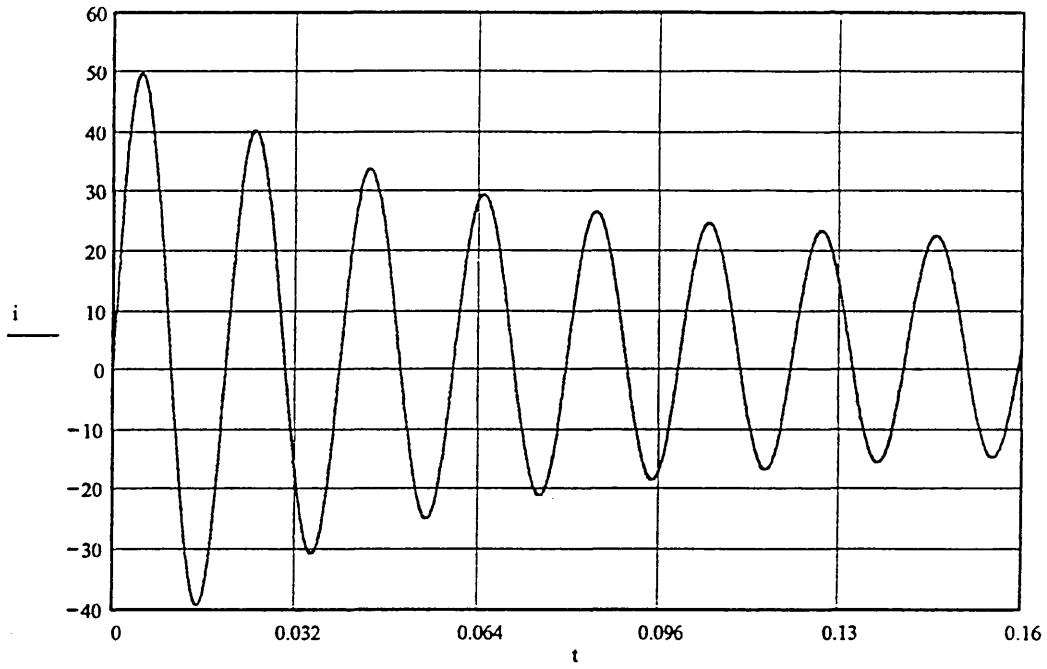


Figure A11.18 Alternator ac current case : long time domain wire current×time (axis : time(ms), current (A))

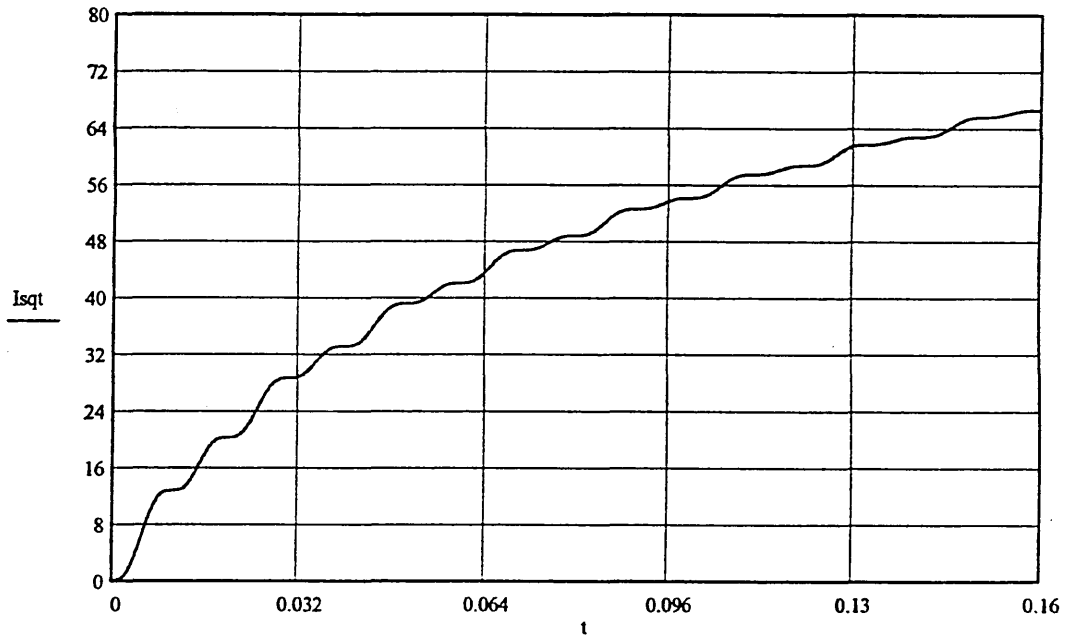


Figure A11.19 Alternator ac current case : long time domain : wire $I^2 \times \text{time}$ (axis : time(ms), $I^2 t (A^2 s / m^4 \times S_0^2)$)

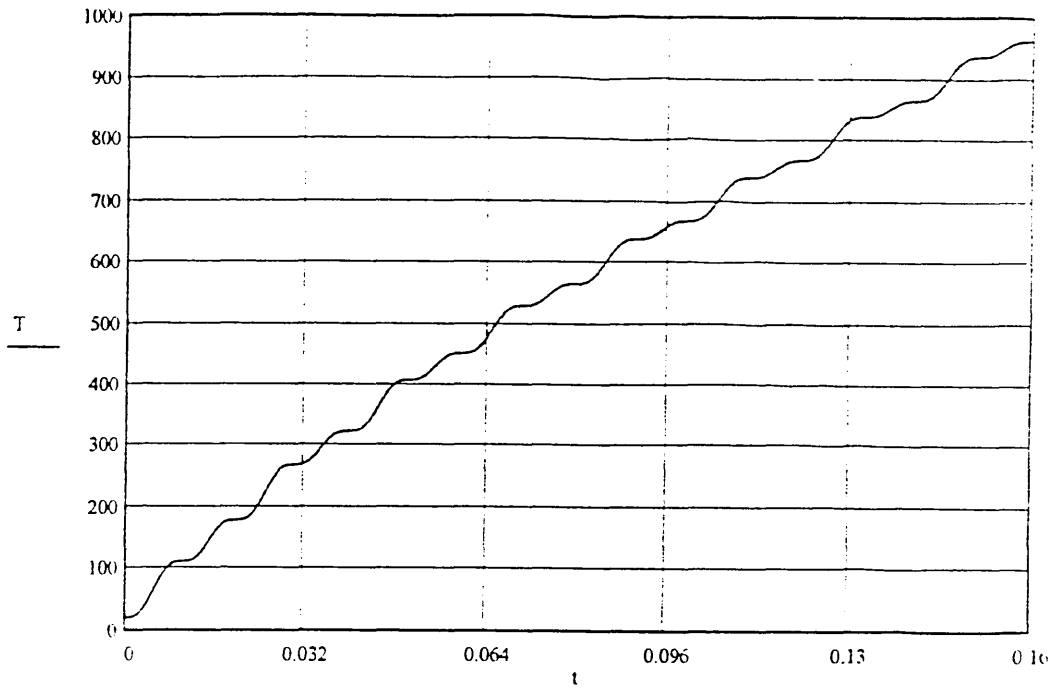


Figure A11.20 Alternator ac current case : long time domain : wire temperature×time (axis : time(ms), temp (°C))

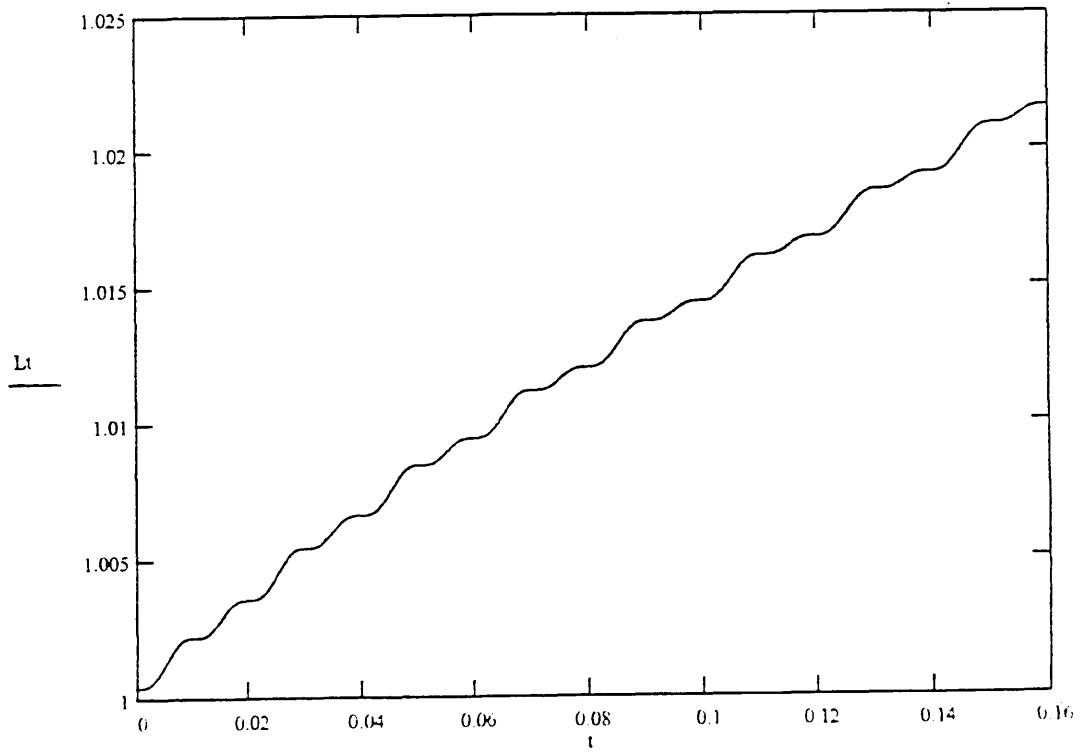


Figure A11.21 Alternator ac current case : long time domain : wire length×time (axis : time(ms), length (L + ΔL))

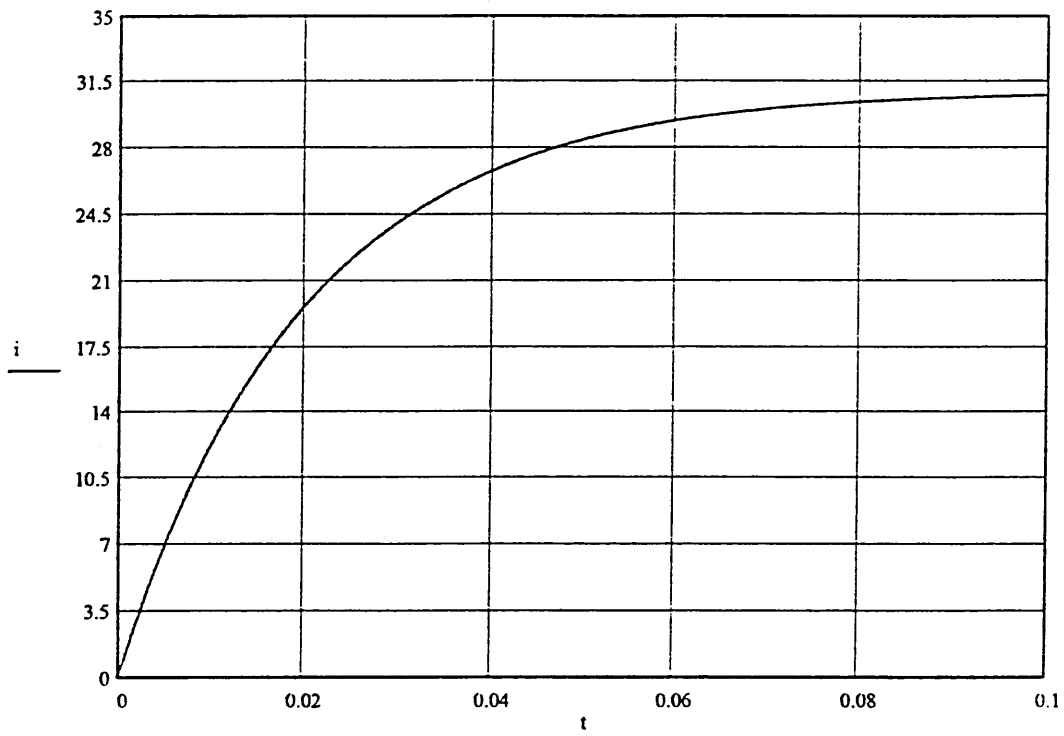


Figure A11.22 DC current case : long time domain wire current \times time (axis : time(ms), current (A))

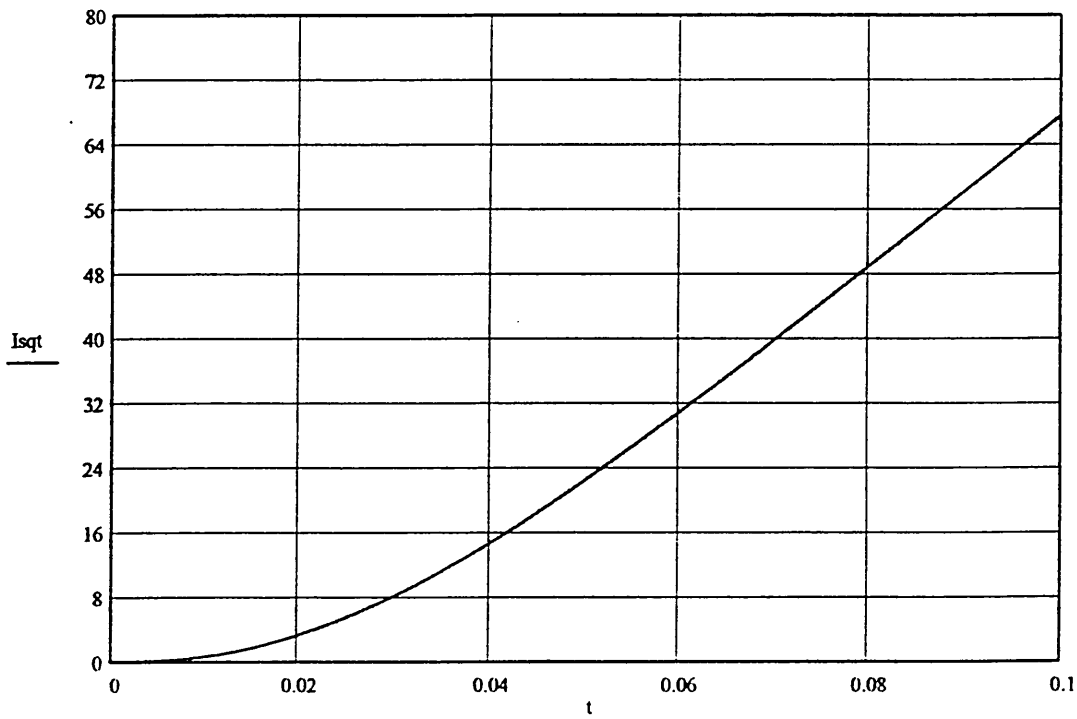


Figure A11.23 DC current case : long time domain : wire I^2t \times time (axis : time(ms), $I^2t(A^2s/m^4 \times S_o^2)$)

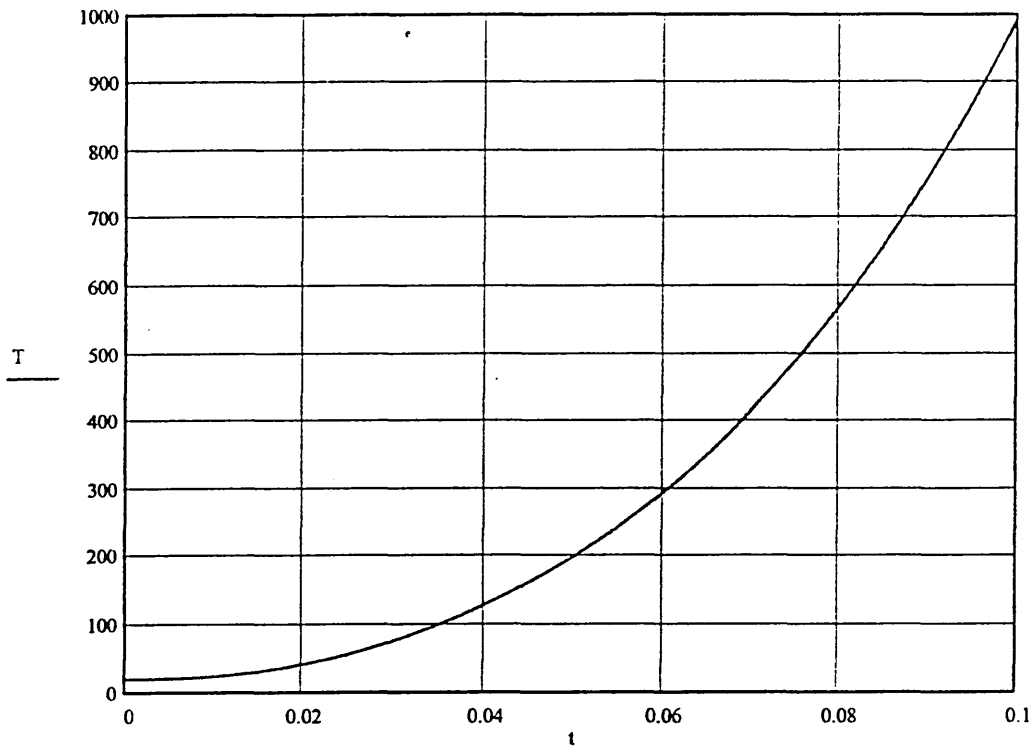


Figure A11.24 DC current case : long time domain : wire temperature \times time (axis : time(ms), temp ($^{\circ}\text{C}$))

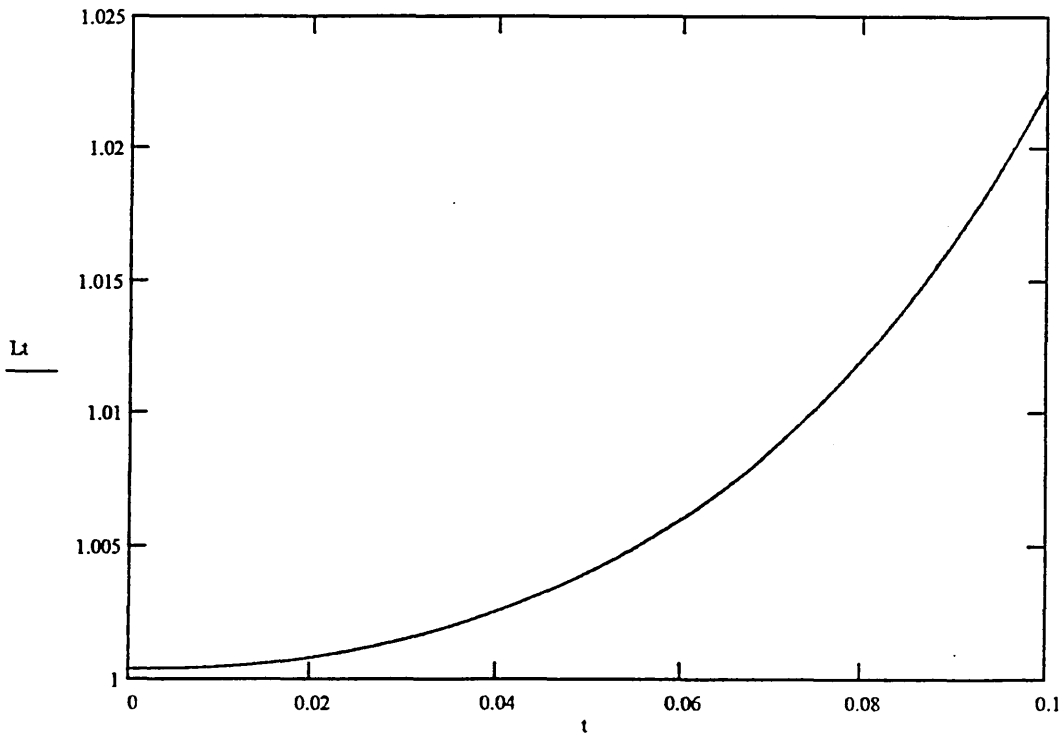


Figure A11.25 DC current case : long time domain : wire length \times time (axis : time(ms), length ($l_0 + \Delta l/l_0$))

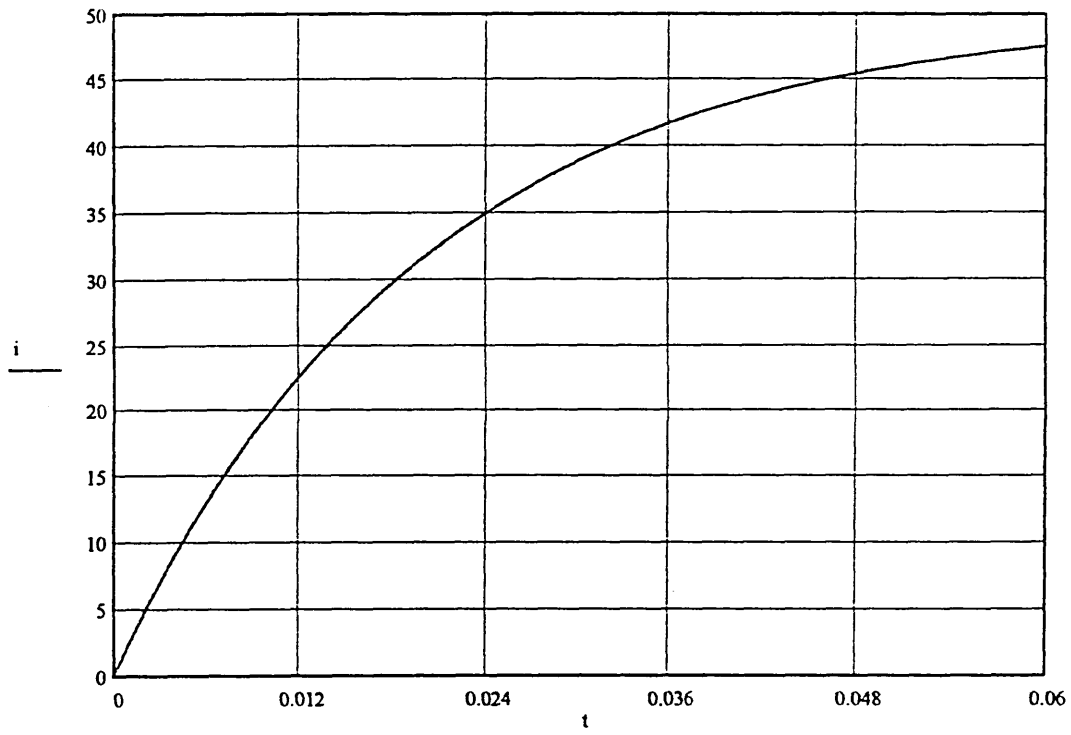


Figure A11.26 DC current case : short time domain wire current \times time (axis : time(ms), current (A))

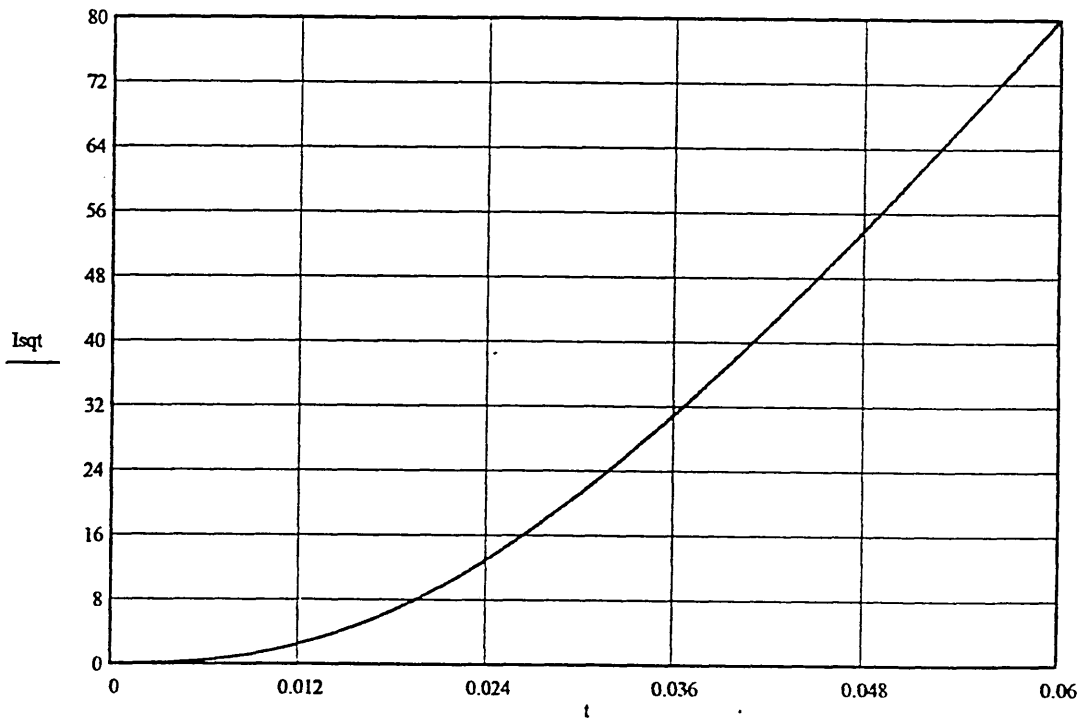


Figure A11.27 DC current case : short time domain : wire I^2t \times time (axis : time(ms), $I^2t(A^2s/m^4 \times S_o^2)$)

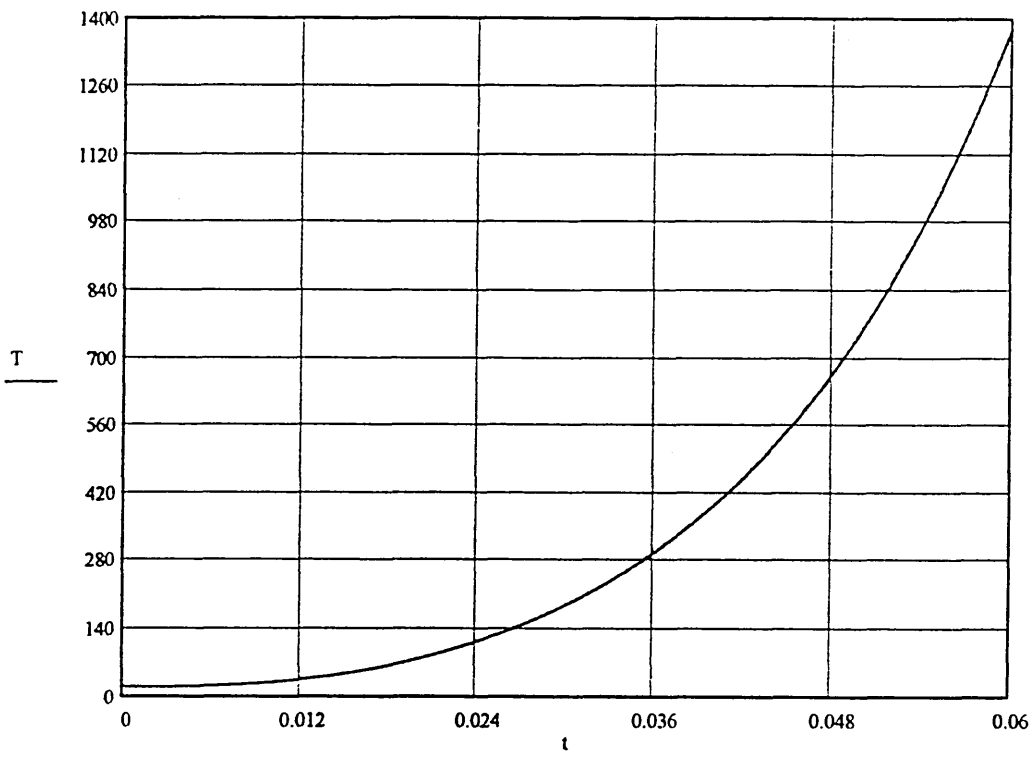


Figure A11.28 DC current case : short time domain : wire temperature \times time (axis : time(ms), temp ($^{\circ}\text{C}$))

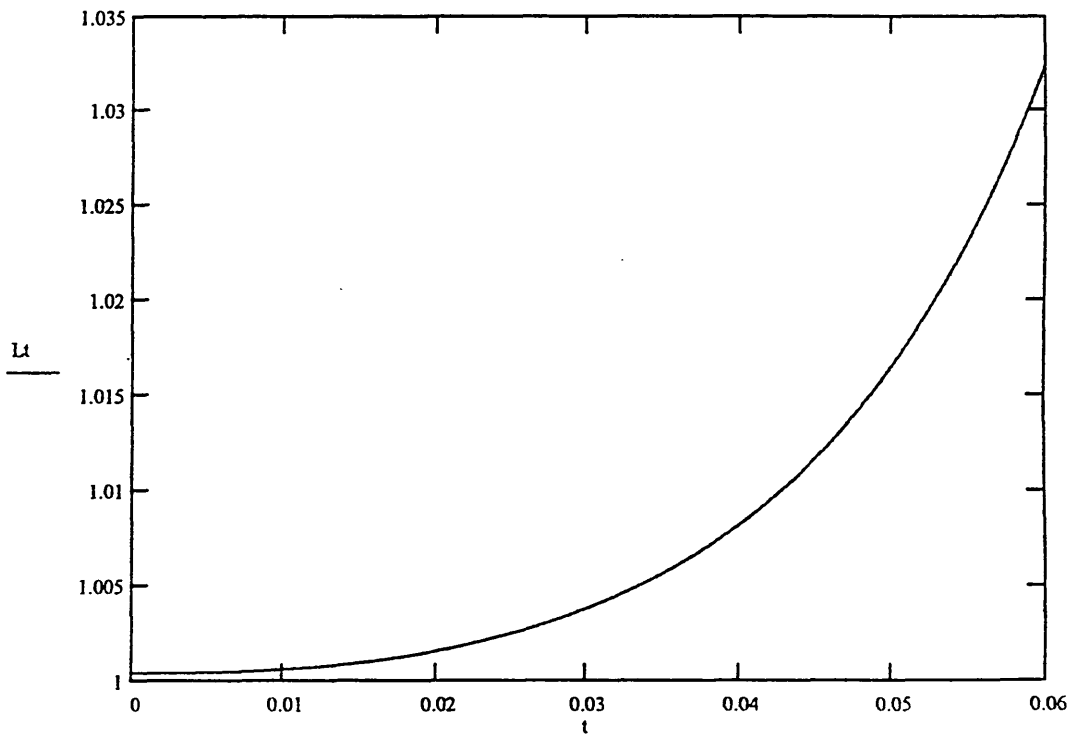


Figure A11.29 DC current case : short time domain : wire length \times time (axis : time(ms), length ($l_0 + \Delta l/l_0$))

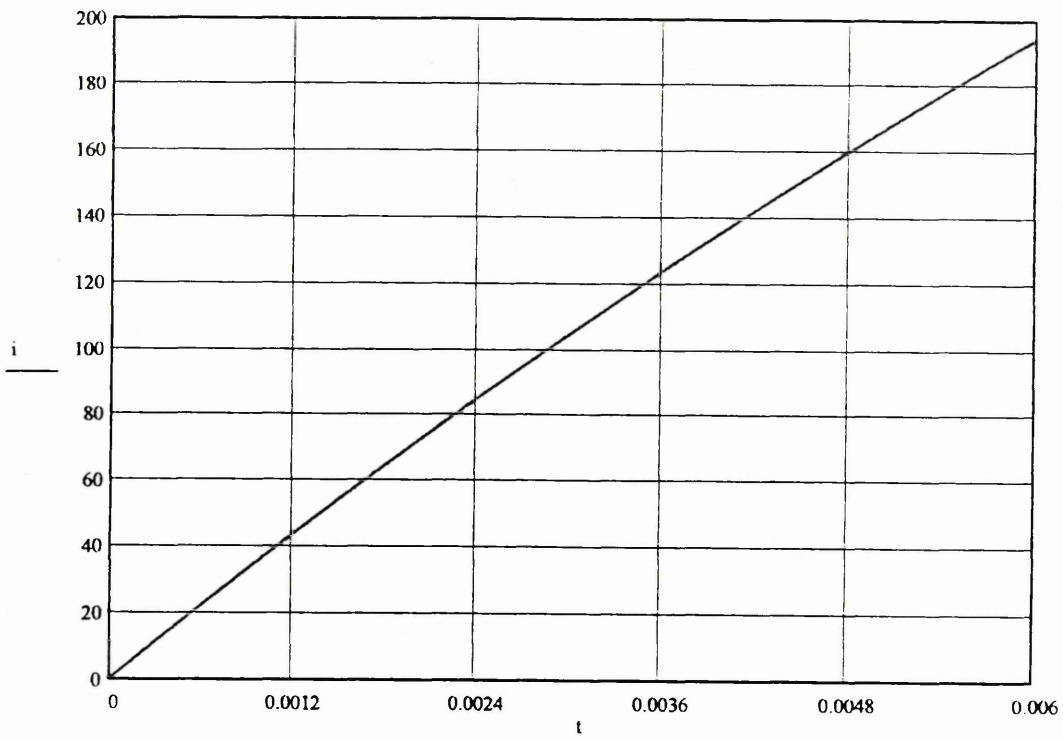


Figure A11.30 DC current case : very short time domain wire current \times time (axis : time(ms), current (A))

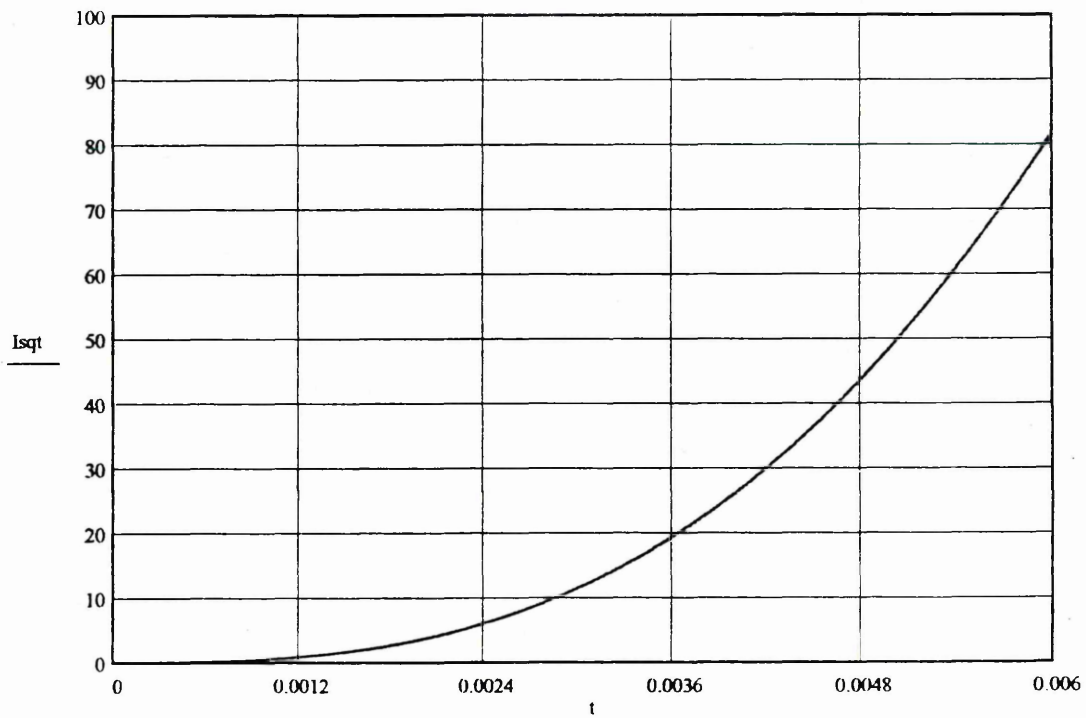


Figure A11.31 DC current case : very short time domain : wire $I^2t \times$ time (axis : time(ms), $I^2t(A^2s/m^4 \times S_o^2)$)

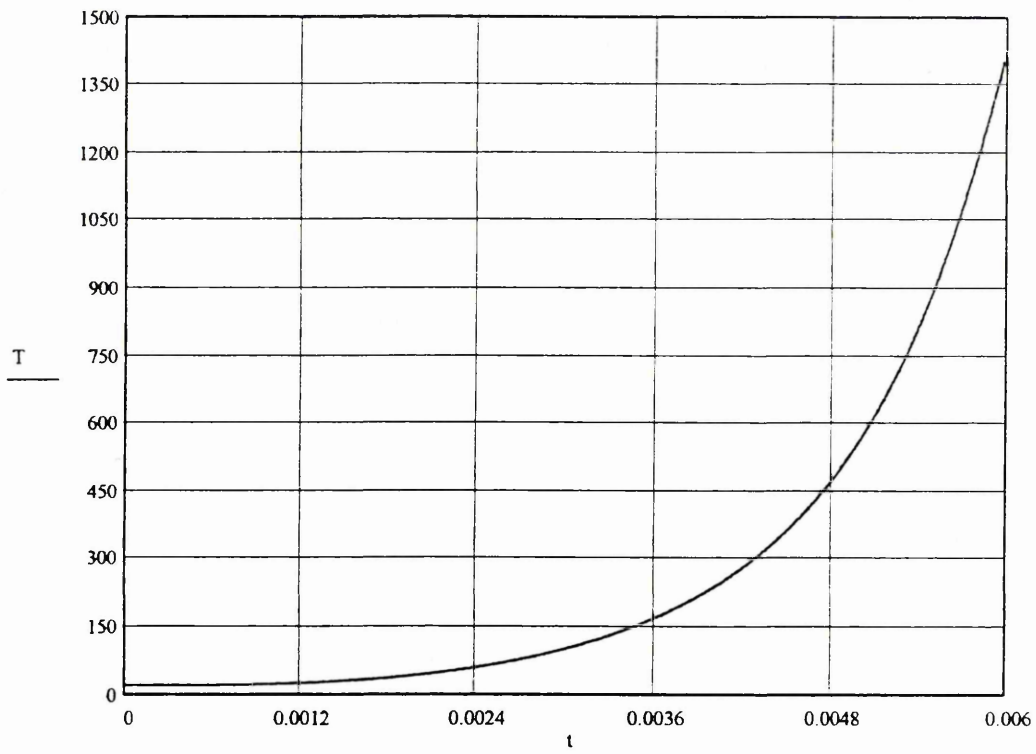


Figure A11.32 DC current case : very short time domain : wire temperature×time (axis : time(ms), temp (°C))

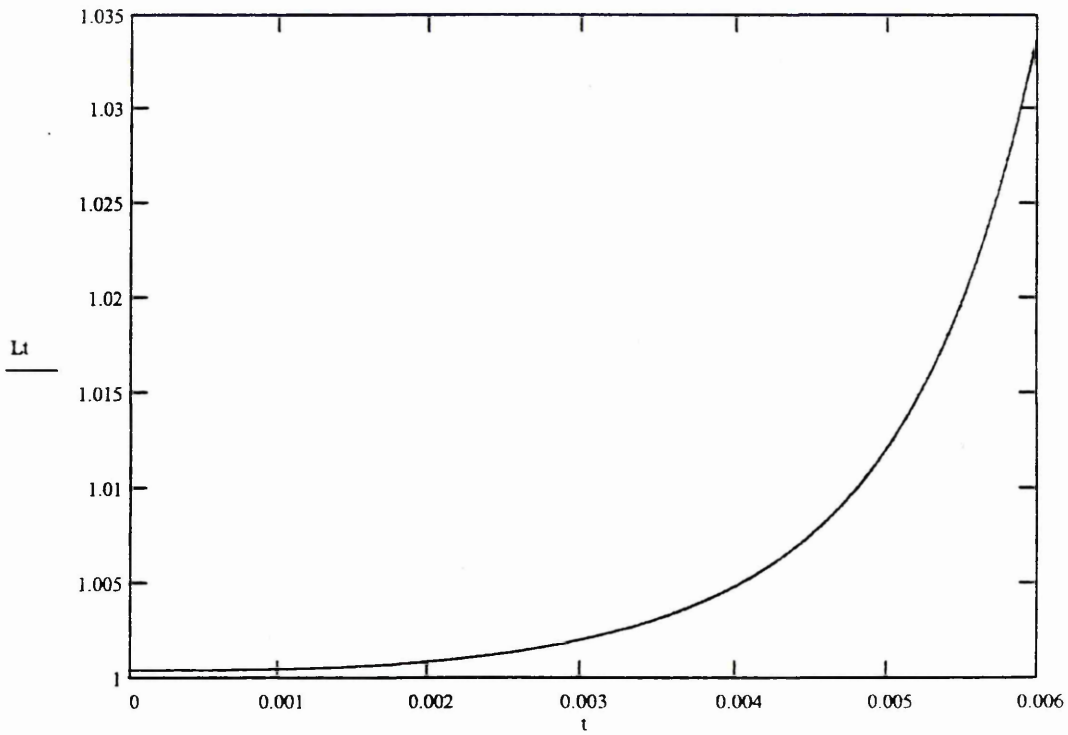


Figure A11.33 DC current case : very short time domain : wire length×time (axis : time(ms), length ($l_0 + \Delta l/l_0$))

Appendix 12

Finite Element CAD Analysis of Wire Displacement and Stress Distribution

The very short time domain analysis and simulation of the displacement and stress distribution of a uniform section wire, suspended in an un-constricting medium was carried out by Wilniewicz [77] using ABACUS finite element analysis CAD package.

For a pre-dispositioned wire the analysis indicates that the deformation of the wire tends to be catenary in shape (Figures A12.1 – A12.4). Moreover, the analysis also indicates that, the concentration of trapped stress is greatest at the conductor terminals.

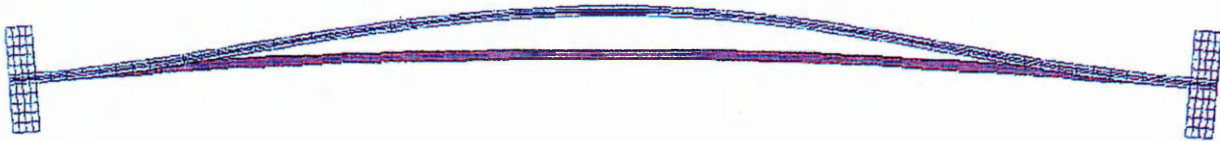
However, the CAD analysis also indicated that, for an homogenous wire no deformation of the wire occurs since ABACUS identified this as a perfect condition and could not compute the deformation or stress distribution in the conductor. Logically this confirms that, some pre-disposition of the wire is fundamentally the causation phenomena for the initial deformation of the wire. Hence, for ABACUS to predict a solution some pre-disposition of the conductor was fixed, which can be seen in Figure A12.1



t = 20 ms

DISPLACEMENT MAGNIFICATION FACTOR = 1.00 ORIGINAL MESH DISPLACED MESH
 TIME COMPLETED IN THIS STEP 1.00 TOTAL ACCUMULATED TIME 1.00
 ABAQUS VERSION: 5.5-1 DATE: 29-JUL-96 TIME: 19:14:04
 STEP 1 INCREMENT 4

Fig.1 Displaced plot after t=20ms.



t = 40 ms

DISPLACEMENT MAGNIFICATION FACTOR = 1.00 ORIGINAL MESH DISPLACED MESH
 TIME COMPLETED IN THIS STEP 1.00 TOTAL ACCUMULATED TIME 1.00
 ABAQUS VERSION: 5.5-1 DATE: 29-JUL-96 TIME: 19:14:04
 STEP 1 INCREMENT 4

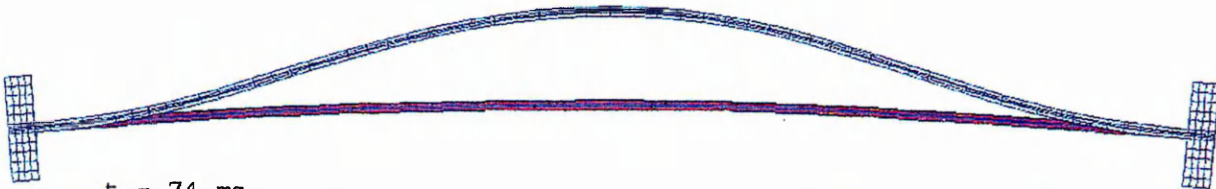
Fig.2 Displaced plot after t=40ms.



t = 60 ms

DISPLACEMENT MAGNIFICATION FACTOR = 1.00 ORIGINAL MESH DISPLACED MESH
 TIME COMPLETED IN THIS STEP 1.00 TOTAL ACCUMULATED TIME 1.00
 ABAQUS VERSION: 5.5-1 DATE: 29-JUL-96 TIME: 19:14:04
 STEP 1 INCREMENT 4

Fig.3 Displaced plot after t=60ms.



t = 74 ms

DISPLACEMENT MAGNIFICATION FACTOR = 1.00 ORIGINAL MESH DISPLACED MESH
 TIME COMPLETED IN THIS STEP 1.00 TOTAL ACCUMULATED TIME 1.00
 ABAQUS VERSION: 5.5-1 DATE: 29-JUL-96 TIME: 19:14:04
 STEP 1 INCREMENT 4

Fig.4 Displaced plot after t=74ms.

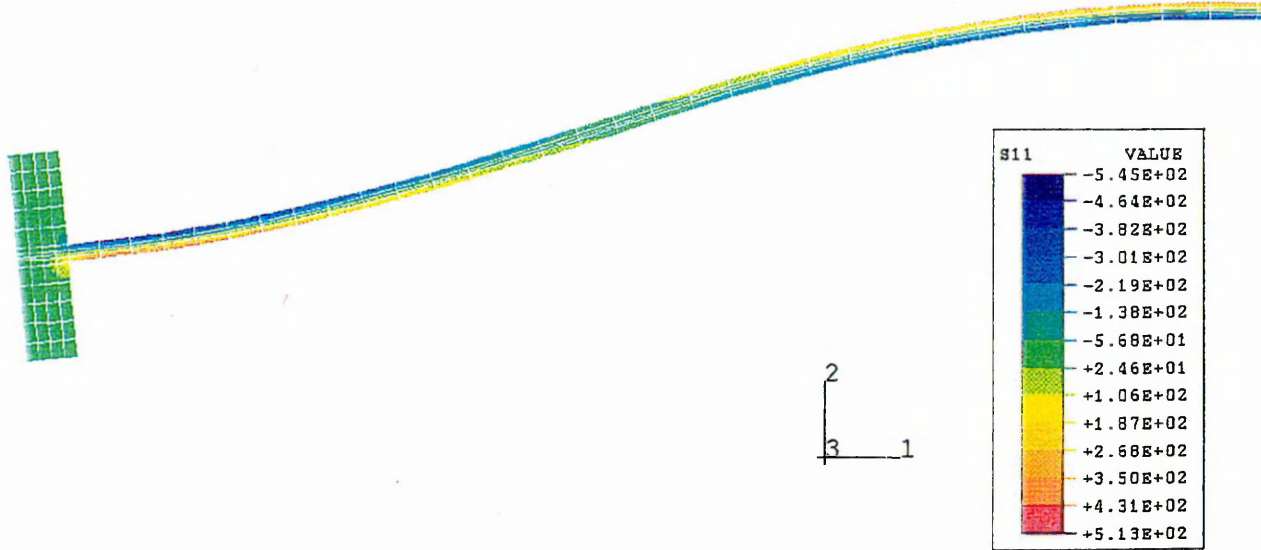


Fig.5 Stress S11 distribution at $t=74\text{ms}$.

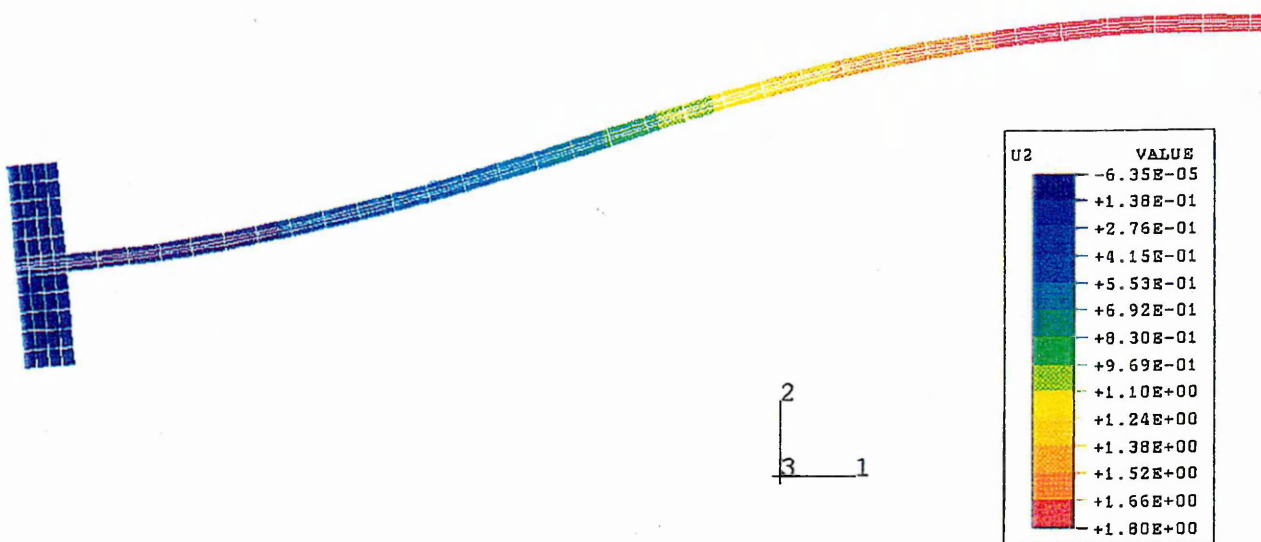


Fig.6 Displacement U2 distribution at $t=74\text{ms}$.

Appendix 13

Evaluation of the Extent of Fragmentation of a Cylindrical Column Suspended in Un-Confined and Constricted Media.

The following analysis indicates that for the models of similar cylindrical columns suspended in un-confined and constricted media, the extent of column fragmentation increases.

Consider, part of a cylindrical column suspended in an un-confined media of length l and sectional area S which evolves into one spheroid ($n_1=1$) [45] (Figure A13.1).

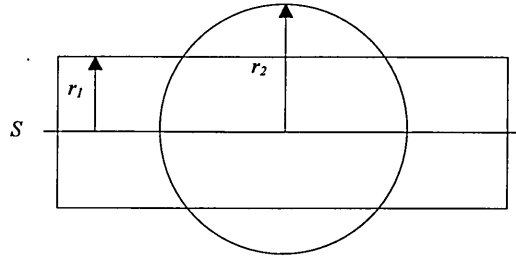


Figure A13.1 Geometrical diagram indicating the evolution of a cylindrical column in an un-confined media

Hence when $n_1 = n_2 = 1$, then,

$$n_1 l S = n_1 \pi r_1^2 = n_2 1.333 \pi r_2^3 \quad \text{Eq. A13.1}$$

Consider the same column in a confined media (Figure A13.2), in this case, $r_1 = r_2 = r$

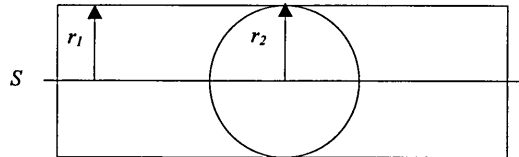


Figure A13.2 Geometrical diagram indicating the evolution of a cylindrical column in a confined media

Logically, $n_1 \neq n_2$ and therefore,

$$n_1/n_2 = l \pi r^2 / 1.333 \pi r^3 = 3l/4r \quad \text{Eq. A13.2}$$

If for the column $r = l$, then,

$$n_1/n_2 = 0.75 \quad \text{Eq. A13.3}$$

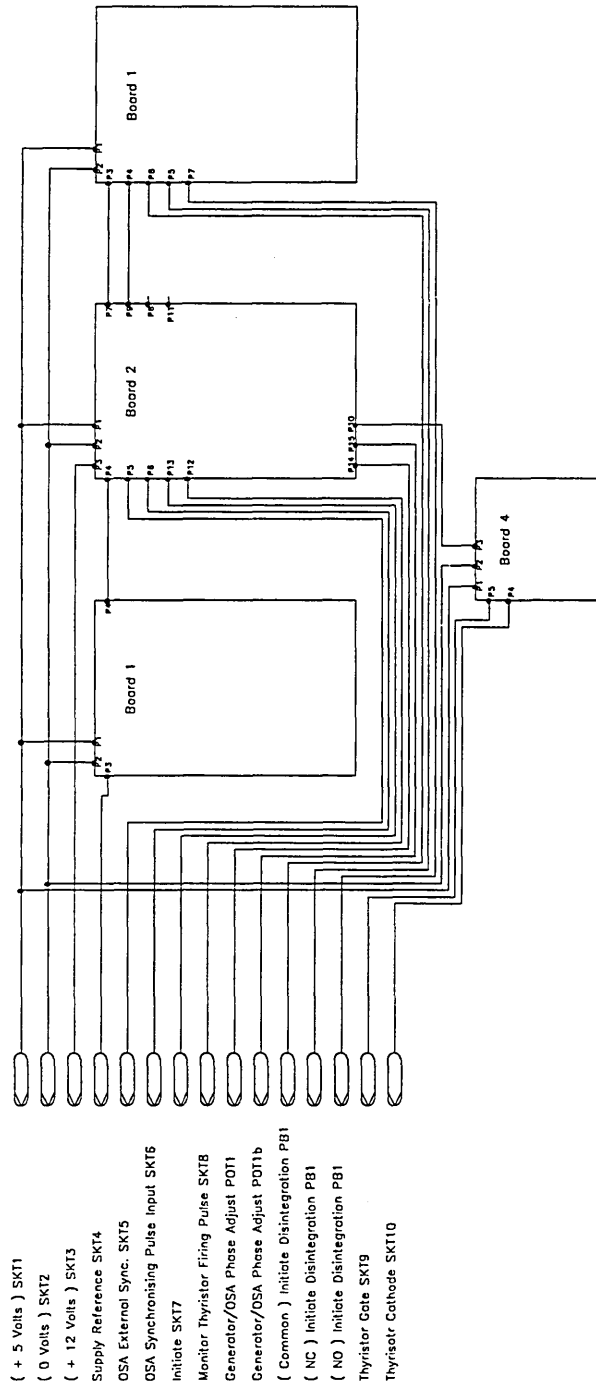
Therefore if the column is totally confined,

$$n_2 = 0.75 / n_1 = 1 / 0.75 = 1.33 \quad \text{Eq. A13.4}$$

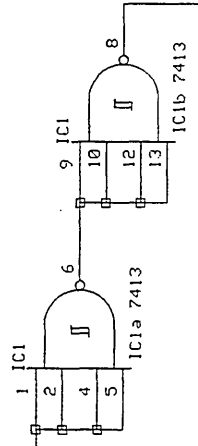
Appendix 14

Fuse Test Facility, Optical Spectrum Analyser Interfacing.

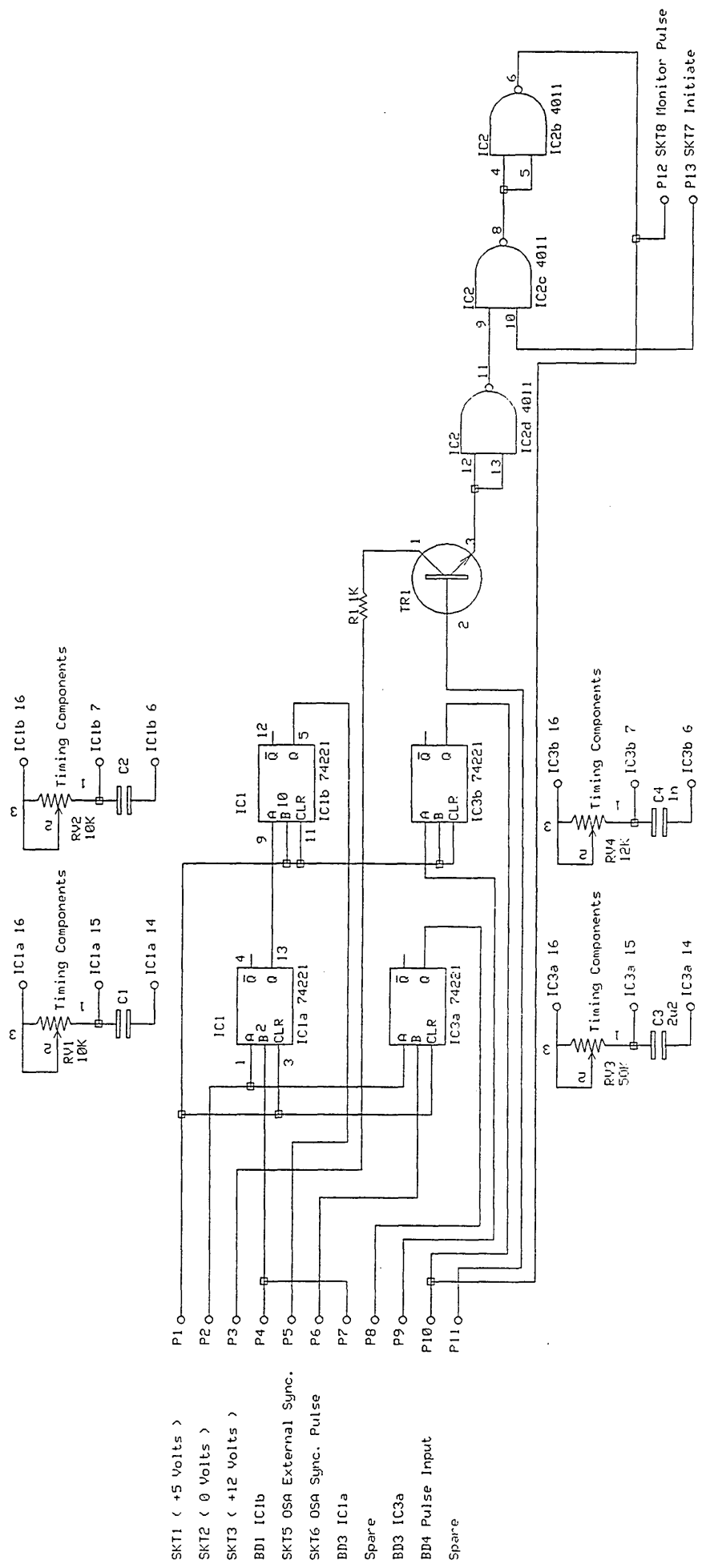
The following pages present the interconnecting wiring diagrams and the schematic diagrams of the circuits which enabled the Optical Spectrum Analyser to monitor the fuse test facility generated supply and subsequently synchronise disintegration of the fuse with the monochromator of the OSA as described in Subsection 5.6.10.



SKT1 (+5 Volts) P1 O-
 SKT2 (0 Volts) P2 O-
 SKT4 Supply Reference P3 O-
 BD2 IC1a P4 O-

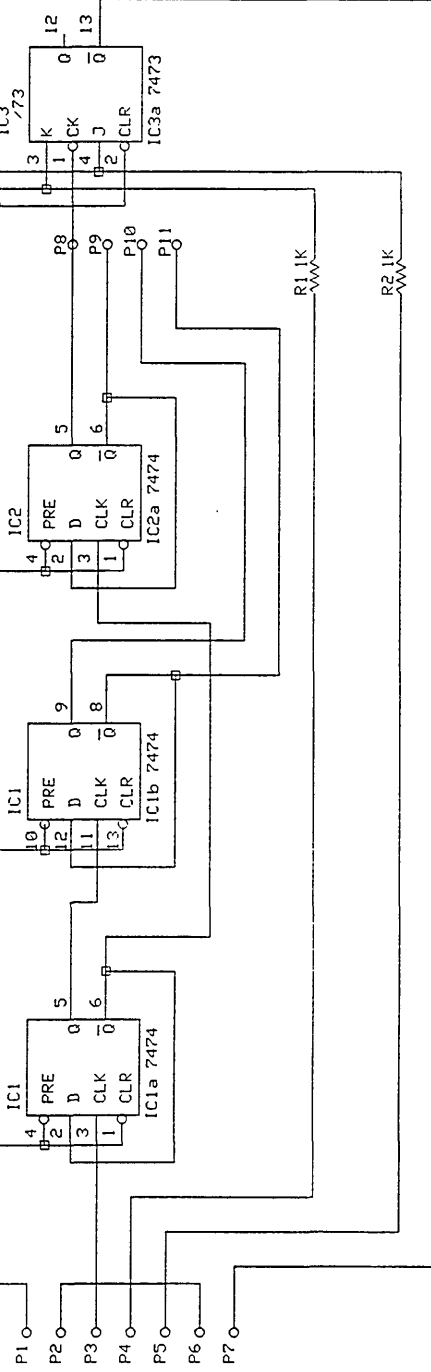


Optical Spectrum Analyser
 Interface
 Wiring Schematic
 Board 1
 Sheffield Hallam University
 School of Engineering
 Drawn by R.E. Brown
 Date : 29/March/1999
 Page 1 of 4

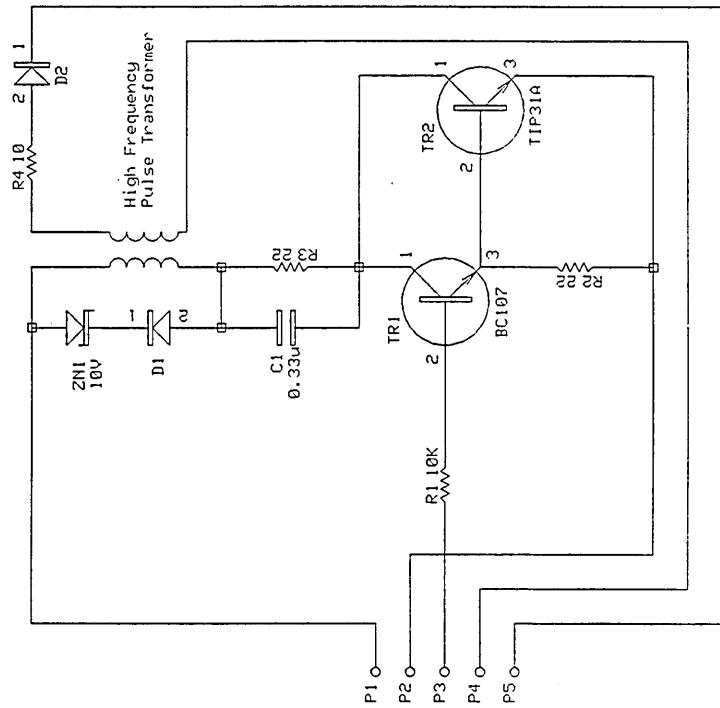


- SKT1 (+5 Volts)
- SKT2 (0 Volts)
- SKT3 (+12 Volts)
- BD1 IC1b
- SKT5 OSA External Sync.
- SKT6 OSA Sync. Pulse
- BD3 IC1a
- Spare
- BD3 IC3a
- BD4 Pulse Input
- Spare

Optical Spectrum Analyzer
 Interface
 Wiring Schematic
 Board 2
 Sheffield Hallam University
 School of Engineering
 Drawn by R.E. Brown
 Date : 29:March:1999
 Page 2 of 4



- SKT1 (+5 Volts)
- SKT2 (0 Volts)
- BD2 IC1a
- BD2 IC2b
- PB1 (NC) Init. Disintegration
- PB1 (Com) Init. Disintegration
- PB1 (H0) Init. Disintegration



- SKT1 (+5 Volts)
- SKT2 (0 Volts)
- BD2 1C3b
- SKT10 Thyristor Cathode
- SKT9 Thyristor Gate